

Distribution Agreement

In presenting this thesis or dissertation as a partial fulfillment of the requirements for an advanced degree from Emory University, I hereby grant to Emory University and its agents the non-exclusive license to archive, make accessible, and display my thesis or dissertation in whole or in part in all forms of media, now or hereafter known, including display on the world wide web. I understand that I may select some access restrictions as part of the online submission of this thesis or dissertation. I retain all ownership rights to the copyright of the thesis or dissertation. I also retain the right to use in future works (such as articles or books) all or part of this thesis or dissertation.

Signature:

Brooke M. Katzman

Date

Navigating the Roads to Drug Discovery:

Part 1: Design, Synthesis, and Biological Evaluation of a Novel Class of Allosteric Modulators of
N-Methyl-D-Aspartate Receptor Function

Part 2: Discovery of Novel Tetrahydroisoquinoline (THIQ)-Based CXCR4 Antagonists and
Conformational Analysis of Structurally Similar CXCR4 Antagonists

By

Brooke M. Katzman
Doctor of Philosophy

Chemistry

Dennis C. Liotta
Advisor

Stefan A. Lutz
Committee Member

Frank E. McDonald
Committee Member

Accepted:

Lisa A. Tedesco, Ph.D.
Dean of the James T. Laney School of Graduate Studies

Date

Navigating the Roads to Drug Discovery:

Part 1: Design, Synthesis, and Biological Evaluation of a Novel Class of Allosteric Modulators of
N-Methyl-D-Aspartate Receptor Function

Part 2: Discovery of Novel Tetrahydroisoquinoline (THIQ)-Based CXCR4 Antagonists and
Conformational Analysis of Structurally Similar CXCR4 Antagonists

By

Brooke M. Katzman
B.S. and B.A., Youngstown State University, 2009

Advisor: Dennis C. Liotta, Ph.D.

An abstract of
A dissertation submitted to the Faculty of the
James T. Laney School of Graduate Studies of Emory University
in partial fulfillment of the requirements for the degree of
Doctor of Philosophy
in Chemistry
2014

Abstract

Navigating the Roads to Drug Discovery:

Part 1: Design, Synthesis, and Biological Evaluation of a Novel Class of Allosteric Modulators of *N*-Methyl-D-Aspartate Receptor Function

Part 2: Discovery of Novel Tetrahydroisoquinoline (THIQ)-Based CXCR4 Antagonists and Conformational Analysis of Structurally Similar CXCR4 Antagonists

By Brooke M. Katzman

Part 1:

The *N*-methyl-D-aspartate receptor (NMDA) is an ionotropic glutamate receptor that mediates excitatory synaptic transmission. Under normal physiological conditions, NMDA receptors are involved in many neurological processes including learning and memory. NMDA receptor dysfunction has been implicated in several neuropathological conditions, such as Parkinson's disease, Alzheimer's disease, and neuronal damage during ischemia. Therapeutic agents acting at NMDA receptors have been proposed for treating disorders, however side effects have complicated the clinical evaluation. This dissertation describes a novel class of allosteric modulators that have a modest preference for GluN2C/D receptors. Several molecules in this series exhibit sub-maximal inhibition. The mechanism of action for a typifying member of this class was determined. We show that this compound is active in neurons, with potent inhibition of NMDA receptor function in cerebellar granule cells. Additionally, this compound possesses neuroprotective properties against NMDA-induced toxicity in primary neuronal cultures. We are optimistic that this series of compounds could be useful neuroprotective agents in stroke or neurodegenerative diseases, with their partial antagonism potentially lessening undesirable side effects.

Part 2:

The CXC chemokine receptor 4 (CXCR4) is a G protein-coupled receptor (GPCR) that interacts with the CXCL12 chemokine to regulate several diverse processes such as cell migration, proliferation, and angiogenesis. Additionally, it plays a pivotal role in HIV pathogenesis as this protein is utilized by T-Tropic HIV-1 variants as a co-receptor for viral entry. Several peptides and small molecules have been developed that target CXCR4 and exploit these biological roles. The second part of this dissertation describes the discovery of a novel series of small molecule CXCR4 antagonists. During the development of a structure activity relationship (SAR), several important details regarding the requirements for effective binding were revealed. A combination of computational and experimental methods was employed with our most potent compound to predict its binding interactions to CXCR4. With knowledge of its conformation in solution and a predicted bioactive pose, we were able to better understand the fundamental factors that contribute to its favorable interactions with the protein. Furthermore, we used this information to design new molecules predicted to be more potent than our lead compound.

Navigating the Roads to Drug Discovery

Part 1: Design, Synthesis, and Biological Evaluation of a Novel Class of Allosteric Modulators of
N-Methyl-D-Aspartate Receptor Function

Part 2: Discovery of Novel Tetrahydroisoquinoline (THIQ)-Based CXCR4 Antagonists and
Conformational Analysis of Structurally Similar CXCR4 Antagonists

By

Brooke M. Katzman
B.S. and B.A., Youngstown State University, 2009

Advisor: Dennis C. Liotta, Ph.D.

A dissertation submitted to the Faculty of the
James T. Laney School of Graduate Studies of Emory University
in partial fulfillment of the requirements for the degree of
Doctor of Philosophy
in Chemistry
2014

Table of Contents

List of Illustrations

Figures
Tables
Schemes
Graphs
Charts

List of Abbreviations

Part 1: Design, Synthesis, and Biological Evaluation of a Novel Class of Allosteric Modulators of *N*-Methyl-D-Aspartate Receptor Function

CHAPTER 1

1.1 Statement of Purpose	1
1.2 Introduction and Background	2
1.2.1 Receptor Structure, Function, and Synaptic Localization	2
1.2.2 NMDA Receptor Pharmacology	6
1.2.3 Clinical Implications of NMDA Receptor Dysfunction	11
1.2.4 NMDA Receptor as a Therapeutic Target	12
1.2.5 Rationale for 1794-Series Analogues	14
1.3 Synthesis of 1794-Series Analogues	15
1.4 Results and Discussion	23
1.4.1 Structure Activity Relationships of 1794 Series	23
1.4.2 <i>In Vitro</i> Analysis of 1794 Series Mechanism of Action	33
1.4.3 <i>In Vitro</i> Analysis of 1794 Series in Primary Cultured Neurons	35
1.4.4 <i>In Vitro</i> Analysis of 1794 Series in Neuroprotection Model	36
1.5 Conclusions	37
1.6 Chemistry Experimental Detail	38
1.6.1 Synthetic Chemistry Experimental Detail	39
1.6.2 Crystal Structure Data	80
1.7 Biology Experimental Detail	96
1.7.1 <i>In Vitro</i> Antagonism Assay	96
1.7.2 Patch Clamp Recordings from Cerebellar Granule Cells	98
1.7.3 Lactate Dehydrogenase (LDH) Assay	99

Part 2: Discovery of Novel Tetrahydroisoquinoline (THIQ)-Based CXCR4 Antagonists and Conformational Analysis of Structurally Similar CXCR4 Antagonists

CHAPTER 2

2.1 Statement of Purpose	102
2.2 Introduction and Background	103
2.2.1 Chemokines and Chemokine Receptors	103
2.2.2 CXCR4 and its Ligand CXCL12	106
2.2.3 CXCR4/CXCL12 Signaling Pathway	108
2.2.4 Therapeutic Rationale for Targeting CXCR4/CXCL12 Axis	109
2.2.5 Clinically Relevant CXCR4 Antagonists	113
2.2.6 Rationale for THIQ-Based CXCR4 Antagonists	115

2.2.7 Rationale for Masking the Basicity of the Butylamine Nitrogen	120
2.3 Synthesis of THIQ Analogues	123
2.3.1 Retrosynthetic Analysis Toward THIQ Analogues	123
2.3.2 Optimization of Synthetic Routes Toward Analogues	124
2.3.3 Forward Synthesis of THIQ Analogues	127
2.4 Results and Discussion	134
2.4.1 Structure Activity Relationship of THIQ Analogues	134
2.4.2 Interpretation of Biological Data Through Molecular Modeling	137
2.4.3 <i>In Vitro</i> Analysis of Drug Efflux and Permeability	139
2.5 Conclusions	142
2.6 Chemistry Experimental Detail	144
2.6.1 Synthetic Chemistry Experimental Detail	144
2.6.2 Crystal Structure Data	161
2.7 Biology Experimental Detail	167
2.7.1 MAGI Antiviral Assay with HIV-1IIIIB	167
2.7.2 Calcium Flux Assay	169
2.7.3 Caco-2 Permeability Assay	170

CHAPTER 3

3.1 Statement of Purpose	172
3.2 Introduction and Background	173
3.2.1 History of Medicine and Drug Discovery	173
3.2.2 Structured-based Drug Design	175
3.2.3 Conformation and Drug Design	175
3.2.4 Tools for Conformational Analysis	177
3.2.5 NMR Analysis of Molecular Flexibility in Solution (NAMFIS)	182
3.3 Conformational Analysis of CXCR4 Antagonists	183
3.3.1 Introduction	183
3.3.2 Synthesis of CXCR4 Antagonists for NAMFIS Studies	184
3.3.3 Results and Discussion	186
3.4 Design of Constrained Analogues	200
3.4.1 Introduction	200
3.4.2 Synthesis of Constrained Analogues	202
3.4.3 Results and Discussion	208
3.5 Conclusions	210
3.6 Chemistry Experimental Detail	212
3.6.1 Synthetic Chemistry Experimental Detail	212
3.6.2 NMR Experimental Detail	234
3.6.3 Crystal Structure Data	242
3.7 Computational Methods	254

List of Illustrations

<u>Page Number</u>	<u>List of Figures</u>
1	Figure 1.1 Structure of Screening Hit in which 1794-Series Originated.
3	Figure 2.2 Structures of Synthetic Glutamate Mimics which Selectively Bind Respective iGluRs.
3	Figure 1.3 Tetrameric NMDA Receptor Assembly.
4	Figure 1.4 Linear Amino Acid Sequence and Cartoon Depiction of NMDA Receptor Subunit Architecture.
5	Figure 1.5 <i>In Situ</i> Hybridization of the NMDA Receptor Subunit mRNA Throughout Rat Development.
8	Figure 1.6 Structures of NMDA Receptor Competitive Antagonists.
9	Figure 1.7 Structures of Uncompetitive NMDA Receptor Antagonists.
10	Figure 1.8 Structures of Noncompetitive NMDA Receptor Modulators.
15	Figure 1.9 Generic Structure Illustrating the Planned Modifications to the Screening Hit (1794).
31	Figure 1.10 Rationale for Hybrid Analogues.
33	Figure 1.11 Inhibition and Subunit-Selectivity of 1794-2 .
34	Figure 1.12 Noncompetitive Inhibition of Recombinant GluN1/GluN2D Receptor by 1794-2 .
35	Figure 1.13 Voltage-Independent Mechanism of GluN1/GluN2C Receptor Inhibition by 1794-2 .
36	Figure 1.14 Negative Allosteric Modulation of NMDA Receptors Expressed on Cultured Primary granule Cells from Rat Cerebellum by 1794-2 .
37	Figure 1.15 Neuroprotection by 1794-2 against NMDA-Induced Excitotoxicity of Cultured Primary Hippocampal Neurons.
102	Figure 2.1 Structure of Potent CXCR4 Antagonist Developed in the Liotta Laboratory.
103	Figure 2.2 Family of Chemokine Receptors.
104	Figure 2.3 Topology of a Typical Chemokine.
105	Figure 2.4 Chemokine Receptors and Their Ligands.
107	Figure 2.5 Cartoon Representation of CXCR4 Structure.
108	Figure 2.6 Proposed Two-Step Mechanism for CXCL12 and CXCR4 Binding.
109	Figure 2.7 CXCR4 Signaling Pathway.
110	Figure 2.8 Mechanism of HIV-1 Cell Entry.
112	Figure 2.9 Hematopoietic Stem Cell (HSC) Niche in Bone Marrow (BM).
115	Figure 2.10 Structures of Selected CXCR4 Antagonists.
116	Figure 2.11 Initial Hit-to-Lead Efforts.
117	Figure 2.12 Conclusions on Initial Hit-to-Lead Efforts.
121	Figure 2.13 Equations for Octanol/Water Partition and Distribution Coefficients.
138	Figure 2.14 Proposed Bioactive Pose of ECXC-00947 (blue tube) Docked into CXCR4:CVX15 Crystal Structure (grey ribbon).
139	Figure 2.15 Proposed Bioactive Pose of 14 (blue tube) Docked into CXCR4:CVX15 Crystal Structure (grey ribbon).
140	Figure 2.16 Diagram of the Caco-2 Permeability Assay.

141 **Figure 2.17** Equation Used to Calculate Permeability Coefficient (P_{app}).
172 **Figure 3.1** Structures of CXCR4 Antagonists used in Computational and
Experimental Studies.
179 **Figure 3.2** Pictorial Representation of Rapid Conformational Interconversion that
Takes Place on the NMR Time Scale.
179 **Figure 3.3** NMR Spectrum of Cyclohexane- d_{11} Illustrating the Effect of
Temperature on Conformational Exchange.
185 **Figure 3.4** Crystal Structure of **IT1t**.
187 **Figure 3.5** Cartoon Representation of Crystal Structure with **IT1t** (magenta)
Bound to CXCR4 and Schematic Representation of Selected Interactions
between CXCR4 and **IT1t**.
189 **Figure 3.6** Overlay of AFITT Structure (pink) with **IT1t** (blue) from the Crystal
Structure within the X-ray Electron Density (gray mesh).
192 **Figure 3.7** Top Pose of **AMD11070** (blue) Docked into **A**) CXCR4:CVX15
Peptide Crystal Structure (gray) **B**) CXCR4:IT1t Crystal Structure (gray).
194 **Figure 3.8** Comparison of the Bioactive Pose of **AMD11070** from the
CXCR4:CVX15 Crystal Structure (light gray) with **A**) the **AMD11070** Small
Molecule Crystal Structure (dark gray) and **B**) NAMFIS-3 (dark gray).
194 **Figure 3.9** Structure of **AMD11070** and Internal Ruler Used to Derive the
Interproton Distances.
195 **Figure 3.10** Alignment of the **AMD11070** Small Molecule X-ray Structure
(blue) with **A**) NAMFIS-4 (yellow) and **B**) NAMFIS-9 (green).
197 **Figure 3.11** Model of **ECXC00947** Binding to CXCR4 Derived from the
CXCR4:IT1t Small Molecule Crystal Structure (PDB 3ODU).
198 **Figure 3.12** Model of **ECXC00947** Binding to CXCR4 Derived from the
CXCR4:CVX15 Peptide Crystal Structure (PDB 3OE0).
199 **Figure 3.13** Overlay of NAMFIS Conformer (green) with Best Fit to Poses
Derived from **A**) CXCR4:IT1t Model (red) and **B**) CXCR4:CVX15 Model
(blue).
202 **Figure 3.14** NAMFIS-derived Conformations of **ECXC00947** Butylamine Side
Chain Represented as Fragments.
203 **Figure 3.15** Target Compounds to Designed to Probe the Effects of
Conformational Flexibility.

List of Tables

6 **Table 1.1** Glycine Site Agonists.
7 **Table 1.2** Glutamate Site Agonists.
13 **Table 1.3** Examples of NMDA Receptor Antagonists Utilized in Clinical Trials.
19 **Table 1.4** Sample of Attempted Coupling Conditions.
25 **Table 1.5** Effect of A-ring Substitutions on the Potency of 1794 Analogues.
25 **Table 1.6** Effect of A-ring Replacement on the Potency of 1794 Analogues.
26 **Table 1.7** Effect of Alkyl Substitutions to the Thiophene Ring on the Potency of
1794 Analogues.
28 **Table 1.8** Effect of Substituted Tetrahydrobenzothiophenes on the Potency of
1794 Analogues.

30	Table 1.9 Effect of Varied Ester Substitutions on the Potency and Mode of Receptor Modulation.
32	Table 1.10 Effect of Aryl Thiol Replacements on the Potency of Hybrid Analogues.
32	Table 1.11 Effect of B-ring Bioisosteric Replacements on the Potency of Hybrid Analogues.
118	Table 2.1 MAGI Assay Results for Series of Piperidine Compounds.
122	Table 2.2 Calculated pKa values for side chain nitrogen.
135	Table 2.3 Effect of THIQ Nitrogen Atom Substitutions on Viral Attachment and Calcium Flux.
136	Table 2.4 Effect of Butylamine Nitrogen Substitutions on Viral Attachment and Calcium Flux.
142	Table 2.5 Caco-2 Permeability Data for Selected THIQ Analogues.
211	Table 3.1 Effect of Conformational Restraints on Biological Activity.
235	Table 3.2 Spectral Assignments of IT1t .
235	Table 3.3 NOE-derived Distances for IT1t .
237	Table 3.4 Spectral Assignments of AMD11070 .
238	Table 3.5 NOE-derived Distances for AMD11070 .
240	Table 3.6 Spectral Assignments of ECXC00947 .
241	Table 3.7 NOE-derived Distances for ECXC00947 .

List of Schemes

16	Scheme 1.1 Synthetic Route Toward 1794 Analogues.
17	Scheme 1.2 Synthesis of Imidazolidinone 1794-5 with HATU Coupling Reagent.
18	Scheme 1.3 Convergent Approach Toward 1794-Series Analogues.
20	Scheme 1.4 Synthesis of Iminothiazolidinones from Aryl Maleimides.
21	Scheme 1.5 Microwave-assisted Hydrolysis of <i>t</i> -Butyl Ester.
21	Scheme 1.6 Synthesis of Analogues with Varied A-rings.
22	Scheme 1.7 Synthesis of Aryl Thiols.
22	Scheme 1.8 Synthesis of Imidazolidinedione 1794-26 .
23	Scheme 1.9 Synthesis of Compounds with Both A-ring and B-ring Replacements.
124	Scheme 2.1 Retrosynthetic of THIQ Analogues.
125	Scheme 2.2 Optimization of Aminoaldehyde Synthesis.
127	Scheme 2.3 Synthesis of (<i>R</i>)-THIQ Carboxylic Acid from a Commercial Amino Acid.
128	Scheme 2.4 Synthesis of Half-Scaffold Amine Intermediate.
129	Scheme 2.5 Examples of Reductive Amination Conditions.
131	Scheme 2.6 Divergent Route Toward THIQ Analogues.
132	Scheme 2.7 Attempted Synthesis of Difluoro-Analogue.
133	Scheme 2.8 Synthetic Route to Difluoro Regioisomer.
185	Scheme 3.1 Synthesis of IT1t .
186	Scheme 3.2 Synthesis of AMD11070 .
204	Scheme 3.3 Conditions Employed for Hydrogenolysis of Cbz Group.

205	Scheme 3.4 Synthesis of Side Chain Fragments.
207	Scheme 3.5 Complete Synthesis of Conformationally Restrained Analogues.
	<u>List of Graphs</u>
111	Graph 2.1 Clinical Progression to AIDS: R5 vs. Dual/Mixed Tropic Virus.
200	Graph 3.1 Comparison of Anti-HIV Activity (pIC_{50}) with Prime MM-GBSA Scores Derived from the CXCR4 Binding Models for a Congeneric Series of THIQ-based Compounds.

List of Abbreviations

AMPA	Amino-3-hydroxy-5-methyl-4-isoxazolepropionate
ATD	Amino terminal domain
BBB	Blood-brain barrier
BH ₃ -DMS	Borane-dimethyl sulfide
BHK	Baby hamster kidney
Boc	<i>Tert</i> -butyl carbamate
br s	Broad singlet
Calc'd	Calculated
CDCl ₃	Deuterated chloroform
<i>cis</i> -ACPD	(1 <i>R</i> ,3 <i>R</i>)-aminocyclopentane- <i>cis</i> -dicarboxylate
cLog <i>P</i>	Calculated log P
CNS	Central nervous system
CSF	Cerebrospinal fluid
CTD	Carboxyl-terminal domain
CIQ	3-chlorophenyl)(6,7-dimethoxy-1-((4-methoxyphenoxy)methyl)-3,4-dihydroisoquinolin-2(1 <i>H</i>)-yl)methanone
d	Doublet
dd	Doublet of doublets
ddd	Doublet of doublets of doublets
dq	Doublet of quartets
dt	Doublet of triplets
DCM	Dichloromethane
DIPEA	Diisopropylethyl amine
DMAP	Dimethyl amino pyridine

DMF	Dimethyl formamide
DMSO	Dimethyl sulfoxide
DQP	Dihydro-quinolone pyrazoline
EC ₅₀	Half-maximal effective concentration
EDCI	1-ethyl-3-(3-dimethylaminopropyl)carbodiimide)
ee	Enantiomeric excess
EPSC	Excitatory postsynaptic current
EtOAc	Ethyl acetate
EtOH	Ethanol
FDA	Food and Drug Administration
GPCR	G protein-coupled receptor
GPe	External globus pallidus
GPi	Internal globus pallidus
HMDS	Hexamethyldisilazide
HOBt	Hydroxyl-benzotriazole
HRMS	High resolution mass spectrometry
IC ₅₀	Half-maximal inhibitory concentration
iGluR	Ionotropic glutamate receptor
KA	Kainate
LC-MS	Liquid chromatography mass spectrometry
LBD	Ligand-binding domain
LDH	Lactate dehydrogenase
LTP	Long-term potentiation
m	Multiplet
MeCN	Acetonitrile
MEK	Methyl ethyl ketone

MeOH	Methanol
mGluRs	Metabotropic glutamate receptors
MHz	Megahertz
MK-801	(5 <i>R</i> ,10 <i>S</i>)-5-methyl-10,11-dihydro-5 <i>H</i> -dibenzo[<i>a,d</i>]cyclohepten-5,10-imine
mRNA	Messenger ribonucleic acid
MsCl	Methanesulfonyl-chloride
NaOH	Sodium hydroxide
NIMH	National Institute of Mental Health
NMDA	<i>N</i> -methyl- <i>D</i> -aspartate
NMR	Nuclear magnetic resonance
P_{app}	Permeability coefficient
PCA	1-phenylcyclohexylamine
PCP	Phencyclidine
P-gp	P-glycoprotein
q	Quartet
s	Singlet
SAR	Structure activity relationship
STN	Subthalamic nucleus
t	Triplet
tt	Triplet of triplets
TBI	Traumatic brain injury
TFA	Trifluoro acetic acid
THF	Tetrahydrofuran
TMD	Transmembrane domain

Part 1:

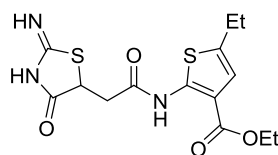
**Design, Synthesis, and Biological Evaluation of a Novel Class of
Allosteric Modulators of *N*-Methyl-D-Aspartate Receptor Function**

CHAPTER 1

1.1 Statement of Purpose

Our research group is interested in the discovery of small molecule modulators of *N*-methyl-D-aspartate (NMDA) receptor function as treatment for neurological diseases. NMDA receptor over-activation is known to cause neuronal toxicity and cell death implicated in ischemic stroke, traumatic brain injury (TBI), epilepsy, Parkinson's disease, Alzheimer's disease, and others. Experimental evidence also indicates that NMDA receptor potentiators have therapeutic potential in the treatment of neurological disorders characterized by receptor hypofunction, including schizophrenia, psychosis, depression, and other anxiety disorders. While both blockade and enhancement of NMDA receptor has been efficacious in animal models, neither of these strategies has translated into positive clinical outcomes. A majority of the clinical failures can be partly attributed to adverse side effects.

In an effort to identify new NMDA receptor modulators, the laboratory of Dr. Stephen Traynelis in the Emory School of Medicine, Department of Pharmacology screened a library of compounds against GluN1/GluN2C- and GluN1/GluN2D-expressing baby hamster kidney (BHK) cells. The fluorescence-based screen resulted in a number of hits. Of these hits, one compound showed inhibition of NMDA-related current and was chosen for further study (1794 series, Figure 1.1, **1794**). This compound displayed modest selectivity for GluN2C- and GluN2D-containing NMDA receptors over GluN2A- and GluN2B-containing receptors.



1794

Figure 1.1 Structure of Screening Hit in which 1794 Series Originated.

The goal of this project was to develop a structure activity relationship (SAR) in collaboration with the Traynelis laboratory. We sought to increase the GluN2C and GluN2D on-target potency of this family of compounds. In addition, exemplary compounds would exhibit selectivity for NMDA receptors across the glutamate receptor ion channel family. These project aims were achieved with the following objectives:

1. Design and synthesis of novel 1794 series analogues, with emphasis on improving potency.
2. Novel analogues were tested for *in vitro* NMDA receptor activity in GluN2A-, GluN2B-, GluN2C-, and GluN2D-containing NMDA receptors. In addition, kainate and AMPA receptor activity was measured. All *in vitro* biological evaluation of NMDA receptors was carried out in the Traynelis laboratory.
3. The mechanism of action was determined for the most potent analogue.
4. *In vitro* analysis of neuroprotection against NMDA-induced toxicity was performed using a lactate dehydrogenase (LDH) assay.

1.2 Introduction and Background

1.2.1 Receptor Structure, Function, and Synaptic Localization

The amino acid glutamate exists as one of the most prevalent excitatory neurotransmitters in the central nervous system (CNS).¹ The glutamate family of receptors can be divided into two distinct classes: metabotropic and ionotropic. Metabotropic glutamate receptors (mGluRs) belong to the group C family of G protein-coupled receptors (GPCRs). To date, eight mGluR subtypes have been cloned (mGluRs 1-8) and classified into three groups (Group I, II, and III) according to their amino acid sequence identity. Ionotropic glutamate receptors (iGluRs) are a major class of cell surface ligand-gated ion channels. The iGluRs are further divided into α -amino-3-hydroxyl-5-methyl-4-isoxazole-propionate (AMPA, **1**), kainate (**2**), and *N*-methyl-D-aspartate (NMDA, **3**) receptors based on their amino acid sequence homology, structure, and

pharmacology.² The three classes of iGluRs have been named according to the synthetic glutamate mimic that binds specifically and selectively to each respective receptor (Figure 1.2).

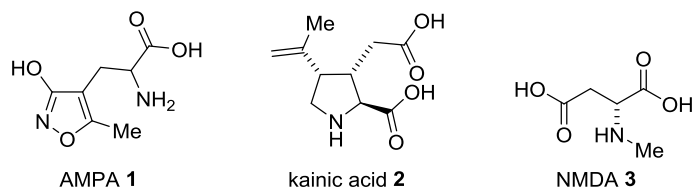


Figure 1.2 Structures of Synthetic Glutamate Mimics which Selectively Bind Respective iGluRs.

NMDA receptors are ligand-gated ion channels that mediate a slow component of excitatory synaptic transmission throughout the central nervous system (CNS). Functional NMDA receptors exist as heterooligomeric assemblies consisting of two glycine-binding GluN1 subunits encoded by eight splice variants of a single gene and two glutamate-binding GluN2 subunits (GluN2A-D) arising from four genes.²⁻⁷ The tetrameric complexes arrange to form an ion conduction pore which controls the flux of cations across the cell membrane (Figure 1.3).

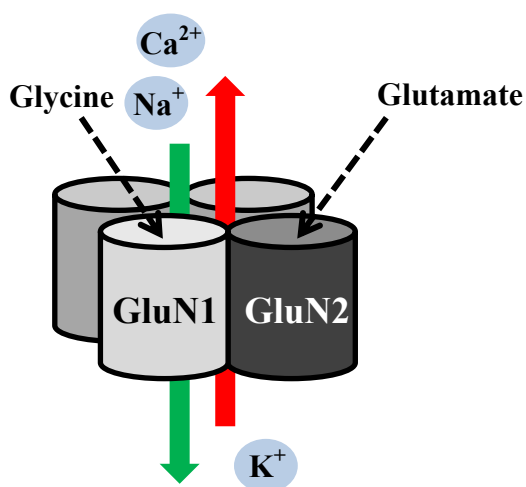


Figure 1.3 Tetrameric NMDA Receptor Assembly.

Each subunit of the NMDA receptors folds into four semi-autonomous domains (Figure 1.4). The amino-terminal domain (ATD), the ligand binding domain (LBD), and the transmembrane domain (TMD) are each thought to have distinct binding sites and structural determinants that account for the actions of endogenous and exogenous modulators.² The carboxy-terminal domain (CTD) is known to bind intracellular proteins and is subject to post-translational modifications that alter the function of the receptor.² Among the iGluRs, NMDA receptors are functionally unique as they require the binding of both glutamate and co-agonist glycine for receptor activation.⁸⁻¹¹ In addition, membrane depolarization is required to relieve voltage-dependent Mg^{2+} block before ions can permeate the channel pore. The combination of chemical and electrical stimuli causes the ion channel to open and allows for the flow of calcium ions into the cell. This process propagates neuron to neuron synaptic transmission which plays an important role in development and in forms of synaptic plasticity that may underlie higher order processes such as learning, memory, and motor function.^{7,12,13}

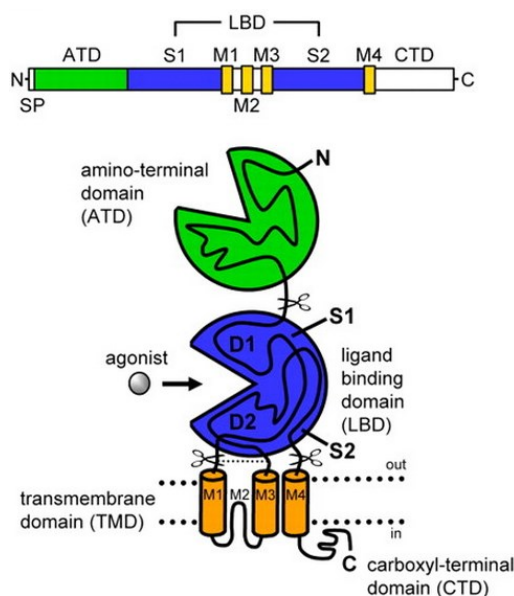


Figure 1.4 Linear Amino Acid Sequence and Cartoon Depiction of NMDA Receptor Subunit Architecture.²

Each of the four GluN2 subunits provides NMDA receptors with unique functional properties, including deactivation time course, agonist potency, mean open time, and open probability.¹⁴ In addition, expression of the four GluN2 subunits is both temporally and spatially controlled throughout brain development.¹⁵ *In situ* hybridization of the mRNA for the GluN1 and each of the four GluN2 subunits shows that GluN1 is ubiquitously expressed throughout the rat brain during development and into adulthood, while GluN2 subunits exhibit differential expression (Figure 1.5).¹⁵ Both GluN2A and GluN2C mRNA expression is not observed at postnatal day 1, but steadily increases throughout the lifetime of the rat. In contrast, GluN2B and GluN2D mRNAs are distinctly expressed throughout most regions of the brain at postnatal day 1, then display a gradual increase in expression to postnatal day 11 followed by a distinct decrease after day 14.

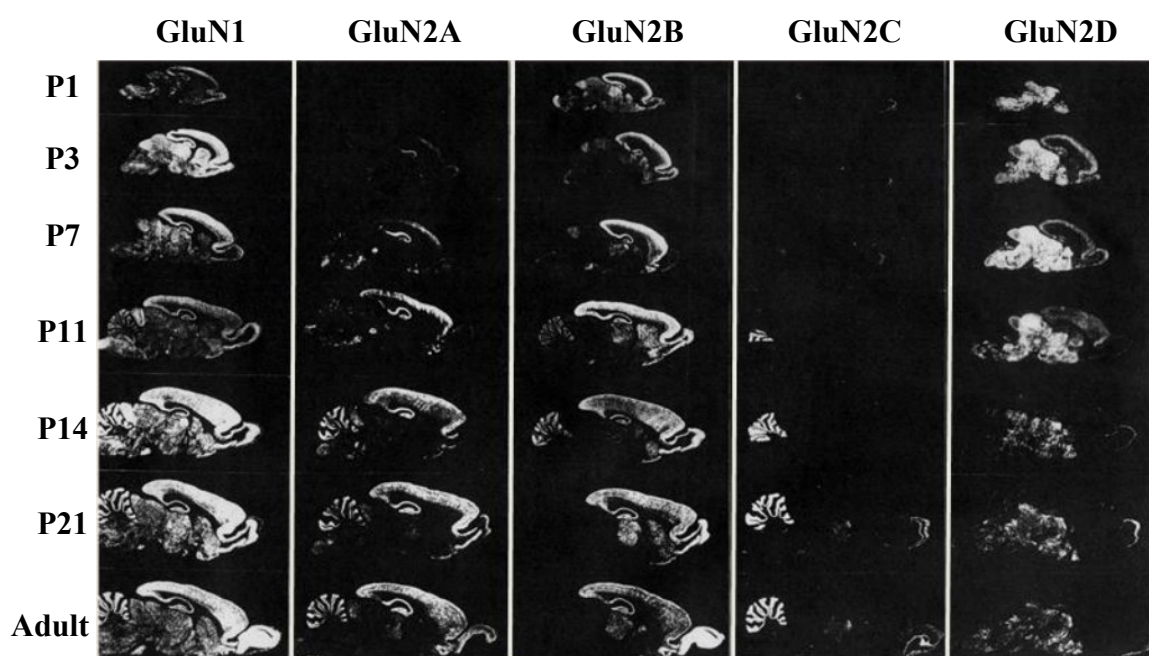


Figure 1.5 *In Situ* Hybridization of the NMDA Receptor Subunit mRNA Throughout Rat Development.¹⁵

The GluN2A subunit mRNA is highly expressed in the cerebellar cortex and hippocampus. GluN2B mRNA is prominent in the telencephalic regions and thalamus of the adult rat brain. A high concentration of GluN2C mRNA is found in the cerebellum, while GluN2D mRNA is moderately expressed in the adult brainstem regions and cortex of the olfactory bulb.

1.2.2 NMDA Receptor Pharmacology

NMDA Receptor Agonists

The ligand binding domain has been thoroughly studied with partial and full agonists acting at either the glutamate binding site of the GluN2 subunits or the glycine binding site of the GluN1 subunits. The discovery that glycine is an essential co-agonist at NMDA receptors prompted scientists to focus their efforts on exploiting the pharmacological potential of the agonist binding pocket.¹⁰ The crystal structure of glycine bound to the GluN1 LBD revealed key structural determinants of agonist binding.¹⁶ Endogenous and exogenous compounds have been shown to act at the glycine binding site with a broad range of potency and efficacy (Table 1.1).^{2,16-18}

Table 1.1 Glycine Site Agonists.

Glycine Site Agonist	GluN2A μM (efficacy)	GluN2B μM (efficacy)	GluN2C μM (efficacy)	GluN2C μM (efficacy)
Glycine	1.1 (100)	0.72 (100)	0.34 (100)	0.13 (100)
L-Serine	212 (95)	77 (98)	27 (110)	15 (98)
D-Serine	1.3 (98)	0.65 (96)	0.32 (110)	0.16 (93)
L-Alanine	3.1 (96)	0.89 (84)	0.56 (96)	0.22 (99)
D-Alanine	55 (100)	52 (100)	12 (89)	14 (90)
D-Cycloserine	19 (90)	8.2 (65)	3.3 (190)	2.9 (94)
HA 966	12 (12)	4.6 (14)	--	--
β-CI-D-Alanine	21 (84)	9.9 (88)	3.7 (79)	1.7 (81)
β-F-DL-Alanine	11 (92)	0.98 (88)	0.40 (84)	0.40 (91)
Tri-F-DL-Alanine	1.3 (130)	0.65 (64)	0.32 (110)	0.16 (93)
ACPC	1.3 (79)	0.65 (89)	0.35 (88)	0.083 (89)
ACBC	45 (13)	6.6 (33)	--	--

Percentage relative efficacy (in parentheses) is the current response to a maximally effective concentration of agonist relative to the response to a maximally effective concentration of glycine. All values are from recombinant rat NMDA receptors expressed in *Xenopus laevis* oocytes and co-activated by glutamate, except HA 966 and ACBC. Abbreviations: HA 966, (+)-(1-hydroxy-3-aminopyrrolidine-2-one); ACPC, 1-aminocyclopropane-1-carboxylic acid; ACBC, 1-aminocyclobutane-1-carboxylic acid.^{2,19-24}

Additional studies have also identified ligands that are full or partial agonists at the glutamate binding site of GluN2 subunits (Table 1.2).^{19–24} Key interactions for agonist binding have been identified through the crystal structure of the agonist-bound GluN1-GluN2A LBD heterodimer.^{16,25} In addition to L-glutamate, endogenous ligands such as D- and L-aspartate, homocysteate, and cysteinesulfinat act as agonists at the GluN2 LBD.^{11,21,26–28}

Table 1.2 Glutamate Site Agonists.

Glutamate Site Agonist	GluN2A μM (efficacy)	GluN2B μM (efficacy)	GluN2C μM (efficacy)	GluN2C μM (efficacy)
L-Glutamate	3.3 (100)	2.9 (100)	1.7 (100)	0.51 (100)
D-Glutamate	250 (99)	160 (120)	110 (100)	42 (110)
L-Aspartate	48 (99)	14 (78)	41 (110)	12 (91)
D-Aspartate	30 (103)	10 (91)	9.3 (99)	2.1 (90)
N-Methyl-L-aspartate	580 (99)	130 (69)	150 (66)	40 (75)
N-Methyl-D-aspartate	94 (93)	30 (78)	22 (86)	7.3 (92)
SYM2081	140 (72)	25 (89)	18 (71)	3.2 (75)
L-Homocysteinsulfinat	73 (91)	18 (94)	14 (70)	6.2 (84)
D-Homocysteinsulfinat	36 (89)	14 (99)	7.9 (92)	3.0 (100)
L-Homocysteate	34 (86)	8.1 (90)	12 (53)	3.4 (69)
D-Homocysteate	180 (92)	86 (94)	110 (74)	22 (87)
L-Cysteinesulfinat	140 (110)	100 (81)	22 (100)	9.2 (98)
L-Cysteate	560 (95)	180 (77)	80 (82)	30 (83)
D-Cysteate	220 (31)	210 (67)	580 (110)	100 (97)
Homoquinolinate	22 (75)	16 (96)	81 (51)	32 (88)
Ibotenate	160 (99)	26 (89)	40 (72)	13 (78)
(R,S)-(Tetrazol-5-yl)glycine	1.7 (98)	0.52 (97)	0.49 (89)	0.099 (78)
L-CCG-IV	0.26 (99)	0.083 (120)	0.11 (90)	0.036 (110)
trans-ACBD	3.1 (91)	0.99 (81)	1.2 (67)	0.51 (81)
cis-ADA	890 (100)	220 (95)	80 (81)	32 (140)
trans-ADC	470 (38)	170 (48)	95 (73)	50 (80)
cis-ACPD	61 (76)	21 (75)	22 (49)	11 (77)
cis-2,3-Piperidinedicarboxylic acid	21 (3)	38 (7)	--	--
(R)-NHP4G	150 (33)	61 (76)	120 (54)	48 (77)
(R,S)-Ethyl-NHP5G	47 (5)	68 (45)	91 (52)	43 (70)
(R)-Propyl-NHP5G	N.E.	105 (6)	429 (22)	153 (37)

Percentage relative efficacy (in parentheses) is the current response to a maximally effective concentration of agonist relative to the response to a maximally effective concentration of glutamate. All values are from recombinant rat NMDA (GluN1 plus the indicated GluN2) receptors expressed in *Xenopus laevis* oocytes activated by agonist plus maximally effective concentration of glycine. Abbreviations: SYM2081, (2*S*,4*R*)-methylglutamate; L-CCG-IV, (2*S*,3*R*,4*S*)-2-(carboxycyclopropyl)glycine; *trans*-ACBD, *trans*-1-aminocyclobutane-1,3-dicarboxylate; *cis*-ADA, *cis*-azetidine-2,4-dicarboxylic acid; *trans*-ADC, *trans*-azetidine-2,3-dicarboxylic acid; *cis*-ACPD, (1*R*,3*R*)-aminocyclopentane-*cis*-dicarboxylate; (R)-NHP4G, (R)-2-(*N*-hydroxylpyrazol-4-yl)glycine; NHP5G, (R*S*)-2-(*N*-hydroxypyrazol-5-yl)glycine.²

A number of other pharmacological sites have been exploited by pharmaceutical companies and academic laboratories in pursuit of antagonists that attenuate NMDA receptor function. The vast majority of the compounds described in the literature can be categorized into three distinct classes: competitive antagonists, uncompetitive antagonists, and noncompetitive antagonists.

Competitive Antagonists of the NMDA Receptor

Antagonists that bind to either the glycine site on GluN1 or the glutamate site on GluN2 have been described in the literature.^{29–33} The first class of competitive glycine site antagonists to be identified included halogenated quinoxalinediones, exemplified by licostinel (**4**, Figure 1.6), while classical competitive antagonists of the glutamate site have included phosphono derivatives of short-chain amino acids typified by selfotel (**5**, Figure 1.6). Licostinel and related analogues displayed potent inhibition of the NMDA receptor ($IC_{50} = 5.9$ nM) and also exhibited modest activity against related ionotropic glutamate receptors such as AMPA ($IC_{50} = 2$ μ M). In addition to their poor selectivity, these compounds suffered from low blood brain barrier permeability due to positive charge they carry at physiological pH. Clinical trials conducted with licostinel confirmed that the compound was safe; however poor aqueous solubility and lack of metabolism of the drug led to the observation of crystals in some of the patients' urine samples.

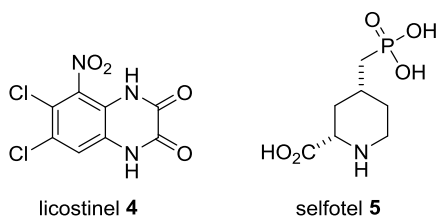


Figure 1.6 Structures of NMDA Receptor Competitive Antagonists.

Uncompetitive Modulators of the NMDA Receptor

The class of uncompetitive modulators is largely comprised of organic cation channel blockers that require the receptor pore to be open to allow access to the blockers' binding site to cause

subsequent blockade of receptor function.³⁴⁻³⁶ This unique requirement results in use-dependent onset of inhibition that generally increases with increasing channel open probability. Due to the global NMDA antagonism imparted by the blocking of the channel pore, these compounds are frequently associated with severe side effects. Memantine (**6**, Figure 1.7), a drug clinically approved for use in the treatment of Alzheimer's disease, belongs to this class of modulators. It is characterized by low affinity binding to the open state of the receptor and a rapid dissociation rate that is thought to improve its clinical utility by preferentially inhibiting overactive NMDA receptors.^{7,37-39} In contrast, **MK-801** (Figure 1.7) has been associated with adverse side effects, potentially due to its ability to bind more tightly and with a longer duration in the pore of the closed receptor.³⁹⁻⁴¹

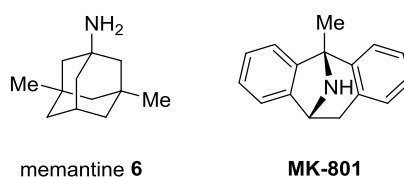


Figure 1.7 Structures of Uncompetitive NMDA Receptor Antagonists.

Noncompetitive Modulators of the NMDA Receptor

Several endogenous and exogenous ligands have been identified with predicted binding sites at the extracellular ATD of various GluN1/GluN2 receptors. The discovery of the first subunit-selective antagonist of GluN2B-containing receptors, ifenprodil (**7**, Figure 1.8), has enhanced our understanding of iGluR functions.²⁹ This polyamine and others have found widespread use as tools to study NMDA receptor subtypes both *in vitro* and *in vivo* and for molecular studies of the properties and regulation of NMDA receptors. Specifically, ifenprodil and structurally-similar analogues have been utilized in investigations regarding the biophysical properties of the channels, studies aimed at identifying the contributions of the receptor in long-term potentiation

(LTP), long-term depression (LTD), learning and memory formation, ischemic cell death, Parkinson's disease and several other phenomena. Data collected with these noncompetitive antagonists have validated the NMDA receptor as a tractable target for therapeutic intervention.

More recently, several other classes of subunit-selective allosteric modulators have been identified and characterized, including the GluN2C- and GluN2D-selective dihydroquinilone-pyrazoline (**DQP-1105**) family of compounds and the quinazolin-4-one (**QNZ-46**) scaffold of inhibitors, a series of negative modulators typified by **TCN-201** shown to be highly selective for GluN2A-containing receptors, and the class of tetrahydroisoquinoline GluN2C- and GluN2D-selective potentiators typified by **CIQ-1390** (Figure 1.8).⁴²⁻⁴⁶ These ligands possess unique structural determinants of action suggesting unique binding sites. Consequently, the compounds have the potential to establish a precedent for therapeutically relevant modulatory sites in regions other than the ATD.

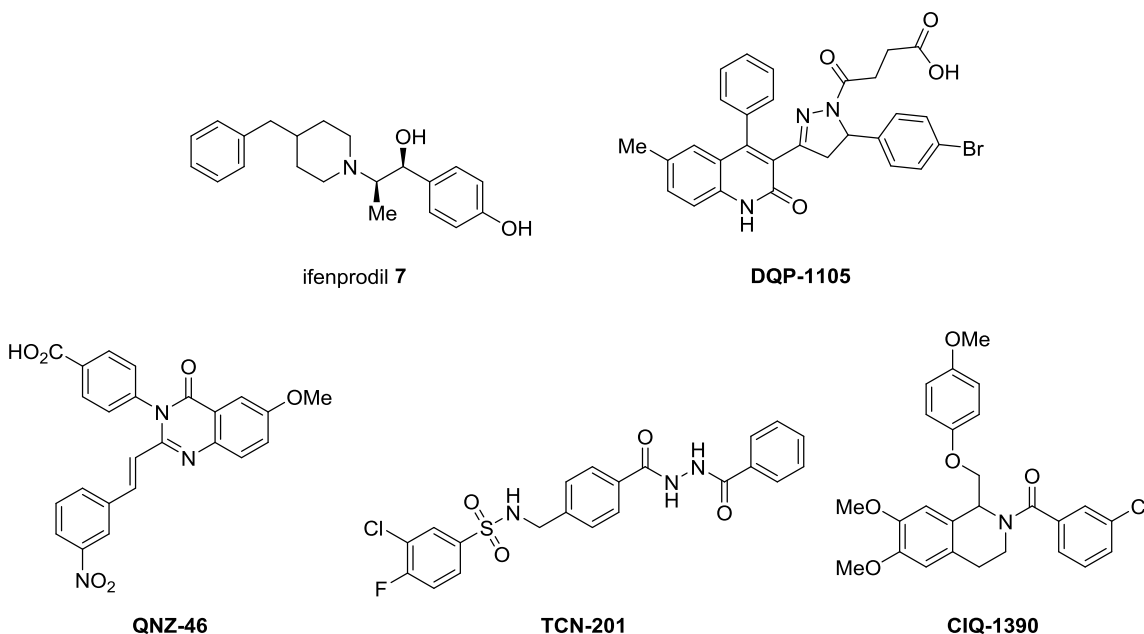


Figure 1.8 Structures of Noncompetitive NMDA Receptor Modulators.

1.2.3 Clinical Implications of NMDA Receptor Dysfunction

The term “excitotoxicity” was first introduced by Olney as a description of the process by which an excitatory neurotransmitter such as glutamate elicits toxicity. Under normal physiological conditions, activation of NMDA receptors by glutamate results in an influx of Ca^{2+} ions that stimulate both electrochemical signaling along the axon and intracellular signaling cascades. However at high concentrations of glutamate, over-activation of NMDA receptors triggers Ca^{2+} ions to flood the intracellular space inducing cell death by excitotoxic signaling, necrosis, and apoptosis. The effects of over-stimulation are exacerbated by affected cells through the enhanced release of glutamate at presynaptic terminals.² This glutamate and calcium feedback mechanism amplifies neuronal insult and can cause significant and irreversible damage to brain tissues of affected areas. Increased intracellular glutamate and NMDA receptor over-activation has been associated with cerebral ischemia, epilepsy, brain trauma, neuropathic pain and inflammation. Likewise, excess of the neurotransmitter has also been proposed to contribute to neurodegenerative diseases such as Alzheimer’s, Parkinson’s, or Huntington’s diseases by sensitizing neurons to excitotoxic damage.²

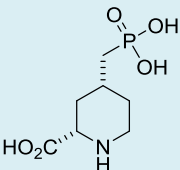
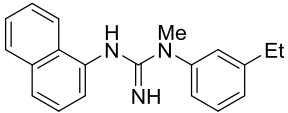
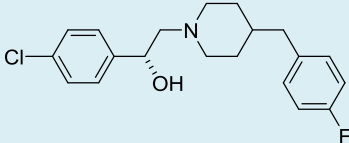
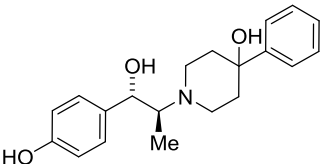
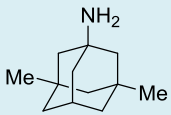
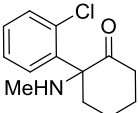
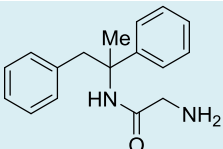
While it is evident that NMDA receptor over-activation is responsible for neuronal death in several disease states, receptor hypofunction and its connection to neurological conditions is not as clearly understood. Schizophrenia and related diseases of psychosis present negative symptoms that seem to be associated with the hypofunction of NMDA receptors. Genetic risk prediction studies have identified schizophrenia risk genes known to affect NMDA receptor function or glutamatergic neurotransmission. Other investigations have reported deficiencies in NMDA receptor subunit density in specific regions of post-mortem brain tissues of schizophrenic patients. Reports of decreased glutamate concentrations in cerebrospinal fluid (CSF) of schizophrenic patients resulted in the glutamate hypofunction hypothesis.⁴⁷ Although the findings reported in the seminal paper have not been successfully replicated,^{48–50} data from post-

mortem studies in schizophrenic patients support the hypothesis and suggest that hypofunction of glutamatergic processes may play a role in schizophrenic etiology.

1.2.4 NMDA Receptor as a Therapeutic Target

Due to the aberrant NMDA receptor behavior demonstrated for a variety of disease states in animal models, NMDA receptor modulators have been tested in a number of clinical trials toward the treatment of the aforementioned diseases (a number of compounds utilized in clinical studies are highlighted in Table 1.3).⁵¹⁻⁵⁴ Both blockade and potentiation of receptor function have been efficacious in animal models, however these results have yet to translate into positive clinical outcomes. While a few clinical studies have included positive modulators of NMDA function, such as glycine transport inhibitors and agonists that act at the glycine site aimed at improving the negative effects of schizophrenia, the majority of clinical work has explored the use of NMDA receptor antagonists in the fields of stroke, TBI, and dementia.^{2,55}

Table 1.3 Examples of NMDA Receptor Antagonists Utilized in Clinical Trials.

Drug	Structure	Mechanism of Action	Clinical Trial Indication
Selfotel		Competitive antagonist (glutamate site)	Stroke, TBI
Aptiganel		Noncompetitive channel blocker	Stroke, TBI
Eliprodil		Allosteric GluN2B-selective antagonist	Stroke, TBI
CP-101,606		Allosteric GluN2B-selective antagonist	TBI
Memantine		Noncompetitive channel blocker	Dementia, Huntington's Disease
Ketamine		Noncompetitive channel blocker	Anesthesia
Remacemide		Uncompetitive antagonist	Epilepsy, Stroke, Huntington's Disease

Stroke and TBI trials have included over 9000 patients, unfortunately, none of these studies have resulted in therapeutically useful agents. The reasons for failure of clinical trials with NMDA receptor antagonists have been extensively discussed. Specifically, failure has been attributed to difficulty of carrying out the clinical trials, heterogeneity of sampled stroke populations, and the narrow treatment window with which antagonists have been shown to be effective.^{2,56} Additionally, severe dose-limiting side effects were observed at therapeutically relevant concentrations. Several of the compounds studied required large plasma drug

concentrations in order to elicit significant neuroprotective effects. However, at high levels these compounds have been shown to alter cardiovascular function and disrupt cognition, resulting in psychotomimetic effects such as delusion, agitation, hallucination, and confusion. It was thought that these negative effects were also a result of global NMDA receptor inhibition.

More recent clinical trials with low-affinity channel blockers have resulted in positive clinical outcomes. Memantine and amantadine have been approved by the Food and Drug Administration (FDA) for use in Alzheimer's disease and Parkinson's disease, respectively.^{38,55} While the efficacy of these agents is not completely understood, their tolerability is attributed to their uncompetitive nature and rapid off-rate kinetics.^{38,39,57} The compounds bind to the NMDA receptor at the open channel Mg²⁺ binding site, then quickly dissociate with a long "off-time". It is thought that this unique mechanism preserves normal synaptic transmission and reduces the side effects commonly observed with channel blockers.

Significant efforts to target a single receptor subtype, namely GluN1A/GluN2B-containing NMDA receptors have also resulted in compounds with decreased psychosis-like side effects. However, these compounds have proven ineffective in the clinic either by failing to reach a statistically significant improvement at the end-point for the desired indications or cardiotoxicity associated with off-target receptors (human ether-a-go-go potassium channel, opioid, α_1 -adrenergic, sigma receptors, and others).

1.2.5 Rationale for 1794 Series Analogues

Although a variety of NMDA receptor antagonists have been shown to be neuroprotective in many animal studies of Parkinson's disease, traumatic brain injury, and stroke, it is clear that the majority of these compounds have been unsuccessful due to complications involving side effect profile and mechanism of action of the drugs tested. It has been proposed that allosteric antagonists of NMDA receptors with submaximal inhibition might be an effective alternative therapeutic strategy, but candidate modulators have not been available to test this hypothesis.

In an attempt to break this impasse, the Traynelis laboratory developed and implemented a high-throughput screen designed to identify noncompetitive allosteric modulators of GluN2C- and GluN2D-containing NMDA receptors.² They believe that some of the identified compounds would not only serve as useful research tools in studies of receptor subunit function, but also they would have the potential to treat a number of CNS-related disease states. The Traynelis lab performed a fluorescence-based primary screen of nearly 100,000 compounds from ChemDiv and Asinex diversity libraries and discovered a dozen new and unique classes of modulators. Among the hits, compound **1794** (Figure 1.9) was selected due to its initial distinct synthetic and pharmacological properties. The compound is characterized by an iminothiazolidinone ring with an acetamide linkage to a substituted thiophene ring. It was envisioned that the SAR could be developed through structural modifications to the original screening hit (**1794**) according to the general structure (**8**) depicted in Figure 1.9.

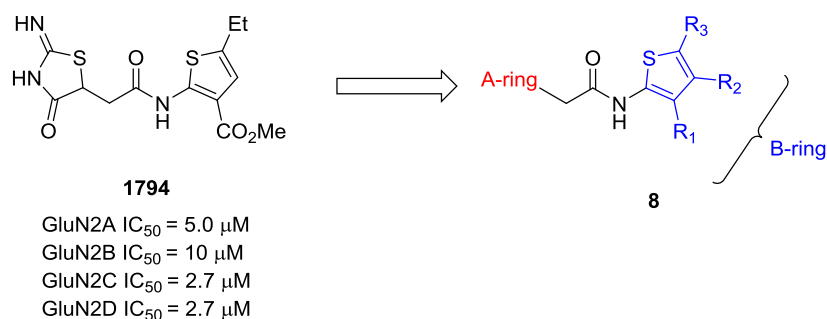
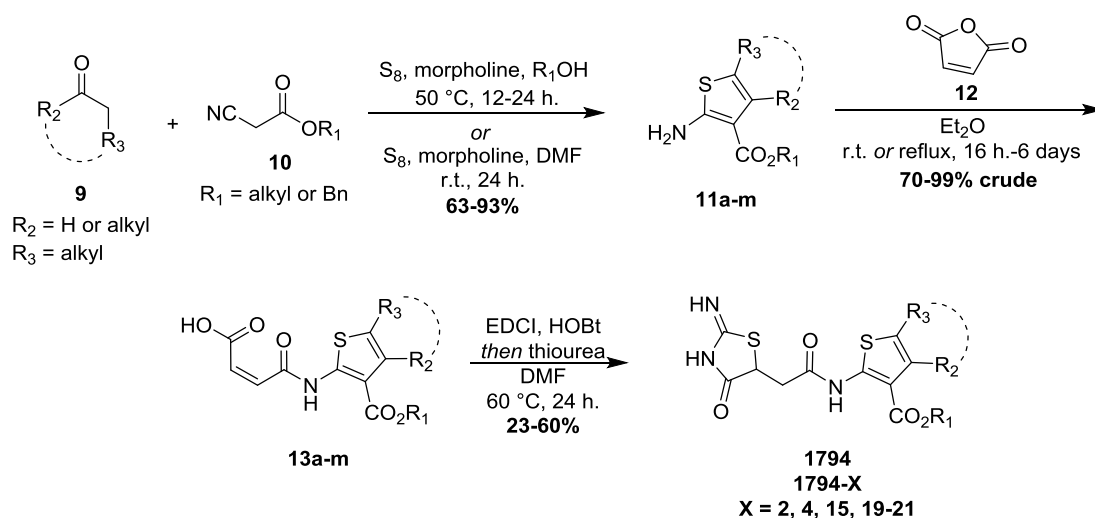


Figure 1.9 Generic Structure Illustrating the Planned Modifications to the Screening Hit (**1794**).

1.3 Synthesis of 1794 Series Analogues

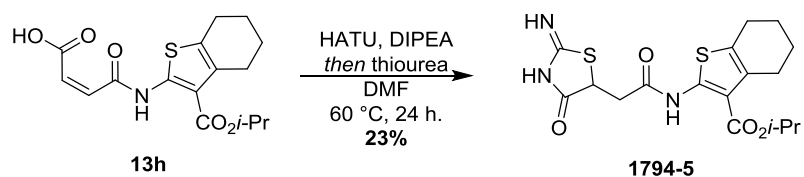
A family of iminothiazolidinones was initially generated according to a three-step sequence (Scheme 1.1).⁵⁸ Within this route, particular attention was paid to the thiophene ring due to the ease at which changes could be made. The first step of the synthesis employed a Gewald reaction. Briefly, in the presence of elemental sulfur under basic conditions, commercially

available cyanoacetates (**10**) reacted with readily available aldehydes or ketones (**9**) providing substituted aminothiophenes (**11a-m**) in generally high yields.⁵⁸ Subsequent ring opening of maleic anhydride (**12**) with compounds **11a-m** afforded maleamic acids (**13a-m**).⁵⁹ Finally, the crude acids underwent EDCI and HOBt coupling with thiourea, followed by conjugate addition and cyclization to provide the target iminothiazolidinones (**1794-X**, **X = 2, 4, 15, 19-21**) in low to modest yields.⁵⁹



Scheme 1.1 Synthetic Route Toward 1794 Analogues.

The poor yields observed in the final transformation were attributed to side reactions that occurred in the amide bond forming step. As such, we looked toward a different coupling reagent, HATU, due to the high coupling efficiencies and fast reaction rates observed with its use. However, as shown in Scheme 1.2, treatment of compound **13h** with HATU resulted in a low yield of **1794-5**, similar to the previous conditions.

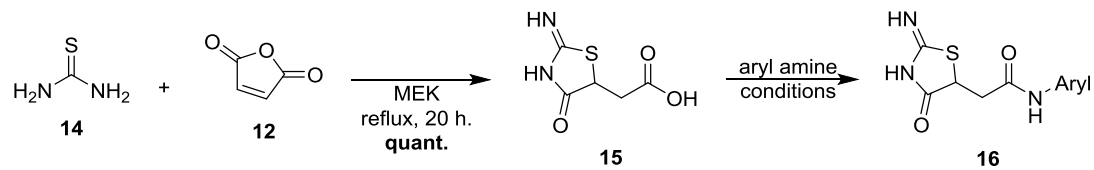


Scheme 1.2 Synthesis of Imidazolidinone **1794-5** with HATU Coupling Reagent.

In an attempt to rapidly gain access to diverse molecules, a convergent synthetic approach was pursued (Scheme 1.3). Reaction of thiourea (**14**) and maleic anhydride (**12**) refluxed in MEK resulted in quantitative formation of carboxylic acid **15**.⁶⁰ Many attempts were made to couple aryl amines with the carboxylic acid *via* standard peptide coupling conditions or acylation with the acid chloride generated from the carboxylic acid. However, low solubility of **15** in organic solvents and the poor nucleophilicity of the amines prohibited product formation. Reactions carried out with various temperatures, solvents, and coupling reagents were unable to generate the desired products.⁶¹ A sample of attempted reaction conditions is illustrated in Table 1.4.

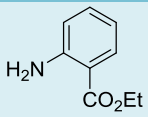
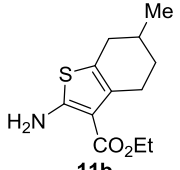
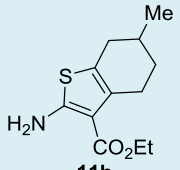
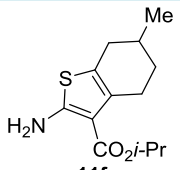
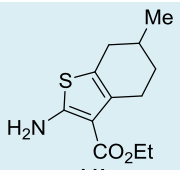
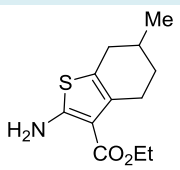
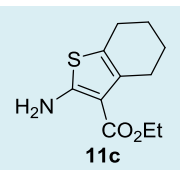
Aniline **17** did not react with the carboxylic acid (**15**) under traditional amidation conditions with EDCI and HOBT. When DMAP was used as an activating agent in place of HOBT, a complex mixture devoid of any desired product was observed. Trace amount of product was detected when acid **15**, EDCI, and aminothiophene **11b** were heated in a DCM and DMF solvent mixture. However, the majority of the reaction mixture contained starting material, and pure product was never isolated. In order to solubilize compound **15**, it was refluxed with excess HMDS and catalytic ammonium sulfate to generate the persilylated compound.⁶² When this material was treated with aminothiophene **11f** and EDCI, a complex mixture of starting material and other unidentifiable products was obtained. Treatment with Mukaiyama's reagent for the coupling reaction with **11b** offered no improvement over reactions carried out with EDCI.⁶³ Finally, acylations were attempted with acid chlorides generated from acid **15**.⁶³ Reaction with

the acid chloride in the presence of either pyridine or TEA resulted in recovery of starting material and unidentifiable side products.



Scheme 1.3 Convergent Approach Toward 1794 Series Analogues.

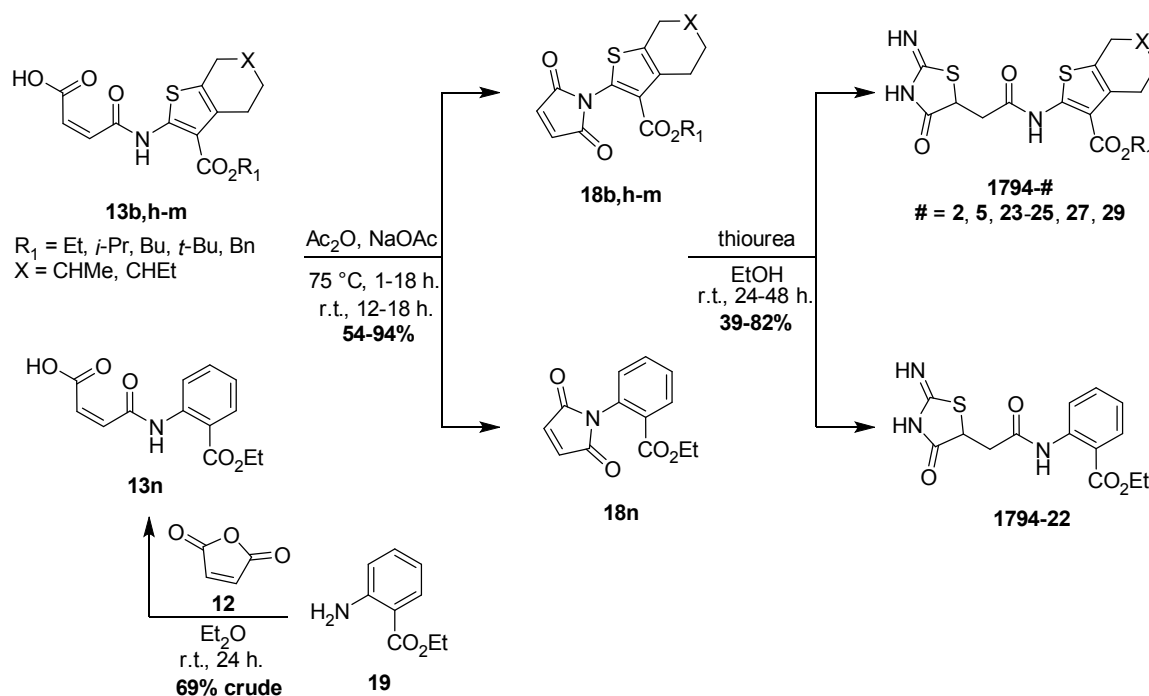
Table 1.4 Sample of Attempted Coupling Conditions.

Aryl Amine	Reagents	Solvent	Temperature	Result
 17	EDCI, HOBT	DMF	r.t. 16 h.	N.R.
 11b	EDCI, DMAP	DMF	0 °C to r.t. 16 h.	decomposition
 11b	EDCI	1 : 1 DCM : DMF	40 °C 16 h.	trace product, S.M.
 11f	HMDS (NH ₄) ₂ SO ₄ (0.1 eq.) <i>then</i> EDCI, DMAP	HMDS <i>then</i> DMF	reflux 1 h. <i>then</i> 0 °C to r.t. 3 days	S.M., complex mixture
 11b	Mukaiyama's reagent (2-chloro-1- methylpyridinium iodide), TEA	DCM	r.t. 16 h.	N.R.
 11b	(COCl) ₂ (6 eq.) DMF (0.01 eq.) <i>then</i> 11b pyridine (3 eq.)	DCM	r.t. 30 min. <i>then</i> r.t. 16 h.	S.M., complex mixture
 11c	(COCl) ₂ (6 eq.) DMF (0.01 eq.) <i>then</i> 11c TEA (3 eq.)	DCM	r.t. 30 min. <i>then</i> 0 °C to r.t. 16 h.	S.M., complex mixture

N.R. = no reaction, S.M. = starting material

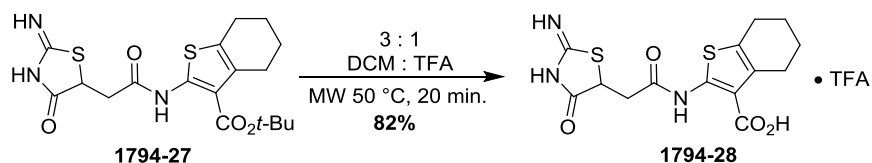
On account of the difficulty faced when preparing the target iminothiazolidinones with conventional coupling agents, a final route was explored (Scheme 1.4).⁶⁴ In this approach, maleamic acids **13b,h-n** were converted to the corresponding maleimides **18b,h-n** through an

intramolecular cyclization onto the mixed anhydride generated *in situ*.⁶⁴ Finally, thia-Michael addition of thiourea to the aryl maleimides and subsequent cyclization generated the desired target compounds (**1794-#**, # = **2, 5, 22-25, 27, 29**) in appreciable yields.



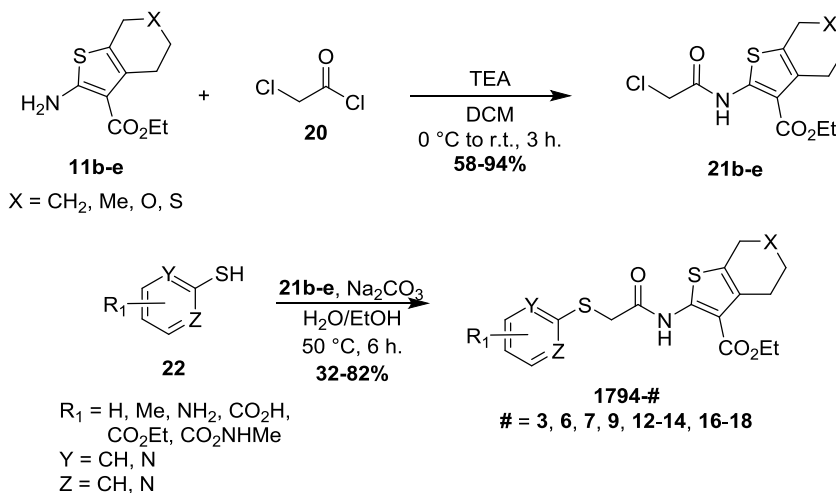
Scheme 1.4 Synthesis of Iminothiazolidinones from Aryl Maleimides.

Synthesis of a **1794** compound with a carboxylic acid moiety in place of the ester on the thiophene ring was prepared as illustrated in Scheme 1.5. Initial attempts at base catalyzed hydrolysis (data not shown) suffered from low conversion due to poor compound solubility and cleavage primarily at the amide functionality. Additionally, hydrogenolysis with palladium on activated carbon under an atmosphere of hydrogen was also unsuccessful when attempted with a compound containing a benzyl ester (compound not shown). When *t*-butyl ester **1794-27** was subjected to microwave irradiation at 50 °C in the presence of acid, the desired carboxylic acid-containing compound (**1794-28**) could be isolated as the TFA salt.



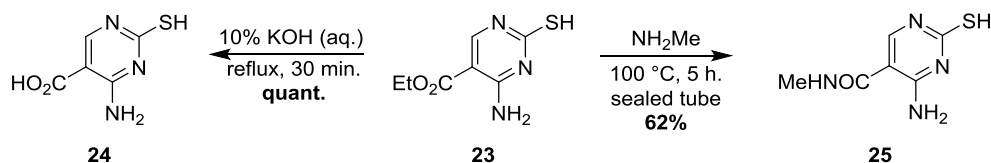
Scheme 1.5 Microwave-assisted Hydrolysis of *t*-Butyl Ester.

Synthesis of 1794 analogues with various replacements for the iminothiazolidinone ring was carried out as illustrated in Scheme 1.6.⁶⁵ Treatment of aminothiophenes (**11b-e**) (synthesized according to Scheme 1.1) with chloroacetyl chloride provided α -chloroamides (**21b-e**) in good yields. The chloride was then displaced in a substitution reaction with an appropriately substituted aryl thiol (**22**) to afford amides with a thioether (**1794-#**, # = 3, 6, 7, 9, 12-14, 16-18) linkage.



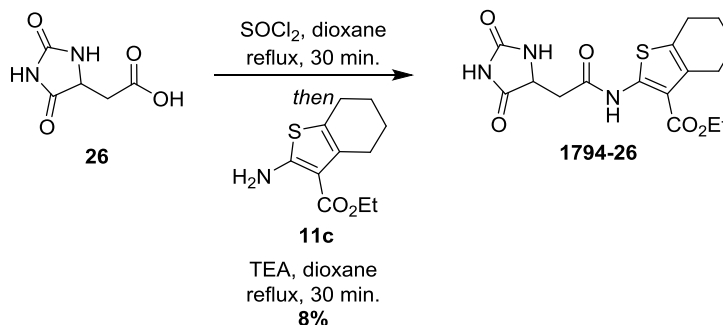
Scheme 1.6 Synthesis of Analogues with Varied A-rings.

For aryl thiols that were not commercially available, the one step synthesis was performed as depicted in Scheme 1.7.⁶⁶ The commercially available ethyl-mercaptopyrimidine carboxylate (**23**) was refluxed with 10% KOH or heated with methylamine in a sealed tube to give the carboxylic acid (**24**) and methylamide (**25**) derivatives, respectively.



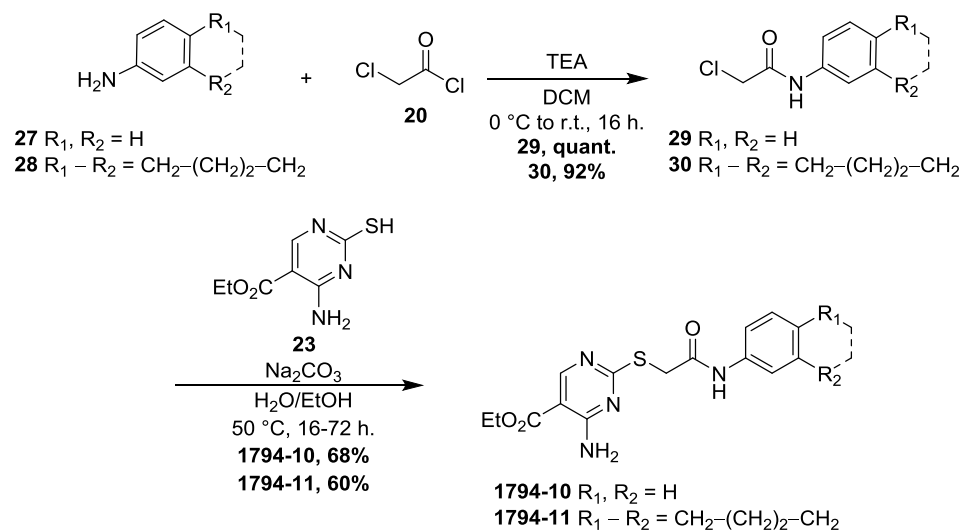
Scheme 1.7 Synthesis of Aryl Thiols.

Synthesis of a compound with a subtle replacement of the iminothiazolidinone ring was carried out as shown in Scheme 1.8. Imidazolidinedione **1794-26** was synthesized through an acylation of aminothiophene **11c** with the acid chloride generated from the treatment of a commercially available carboxylic acid (**26**) with thionyl chloride. Similar to the results observed for the attempted reactions highlighted in Scheme 1.3 and Table 1.4, it was presumed that low compound solubility was responsible for the poor yield of **1794-26**.



Scheme 1.8 Synthesis of Imidazolidinedione **1794-26**.

Two additional compounds were synthesized in which both the A-ring and the B-ring were replaced with bioisosteres (Scheme 1.9).⁶⁵ Acylation of aniline **27** and tetrahydronaphthalen-2-amine **28** with chloroacetyl chloride gave the corresponding α -chloroamides (**29** and **30**, respectively) in high yields. Finally, chloride displacement with ethyl-mercaptopyrimidine carboxylate (**23**) provided the desired compounds (**1794-10** and **1794-11**) for biological testing.



Scheme 1.9 Synthesis of Compounds with Both A-ring and B-ring Replacements.

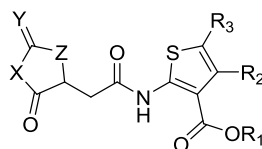
1.4 Results and Discussion

1.4.1 Structure Activity Relationships of 1794 Series

Upon discovery of the original screening hit (**1794**), the Traynelis laboratory ordered a small library of structurally related compounds in addition to the compounds synthesized according to the routes described in the previous section. Our initial efforts were directed toward identifying critical contact points in the A-ring (Table 1.5). Consequently, we noted that none of the changes were well-tolerated. Specifically, replacement of the imine in **1794** with a carbonyl group in **1972** and **1974** abolished activity at all receptor subtypes. Similar results were observed for **2098** where both nitrogen atoms were alkylated. In addition, replacement of the iminothiazolidinone moiety of **1794** with the imidazolidinedione ring of compound **1794-26** abrogated NMDA activity at GluN2A- and GluN2B-containing receptors, while GluN2C- and GluN2D-containing receptors retained modest activity ($IC_{50} = 17 \mu M$ and $37 \mu M$, respectively). Two additional compounds where the entire A-ring was replaced with another heterocycle also

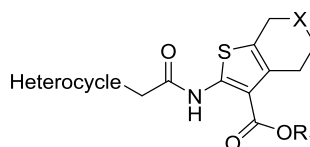
resulted in a complete loss of activity (Table 1.6). Taken together, the data suggest that the presence and position of the hydrogen bond donating atoms are important for activity.

An interesting observation was made regarding the extent of inhibition that resulted from application of **1794-26**. At the highest concentration of drug tested (100 μ M), only 40% inhibition was observed for GluN2C-containing receptors, while 77% inhibition was noted for GluN2D-containing receptors. Initially, we suspected that at high concentrations of **1794-26**, a significant portion of the molecule precipitated out of solution, thus accounting for the submaximal inhibition. However, if compound solubility were the only parameter responsible for the incomplete inhibition, we would not have expected to see differences in the percent maximal inhibition across the various receptor subtypes tested. Solubility measurements were taken for a select compound to rule out this possibility. Nonetheless, the results obtained for **1794-26** and others described in the following sections were intriguing from a therapeutic standpoint on account of their partial inhibition. Given the adverse side effects commonly associated with full receptor inhibition, we were hopeful that certain compounds from this series could circumvent these issues through submaximal inhibition.

Table 1.5 Effect of A-ring Substitutions on the Potency of 1794 Analogues.

Compound ID	X	Y	Z	R ₁	R ₂	R ₃	IC ₅₀ (μM) ^a (% maximal inhibition) [‡]			
							GluN2A	GluN2B	GluN2C	GluN2D
1794	NH	NH	S	Me	H	Et	5.0 (100)	10 (100)	2.7 (100)	2.7 (100)
1972	NH	O	S	Et	CH ₂ -CH ₂ -CH ₂		--	--	--	--
1974	NH	O	S	Et	CH ₂ -(CH ₂) ₂ -CH ₂		--	--	--	--
2098	NMe	NMe	S	Et	CH ₂ -(CH ₂) ₂ -CH ₂		--	--	--	--
1794-26	NH	O	NH	Et	CH ₂ -(CH ₂) ₂ -CH ₂		--	--	17 (40)	37 (77)

^aIC₅₀ values were obtained by fitting the Hill equation to the average composite concentration-effect curves (see Biology Experimental Detail). Data are from 3-13 oocytes between 1-2 frogs. Compounds producing less than 25% inhibition at 30 μM were considered to have no effect (--). [‡]Values in parentheses represent the percentage of inhibition at the maximal concentration of drug tested.

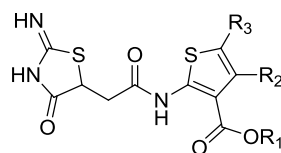
Table 1.6 Effect of A-ring Replacement on the Potency of 1794 Analogues.

Compound ID	A-ring	X	R ₁	IC ₅₀ (μM) (% maximal inhibition)			
				GluN2A	GluN2B	GluN2C	GluN2D
2099		CH ₂	Me	--	--	--	--
2126		CHMe	Et	--	--	--	--

To further expand the SAR, we also investigated alkyl substitutions at three positions on the thiophene ring (Table 1.7). Replacement of the methyl ester of **1794** with an ethyl ester in compound **1969** retained potency. However, exchange of the ethyl group for a methyl group at

the position proximal to the sulfur atom in the thiophene ring in analog **2127** resulted in >4-fold decrease in potency. This compound also exhibited a slight preference for GluN2C- and GluN2D-containing receptors over receptors comprised of GluN2A or GluN2B. Addition of alkyl substituents at the R₂ position of the thiophene ring in compounds **2124**, **1973**, and **2125** all resulted in diminished biological activity. However, **1973** offered a slight increase in subunit-selectivity for GluN2D over GluN2A. The replacement of alkyl substituents with hydrogen atoms at both the R₂ and R₃ positions drastically reduced activity. While no improvements in potency were observed for these compounds, the data indicated that one or more alkyl substituents on the thiophene ring are necessary for activity, potentially by burying the compound into a hydrophobic binding pocket.

Table 1.7 Effect of Alkyl Substitutions to the Thiophene Ring on the Potency of 1794 Analogues.



Compound ID	R ₁	R ₂	R ₃	IC ₅₀ (μM) ^a (% maximal inhibition) [‡]			
				GluN2A	GluN2B	GluN2C	GluN2D
1794	Me	H	Et	5.0 (100)	10 (100)	2.7 (100)	2.7 (100)
1969	Et	H	Et	6.3 (97)	9.9 (96)	3.9 (98)	2.6 (94)
2127	Et	H	Me	35 (83)	41 (88)	11 (99)	13 (100)
2124	Me	Me	Me	21 (83)	24 (63)	9.6 (88)	10 (94)
1973	Et	Me	Me	58 (100)	--	9.8 (79)	11 (78)
2125	Me	Et	Me	26 (78)	44 (77)	6.7 (85)	9.1 (82)
1971	Me	H	H	--	--	43 (100)	44 (100)

^aIC₅₀ values were obtained by fitting the Hill equation to the average composite concentration-effect curves (see Biology Experimental Detail). Data are from 8-13 oocytes between 2 frogs. Compounds producing less than 25% inhibition at 30 μM were considered to have no effect (--). [‡]Values in parentheses represent the percentage of inhibition at the maximal concentration of drug tested. Data for **1794** is presented in Table 1.5 and repeated here to facilitate comparisons.

The preference for lipophilic functionality on the thiophene ring was further demonstrated through the improved potency observed with several of the compounds summarized in Table 1.8.

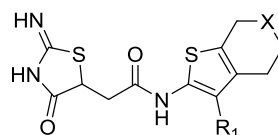
Specifically, we evaluated compounds containing a bicyclic thiophene as a replacement for the thiophene ring with short alkyl appendages present in compounds like **1794**. We also hypothesized that by increasing the hydrophobic character of these compounds, we would also reduce the total polar surface area toward a more drug-like value common to CNS drugs. Gratifyingly, introduction of the tetrahydrobenzothiophene moiety provided several potent NMDA inhibitors.

Comparison of both **2100** and **1794-4** showed that moving from the methyl ester to the ethyl ester, respectively, did not significantly affect potency, but resulted in a slight increase in GluN2D selectivity over GluN2A. Furthermore, when compared to the original screening hit (**1794**, Table 1.5), the analogues with the fused cyclohexyl ring pleasingly demonstrated either a 2-fold increase (**2100**) or a 5-fold increase (**1794-4**) in potency at GluN2D and surprisingly exhibited varying degrees of submaximal inhibition at all receptor combinations tested. The importance of the ester moiety was made apparent by the complete loss of activity observed with carboxylic acid **1794-28** and nitrile **1967**. This result further supported our hypothesis that this portion of the molecule is buried in a hydrophobic region of the receptor.

A number of compounds were designed to further our understanding of the chemical space surrounding the analogues so that we might be able to take advantage of additional binding interactions and improve potency, selectivity, or both. Various substitutions were made exclusively at the 6-position of the tetrahydrobenzothiophene ring system so as to avoid regioisomers that could form in the condensation reaction toward the aminothiophene building blocks (Scheme 1.1). Introduction of a single methyl unit onto the cyclohexyl ring (**1749-2**) resulted in activity comparable to its unsubstituted counterpart (**1794-4**). However, the vast difference in activity between the methyl ester analogue (**1968**) and the ethyl ester in **1794-2** (most apparent in 55-fold difference at GluN2A) was significantly greater than that which was noted with the same ester combinations for the unsubstituted analogues (**2100** and **1794-4**). An increase in steric bulk at the position denoted X (compounds **1794-24**, **1970**, and **1794-20**)

trended toward decreased inhibitor potency. This indicated that the antagonist binding site is of finite size and able to accommodate ligands up to a specific molecular volume. While the gem-difluoro isostere (**1794-23**) was well tolerated, it possessed lower potency at GluN2D ($IC_{50} = 2.1 \mu\text{M}$) than **1794-4** and **1794-2** ($IC_{50} = 0.5 \mu\text{M}$). Likewise, the incorporation of heteroatoms ($X = \text{S}$ or O) was also tolerated and resulted in a submicromolar inhibitor (**1794-15**, $X = \text{S}$) with greater selectivity for GluN2D-containing receptors over GluN2A (7-fold selectivity).

Table 1.8 Effect of Substituted Tetrahydrobenzothiophenes on the Potency of 1794 Analogues.

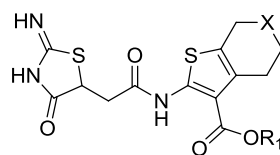


Compound ID	R_1	X	$IC_{50} (\mu\text{M})^a$ (% maximal inhibition) [‡]			
			GluN2A	GluN2B	GluN2C	GluN2D
2100	CO ₂ Me	CH ₂	2.6 (65)	4.9 (86)	1.1 (90)	1.2 (87)
1794-4	CO ₂ Et	CH ₂	2.5 (66)	--	1.0 (50)	0.5 (58)
1794-28	CO ₂ H	CH ₂	--	--	--	--
1967	CN	CH ₂	--	--	--	--
1968	CO ₂ Me	CHMe	55 (100)	52 (100)	12 (89)	14 (90)
1794-2	CO ₂ Et	CHMe	1.0 (85)	3.0 (82)	0.7 (79)	0.5 (70)
1794-24	CO ₂ Et	CHEt	--	15 (67)	23 (100)	15 (93)
1970	CO ₂ Me	<i>Ct</i> -Bu	--	--	--	--
1794-20	CO ₂ Et	CMe ₂	25 (66)	43 (62)	3.5 (75)	7.4 (85)
1794-23	CO ₂ Et	CF ₂	6.3 (77)	12 (80)	2.4 (81)	2.1 (77)
1794-15	CO ₂ Et	S	6.3 (82)	11 (73)	0.9 (88)	0.9 (84)
1794-21	CO ₂ Et	O	3.7 (74)	6.4 (71)	5.5 (74)	3.4 (43)

^a IC_{50} values were obtained by fitting the Hill equation to the average composite concentration-effect curves (see Biology Experimental Detail). Data are from 4-17 oocytes between 1-4 frogs. Compounds producing less than 25% inhibition at 30 μM were considered to have no effect (--). [‡]Values in parentheses represent the percentage of inhibition at the maximal concentration of drug tested.

Although it was apparent from the bicyclic analogues that an alkyl ester is critical for activity, only methyl esters and ethyl esters had been tested. A number of esters with varied chain length and branching were incorporated into compounds that included either the unsubstituted or methyl-substituted tetrahydrobenzothiophene moiety (Table 1.9). Interestingly, replacement of

the ethyl ester of **1794-4** with an isopropyl ester resulted in a compound (**1794-5**) that selectively potentiated GluN2C- and GluN2D-containing NMDA receptors with EC_{50} measurements in the low micromolar range. In contrast, when this same change was made for the methyl-substituted tetrahydrobenzothiophene, compound **1794-19** produced receptor inhibition on par with what was observed for the corresponding ethyl ester analogue (**1794-2**). The data suggested that these compounds could share the same binding site and slight perturbations to their chemical structures promote a switch from receptor inhibition to receptor potentiation. The addition of steric bulk to the alkyl group as in *t*-butyl ester **1794-27** resulted in substantial potentiation with EC_{50} measurements just above 2 μ M for all receptor subtypes, except for GluN2A-containing receptors where submaximal inhibition was observed with an $IC_{50} = 10 \mu$ M. With increasing chain length and volume, receptor potentiation was still observed, however butyl ester **1794-29** and benzyl ester **1794-25** were considerably less potent ($EC_{50} = 87 \mu$ M and 79 μ M, respectively at GluN2D). It seemed that there was an inverse relationship between the ester size and potency. Likewise, the trend indicated that there is some space, while limited, within the binding pocket where these alkyl chains interact with the protein.

Table 1.9 Effect of Varied Ester Substitutions on the Potency and Mode of Receptor Modulation.

Compound ID	R ₁	X	IC ₅₀ (μM) ^a (% maximal inhibition) [‡]			
			GluN2A	GluN2B	GluN2C	GluN2D
1794-4	Et	CH ₂	2.5 (66)	--	1.0 (50)	0.5 (58)
1794-2	Et	CHMe	1.0 (85)	3.0 (82)	0.7 (79)	0.5 (70)
1794-5*	<i>i</i> -Pr	CH ₂	--	--	3.7 (141)	9.2 (158)
1794-19	<i>i</i> -Pr	CHMe	3.2 (68)	1.8 (57)	0.7 (60)	0.9 (61)
1794-27*	<i>t</i> -Bu	CH ₂	10 (47)	2.1 (139)	2.5 (240)	2.7 (248)
1794-29*	Bu	CH ₂	70 (66)	65 (194)	61 (162)	87 (239)
1794-25*	Bn	CH ₂	41 (140)	34 (362)	79 (516)	79 (648)

^aIC₅₀ values were obtained by fitting the Hill equation to the average composite concentration-effect curves (see Biology Experimental Detail). Data are from 3-18 oocytes between 1-4 frogs. Compounds producing less than 25% inhibition at 30 μM were considered to have no effect (--). [‡]Values in parentheses represent the percentage of inhibition at the maximal concentration of drug tested. *Compounds with percentages (value in parentheses) greater than 100 potentiated the receptor above the initial glutamate and glycine response. These compounds were fit to the corresponding EC₅₀ values. Data for **1794-4** and **1794-2** is presented in Table 1.7 and repeated here to facilitate comparisons.

Comparison of the new lead compound, **1794-2**, and another screening hit (**1649**), highlighted structural similarities between the two compounds (Figure 1.10). Interestingly, **1794-2** displayed desirable potency with poor selectivity, while **1649** selectively inhibited GluN2C- and GluN2D-containing receptors with modest potency. We hypothesized that a hybrid molecule with a combination of features from both of these compounds may show a synergistic effect (Figure 1.9). However to our surprise, initial biological experiments revealed that **1794-3** selectively inhibited GluN2A-containing receptors with modest potency and **1794-22** selectively inhibited NMDA receptors comprised of GluN2C or GluN2D with diminished potency (IC₅₀ = 36 μM and 49 μM, respectively). On account of this unexpected result, we pursued additional compounds with similar biological activity. As illustrated in Table 1.10, unfortunately only one compound (**1794-14**) demonstrated appreciable activity. Similarly, when the B-ring thiophene was replaced with bioisosteres and the ethyl-mercaptopyrimidine carboxylate moiety was held constant at the

B-ring (Table 1.11), inhibitory activity was not observed, with the exception of **1794-11** only with GluN2B-containing receptors ($IC_{50} = 27 \mu\text{M}$).

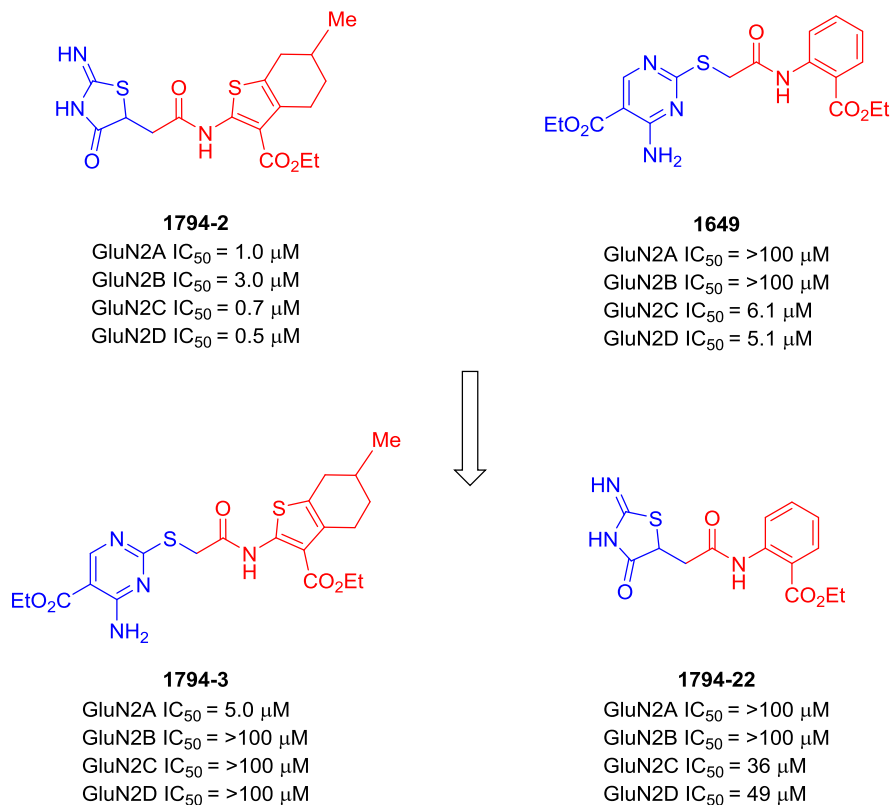
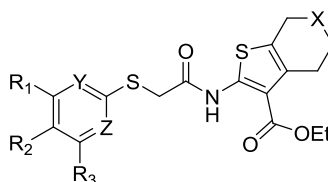
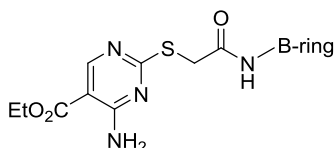


Figure 1.10 Rationale for Hybrid Analogues.

Table 1.10 Effect of Aryl Thiol Replacements on the Potency of Hybrid Analogues.

Compound ID	X	Y	Z	R ₁	R ₂	R ₃	IC ₅₀ (μM) ^a (% maximal inhibition) [‡]			
							GluN2A	GluN2B	GluN2C	GluN2D
1794-3	CHMe	N	N	NH ₂	CO ₂ Et	H	5.0 (72)	--	--	--
1794-16	S	N	N	NH ₂	CO ₂ Et	H	--	--	--	--
1794-17	O	N	N	NH ₂	CO ₂ Et	H	--	--	--	--
1794-18	CHMe	N	N	NH ₂	CO ₂ NHMe	H	--	--	--	--
1794-14	CHMe	N	N	NH ₂	CO ₂ H	H	18 (82)	10 (95)	3.4 (97)	3.1 (95)
1794-9	CHMe	N	N	NH ₂	H	H	--	--	--	--
1794-7	CH ₂	N	N	Me	H	Me	--	--	--	--
1794-6	CH ₂	N	N	H	H	H	--	--	--	--
1794-13	CHMe	N	CH	H	H	H	--	--	--	--
1794-12	CHMe	CH	CH	H	H	H	--	--	--	--

^aIC₅₀ values were obtained by fitting the Hill equation to the average composite concentration-effect curves (see Biology Experimental Detail). Data are from 4-16 oocytes between 1-3 frogs. Compounds producing less than 25% inhibition at 30 μM were considered to have no effect (--). [‡]Values in parentheses represent the percentage of inhibition at the maximal concentration of drug tested.

Table 1.11 Effect of B-ring Bioisosteric Replacements on the Potency of Hybrid Analogues.

Compound ID	B-ring	IC ₅₀ (μM) ^a (% maximal inhibition) [‡]			
		GluN2A	GluN2B	GluN2C	GluN2D
1794-10		--	--	--	--
1794-11		--	27 (54)	--	--

^aIC₅₀ values were obtained by fitting the Hill equation to the average composite concentration-effect curves (see Biology Experimental Detail). Data are from 6-10 oocytes between 2 frogs. Compounds producing less than 25% inhibition at 30 μM were considered to have no effect (--). [‡]Values in parentheses represent the percentage of inhibition at the maximal concentration of drug tested.

1.4.2 In Vitro Analysis of 1794 Series Mechanism of Action

Since several compounds in this class presented with submaximal inhibition, we sought to examine the specific interactions of a selected compound and NMDA receptors that gave rise to the observed pharmacological effects. The actions of **1794-2** against current responses from recombinant NMDA receptors expressed in *Xenopus laevis* oocytes were evaluated (Figure 1.11) to determine its potency and selectivity across the NMDA receptor subtypes. When co-applied in solutions containing maximally effective concentrations of glutamate and glycine, **1794-2** inhibited recombinant NMDA receptors containing the GluN1/GluN2C and GluN1/GluN2D subunits up to 80% with IC_{50} values that were two-fold lower than that for inhibition of GluN1/GluN2A.

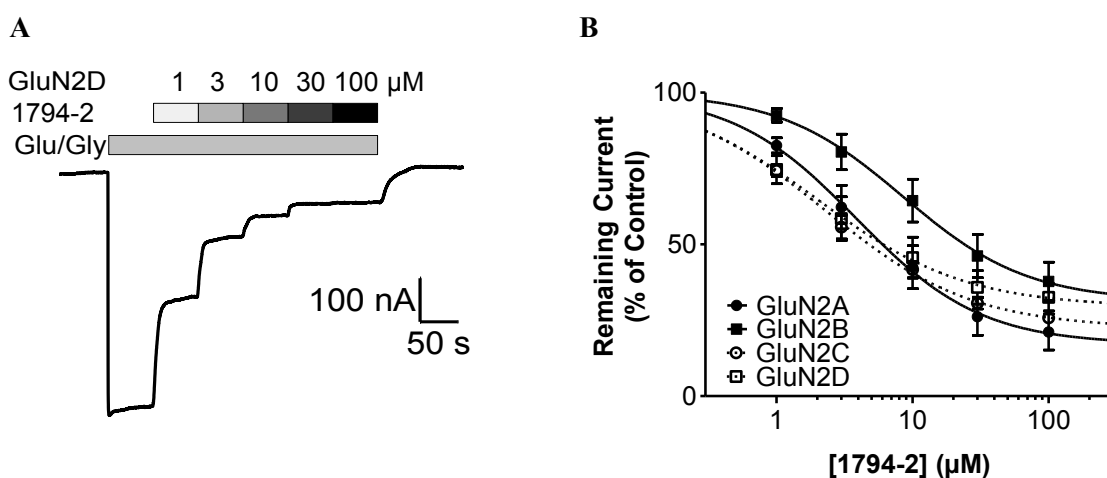


Figure 1.11 Inhibition and Subunit-Selectivity of **1794-2**. **A**) Representative trace of a two-electrode voltage clamp recording from *Xenopus laevis* oocyte expressing GluN1/GluN2D NMDA receptors in response to saturating glutamate and glycine (100 μM and 30 μM, respectively) in the absence and presence of increasing concentrations of **1794-2**. **B**) Summary of the concentration-dependent effect of **1794-2** on maximally activated GluN2 diheteromeric receptors. The IC_{50} values were determined to be 1.0, 3.0, 0.7, and 0.5 μM for diheteromeric receptors containing GluN2A-D, respectively. Maximum extent of inhibition was determined to be 85, 82, 79, and 70%.

To begin to determine the mechanism of **1794-2** inhibition, we evaluated whether the actions of the compound were dependent on the agonist concentration for GluN1/GluN2D receptor

responses recorded in *Xenopus* oocytes. We attempted to out compete **1794-2** by applying an excessively saturating dose of glutamate (1000 μM) or glycine (2000 μM). Submaximal inhibition of GluN1/GluN2D receptor responses by 5 μM **1794-2** could not be surmounted by significant increases in either glutamate or glycine concentration, which suggested that the compound acts by a noncompetitive mechanism (Figure 1.12).

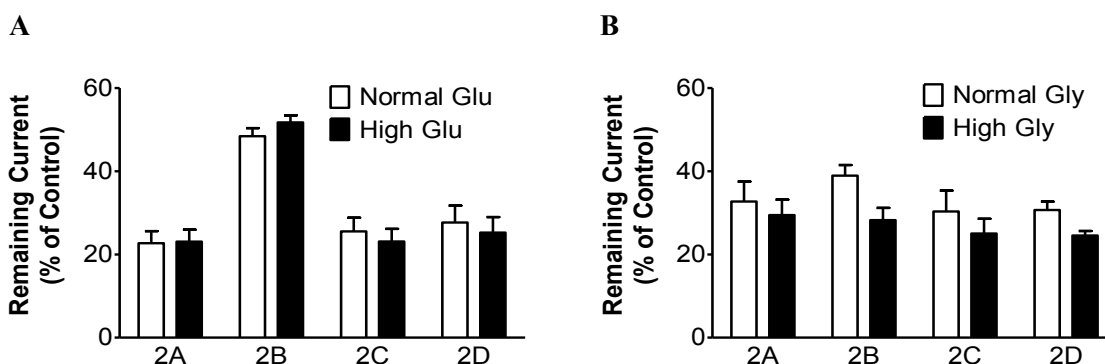


Figure 1.12 Noncompetitive Inhibition of Recombinant GluN1/GluN2D Receptor by **1794-2**. Graph depicting the mean inhibition, by 5 μM **1794-2**, of NMDA receptor currents in both saturating concentrations of glutamate and glycine (100 μM and 30 μM , respectively) and super-saturating concentrations of either **A**) glutamate (1000 μM) or **B**) glycine (2000 μM).

In order to determine whether **1794-2** inhibition had any voltage dependence, we evaluated the receptor inhibition at various membrane potentials. Two electrode voltage clamp recordings were performed with 3 μM **1794-2** at different membrane potentials between -60 and +60 mV and in the absence of Mg^{2+} . The degree of inhibition produced by **1794-2** was the same at all voltages tested. In addition, as illustrated in Figure 1.13, the mean reversal potential (V_{REV}) was not significantly different between control response to glutamate and glycine and the response to glutamate and glycine plus 3 μM **1794-2**. Based on the aforementioned data, we concluded that **1794-2** neither inhibits receptor function by competing with glutamate or glycine at the agonist

binding domain, nor elicits its inhibitory effects through an interaction with the channel pore in a manner that is influenced by the transmembrane electric field.

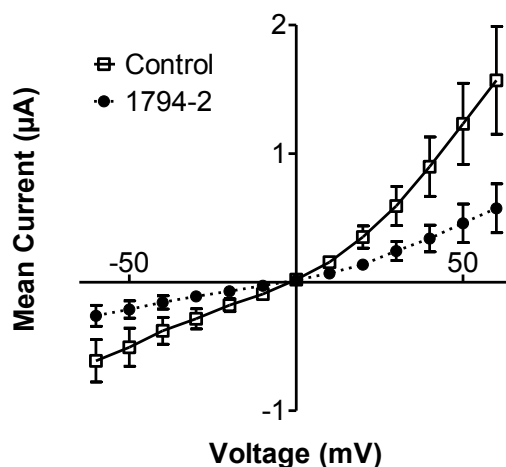


Figure 1.13 Voltage-Independent Mechanism of GluN1/GluN2C Receptor Inhibition by **1794-2**. Mean current-voltage relationship of maximally activated GluN1/GluN2C receptors in the absence of extracellular Mg^{2+} and in the absence and presence of $3 \mu M$ **1794-2**.

1.4.3 *In Vitro* Analysis of 1794 Series in Primary Cultured Neurons

To examine if this compound class could modulate native NMDA receptors, we performed a primary culture of p6-8 rat cerebellar granule cells and performed patch clamp recordings (Figure 1.14 A). Granule cells were first activated with $100 \mu M$ NMDA and $30 \mu M$ glycine and then inhibited with varying concentrations of **1794-2**. The inhibitory responses of the differing concentrations of **1794-2** were fit to a concentration-response curve (Figure 1.14 B). The IC_{50} of **1794-2** in this preparation was similar to the IC_{50} of the compound for GluN2B-containing diheteromeric receptors as expressed in *Xenopus* oocytes. This result which aligned with the expected expression pattern of GluN2 subunits in the cerebellar granule cells cultured in this manner.

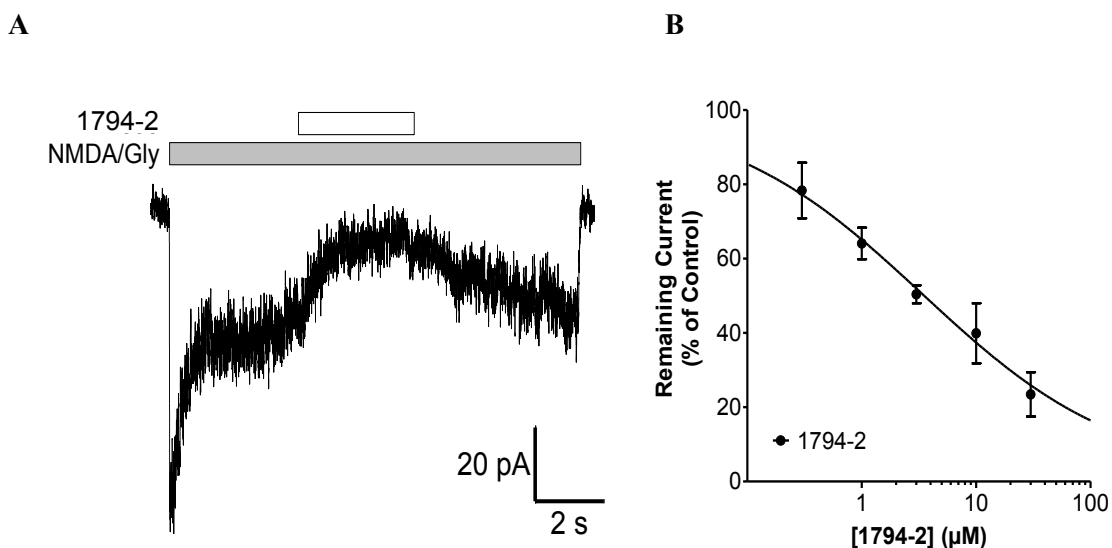


Figure 1.14 Negative Allosteric Modulation of NMDA Receptors Expressed on Cultured Primary granule Cells from Rat Cerebellum by **1794-2**. **A**) Representative trace of from patch clamp recording of a primary cerebellar granule cell culture illustrating the inhibition elicited by 30 μM **1794-2** on NMDA activated currents (100 μM NMDA and 50 μM glycine). **B**) Concentration-effect relationship of **1794-2** on NMDA-induced currents in primary cerebellar granule cell cultures with an $\text{IC}_{50} = 3.4 \mu\text{M}$.

1.4.4 *In Vitro* Analysis of 1794 Series in Neuroprotection Model

We also investigated the potential neuroprotective effects of this class of inhibitors. Cultured primary hippocampal neurons were challenged with NMDA and glycine. The extent of cell death was measured in the absence and presence of **1794-2**. The relative amount of cell death was estimated by performing a lactate dehydrogenase (LDH) assay on the supernatant of the cells 24 hours after treatment. Treatment with 100 μM NMDA and 30 μM glycine for 1 hour caused an increase in the amount of LDH in the media as compared to control (Figure 1.15). However, this cell death was reduced significantly by the addition of 30 μM **1794-2** to just 1-fold more LDH content than control. For comparison, 10 μM **MK-801**, a potent NMDA channel blocker, was used to show that the increase in LDH caused by the application of NMDA and glycine resulted from NMDA receptor activation.

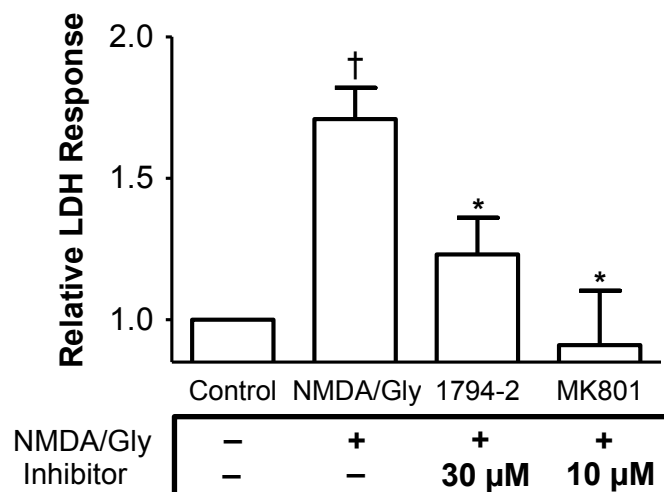


Figure 1.15 Neuroprotection by **1794-2** against NMDA-Induced Excitotoxicity of Cultured Primary Hippocampal Neurons. Attenuation of excitotoxicity of 100 μ M NMDA and 30 μ M glycine by 30 μ M **1794-2** and the open channel blocker, **MK-801** (10 μ M), as measured by relative concentration of LDH released into culture media upon treatment (* p < 0.05 as compared to NMDA/Gly response and † p < 0.05 as compared to control).

1.5 Conclusions

The development of NMDA receptor antagonists, useful for the treatment of a number of neurodegenerative diseases, has been hindered by the presence of untoward side effects as a result of global NMDA receptor antagonism and undesired off-target activity. In the course of this study, we initially sought potent GluN2C- and GluN2D-selective NMDA receptor antagonists that might circumvent the issues with typical NMDA receptor inhibitors.

Beginning with the screening hit **1794**, a novel series of iminothiazolidinone-based compounds were synthesized and evaluated biologically NMDA receptor antagonism. From these data, it was clear that the potency of this series was highly dependent upon the substitution around the aminothiophene ring. Unfortunately, heterocyclic replacements and modifications to the A-ring were not well-tolerated, as the only compounds with appreciable inhibitory effects contained the iminothiazolidinone ring. In contrast, modifications to the B-ring were well-tolerated and even resulted in compounds with increased potency and selectivity. Specifically, introduction of the tetrahydrobenzothiophene ring to compound **1794-4** resulted in

submicromolar inhibition of GluN2C- and GluN2D-containing NMDA receptors. Additionally, heteroatom substitution in the bicyclic ring with S (**1794-15**) and the incorporation of alkyl appendages at the same position (**1794-2**) provided the most selective and potent compounds of the series, respectively. To our surprise, the vast majority of active compounds in this class resulted in submaximal receptor inhibition. The utility of such compounds remains to be seen. Interestingly, a few compounds were also identified in this class that potentiated the NMDA receptor with modest potency upon slight structural changes to the ester moiety of the B-ring.

The mechanism of action was determined for **1794-2**, a typifying member of the inhibitor class. The effectiveness of this compound against native neuronal NMDA receptors and its potential neuroprotective effect was investigated. It was found that **1794-2** is an allosteric antagonist whose inhibitory effects are voltage-independent. The inhibition of NMDA receptors by **1794-2** lead to a reduction in cell death of cultured primary hippocampal neurons, but is hypothesized to allow for a low level of NMDA receptor activity due to the submaximal inhibition observed *in vitro*. We are optimistic that a few of these compounds will be considered for further study as potential neuroprotective agents due to their desirable characteristics of allosteric and submaximal inhibition.

1.6 Chemistry Experimental Detail

1.6.1 Synthetic Chemistry Experimental Detail

All reagents were obtained from commercial suppliers and used without further purification unless specified otherwise. Reaction progress was monitored by thin layer chromatography (TLC) on pre-coated glass plates (silica gel 60 F254, 0.25 mm) or liquid chromatography-mass spectrometry (LC-MS) using an analytical column (Agilent, ZORBAX Eclipse XDB-C18, 4.6 x 50 mm, 3.5 μ m). When noted, flash chromatography was performed on a Teledyne ISCO Combiflash Companion with prepackaged Teledyne Redisep or Silicycle disposable normal phase silica columns. Proton and carbon NMR spectra were recorded on an INOVA-400 (400 MHz),

VNMRS 400 (400 MHz), INOVA-600 (600 MHz), or Unity-600 (600 MHz). All chemical shifts are reported in parts per million and referenced to the residual solvent peak. Mass spectra were performed by the Emory University Mass Spectroscopy Center on either a VG 70-S Nier Johnson or JEOL instrument. The IR spectra were acquired with a Nicolet Avatar 370 DTGS. Final compound purity was established either through high-performance liquid chromatography (HPLC) under the conditions listed or by elemental analysis performed by Atlanta Microlab Inc. where C, H, N agreed with proposed structures within $\pm 0.4\%$ of theoretical values unless indicated otherwise.

General Procedure A: Preparation of aminothiophene compounds in alcohol solvent. To a solution of aldehyde/ketone (1.0 eq.) in alcohol (0.2-0.4 M) was added cyanoacetate (1.1 eq.), elemental sulfur (1.1 eq.), and morpholine (1.4 eq.). The reaction mixture was heated to 50 °C in an oil bath. When TLC or LC-MS indicated complete conversion (12-24 h.), the reaction mixture was concentrated *in vacuo*. The resulting residue was taken up in EtOAc and washed with water (2x) and brine (2x). The organic layer was dried over MgSO₄ and filtered. The solvent was removed *in vacuo*. The resulting product was subjected to flash column chromatography.

General Procedure B: Preparation of aminothiophene compounds in DMF. To a solution of aldehyde/ketone (1.0 eq.) in DMF (1.0 M) was added cyanoacetate (1.1 eq.), elemental sulfur (1.1 eq.), and morpholine (1.4 eq.). The reaction mixture stirred at room temperature for 24 hours and then concentrated *in vacuo*. The resulting residue was taken up in EtOAc and washed with water (3x) and brine (3x). The organic layer was dried over MgSO₄ and filtered. The solvent was removed *in vacuo*. The resulting product was subjected to flash column chromatography.

General Procedure C: Preparation of (Z)-4-oxo-4-(thiophen-2-ylamino)but-2-enoic acid compounds. A solution of the aminothiophene (1.0 eq.) in anhydrous ether was added dropwise to a solution of maleic anhydride (1.0 eq.) in anhydrous ether for a total concentration of 0.1-0.2

M. Reaction was allowed to stir at room temperature or refluxed until complete consumption of starting material was observed by TLC or LC-MS (16 h.-6 days). The resulting precipitate was filtered, washed with ether, and carried on without further purification.

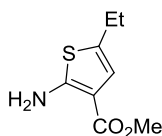
General Procedure D: Preparation of 2-(2-imino-4-oxothiazolidin-5-yl)-N-(thiophen-2-yl)acetamide compounds from (Z)-4-oxo-4-(thiophen-2-ylamino)but-2-enoic acid using EDCI. To a solution of carboxylic acid (1 eq.) in dry DMF (0.15 M) was added HOBt (1.1 eq.) and EDCI (1.5 eq.). The reaction mixture was stirred at room temperature for 1 hour or until all materials were in solution. To the solution was added thiourea (1.1 eq.). The reaction mixture was allowed to stir at room temperature for an additional hour and then heated to 60 °C for 24 hours. The reaction mixture was poured into EtOAc and washed with water (2x) and brine (2x). The organic extracts were combined, dried over anhydrous MgSO₄ and concentrated *in vacuo*. Crude material was dissolved in hot methanol or ethanol and then slowly cooled to room temperature. The resulting precipitate was filtered and washed with cold solvent.

General Procedure E: Preparation of aryl maleimide compounds. A mixture of carboxylic acid (1.0 eq.), acetic anhydride (3.3-7.0 eq.), and sodium acetate (0.2 eq.) was heated to 75 °C in an oil bath. After consumption of starting material, reaction mixture was cooled to room temperature where it stirred for 12-18 hours. The reaction was diluted with water and extracted with DCM (3x). The organic extracts were dried over MgSO₄, filtered, and concentrated. The resulting product was subjected to flash column chromatography.

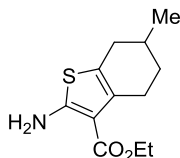
General Procedure F: Preparation of 2-(2-imino-4-oxothiazolidin-5-yl)-N-(thiophen-2-yl)acetamide compounds from aryl maleimides. A mixture of maleimide (1.0 eq.) and thiourea (1.0 eq.) in absolute EtOH (0.1 M) stirred at room temperature for 24-48 hours. Reaction mixture was filtered, and solid material was washed with EtOH and DCM.

General Procedure G: Preparation of 2-chloro-*N*-(thiophen-2-yl)acetamide compounds. A solution of aminothiophene (1.0 eq.) dissolved in dry DCM (0.35 M) was added TEA (1.5 eq.) and brought to 0 °C. To the stirring mixture was added dropwise chloroacetyl chloride (1.1 eq.). The reaction mixture was warmed to room temperature and allowed to stir for 3 hours. The reaction was quenched with 1M HCl (aq.) and extracted with DCM. The organic extracts were washed with brine. Finally, the organic layer was dried over anhydrous MgSO₄, filtered, and concentrated. Crude material was purified by crystallization or flash column chromatography.

General Procedure H: Preparation of 2-(aryltio)-*N*-(thiophen-2-yl)acetamide compounds. A mixture of aryl thiol (1.0 eq.) and 2-chloro-*N*-(thiophen-2-yl)acetamide (1.0 eq.) in 3:1 ratio of water to glacial acetic acid (total concentration 0.1 M) was heated to 50 °C for 6 hours. The reaction mixture was extracted with EtOAc and washed with brine. The organic layer was dried over anhydrous MgSO₄, filtered, and concentrated. The crude solid was purified by flash column chromatography.

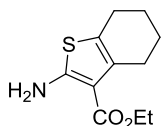


methyl 2-amino-5-ethylthiophene-3-carboxylate (11a). Compound **11a** was prepared according to procedure A using butyraldehyde (1.6 mL, 17.3 mmol) and methyl-2-cyanoacetate (1.7 mL, 19.1 mmol). The crude material was purified by flash column chromatography (ISCO, 80 g silica gel column, 0-11% EtOAc-Hexanes over 25 minutes) to afford the title compound as an off-white solid (1.06 g, 33%). ¹H NMR [400 MHz, CDCl₃] δ 6.23 (s, 1H), 5.76 (br s, 2H), 3.79 (s, 3H), 2.61 (dq, *J* = 1.2, 7.5, 15.0 Hz, 2H), 1.23 (t, *J* = 7.4 Hz, 3H); ¹³C NMR [100 MHz, CDCl₃] δ 165.9, 161.5, 128.7, 120.6, 106.1, 51.0, 23.2, 15.5; HRMS (ESI) [M+H]⁺, calc'd for C₈H₁₂NO₂S 186.05833, found 186.05812.

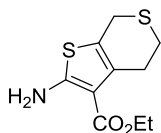


ethyl 2-amino-6-methyl-4,5,6,7-tetrahydrobenzo[b]thiophene-3-carboxylate (11b).

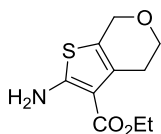
Compound **11b** was prepared according to procedure A using 4-methylcyclohexanone (1.6 mL, 13.4 mmol) and ethyl 2-cyanoacetate (1.6 mL, 14.7 mmol). The crude material was purified by flash column chromatography (ISCO, 120 g silica gel column, 0-10% EtOAc-Hexanes over 25 minutes) to afford the title compound as a white crystalline solid (3.14 g, 98%). ¹H NMR [400 MHz, CDCl₃] δ 5.92 (br s, 2H), 4.26 (q, *J* = 7.0 Hz, 2H), 2.85-2.90 (m, 1H), 2.53-2.63 (m, 2H), 2.11-2.17 (m, 1H), 1.81-1.88 (m, 2H), 1.29-1.37 (m, 4H), 1.05 (d, *J* = 6.4 Hz, 3H); ¹³C NMR [100 MHz, CDCl₃] δ 166.3, 162.0, 132.3, 117.4, 105.8, 59.5, 32.8, 31.3, 29.7, 26.9, 21.7, 14.7; HRMS (ESI) [M+H]⁺, calc'd for C₁₂H₁₈NO₂S 240.10528, found 240.10521.



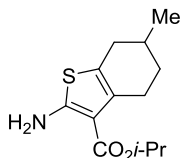
ethyl 2-amino-4,5,6,7-tetrahydrobenzo[b]thiophene-3-carboxylate (11c). Compound **11c** was prepared according to procedure A using cyclohexanone (5.3 mL, 50.9 mmol) and ethyl 2-cyanoacetate (6.0 mL, 56.0 mmol). The crude material was recrystallized from absolute ethanol to afford the title compound as light yellow crystals (10.0 g, 87%). ¹H NMR [400 MHz, CDCl₃] δ 5.96 (br s, 2H), 4.26 (q, *J* = 7.1 Hz, 2H), 2.73-2.69 (m, 2H), 2.52- 2.48 (m, 2H), 1.81-1.71 (m, 4H), 1.34 (t, *J* = 7.2 Hz, 3H); ¹³C NMR [100 MHz, CDCl₃] δ 166.3, 161.9, 132.6, 117.8, 105.9, 59.5, 27.1, 24.7, 23.4, 23.0, 14.7; HRMS (ESI) [M+H]⁺, calc'd for C₁₁H₁₆NO₂S 226.08963, found 226.08966; IR (solid ATR): 3400, 3294, 2982, 2939, 2895, 1644, 1593, 1488, 1271 cm⁻¹.



ethyl 2-amino-4,7-dihydro-5H-thieno[2,3-c]thiopyran-3-carboxylate (11d). Compound **11d** was prepared according to procedure A using tetrahydro-4H-thiopyran-4-one (2.0 g, 17.2 mmol) and ethyl 2-cyanoacetate (2.0 mL, 18.9 mmol). The crude material was purified by column chromatography (ISCO, 80 g silica gel column, 0-18% EtOAc-Hexanes over 20 minutes) to afford the title compound as a white solid (3.69 g, 88%). ^1H NMR [400 MHz, CDCl_3] δ 6.06 (br s, 2H), 4.25 (q, $J = 7.2$ Hz, 2H), 3.56 (s, 2H), 3.00 (t, $J = 5.9$ Hz, 2H), 2.86 (t, $J = 5.8$ Hz, 2H), 1.32 (t, $J = 7.2$ Hz, 3H); ^{13}C NMR [100 MHz, CDCl_3] δ 165.9, 161.3, 132.4, 113.7, 106.0, 59.7, 28.8, 26.2, 25.3, 14.6; HRMS (ESI) $[\text{M}+\text{H}]^+$, calc'd for $\text{C}_{10}\text{H}_{14}\text{NO}_2\text{S}_2$ 244.04605, found 244.04561.

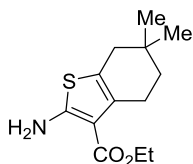


ethyl 2-amino-4,7-dihydro-5H-thieno[2,3-c]pyran-3-carboxylate (11e). Compound **11e** was prepared according to procedure A using tetrahydro-4H-pyran-4-one (2.0 g, 22.0 mmol) and ethyl 2-cyanoacetate (2.6 mL, 24.2 mmol). The crude light brown solid (5.00 g, quant.) was carried on without further purification. ^1H NMR [400 MHz, CDCl_3] δ 6.05 (br s, 2H), 4.55 (t, $J = 2.0$ Hz, 2H), 4.26 (q, $J = 7.1$ Hz, 2H), 3.91 (t, $J = 5.5$ Hz, 2H), 2.82 (tt, $J = 2.0, 5.6$ Hz, 2H), 1.33 (t, $J = 7.2$ Hz, 3H); ^{13}C NMR [100 MHz, CDCl_3] δ 166.0, 162.4, 130.5, 114.9, 105.5, 65.3, 64.8, 59.7, 27.9, 14.6.; HRMS (ESI) $[\text{M}+\text{H}]^+$, calc'd for $\text{C}_{10}\text{H}_{14}\text{NO}_2\text{S}$ 228.06889, found 228.06873.



isopropyl 2-amino-6-methyl-4,5,6,7-tetrahydrobenzo[*b*]thiophene-3-carboxylate (11f).

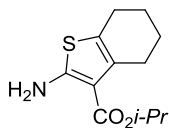
Compound **11f** was prepared according to procedure A using 4-methylcyclohexanone (2.2 mL, 17.8 mmol) and isopropyl 2-cyanoacetate (2.5 mL, 19.6 mmol). The crude material was purified by flash column chromatography (ISCO, 80 g silica gel column, 0-20% EtOAc-Hexanes over 25 minutes) to afford the title compound as an off-white solid (4.42 g, 98%). ¹H NMR [400 MHz, CDCl₃] δ 5.96 (br s, 2H), 5.16 (septet, *J* = 6.3 Hz, 1H), 2.84-2.91 (m, 1H), 2.52-2.65 (m, 2H), 2.10-2.18 (m, 1H), 1.80-1.90 (m, 2H), 1.25-1.35 (m, 1H), 1.32 (d, *J* = 6.4 Hz, 3H), 1.31 (d, *J* = 6.4 Hz, 3H), 1.04 (d, *J* = 6.7 Hz, 3H); ¹³C NMR [100 MHz, CDCl₃] δ 165.9, 161.9, 132.3, 117.4, 106.1, 66.8, 32.9, 31.3, 29.6, 27.0, 22.4, 21.7; HRMS (ESI) [M+H]⁺, calc'd for C₁₃H₂₀NO₂S 254.12093, found 254.12052.



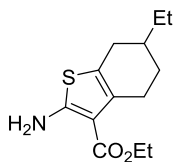
ethyl 2-amino-6,6-dimethyl-4,5,6,7-tetrahydrobenzo[*b*]thiophene-3-carboxylate (11g).

Compound **11g** was prepared according to procedure A using 4,4-dimethylcyclohexanone (2.8 g, 22.0 mmol) and ethyl 2-cyanoacetate (2.6 mL, 24.2 mmol). The crude material was purified by flash column chromatography (ISCO, 80 g silica gel column, 0-20% EtOAc-Hexanes over 14 minutes) to afford the title compound as a white solid (4.48 g, 80%). ¹H NMR [400 MHz, CDCl₃] δ 5.96 (br s, 2H), 4.27 (q, *J* = 7.1 Hz, 2H), 2.71 (tt, *J* = 1.8, 6.7 Hz, 2H), 2.27 (t, *J* = 1.8 Hz, 2H), 1.49 (t, *J* = 6.4 Hz, 2H), 1.35 (t, *J* = 7.0 Hz, 3H), 0.99 (s, 6H); ¹³C NMR [100 MHz, CDCl₃] δ 166.4, 162.0, 131.2, 117.2, 105.7, 59.6, 38.2, 35.6, 30.4, 28.0, 24.8, 14.7; HRMS (ESI) [M+H]⁺, calc'd for C₁₃H₂₀NO₂S 254.12093, found 254.12059; IR (solid ATR): 3405, 3295, 3232, 3162,

2924, 1649, 1591, 1489, 1464, 1440, 1427, 1406, 1368, 1344, 1323, 1278, 1261, 1215, 1171, 1133, 1091, 1036, 973, 908, 880, 840, 776, 733, 637, 619 cm^{-1} .

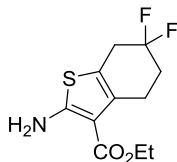


isopropyl 2-amino-4,5,6,7-tetrahydrobenzo[*b*]thiophene-3-carboxylate (11h). Compound **11h** was prepared according to procedure A using cyclohexanone (2.1 mL, 20.4 mmol) and isopropyl 2-cyanoacetate (2.8 mL, 22.4 mmol). The crude material was purified by flash column chromatography (ISCO, 120 g silica gel column, 0-10% EtOAc-Hexanes over 25 minutes) to afford the title compound as a white solid (4.12 g, 84%). ^1H NMR [400 MHz, CDCl_3] δ 6.12 (br s, 2H), 5.16 (septet, $J = 6.2$ Hz, 1H), 2.69-2.71 (m, 2H), 2.46-2.48 (m, 2H), 1.72-1.77 (m, 4H), 1.31 (d, $J = 6.2$ Hz, 6H); ^{13}C NMR [100 MHz, CDCl_3] δ 165.7, 162.0, 132.3, 117.4, 105.6, 66.6, 27.0, 24.5, 23.2, 22.9, 22.1; HRMS (ESI) $[\text{M}+\text{H}]^+$, calc'd for $\text{C}_{12}\text{H}_{18}\text{NO}_2\text{S}$ 240.10528, found 240.10549; Elem. Anal. calc'd for $\text{C}_{12}\text{H}_{17}\text{NO}_2\text{S}$, C, 60.22; H, 7.16; N, 5.85, found C, 60.49; H, 7.26; N, 5.79.



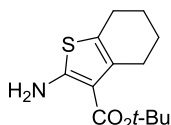
ethyl 2-amino-6-ethyl-4,5,6,7-tetrahydrobenzo[*b*]thiophene-3-carboxylate (11i). Compound **11i** was prepared according to procedure A using 4-ethylcyclohexanone (1.5 g, 11.9 mmol) and ethyl 2-cyanoacetate (1.4 mL, 13.1 mmol). The crude material was purified by flash column chromatography (ISCO, 80 g silica gel, 0-20% EtOAc-Hexanes over 25 minutes) to afford the title compound as an off-white solid (2.79 g, 93%). ^1H NMR [400 MHz, CDCl_3] δ 5.96 (br s, 2H), 4.26 (q, $J = 7.1$ Hz, 2H), 2.92-2.86 (m, 1H), 2.63-2.53 (m, 2H), 2.18-2.10 (m, 1H), 1.91-1.86 (m, 1H), 1.69-1.58 (m, 1H), 1.43-1.31 (m, 3H), 1.34 (t, $J = 7.0$ Hz, 3H), 0.95 (t, 7.5 Hz, 3H); ^{13}C NMR [100 MHz, CDCl_3] δ 166.3, 162.0, 132.6, 117.5, 105.7, 59.5, 36.5, 30.7, 29.1, 28.9, 27.0,

14.6, 11.7; HRMS (ESI) $[M+H]^+$, calc'd for $C_{13}H_{20}NO_2S$ 254.12093, found 254.12052; IR (solid ATR): 3410, 3303, 2963, 2895, 2842, 1646, 1591, 1489, 1409, 1340, 1296, 1267, 1164, 1147, 1026, 780 cm^{-1} .



ethyl 2-amino-6,6-difluoro-4,5,6,7-tetrahydrobenzo[b]thiophene-3-carboxylate (11j).

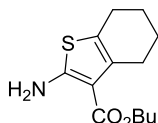
Compound **11j** was prepared according to procedure A using 4,4-difluorocyclohexanone (1.0 g, 7.5 mmol), and ethyl 2-cyanoacetate (0.9 mL, 8.2 mmol). The crude material was purified by flash column chromatography (ISCO, 40 g silica gel column, 0-20% EtOAc-Hexanes over 20 minutes) to afford the title compound as a white solid (1.62 g, 83%). 1H NMR [400 MHz, $CDCl_3$] δ 6.05 (s, 2H), 4.28 (q, $J = 7.1$ Hz, 2H), 3.07-2.94 (m, 4H), 2.23-2.09 (m, 2H), 1.35 (t, $J = 7.1$ Hz, 3H); ^{13}C NMR [100 MHz, $CDCl_3$] δ 165.9, 163.01, 131.3, 123.0 (t, $J_{C-F} = 241.7$ Hz), 111.6 (t, $J_{C-F} = 6.6$ Hz), 105.0, 59.9, 34.3 (t, $J_{C-F} = 28.4$ Hz), 30.8 (t, $J_{C-F} = 24.1$ Hz), 24.6 (t, $J_{C-F} = 5.3$ Hz), 14.6; ^{19}F NMR [400 MHz, $CDCl_3$] δ -97.80 (p, $J = 13.7$ Hz); HRMS (ESI) $[M+H]^+$, calc'd for $C_{11}H_{14}F_2NO_2S$ 262.07078, found 262.07073; IR (solid ATR): 3422, 3307, 1647, 1593, 1489, 1414, 1258 cm^{-1} .



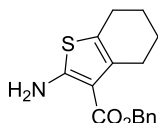
tert-butyl 2-amino-4,5,6,7-tetrahydrobenzo[b]thiophene-3-carboxylate (11k).

Compound **11k** was prepared according to procedure A using cyclohexanone (1.6 mL, 15.3 mmol) and tert-butyl 2-cyanoacetate (2.4 mL, 16.8 mmol) in absolute ethanol (40.0 mL). The crude material was purified by flash column chromatography (ISCO, 80 g silica gel, 0-20% EtOAc-Hexanes over 25 minutes) to afford the title compound as a yellow oil (2.45 g, 63%). 1H NMR [400 MHz, $CDCl_3$] δ 5.83 (br s, 2H), 2.67-2.64 (m, 2H), 2.49-2.46 (m, 2H), 1.76-1.69 (m, 4H), 1.52 (s, 9H); ^{13}C

NMR [100 MHz, CDCl₃] δ 165.8, 161.2, 132.7, 117.7, 107.4, 80.2, 28.8, 27.4, 24.8, 23.5, 23.1; HRMS (ESI) [M+H]⁺, calc'd for C₁₃H₂₀NO₂S 254.12093, found 254.12087; IR (solid ATR): 3434, 3324, 2932, 1732, 1660, 1576, 1484, 1141 cm⁻¹.

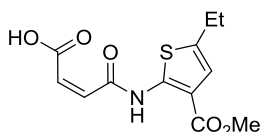


ethyl 2-amino-5,7-dihydro-4H-thieno[2,3-c]thiopyran-3-carboxylate (11l). Compound **11l** was prepared according to procedure B using cyclohexanone (1.2 mL, 11.6 mmol) and butyl 2-cyanoacetate (1.8 mL, 12.8 mmol). The crude material was purified by flash column chromatography (ISCO, 80 g silica gel, 0-10% EtOAc-Hexanes over 20 minutes) to afford the title compound as a yellow oil (2.35 g, 80%). ¹H NMR [400 MHz, CDCl₃] δ 5.96 (br s, 2H), 4.21 (t, *J* = 6.6 Hz, 2H), 2.72-2.69 (m, 2H), 2.52-2.49 (m, 2H), 1.82-1.66 (m, 6H), 1.45 (sextet, *J* = 7.4 Hz, 2H), 0.96 (t, *J* = 7.3 Hz, 3H); ¹³C NMR [100 MHz, CDCl₃] δ 166.5, 161.9, 132.6, 117.8, 106.0, 63.5, 31.1, 27.2, 24.7, 23.4, 23.1, 19.6, 114.0; HRMS (ESI) [M+H]⁺, calc'd for C₁₃H₂₀NO₂S 254.12093, found 254.12061; IR (solid ATR): 3433, 3325, 2932, 2857, 1664, 1576, 1485, 1265 cm⁻¹.



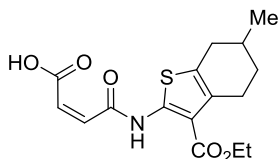
benzyl 2-amino-4,5,6,7-tetrahydrobenzo[b]thiophene-3-carboxylate (11m). Compound **11m** was prepared according to procedure B using cyclohexanone (0.7 mL, 6.5 mmol) and benzyl 2-cyanoacetate (1.1 mL, 7.1 mmol). The crude material was purified by flash column chromatography (ISCO, 40 g silica gel, 0-20% EtOAc-Hexanes over 15 minutes) to afford the title compound as a yellow tinted oil (1.38 g, 74%). ¹H NMR [400 MHz, CDCl₃] δ 7.43-7.33 (m, 5H), 6.00 (br s, 2H), 5.29 (s, 2H), 2.74-2.71 (m, 2H), 2.52-2.49 (m, 2H), 1.81-1.68 (m, 4H); ¹³C NMR [100 MHz, CDCl₃] δ 166.0, 162.4, 136.9, 132.5, 128.7, 128.1, 128.1, 117.8, 105.5, 65.4,

27.2, 24.7, 23.4, 23.0; HRMS (ESI) $[M+H]^+$, calc'd for $C_{16}H_{18}NO_2S$ 288.10528, found 288.10519; IR (solid ATR): 3442, 3325, 2980, 2934, 1659, 1575, 1483, 1261 cm^{-1} .



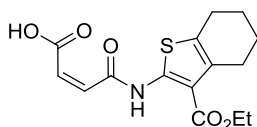
(Z)-4-((5-ethyl-3-(methoxycarbonyl)thiophen-2-yl)amino)-4-oxobut-2-enoic acid (13a).

Compound **13a** was prepared according to procedure C using compound **11a** (1.0 g, 5.5 mmol). The crude yellow solid (1.34 g, 87%) was carried on without further purification. 1H NMR [400 MHz, $CDCl_3$] δ 14.43 (br s, 1H), 11.73 (s, 1H), 6.99 (s, 1H), 6.54 (d, $J = 12.8$ Hz, 1H), 6.48 (d, $J = 12.8$ Hz, 1H), 3.92 (s, 3H), 2.80 (dq, $J = 1.2, 7.5, 14.9$ Hz, 2H), 1.33 (t, $J = 7.6$ Hz, 3H); ^{13}C NMR [100 MHz, $CDCl_3$] δ 166.2, 164.2, 162.2, 143.8, 141.2, 138.1, 129.7, 120.2, 115.6, 52.4, 23.1, 15.6 HRMS (ESI) $[M+H]^+$, calc'd for $C_{12}H_{14}NO_5S$, 284.05872, found 284.05863.

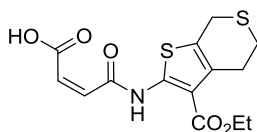


(Z)-4-((3-(ethoxycarbonyl)-6-methyl-4,5,6,7-tetrahydrobenzo[b]thiophen-2-yl)amino)-4-

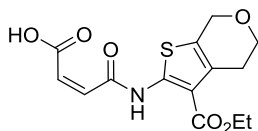
oxobut-2-enoic acid (13b). Compound **13b** was prepared according to procedure C using compound **11b** (2.6 g, 10.7 mmol). The crude yellow solid (3.54 g, 98%) was carried on without further purification. 1H NMR [400 MHz, $CDCl_3$] δ 12.22 (s, 1H), 6.51 (d, $J = 12.8$ Hz, 1H), 6.45 (d, $J = 12.8$ Hz, 1H), 4.38 (q, $J = 7.0$ Hz, 2H), 2.95-2.99 (m, 1H), 2.78 (dd, $J = 4.9, 15.9$ Hz, 1H), 2.66-2.75 (m, 1H), 2.29-2.35 (m, 1H), 1.89-1.93 (m, 2H), 1.42 (t, $J = 7.3$ Hz, 4H), 1.09 (d, $J = 6.7$ Hz, 3H); ^{13}C NMR [100 MHz, $CDCl_3$] δ 166.9, 164.3, 162.1, 144.4, 137.8, 132.1, 130.8, 130.0, 115.0, 61.6, 32.8, 31.0, 29.3, 26.3, 21.5, 14.4; HRMS (ESI) $[M+H]^+$, calc'd for $C_{16}H_{20}NO_5S$, 338.10567, found 338.10550.



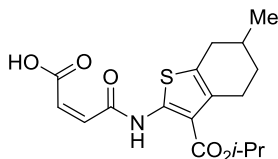
(Z)-4-((3-(ethoxycarbonyl)-4,5,6,7-tetrahydrobenzo[*b*]thiophen-2-yl)amino)-4-oxobut-2-enoic acid (13c). Compound **13c** was prepared according to procedure C using compound **11c** (3.0 g, 13.3 mmol). The crude yellow solid (4.02 g, 93%) was carried on without further purification. ^1H NMR [400 MHz, CDCl_3] δ 12.18 (br s, 1H), 6.49 (d, $J = 12.8$ Hz, 1H), 6.45 (d, $J = 12.8$ Hz, 1H), 4.36 (q, $J = 7.1$ Hz, 2H), 2.78 (app. t, $J = 5.2$ Hz, 2H), 2.69 (app. t, $J = 4.9$ Hz, 2H), 1.78-1.83 (m, 4H), 1.40 (t, $J = 7.3$ Hz, 3H); ^{13}C NMR [100 MHz, CDCl_3] δ 166.8, 164.3, 162.0, 144.2, 137.7, 132.3, 131.0, 130.0, 115.1, 61.5, 26.4, 24.7, 22.9, 22.7, 14.4; HRMS (ESI) $[\text{M}+\text{H}]^+$, calc'd for $\text{C}_{15}\text{H}_{18}\text{NO}_5\text{S}$ 324.09002, found 324.08965.



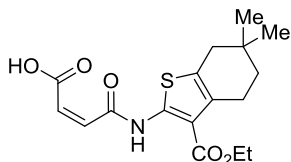
(Z)-4-((3-(ethoxycarbonyl)-4,7-dihydro-5H-thieno[2,3-*c*]thiopyran-2-yl)amino)-4-oxobut-2-enoic acid (13d). Compound **13d** was prepared according to procedure C using compound **11d** (1.0 g, 4.1 mmol). The crude yellow solid (1.14 g, 81%) was carried on without further purification. ^1H NMR [400 MHz, CDCl_3] δ 12.22 (br s, 1H), 6.51 (d, $J = 12.8$ Hz, 1H), 6.47 (d, $J = 12.8$ Hz, 1H), 4.38 (q, $J = 6.9$ Hz, 2H), 3.75 (s, 2H), 3.10 (t, $J = 5.7$ Hz, 2H), 2.93 (t, $J = 6.0$ Hz, 2H), 1.41 (t, $J = 7.1$ Hz, 3H); ^{13}C NMR [100 MHz, CDCl_3] δ 166.5, 164.1, 162.3, 144.2, 137.9, 131.8, 129.8, 126.8, 115.4, 61.8, 28.3, 26.3, 25.5, 14.4; HRMS (ESI) $[\text{M}+\text{H}]^+$, calc'd for $\text{C}_{14}\text{H}_{16}\text{NO}_5\text{S}_2$ 342.04644, found 342.04630.



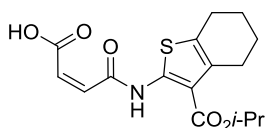
(Z)-4-((3-(ethoxycarbonyl)-4,7-dihydro-5H-thieno[2,3-c]pyran-2-yl)amino)-4-oxobut-2-enoic acid (13e). Compound **13e** was prepared according to procedure C using compound **11e** (1.0 g, 4.4 mmol). The crude yellow solid (1.02 g, 71%) was carried on without further purification. ^1H NMR [400 MHz, CDCl_3] δ 12.05 (s, 1H), 6.46 (d, $J = 12.8$ Hz, 1H), 6.41 (d, $J = 12.8$ Hz, 1H), 4.67 (t, $J = 1.8$ Hz, 2H), 4.32 (q, $J = 7.1$ Hz, 2H), 3.89 (t, $J = 5.8$ Hz, 2H), 2.83-2.86 (m, 2H), 1.34 (t, $J = 7.0$ Hz, 3H); ^{13}C NMR [100 MHz, CDCl_3] δ 166.5, 164.2, 162.2, 145.2, 138.0, 130.0, 129.7, 128.2, 114.7, 65.1, 64.8, 61.8, 27.1, 14.4; HRMS (ESI) $[\text{M}+\text{H}]^+$, calc'd for $\text{C}_{14}\text{H}_{16}\text{NO}_6\text{S}$ 326.06929, found 326.06895.



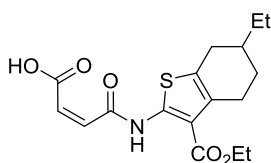
(Z)-4-((3-(isopropoxycarbonyl)-6-methyl-4,5,6,7-tetrahydrobenzo[b]thiophen-2-yl)amino)-4-oxobut-2-enoic acid (13f). Compound **13f** was prepared according to procedure C using compound **11f** (2.0 g, 7.9 mmol). The crude yellow solid (2.69 g, 97%) was carried on without further purification. ^1H NMR [400 MHz, CDCl_3] δ 12.25 (br s, 1H), 6.49 (d, $J = 12.8$ Hz, 1H), 6.45 (d, $J = 12.8$ Hz, 1H), 5.22 (septet, $J = 6.2$ Hz, 1H), 2.93-2.97 (m, 1H), 2.64-2.79 (m, 2H), 2.26-2.33 (m, 1H), 1.84-1.92 (m, 2H), 1.29-1.43 (m, 7H), 1.08 (d, $J = 6.1$ Hz, 3H); ^{13}C NMR [100 MHz, CDCl_3] δ 166.4, 164.3, 162.0, 144.2, 137.8, 132.0, 130.7, 130.1, 115.3, 69.5, 32.7, 31.0, 29.3, 26.3, 22.1, 21.5; HRMS (ESI) $[\text{M}-\text{H}]^-$, calc'd for $\text{C}_{17}\text{H}_{22}\text{NO}_5\text{S}$ 350.10677, found 350.10666.



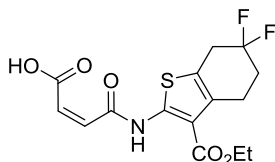
(Z)-4-((3-(ethoxycarbonyl)-6,6-dimethyl-4,5,6,7-tetrahydrobenzo[*b*]thiophen-2-yl)amino)-4-oxobut-2-enoic acid (13g). Compound **13g** was prepared according to procedure C using compound **11g** (2.0 g, 7.9 mmol). The crude yellow solid was carried on without further purification. HRMS (ESI) $[M-H]^-$, calc'd for $C_{17}H_{20}NO_5S$ 350.10677, found 350.10654.



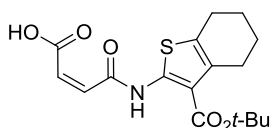
(Z)-4-((3-(isopropoxycarbonyl)-4,5,6,7-tetrahydrobenzo[*b*]thiophen-2-yl)amino)-4-oxobut-2-enoic acid (13h). Compound **13h** was prepared according to procedure C using compound **11h** (1.5 g, 6.3 mmol). The crude yellow solid (2.01 g, 95%) was carried on without further purification. 1H NMR [600 MHz, $CDCl_3$] δ 12.27 (br s, 1H), 6.50 (d, $J = 12.8$ Hz, 1H), 6.46 (d, $J = 12.8$ Hz, 1H), 5.23 (septet, $J = 6.3$ Hz, 1H), 2.79-2.80 (m, 2H), 2.69-2.70 (m, 2H), 1.81-1.82 (m, 4H), 1.39 (d, $J = 6.0$ Hz, 6H); ^{13}C NMR [150 MHz, $CDCl_3$] δ 166.5, 164.3, 162.1, 144.1, 137.8, 132.4, 131.1, 130.1, 115.5, 69.5, 26.6, 24.7, 22.9, 22.8, 22.2; HRMS (ESI) $[M+H]^+$, calc'd for $C_{16}H_{20}NO_5S$ 338.10567, found 338.10578.



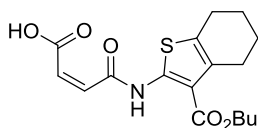
(Z)-4-((3-(ethoxycarbonyl)-6-ethyl-4,5,6,7-tetrahydrobenzo[*b*]thiophen-2-yl)amino)-4-oxobut-2-enoic acid (13i). Compound **13i** was prepared according to procedure C using compound **11i** (1.0 g, 4.0 mmol). The crude yellow solid (1.21 g, 87%) was carried on without further purification. HRMS (ESI) $[M+H]^+$, calc'd for $C_{17}H_{20}NO_5S$ 350.10677, found 350.10657.



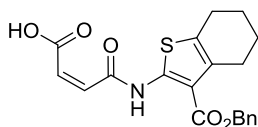
(Z)-4-((3-(ethoxycarbonyl)-6,6-difluoro-4,5,6,7-tetrahydrobenzo[b]thiophen-2-yl)amino)-4-oxobut-2-enoic acid (13j). Compound **13j** was prepared according to procedure C using compound **11j** (0.6 g, 2.3 mmol). The crude yellow solid (0.826 g, quant.) was carried on without further purification. HRMS (ESI) $[M+H]^+$, calc'd for $C_{15}H_{16}F_2NO_5S$ 360.07118, found 360.07132.



(Z)-4-((3-(tert-butoxycarbonyl)-4,5,6,7-tetrahydrobenzo[b]thiophen-2-yl)amino)-4-oxobut-2-enoic acid (13k). Compound **13k** was prepared according to procedure C using compound **11k** (2.4 g, 9.6 mmol). The crude yellow solid (2.88 g, 86%) was carried on without further purification. HRMS (ESI) $[M+H]^+$, calc'd for $C_{17}H_{22}NO_5S$ 352.12132, found 352.12107.

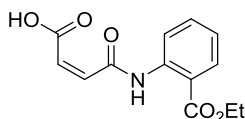


(Z)-4-((3-(butoxycarbonyl)-4,5,6,7-tetrahydrobenzo[b]thiophen-2-yl)amino)-4-oxobut-2-enoic acid (13l). Compound **13l** was prepared according to procedure C using compound **11l** (1.5 g, 5.8 mmol). The crude yellow solid (1.73 g, 85%) was carried on without further purification. HRMS (ESI) $[M+H]^+$, calc'd for $C_{17}H_{22}NO_5S$ 352.12132, found 352.12111.

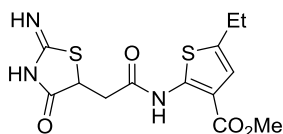


(Z)-4-((3-((benzyloxy)carbonyl)-4,5,6,7-tetrahydrobenzo[b]thiophen-2-yl)amino)-4-oxobut-2-enoic acid (13m). Compound **13m** was prepared according to procedure C using compound

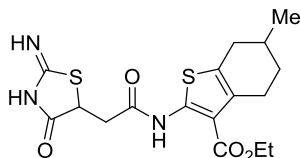
11m (0.6 g, 2.1 mmol). The crude yellow solid (0.573 g, 70%) was carried on without further purification. HRMS (ESI) $[M+H]^+$, calc'd for $C_{20}H_{20}NO_5S$ 386.10567, found 386.10587.



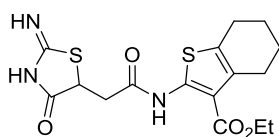
(Z)-4-((2-(ethoxycarbonyl)phenyl)amino)-4-oxobut-2-enoic acid (13n). To a solution of maleic anhydride (0.9 g, 9.1 mmol) dissolved in anhydrous ether (40.0 mL) was added ethyl 2-aminobenzoate (1.3 mL, 9.1 mmol). The reaction was allowed to stir for 48 hours. The precipitate was filtered and rinsed with ether. The crude white solid (1.65 g, 69%) was carried on without further purification. HRMS (ESI) $[M+Na]^+$, calc'd for $C_{13}H_{13}NNaO_5$ 286.06859, found 286.06873.



methyl 5-ethyl-2-(2-(2-imino-4-oxothiazolidin-5-yl)acetamido)thiophene-3-carboxylate (1794). Compound **1794** was prepared according to procedure D using compound **13a** (0.5 g, 1.8 mmol). The crude material was precipitated from hot methanol to afford the title compound as a light yellow solid (0.143 g, 24%). 1H NMR [400 MHz, $DMSO-d_6$] δ 10.78 (s, 1H), 9.04 (s, 1H), 8.80 (s, 1H), 6.68 (s, 1H), 4.44 (dd, $J = 3.7, 10.1$ Hz, 1H), 3.8 (s, 3H), 3.44 (dd, $J = 3.5, 16.9$ Hz, 1H), 3.02 (dd, $J = 10.1, 16.8$, 1H), 2.70 (q, $J = 7.4$ Hz, 2H), 1.20 (t, $J = 6.9$ Hz, 3H); ^{13}C NMR [100 MHz, $DMSO-d_6$] (^{13}C resonance obstructed by solvent peak) δ 188.5, 182.0, 168.0, 164.1, 145.0, 136.5, 119.4, 112.1, 51.7, 51.3, 22.0, 15.4; HRMS (ESI) $[M+H]^+$, calc'd for $C_{13}H_{16}N_3O_4S_2$, 342.05768, found 342.05759; IR (solid ATR): 3224, 2927, 1673, 1562, 1534, 1496, 1460, 1435, 1376, 1284, 1257, 1231, 1166, 1142, 1081, 1027, 960, 843, 775, 741, 698, 636 cm^{-1} ; m.p. = 226-234 $^{\circ}C$ (dec.); Elem. Anal. calc'd for $C_{13}H_{15}N_3O_4S_2$, C, 45.73; H, 4.43; N, 12.31, found C, 45.88; H, 4.46; N, 11.93.

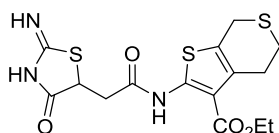


Ethyl 2-(2-(2-imino-4-oxothiazolidin-5-yl)acetamido)-6-methyl-4,5,6,7-tetrahydrobenzo[b]thiophene-3-carboxylate (1794-2). Compound **1794-2** was prepared according to procedure D using compound **13b** (0.3 g, 0.7 mmol). The crude material was precipitated from hot ethanol to afford the title compound (inseparable mixture of diastereomers) as a light yellow solid (0.0779 g, 27%). Compound **1794-2** was also prepared according to procedure F using compound **18b** (0.4 g, 1.3 mmol). The precipitate was rinsed with DCM to afford the title compound (inseparable mixture of diastereomers) as an off-white solid (0.406 g, 82%). ^1H NMR [400 MHz, DMSO- d_6] δ 10.98 (s, 1H), 9.03 (s, 1H), 8.80 (s, 1H), 4.42 (dd, J = 3.7, 10.4 Hz, 1H), 4.27 (q, J = 6.9 Hz, 2H), 2.99 (dd, J = 10.4, 15.3 Hz, 1H), 2.83-2.88 (m, 1H), 2.59-2.70 (m, 2H), 2.16-2.22 (m, 1H), 1.80 (m, 2H), 1.30 (t, J = 7.0 Hz, 4H), 1.01 (d, J = 6.7 Hz, 4H); ^{13}C NMR [100 MHz, DMSO- d_6] (^{13}C resonance obstructed by solvent peak) δ 188.5, 182.0, 167.8, 164.7, 145.4, 130.2, 125.9, 111.7, 60.4, 51.4, 31.7, 30.5, 28.7, 25.6, 21.2, 14.1; HRMS (ESI) $[\text{M}+\text{H}]^+$, calc'd for $\text{C}_{13}\text{H}_{16}\text{N}_3\text{O}_4\text{S}_2$, 342.05768, found 342.05759; IR (solid ATR): 3224, 2927, 1673, 1562, 1534, 1496, 1460, 1435, 1376, 1284, 1257, 1231, 1166, 1142, 1081, 1027, 960, 843, 775, 741, 698, 636 cm^{-1} ; m.p. = 190-204 $^\circ\text{C}$ (dec.); Elem. Anal. calc'd for $\text{C}_{13}\text{H}_{15}\text{N}_3\text{O}_4\text{S}_2$, C, 45.73; H, 4.43; N, 12.31, found C, 45.88; H, 4.46; N, 11.93.

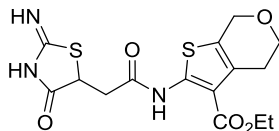


Ethyl 2-(2-(2-imino-4-oxothiazolidin-5-yl)acetamido)-4,5,6,7-tetrahydrobenzo[b]thiophene-3-carboxylate (1794-4). Compound **1794-4** was prepared according to procedure D using compound **13c** (0.4 g, 1.2 mmol). The crude material was precipitated from hot ethanol to afford the title compound as a light yellow solid (0.281 g, 60%). ^1H NMR [400 MHz, DMSO- d_6] δ

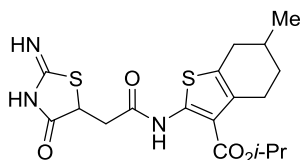
11.00 (s, 1H), 9.06 (s, 1H), 8.82 (s, 1H), 4.43 (dd, $J = 3.9, 10.2$ Hz, 1H), 4.28 (q, $J = 7.0$ Hz, 2H), 3.36-3.42 (m, 1H), 3.01 (dd, $J = 10.2, 16.8$, 1H), 2.69 (s, 2H), 2.59 (s, 2H), 1.72 (s, 4H), 1.31 (t, $J = 7.0$ Hz, 3H); ^{13}C NMR [100 MHz, DMSO- d_6] (^{13}C resonance obstructed by solvent peak) δ 188.5, 182.0, 167.8, 164.7, 145.3, 130.5, 126.3, 111.8, 60.3, 51.4, 25.8, 23.7, 22.5, 22.3, 14.1; HRMS (ESI) $[\text{M}+\text{H}]^+$, calc'd for $\text{C}_{16}\text{H}_{20}\text{N}_3\text{O}_4\text{S}_2$, 382.08952, found 382.08902; IR (solid ATR): 3661, 3269, 3195, 2933, 1655, 1563, 1527, 1439, 1408, 1366, 1326, 1231, 1134, 1032, 996, 969, 784, 703, 629 cm^{-1} ; m.p. = 163 $^{\circ}\text{C}$ (dec.); Elem. Anal. calc'd for $\text{C}_{16}\text{H}_{19}\text{N}_3\text{O}_4\text{S}_2$, C, 50.38; H, 5.02; N, 11.02, found C, 49.31; H, 5.00; N, 10.73 (Value did not fall within ± 0.4).



ethyl 2-(2-(2-imino-4-oxothiazolidin-5-yl)acetamido)-4,7-dihydro-5H-thieno[2,3-c]thiopyran-3-carboxylate (1794-15). Compound **1794-15** was prepared according to procedure D using compound **13d** (0.4 g, 1.2 mmol). The crude material was precipitated from hot ethanol to afford the title compound as a light brown solid (0.140 g, 30%). ^1H NMR [400 MHz, DMSO- d_6] δ 11.01 (br s, 1H), 9.03 (br s, 1H), 8.80 (br s, 1H), 4.43 (dd, $J = 3.7, 10.4$ Hz, 1H), 4.29 (q, $J = 7.2$ Hz, 2H), 3.73 (s, 2H), 3.40 (dd, $J = 4.0, 16.8$ Hz, 1H), 3.01 (dd, $J = 10.1, 16.8$ Hz, 1H), 2.94-3.00 (m, 2H), 2.88 (app. t, $J = 5.7$ Hz, 2H), 1.31 (t, $J = 7.0$ Hz, 3H); ^{13}C NMR [100 MHz, DMSO- d_6] δ 188.5, 181.9, 168.0, 164.3, 144.7, 130.2, 123.0, 112.4, 60.6, 51.3, 39.2, 27.6, 25.33, 24.2, 14.1; HRMS (ESI) $[\text{M}+\text{H}]^+$, calc'd for $\text{C}_{15}\text{H}_{18}\text{N}_3\text{O}_4\text{S}_3$ 400.04540, found 400.04554; IR (solid ATR): 3440, 3345, 3228, 2984, 2360, 1712, 1649, 1561, 1518, 1442, 1405, 1372, 1325, 1284, 1227, 1128, 1035, 949, 881, 816, 781, 748, 667, 628 cm^{-1} ; m.p. = 158-162 $^{\circ}\text{C}$ (dec.); HPLC purity: >95% $t_{\text{R}} = 0.731$ min. (85% MeOH/Water with 0.1% formic acid, isocratic, 1.0 mL/min.); $t_{\text{R}} = 0.586$ min. (75% MeCN/Water with 0.1% formic acid, isocratic, 1.0 mL/min.).

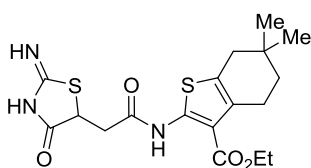


ethyl 2-(2-(2-imino-4-oxothiazolidin-5-yl)acetamido)-4,7-dihydro-5H-thieno[2,3-c]pyran-3-carboxylate (1794-21). Compound **1794-21** was prepared according to procedure D using compound **13e** (0.5 g, 1.5 mmol). The crude material was precipitated from hot ethanol to afford the title compound as an off-white solid (0.0590 g, 10%). ^1H NMR [400 MHz, DMSO- d_6] δ 11.00 (s, 1H), 9.03 (s, 1H), 8.80 (s, 1H), 4.62 (s, 2H), 4.44 (dd, J = 3.8, 10.2 Hz, 1H), 4.29 (q, J = 7.0 Hz, 2H), 3.84 (t, J = 5.5 Hz, 2H), 3.42 (dd, J = 4.0, 16.8 Hz, 1H), 3.02 (dd, J = 10.4, 16.8 Hz, 1H), 2.78-2.79 (m, 2H), 1.31 (t, J = 7.0 Hz, 3H); ^{13}C NMR [100 MHz, DMSO- d_6] δ 188.5, 181.9, 168.0, 164.3, 146.1, 128.4, 124.4, 111.4, 64.1, 63.9, 60.5, 51.3, 39.2, 26.5, 14.1; HRMS (ESI) $[\text{M}+\text{Na}]^+$, calc'd for $\text{C}_{15}\text{H}_{17}\text{N}_3\text{NaO}_5\text{S}_2$ 406.05019, found 406.05093; IR (solid ATR): 3256, 1651, 1564, 1526, 1446, 1419, 1369, 1330, 1273, 1236, 1089, 1033, 977, 870, 781, 683 cm^{-1} ; m.p. = 243-246 $^\circ\text{C}$ (dec.); HPLC purity: >95% t_{R} = 0.607 min. (85% MeOH/Water with 0.1% formic acid, isocratic, 1.0 mL/min.); t_{R} = 0.517 min. (75% MeCN/Water with 0.1% formic acid, isocratic, 1.0 mL/min.).

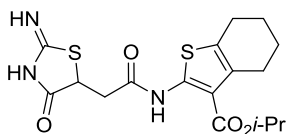


isopropyl 2-(2-(2-imino-4-oxothiazolidin-5-yl)acetamido)-6-methyl-4,5,6,7-tetrahydrobenzo[b]thiophene-3-carboxylate (1794-19). Compound **1794-19** was prepared according to procedure D using compound **13f** (0.7 g, 2.0 mmol). The crude material was precipitated from hot ethanol to afford the title compound as a white solid (0.134 g, 16%). ^1H NMR [400 MHz, DMSO- d_6] δ 11.00 (s, 1H), 9.04 (s, 1H), 8.81 (s, 1H), 4.43 (dd, J = 3.8, 10.2 Hz, 1H), 4.29 (q, J = 7.1 Hz, 2H), 3.39 (dd, J = 3.8, 16.9 Hz, 1H), 3.00 (dd, J = 10.4, 16.8 Hz, 1H), 2.71 (app. t, J = 5.9 Hz, 2H), 2.38 (app. s, 2H), 1.48 (app. t, J = 6.3 Hz, 2H), 1.32 (t, J = 7.0

Hz, 3H), 0.95 (s, 6H); ^{13}C NMR [100 MHz, DMSO- d_6] δ 188.5, 181.9, 167.7, 164.7, 145.5, 129.1, 125.6, 111.5, 60.4, 51.4, 39.2, 37.1, 35.0, 29.7, 27.4, 27.3, 23.5, 14.0; HRMS (ESI) $[\text{M}+\text{H}]^+$, calc'd for $\text{C}_{16}\text{H}_{24}\text{N}_3\text{O}_4\text{S}_2$ 410.12028, found 410.12066; IR (solid ATR): 3205, 2923, 1655, 1561, 1531, 1492, 1386, 1293, 1233, 1148, 1106, 1074, 1011, 979, 960, 912, 835, 783, 761, 736, 698, 645 cm^{-1} ; m.p. = 229 °C (dec.); HPLC purity: >95% t_{R} = 1.300 min. (85% MeOH/Water with 0.1% formic acid, isocratic, 1.0 mL/min.); t_{R} = 0.995 min. (75% MeCN/Water with 0.1% formic acid, isocratic, 1.0 mL/min.).

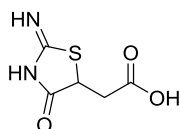


ethyl **2-(2-(2-imino-4-oxothiazolidin-5-yl)acetamido)-6,6-dimethyl-4,5,6,7-tetrahydrobenzo[b]thiophene-3-carboxylate (1794-20)**. Compound **1794-20** was prepared according to procedure D using compound **13g** (1.0 g, 2.9 mmol). The crude material was precipitated from hot ethanol to afford the title compound as a light brown solid (0.0400 g, 3%). ^1H NMR [400 MHz, DMSO- d_6] δ 11.03 (s, 1H), 9.03 (s, 1H), 8.80 (s, 1H), 5.10 (septet, J = 6.2 Hz, 1H), 4.42 (dd, J = 4.0, 10.1 Hz, 1H), 3.37 (dt, J = 3.4, 16.9 Hz, 1H), 2.95-3.03 (m, 1H); ^{13}C NMR [100 MHz, DMSO- d_6] δ 188.5, 181.9, 167.7, 164.4, 145.6, 130.1, 125.9, 111.8, 68.0, 51.4, 31.7, 30.6, 28.7, 25.7, 21.7 (2C), 21.2; HRMS (ESI) $[\text{M}+\text{H}]^+$, calc'd for $\text{C}_{18}\text{H}_{24}\text{N}_3\text{O}_4\text{S}_2$ 410.12028, found 410.12043; HPLC purity: >95% t_{R} = 1.229 min. (85% MeOH/Water with 0.1% formic acid, isocratic, 1.0 mL/min.); t_{R} = 0.946 min. (75% MeCN/Water with 0.1% formic acid, isocratic, 1.0 mL/min.).



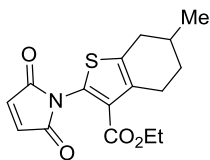
isopropyl **2-(2-(2-imino-4-oxothiazolidin-5-yl)acetamido)-4,5,6,7-tetrahydrobenzo[b]thiophene-3-carboxylate (1794-5)**. To a solution of **13h** (0.2 g, 0.6 mmol)

dissolved in dry DMF (5.0 mL) was added HATU (0.2 g, 0.6 mmol). The reaction mixture was allowed to stir at room temperature for 10 minutes. To the stirring mixture was added thiourea (0.1 g, 1.5 mmol) and DIPEA (0.5 mL, 3.0 mmol). The reaction was allowed to stir an additional 30 minutes before heating to 60 °C for 72 hours. The solvent was removed *in vacuo*. The crude material was purified by flash column chromatography (ISCO, 12 g silica gel column, 3-11% MeOH-DCM over 15 minutes). The resulting fractions were found to contain impurities. Material was re-purified by flash column chromatography (12 g silica gel column, 0-8% MeOH-DCM over 15 minutes) to afford the title compound as a light brown solid (0.0551 g, 23%). Compound **1794-5** was also prepared according to procedure F using **18h** (0.2 g, 0.7 mmol). The precipitate was rinsed with DCM to afford the title compound as a white solid (0.119 g, 42%). ¹H NMR [400 MHz, DMSO-*d*₆] δ 11.04 (s, 1H), 9.04 (s, 1H), 8.81 (s, 1H), 5.10 (septet, *J* = 6.3 Hz, 1H), 4.42 (dd, *J* = 3.9, 10.2 Hz, 1H), 3.40 (d, *J* = 3.5 Hz, 1H), 3.00 (dd, *J* = 10.2, 16.8, 1H), 2.69 (br s, 2H), 2.58 (br s, 2H), 1.71 (br s, 4H), 1.31 (d, *J* = 6.3 Hz, 6H); ¹³C NMR [100 MHz, DMSO-*d*₆] (¹³C resonance obstructed by solvent peak) δ 188.5, 181.9, 167.7, 164.4, 145.4, 130.4, 126.3, 112.0, 68.0, 51.4, 25.9, 23.7, 22.5, 22.3, 21.7 (2C); HRMS (ESI) [M+H]⁺, calc'd for C₁₇H₂₂N₃O₄S₂ 396.10463, found 396.10409; m.p. = 152-154 °C; HPLC purity: >95% *t*_R = 2.082 min. (75-95% MeOH/Water with 0.1% formic acid, gradient over 3 minutes, 1.0 mL/min.); *t*_R = 0.698 min. (85% MeCN/Water with 0.1% formic acid, isocratic, 1.0 mL/min.).

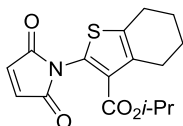


2-(2-imino-4-oxothiazolidin-5-yl)acetic acid (15). Thiourea (0.4 g, 5.7 mmol) and maleic anhydride (0.6 g, 5.7 mmol) were suspended in methyl ethyl ketone (25.0 mL). The yellow suspension was refluxed for 20 hours. The reaction mixture was concentrated *in vacuo* to a yellow solid. The crude light yellow solid (0.997 g, quant.) was carried on without further purification. ¹H NMR [400 MHz, DMSO-*d*₆] δ 9.01 (br s, 1H), 8.78 (s, 1H), 4.32 (dd, *J* = 3.1,

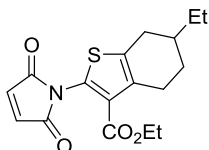
10.7 Hz, 1H), 3.04 (dd, $J = 3.5, 17.2$, 1H), 2.60 (dd, $J = 10.7, 17.4$ Hz, 1H); ^{13}C NMR [100 MHz, DMSO- d_6] δ 188.6, 182.0, 172.5, 51.6, 37.8; HRMS (APCI) $[\text{M}+\text{H}]^+$, calc'd for $\text{C}_5\text{H}_6\text{N}_2\text{O}_3\text{S}$ 175.01719, found 175.01698.



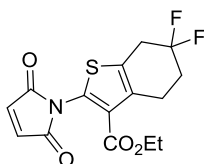
ethyl **2-(2,5-dioxo-2,5-dihydro-1H-pyrrol-1-yl)-6-methyl-4,5,6,7-tetrahydrobenzo[b]thiophene-3-carboxylate (18b)**. Compound **18b** was prepared according to procedure E using compound **13b** (1.0 g, 3.0 mmol). The crude material was purified by flash column chromatography (ISCO, 24 g silica gel, 0-18% EtOAc-Hexanes over 15 minutes) to afford the title compound as a yellow oil that solidified upon standing (0.769 g, 81%). HRMS (APCI) $[\text{M}+\text{H}]^+$, calc'd for $\text{C}_{16}\text{H}_{18}\text{NO}_4\text{S}$ 320.09511, found 320.09520.



isopropyl **2-(2,5-dioxo-2,5-dihydro-1H-pyrrol-1-yl)-4,5,6,7-tetrahydrobenzo[b]thiophene-3-carboxylate (18h)**. Compound **18h** was prepared according to procedure E using compound **13h** (0.8 g, 2.4 mmol). The crude material was purified by flash column chromatography (ISCO, 24 g silica gel, 0-25% EtOAc-Hexanes over 20 minutes) to afford the title compound as a golden brown oil (0.712 g, 94%). ^1H NMR [400 MHz, CDCl_3] δ 6.91 (s, 2H), 5.09 (septet, $J = 5.3$ Hz, 1H), 2.84 (app. t, $J = 5.8$ Hz, 2H), 2.75 (app. t, $J = 5.5$ Hz, 2H), 1.80-1.86 (m, 4H), 1.20 (d, $J = 6.1$ Hz, 6H); HRMS (APCI) $[\text{M}+\text{H}]^+$, calc'd for $\text{C}_{16}\text{H}_{18}\text{NO}_4\text{S}$ 320.09511, found 320.09527.

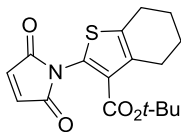


ethyl 2-(2,5-dioxo-2,5-dihydro-1H-pyrrol-1-yl)-6-ethyl-4,5,6,7-tetrahydrobenzo[b]thiophene-3-carboxylate (18i). Compound **18i** was prepared according to procedure E using compound **13i** (0.5 g, 1.4 mmol). The crude material was purified by flash column chromatography (ISCO, 24 g silica gel, 0-25% EtOAc-Hexanes over 15 minutes) to afford the title compound as a light yellow oil (0.399 g, 84%). ^1H NMR [400 MHz, CDCl_3] δ 6.91 (s, 2H), 4.24-4.10 (m, 2H), 3.06-2.98 (m, 1H), 2.90-2.82 (m, 1H), 2.78-2.67 (m, 1H), 2.36 (dddd, $J = 16.4, 10.1, 2.7, 1.6$ Hz, 1H), 2.01-1.92 (m, 1H), 1.77-1.64 (m, 1H), 1.50-1.33 (3H, m), 1.22 (t, $J = 7.1$ Hz, 3H), 0.98 (t, $J = 7.4$ Hz, 3H); ^{13}C NMR [100 MHz, CDCl_3] δ 169.2 (2C), 162.1, 136.7, 135.9, 135.1 (2C), 133.1, 128.5, 60.7, 36.0, 31.3, 28.8, 28.7, 26.3, 14.5, 11.7; HRMS (APCI) $[\text{M}+\text{H}]^+$, calc'd for $\text{C}_{17}\text{H}_{19}\text{NO}_4\text{S}$ 334.11076, found 334.11084; IR (solid ATR): 2971, 2914, 1709, 1670, 1534, 1372, 1242, 692 cm^{-1} .

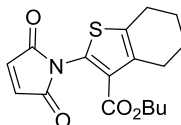


Ethyl 2-(2,5-dioxo-2,5-dihydro-1H-pyrrol-1-yl)-6,6-difluoro-4,5,6,7-tetrahydrobenzo[b]thiophene-3-carboxylate (18j). Compound **18j** was prepared according to procedure E using compound **13j** (0.5g, 1.4 mmol). The crude material was purified by flash column chromatography (ISCO, 24 g silica gel, 0-25% EtOAc-Hexanes over 15 minutes) to afford the title compound as a light yellow solid (0.269 g, 57%). ^1H NMR [400 MHz, CDCl_3] δ 6.93 (s, 2H), 4.20 (q, $J = 7.1$ Hz, 2H), 3.26 (t, $J = 13.4$ Hz, 2H), 3.13 (tt, $J = 6.7, 1.5$ Hz, 2H), 2.23 (tt, $J = 13.6, 6.7$ Hz, 2H), 1.23 (t, $J = 7.1$ Hz, 3H); ^{13}C NMR [100 MHz, CDCl_3] δ 168.8 (2C), 161.6, 135.2 (3C), 134.2, 130.7 (t, $J_{\text{C-F}} = 6.5$ Hz), 128.0, 122.2 (t, $J_{\text{C-F}} = 242.3$ Hz), 61.1,

34.8 (t, $J_{C-F} = 29.5$ Hz), 30.5 (t, $J_{C-F} = 24.2$ Hz), 24.0, 14.4; ^{19}F NMR [400 MHz, CDCl_3] δ -97.80 (p, $J = 13.5$ Hz); HRMS (APCI) $[\text{M}+\text{H}]^+$, calc'd for $\text{C}_{15}\text{H}_{14}\text{F}_2\text{NO}_4\text{S}$ 342.06061, found 342.06086; IR (solid ATR): 2978, 1711, 1669, 1563, 1533, 1373, 1242, 693 cm^{-1} .

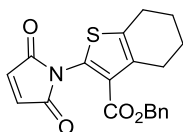


tert-butyl 2-(2,5-dioxo-2,5-dihydro-1H-pyrrol-1-yl)-4,5,6,7-tetrahydrobenzo[b]thiophene-3-carboxylate (18k). Compound **18k** was prepared according to procedure E using compound **13k** (2.0 g, 5.7 mmol). The crude material was purified by flash column chromatography (ISCO, 40 g silica gel, 0-18% EtOAc-Hexanes over 15 minutes) to afford the title compound as a light yellow solid (1.44 g, 76%). ^1H NMR [400 MHz, CDCl_3] δ 6.90 (s, 2H), 2.83-2.79 (m, 2H), 2.75-2.72 (m, 2H), 1.86-1.76 (m, 4H), 1.44 (s, 9H); ^{13}C NMR [100 MHz, CDCl_3] δ 169.1 (2C), 161.4, 136.6, 135.7, 135.1 (2C), 131.6, 130.4, 81.6, 28.4 (3C), 26.6, 25.4, 22.9, 22.6; HRMS (APCI) $[\text{M}-\text{O}t\text{-Bu}]^+$, calc'd for $\text{C}_{13}\text{H}_{10}\text{NO}_3\text{S}$ 260.03759, found 260.03737; IR (solid ATR): 2918, 1709, 1565, 1410, 1393, 1367, 1136, 691 cm^{-1} .

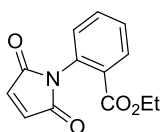


tert-butyl 2-(2,5-dioxo-2,5-dihydro-1H-pyrrol-1-yl)-4,5,6,7-tetrahydrobenzo[b]thiophene-3-carboxylate (18l). Compound **18l** was prepared according to procedure E using compound **13l** (1.2 g, 3.4 mmol). The crude material was purified by flash column chromatography (ISCO, 40 g silica gel, 0-18% EtOAc-Hexanes over 15 minutes) to afford the title compound as a light yellow solid (1.04 g, 91%). ^1H NMR [400 MHz, CDCl_3] δ 6.91 (s, 2H), 4.13 (t, $J = 6.7$ Hz, 2H), 2.84 (app. T, $J = 5.8$ Hz, 2H), 2.75 (app. t, $J = 5.8$ Hz, 2H), 1.87-1.78 (m, 4H), 1.57 (p, $J = 7.2$ Hz, 2H), 1.34 (sextet, $J = 7.5$ Hz, 2H), 0.91 (t, $J = 7.5$ Hz, 3H); ^{13}C NMR [100 MHz, CDCl_3] δ 169.2 (2C), 162.21, 136.8, 135.9, 135.1 (2C), 133.0, 128.7, 64.7, 30.8, 26.6, 25.4, 22.8, 22.6, 19.3, 13.9;

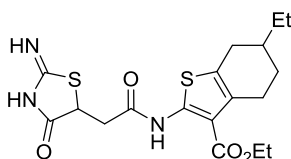
HRMS (APCI) $[M+H]^+$, calc'd for $C_{17}H_{20}NO_4S$ 334.11076, found 334.11128; IR (solid ATR): 3097, 2944, 1710, 1414, 1364, 1175, 836, 693 cm^{-1} .



benzyl 2-(2,5-dioxo-2,5-dihydro-1H-pyrrol-1-yl)-4,5,6,7-tetrahydrobenzo[b]thiophene-3-carboxylate (18m). Compound **18m** was prepared according to procedure E using compound **13m** (0.4 g, 1.0 mmol). The crude material was purified by flash column chromatography (ISCO, 24 g silica gel, 0-25% EtOAc-Hexanes over 15 minutes) to afford the title compound as a light yellow solid (0.299 g, 78%). 1H NMR [400 MHz, $CDCl_3$] δ 7.40-7.21 (m, 5H), 6.44 (s, 2H), 5.07 (s, 2H), 2.91-2.78 (m, 2H), 2.75-2.64 (m, 2H), 1.88-1.71 (m, 4H); ^{13}C NMR [100 MHz, $CDCl_3$] δ 169.2 (2C), 161.6, 137.0, 136.3, 135.4, 134.2 (2C), 133.3, 129.4 (2C), 128.8 (2C), 128.7, 128.3, 67.0, 26.4, 25.4, 22.8, 22.5; HRMS (APCI) $[M+H]^+$, calc'd for $C_{20}H_{18}NO_4S$ 368.09511, found 368.09512; IR (solid ATR): 2942, 2850, 1763, 1672, 1638, 1537, 1176, 1137, 691 cm^{-1} .

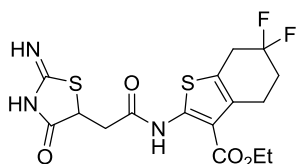


ethyl 2-(2,5-dioxo-2,5-dihydro-1H-pyrrol-1-yl)benzoate (18n). Compound **18n** was prepared according to procedure E using compound **13n** (0.2 g, 0.8 mmol). The crude material was recrystallized from absolute ethanol to afford the title compound a clear crystalline solid (0.104 g, 54%). HRMS (APCI) $[M]^+$, calc'd for $C_{13}H_{11}NO_4$ 245.06826, found 245.06829.



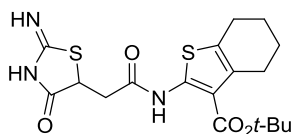
ethyl 6-ethyl-2-(2-(2-imino-4-oxothiazolidin-5-yl)acetamido)-4,5,6,7-tetrahydrobenzo[b]thiophene-3-carboxylate (1794-24). Compound **1794-24** was prepared according to procedure F using compound **18i** (0.2 g, 0.7 mmol). The precipitate was rinsed with

EtOH and DCM to afford the title compound as an off-white solid (0.197 g, 75%). ^1H NMR [400 MHz, DMSO- d_6] δ 10.99 (s, 1H), 9.04 (s, 1H), 8.80 (s, 1H), 4.42 (dd, J = 10.2, 3.8 Hz, 1H), 4.28 (d, J = 7.1 Hz, 2H), 3.42-3.35 (m, 1H), 2.99 (ddd, J = 16.9, 10.3, 1.8 Hz, 1H), 2.86 (d, J = 16.6 Hz, 1H), 2.70 (dd, J = 16.5, 3.8 Hz, 1H), 2.67-2.51 (m, 1H), 2.20 (dd, J = 15.3, 10.3 Hz, 1H), 1.93-1.82 (m, 1H), 1.64-1.50 (m, 1H), 1.39-1.22 (m, 3H), 1.30 (t, J = 7.1 Hz, 3H), 0.92 (t, J = 7.4 Hz, 3H); ^{13}C NMR [100 MHz, DMSO- d_6] (^{13}C resonance obstructed by solvent peak) δ 188.5, 182.0, 167.7, 164.7, 145.5, 130.4, 126.0, 111.6, 60.4, 51.4, 35.4, 29.6, 28.3, 28.1, 25.6, 14.1, 11.4; HRMS (ESI) $[\text{M}+\text{H}]^+$, calc'd for $\text{C}_{18}\text{H}_{24}\text{N}_3\text{O}_4\text{S}_2$ 410.12028, found 410.12044; IR (solid ATR): 2924, 1670, 1637, 1534, 1405, 1168, 1027 cm^{-1} ; m.p. = 189-193 $^\circ\text{C}$; HPLC purity: >95% t_{R} = 0.815 min. (95% MeOH/Water with 0.1% formic acid, isocratic, 1.0 mL/min.).

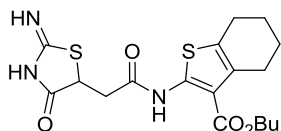


ethyl 6,6-difluoro-2-(2-(2-imino-4-oxothiazolidin-5-yl)acetamido)-4,5,6,7-tetrahydrobenzo[b]thiophene-3-carboxylate (1794-23). Compound **1794-23** was prepared according to procedure F using compound **18j** (0.2 g, 0.6 mmol). The precipitate was rinsed with DCM to afford the title compound as an off-white solid (0.144 g, 59%). ^1H NMR [400 MHz, DMSO- d_6] δ 11.02 (s, 1H), 9.05 (s, 1H), 8.81 (s, 1H), 4.44 (dd, J = 10.1, 3.9 Hz, 1H), 4.30 (q, J = 7.1 Hz, 2H), 3.42 (dd, J = 16.9, 3.9 Hz, 1H), 3.22 (t, J = 13.8 Hz, 2H), 3.03 (dd, J = 16.9, 10.2 Hz, 1H), 2.94 (t, J = 6.7 Hz, 2H), 2.21 (tt, J = 13.7, 6.8 Hz, 2H), 1.32 (t, J = 7.1 Hz, 3H); ^{13}C NMR [100 MHz, DMSO- d_6] δ 188.5, 182.0, 168.2, 164.3, 146.8, 128.9, 123.6 (t, $J_{\text{C-F}}$ = 239.0 Hz), 121.1, 110.9, 60.6, 51.3, 39.2, 33.1 (t, $J_{\text{C-F}}$ = 28.3 Hz), 29.7 (t, $J_{\text{C-F}}$ = 24.1 Hz), 23.6, 14.1; ^{19}F NMR [400 MHz, DMSO- d_6] δ -96.15 (p, J = 14.2 Hz); HRMS (ESI) $[\text{M}+\text{H}]^+$, calc'd for $\text{C}_{16}\text{H}_{18}\text{F}_2\text{N}_3\text{O}_4\text{S}_2$ 418.07013, found 418.07021; IR (solid ATR): 3275, 2976, 1657, 1563, 1531, 1509, 1441, 1410, 1368, 1326, 1268, 1230, 1160, 1117, 1075, 1036, 997, 959, 883, 838, 784, 767,

710, 640 cm^{-1} ; m.p. = >250 $^{\circ}\text{C}$; HPLC purity: $>95\%$ $t_{\text{R}} = 1.066$ min. (75-95% MeOH/Water with 0.1% formic acid, gradient over 3 minutes, 1.0 mL/min.).

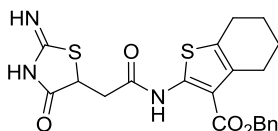


tert-butyl 2-(2-(2-imino-4-oxothiazolidin-5-yl)acetamido)-4,5,6,7-tetrahydrobenzo[b]thiophene-3-carboxylate (1794-27). Compound **1794-27** was prepared according to procedure F using compound **18k** (0.5 g, 1.5 mmol). The precipitate was rinsed with EtOH and EtOAc to afford the title compound as a light yellow solid (0.403 g, 66%). ^1H NMR [400 MHz, $\text{DMSO-}d_6$] δ 11.03 (s, 1H), 9.03 (s, 1H), 8.80 (s, 1H), 4.43 (dd, $J = 4.0, 10.2$ Hz, 1H), 3.38 (dd, $J = 3.7, 16.8$ Hz, 1H), 3.00 (dd, $J = 10.4, 16.8$ Hz, 1H), 2.68 (app. br s, 2H), 2.58 (app. br s, 2H), 1.70 (app. br s, 4H), 1.54 (s, 9H); ^{13}C NMR [100 MHz, $\text{DMSO-}d_6$] (^{13}C resonance obstructed by solvent peak) δ 188.5, 182.0, 167.7, 164.3, 145.2, 130.5, 126.1, 112.8, 81.5, 51.4, 28.0 (3C), 26.1, 23.8, 22.5, 22.4; HRMS (ESI) $[\text{M}+\text{H}]^+$, calc'd for $\text{C}_{18}\text{H}_{24}\text{N}_3\text{O}_4\text{S}_2$ 410.12027, found 410.12011; IR (solid ATR): 3372, 2919, 1705, 1565, 1524, 1367, 1240, 1138 cm^{-1} ; HPLC purity: $>95\%$ $t_{\text{R}} = 0.765$ min. (95% MeOH/Water with 0.1% formic acid, isocratic, 1.0 mL/min.).

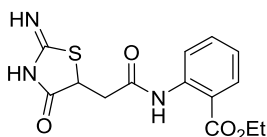


butyl 2-(2-(2-imino-4-oxothiazolidin-5-yl)acetamido)-4,5,6,7-tetrahydrobenzo[b]thiophene-3-carboxylate (1794-29). Compound **1794-29** was prepared according to procedure F using compound **18l** (0.5 g, 1.5 mmol). The precipitate was rinsed with EtOH to afford the title compound as a light yellow solid (0.325 g, 53%). ^1H NMR [400 MHz, $\text{DMSO-}d_6$] δ 11.38 (s, 1H), 10.05 (br s, 1H), 7.53 (s, 1H), 4.55 (dd, $J = 3.2, 11.1$ Hz, 1H), 4.24 (t, $J = 6.6$ Hz, 2H), 3.54 (dd, $J = 3.1, 16.8$ Hz, 1H), 2.96 (dd, $J = 11.3, 16.8$ Hz, 1H), 2.72 (app. br s, 2H), 2.57 (app. br s, 2H), 1.76 (app. br s, 4H), 1.70 (p, $J = 7.2$ Hz, 2H), 1.44 (sextet, $J = 7.4$ Hz, 2H), 0.96 (t, $J = 7.3$

Hz, 3H); ^{13}C NMR [100 MHz, $\text{DMSO-}d_6$] δ 189.1, 184.3, 167.0, 166.7, 146.9, 131.0, 127.2, 112.2, 64.7, 52.0, 40.2, 30.9, 26.5, 24.5, 23.1, 23.0, 19.6, 13.9; HRMS (ESI) $[\text{M}+\text{H}]^+$, calc'd for $\text{C}_{18}\text{H}_{24}\text{N}_3\text{O}_4\text{S}_2$ 410.12027, found 410.11979; IR (solid ATR): 3307, 2939, 1650, 1567, 1521, 1414, 1245, 1115cm^{-1} ; HPLC purity: >95% $t_R = 1.479$ min. (85% MeOH/Water with 0.1% formic acid, isocratic, 1.0 mL/min.).

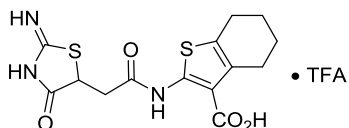


benzyl 2-(2-(2-imino-4-oxothiazolidin-5-yl)acetamido)-4,5,6,7-tetrahydrobenzo[b]thiophene-3-carboxylate (1794-25). Compound **1794-25** was prepared according to procedure F using compound **18m** (0.3 g, 0.7 mmol). The precipitate was rinsed with DCM to afford the title compound as an off-white solid (0.124 g, 41%). ^1H NMR [400 MHz, $\text{DMSO-}d_6$] δ 10.98 (s, 1H), 9.04 (s, 1H), 8.80 (s, 1H), 7.49-7.29 (m, 5H), 5.33 (s, 2H), 4.42 (dd, $J = 3.8, 10.2$ Hz, 1H), 3.37 (dd, $J = 4.0, 16.8$ Hz, 1H), 2.96 (dd, 1H, $J = 10.2, 16.9$ Hz, 1H), 2.72-2.64 (m, 2H), 2.62-2.54 (m, 2H), 1.77-1.61 (m, 4H); ^{13}C NMR [100 MHz, $\text{DMSO-}d_6$] (^{13}C resonance obstructed by solvent peak) δ 188.5, 181.97, 167.9, 164.4, 145.7, 136.1, 130.5, 128.6 (2C), 128.2, 128.1 (2C), 126.4, 111.6, 65.9, 51.4, 25.9, 23.7, 22.5, 22.3; HRMS (ESI) $[\text{M}+\text{H}]^+$, calc'd for $\text{C}_{21}\text{H}_{22}\text{N}_3\text{O}_4\text{S}_2$ 444.10463, found 444.10497; IR (solid ATR): 2936, 1649, 1564, 1517, 1237, 1191, 1020cm^{-1} ; HPLC purity: >95% $t_R = 2.470$ min. (75-95% MeOH/Water with 0.1% formic acid, gradient over 3 minutes, 1.0 mL/min.).



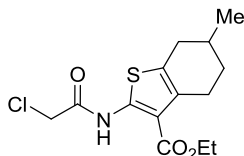
ethyl 2-(2-(2-imino-4-oxothiazolidin-5-yl)acetamido)benzoate (1794-24). A suspension of **18n** (0.05 g, 0.2 mmol) and thiourea (0.02 g, 0.2 mmol) in absolute ethanol (2.0 mL) was allowed to stir at room temperature for 22 hours. The precipitate was rinsed with DCM to afford the title

compound as a white solid (0.0250 g, 39%). ^1H NMR [400 MHz, $\text{DMSO-}d_6$] δ 10.56 (s, 1H), 8.88 (br s, 2H), 8.04 (d, $J = 7.6$ Hz, 1H), 7.88 (dd, $J = 1.5, 7.9$ Hz, 1H), 7.60 (dt, $J = 1.5, 7.9$ Hz, 1H), 7.22 (dt, $J = 0.9, 7.6$ Hz, 1H), 4.38 (dd, $J = 3.4, 11.0$ Hz, 1H), 4.30 (q, $J = 7.1$ Hz, 2H), 3.28 (dd, $J = 3.5, 16.6$ Hz, 1H), 2.79 (dd, $J = 11.0, 16.5$ Hz, 1H), 1.32 (t, $J = 7.2$ Hz, 3H); ^{13}C NMR [100 MHz, $\text{DMSO-}d_6$] δ 188.7, 182.2, 168.9, 166.8, 138.6, 133.6, 130.4, 123.7, 122.0, 119.6, 61.1, 51.5, 40.4, 14.0; HRMS (ESI) $[\text{M}+\text{H}]^+$, calc'd for $\text{C}_{14}\text{H}_{16}\text{N}_3\text{O}_4\text{S}$ 322.08560; found 322.08566; HPLC purity: >95% $t_{\text{R}} = 0.607$ min. (85% MeOH/Water with 0.1% formic acid, isocratic, 1.0 mL/min.); $t_{\text{R}} = 0.526$ min. (75% MeCN/Water with 0.1% formic acid, isocratic, 1.0 mL/min.).

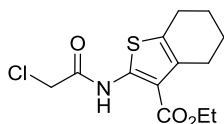


2-(2-(2-imino-4-oxothiazolidin-5-yl)acetamido)-4,5,6,7-tetrahydrobenzo[b]thiophene-3-

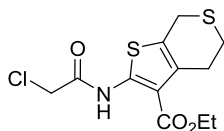
carboxylic acid, trifluoroacetic acid (1794-28). A suspension of compound **1794-27** (0.05 g, 0.1 mmol) in 3:1 DCM (0.45 mL) and TFA (0.15 mL) was heated in a microwave vial at 50 °C for 20 minutes. The reaction mixture was concentrated to a light orange-yellow solid and then washed several times with ether to afford the title compound as a light yellow solid (0.0470 g, 82%). ^1H NMR [400 MHz, $\text{DMSO-}d_6$] δ 11.25 (s, 1H), 9.30 (br s, 1H), 9.15 (s, 1H), 4.49 (dd, $J = 3.7, 9.8$ Hz, 1H), 3.39 (dd, $J = 3.7, 16.5$ Hz, 1H), 3.06 (dd, $J = 9.8, 16.5$ Hz, 1H), 2.70 (app. br s, 2H), 1.71-1.70 (m, 4H); ^{13}C NMR [100 MHz, $\text{DMSO-}d_6$] (^{13}C resonance obstructed by solvent peak) δ 186.5, 181.1, 167.4, 166.7, 158.4 (q, $J_{\text{C-F}} = 38$ Hz), 145.4, 131.0, 125.8, 115.4 (q, $J_{\text{C-F}} = 289$ Hz), 112.4, 50.7, 25.9, 23.7, 22.6, 22.3; HRMS (ESI) $[\text{M}+\text{H}]^+$, calc'd for $\text{C}_{14}\text{H}_{16}\text{N}_3\text{O}_4\text{S}_2$ 354.05767, found 354.05747; IR (solid ATR): 2938, 1763, 1673, 1638, 1538, 1463, 1288, 1254, 1192, 1135 cm^{-1} ; HPLC purity: >95% $t_{\text{R}} = 3.070$ min. (50-95% MeOH/Water with 0.1% formic acid, gradient over 5 minutes, 1.0 mL/min.).



ethyl 2-(2-chloroacetamido)-6-methyl-4,5,6,7-tetrahydrobenzo[*b*]thiophene-3-carboxylate (21b). Compound **21b** was prepared according to procedure G using compound **11b** (0.3 g, 1.1 mmol). The crude material was recrystallized from absolute ethanol to afford the title compound as an off-white solid (0.190 g, 58%). ^1H NMR [400 MHz, CDCl_3] δ 12.12 (s, 1H), 4.37 (q, $J = 7.1$ Hz, 2H), 4.26 (s, 2H), 2.94-2.98 (m, 1H), 2.66-2.74 (m, 2H), 2.24-2.30 (m, 1H), 1.87-1.90 (m, 2H), 1.39 (t, $J = 7.0$ Hz, 4H), 1.07 (d, $J = 6.7$ Hz, 3H); ^{13}C NMR [100 MHz, CDCl_3] δ 166.3, 163.6, 146.1, 131.2, 127.5, 113.1, 60.9, 42.5, 32.6, 31.2, 29.4, 26.3, 21.6, 14.5; HRMS (ESI) $[\text{M}+\text{H}]^+$, calc'd for $\text{C}_{14}\text{H}_{19}\text{ClNO}_3\text{S}$ 316.07687, found 316.07688; Elem. Anal. calc'd for $\text{C}_{14}\text{H}_{18}\text{ClNO}_3\text{S}$, C, 53.24; H, 5.74; N, 4.44, found 53.07; H, 5.74; N, 4.27.

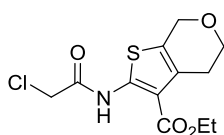


ethyl 2-(2-chloroacetamido)-4,5,6,7-tetrahydrobenzo[*b*]thiophene-3-carboxylate (21c). Compound **21c** was prepared according to procedure G using compound **11c** (2.0 g, 8.9 mmol). The crude material was purified by flash column chromatography (ISCO, 80 g silica gel, 0-15% EtOAc-Hexanes over 25 minutes) to afford the title compound as a light yellow solid (2.51 g, 94%). ^1H NMR [400 MHz, CDCl_3] δ 12.12 (s, 1H), 4.36 (q, $J = 7.1$ Hz, 2H), 4.25 (s, 2H), 2.77-2.79 (m, 2H), 2.64-2.67 (m, 2H), 1.79-1.81 (m, 4H), 1.39 (t, $J = 7.0$ Hz, 3H); ^{13}C NMR [100 MHz, CDCl_3] δ 166.3, 163.6, 146.0, 131.5, 127.8, 113.2, 60.9, 42.5, 26.5, 24.6, 23.1, 22.9, 14.5; HRMS (ESI) $[\text{M}+\text{H}]^+$, calc'd for $\text{C}_{13}\text{H}_{17}\text{ClNO}_3\text{S}$ 302.06122, found 302.06092; Elem. Anal. calc'd for $\text{C}_{13}\text{H}_{16}\text{ClNO}_3\text{S}$, C, 51.74; H, 5.34; N, 4.64, found C, 51.99; H, 5.40; N, 4.42.



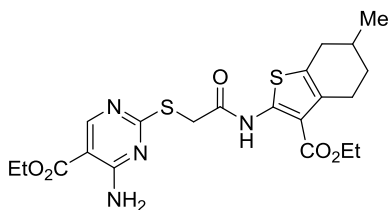
ethyl 2-(2-chloroacetamido)-4,7-dihydro-5H-thieno[2,3-c]thiopyran-3-carboxylate (21d).

Compound **21d** was prepared according to procedure G using compound **11d** (1.0 g, 4.1 mmol). The crude material was filtered over a pad of silica gel to afford the title compound as an orange solid (1.19 g, 91%). ¹H NMR [400 MHz, CDCl₃] δ 12.16 (br s, 1H), 4.38 (q, *J* = 7.1 Hz, 2H), 4.27 (s, 2H), 3.72 (br s, 2H), 3.10 (t, *J* = 5.8 Hz, 2H), 2.91 (t, *J* = 5.8 Hz, 2H), 1.40 (t, *J* = 7.0 Hz, 3H); ¹³C NMR [100 MHz, CDCl₃] δ 165.9, 163.8, 145.8, 131.2, 123.8, 113.6, 61.2, 42.4, 28.3, 26.4, 25.4, 14.5; HRMS (ESI) [M+H]⁺, calc'd for C₁₂H₁₅ClNO₃S₂ 320.01764, found 320.01736.



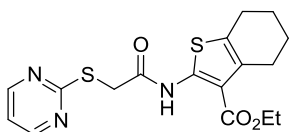
ethyl 2-(2-chloroacetamido)-4,7-dihydro-5H-thieno[2,3-c]pyran-3-carboxylate (21e).

Compound **21e** was prepared according to procedure G using compound **11e** (1.0 g, 4.4 mmol). The crude material was filtered over a pad of silica gel to afford the title compound as a yellow solid (1.19 g, 89%). ¹H NMR [400 MHz, CDCl₃] δ 12.08 (br s, 1H), 4.69 (s, 2H), 4.37 (q, *J* = 7.1 Hz, 2H), 4.27 (s, 2H), 3.94 (t, *J* = 5.5 Hz, 2H), 2.89 (s, 2H), 1.39 (t, *J* = 7.0 Hz, 3H); ¹³C NMR [100 MHz, CDCl₃] δ 165.9, 163.7, 146.7, 129.2, 125.3, 112.8, 65.2, 64.8, 61.1, 42.4, 27.1, 14.5; HRMS (ESI) [M+H]⁺, calc'd for C₁₂H₁₄ClNO₄S 304.04048, found 304.04056.



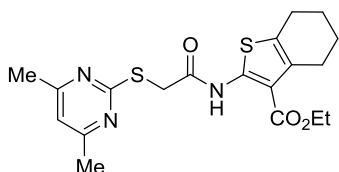
Ethyl 4-amino-2-((2-((3-(ethoxycarbonyl)-6-methyl-4,5,6,7-tetrahydrobenzo[*b*]thiophen-2-yl)amino)-2-oxoethyl)thio)pyrimidine-5-carboxylate (1794-3). Compound **1794-3** was prepared according to procedure H using compound **21b** (0.1 g, 0.3 mmol) and ethyl 4-amino-2-

mercaptopyrimidine-5-carboxylate (0.06 g, 0.3 mmol). The crude material was purified by flash column chromatography (ISCO, 12 g silica gel, 0-35% EtOAc-Hexanes over 15 minutes) to afford the title compound as an off-white solid (0.0865 g, 60%). ^1H NMR [400 MHz, CDCl_3] δ 11.83 (br s, 1H), 8.71 (s, 1H), 7.92 (br s, 1H), 6.67 (br s, 1H), 4.29-4.36 (m, 4H), 3.91 (d, J = 1.3 Hz, 2H), 2.88-2.92 (m, 1H), 2.59-2.72 (m, 2H), 2.20-2.26 (m, 1H), 1.83-1.86 (m, 2H), 1.35-1.40 (m, 7H), 1.04 (d, J = 6.7 Hz, 3H); ^{13}C NMR [100 MHz, CDCl_3] δ 173.9, 166.6, 166.4 (2C), 162.6, 159.5, 147.5, 131.7, 127.1, 112.1, 101.8, 61.2, 60.8, 35.1, 32.6, 31.3, 29.3, 26.3, 21.5, 14.5, 14.4; HRMS (ESI) $[\text{M}+\text{H}]^+$, calc'd for $\text{C}_{21}\text{H}_{27}\text{N}_4\text{O}_5\text{S}_2$ 479.14174, found 479.14128; IR (solid ATR): 2938, 1763, 1673, 1638, 1538, 1463, 1288, 1254, 1192, 1135, 3388, 3133, 2947, 1700, 1686, 1668, 1634, 1566, 1529, 1473, 1434, 1408, 1366, 1338, 1326, 1302, 1263, 1233, 1214, 1195, 1142, 1107, 1061, 1030, 967, 870, 842, 807, 783, 755, 721, 671 cm^{-1} ; Elem. Anal. calc'd for $\text{C}_{21}\text{H}_{26}\text{N}_4\text{O}_5\text{S}_2$, C, 52.70; H, 5.48; N, 11.71, found C, 52.91; H, 5.56; N, 11.43.

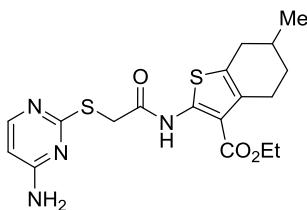


ethyl 2-(2-(pyrimidin-2-ylthio)acetamido)-4,5,6,7-tetrahydrobenzo[b]thiophene-3-carboxylate (1794-6). Compound **1794-6** was prepared according to procedure H using compound **21c** (0.1 g, 0.3 mmol) and pyrimidine-2-thiol (0.04 g, 0.3 mmol). The crude material was purified by flash column chromatography (ISCO, 12 g silica gel, 0-27% EtOAc-Hexanes over 15 minutes) to afford the title compound as a light yellow solid (0.0849 g, 72%). ^1H NMR [400 MHz, CDCl_3] δ 11.98 (br s, 1H), 8.59 (d, J = 4.9 Hz, 2H), 7.02 (t, J = 4.9 Hz, 1H), 4.29 (q, J = 7.1 Hz, 2H), 4.03 (s, 2H), 2.72-2.74 (m, 2H), 2.60-2.63 (m, 2H), 1.75-1.78 (m, 4H), 1.34 (t, J = 7.0, 3H); ^{13}C NMR [100 MHz, CDCl_3] δ 170.5, 166.3, 165.9, 157.9 (2C), 146.9, 131.1, 127.3, 117.3, 112.5, 60.5, 34.9, 26.5, 24.5, 23.1, 23.0, 14.5; HRMS (ESI) $[\text{M}+\text{H}]^+$, calc'd for $\text{C}_{17}\text{H}_{20}\text{N}_3\text{O}_3\text{S}_2$ 378.09406, found 378.09353; IR (solid ATR): 3252, 2925, 2847, 1662, 1562,

1549, 1528, 1441, 1378, 1240, 1200, 1139, 1086, 1029, 814, 776, 744, 674, 631 cm^{-1} ; Elem. Anal. calc'd for $\text{C}_{17}\text{H}_{19}\text{N}_3\text{O}_3\text{S}_2$, C, 54.09; H, 5.07; N, 11.13, found C, 53.98; H, 5.11; N, 10.98.

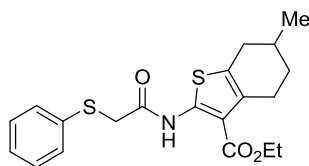


ethyl **2-(2-((4,6-dimethylpyrimidin-2-yl)thio)acetamido)-4,5,6,7-tetrahydrobenzo[b]thiophene-3-carboxylate (1794-7)**. Compound **1794-7** was prepared according to procedure H using compound **21c** (0.2 g, 0.5 mmol) and 4,6-dimethylpyrimidine-2-thiol (0.07 g, 0.5 mmol). The crude material was purified by flash column chromatography (ISCO, 12 g silica gel, 0-25% EtOAc-Hexanes over 25 minutes) to afford the title compound as an off-white solid (0.0534 g, 28%). ^1H NMR [400 MHz, CDCl_3] δ 11.75 (s, 1H), 6.72 (s, 1H), 4.26 (q, $J = 7.1$ Hz, 2H), 4.07 (s, 2H), 2.72-2.75 (m, 2H), 2.61-2.63 (m, 2H), 2.40 (s, 6H), 1.75-1.78 (m, 4H), 1.32 (t, $J = 7.2$ Hz, 3H); ^{13}C NMR [100 MHz, CDCl_3] δ 168.9, 167.8 (2C), 166.6, 165.8, 147.0, 131.1, 121.1, 116.6, 112.2, 60.5, 35.0, 26.5, 24.5, 24.0, 23.1, 23.0 (2C), 14.5; HRMS (ESI) $[\text{M}+\text{H}]^+$, calc'd for $\text{C}_{19}\text{H}_{24}\text{N}_3\text{O}_3\text{S}_2$ 406.12536, found 406.12469; IR (solid ATR): 3227, 2934, 2360, 1668, 1581, 1564, 1528, 1434, 1404, 1365, 1339, 1322, 1266, 1209, 1140, 1113, 1094, 1035, 954, 895, 859, 784, 726, 636, 620 cm^{-1} ; Elem. Anal. calc'd for $\text{C}_{19}\text{H}_{23}\text{N}_3\text{O}_3\text{S}_2$, C, 56.27; H, 5.72; N, 10.36, found C, 56.63; H, 5.79; N, 10.22.

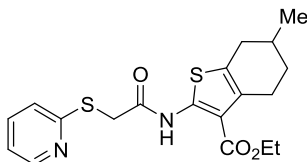


ethyl **2-(2-((4-aminopyrimidin-2-yl)thio)acetamido)-6-methyl-4,5,6,7-tetrahydrobenzo[b]thiophene-3-carboxylate (1794-9)**. Compound **1794-9** was prepared according to procedure H using compound **21b** (0.3 g, 0.8 mmol) and 4-aminopyrimidine-2-thiol (0.1 g, 0.8 mmol). The crude material was recrystallized in absolute ethanol to afford the title

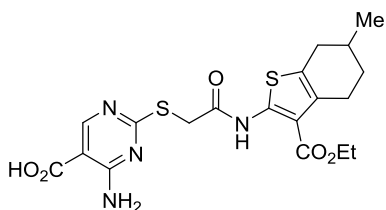
compound as an off-white solid (0.195 g, 61%). ^1H NMR [400 MHz, CDCl_3] δ 11.86 (br s, 1H), 8.04 (d, $J = 6.1$ Hz, 1H), 6.13 (d, $J = 5.5$ Hz, 1H), 5.45 (br s, 2H), 4.30 (q, $J = 7.1$ Hz, 2H), 3.91 (app. q, $J = 14.6$ Hz, 2H), 2.88-2.93 (m, 1H), 2.60-2.72 (m, 2H), 2.20-2.26 (m, 1H), 1.83-1.86 (m, 2H), 1.36 (t, $J = 7.0$ Hz, 4H), 1.05 (d, $J = 6.7$ Hz, 3H); ^{13}C NMR [100 MHz, CDCl_3] δ 169.6, 167.1, 166.3, 163.2, 156.4, 147.4, 130.7, 127.0, 112.2, 101.6, 60.6, 34.8, 32.6, 31.3, 29.4, 26.3, 21.5, 14.5; HRMS (ESI) $[\text{M}+\text{H}]^+$, calc'd for $\text{C}_{18}\text{H}_{23}\text{N}_4\text{O}_3\text{S}_2$ 407.12061, found 407.11990; HPLC purity: >95% $t_{\text{R}} = 1.278$ min. (85% MeOH/Water with 0.1% formic acid, isocratic, 1.0 mL/min.) ; $t_{\text{R}} = 1.149$ min. (75% MeCN/Water with 0.1% formic acid, isocratic, 1.0 mL/min.).



ethyl 6-methyl-2-(2-(phenylthio)acetamido)-4,5,6,7-tetrahydrobenzo[b]thiophene-3-carboxylate (1794-12). Compound **1794-12** was prepared according to procedure H using compound **21b** (0.3 g, 0.8 mmol) and thiophenol (0.08 mL, 0.8 mmol). The crude material was recrystallized in absolute ethanol to afford the title compound as an off-white solid (0.205 g, 67%). ^1H NMR [400 MHz, CDCl_3] δ 12.19 (br s, 1H), 7.37-7.40 (m, 2H), 7.23-7.27 (m, 2H), 7.16-7.20 (m, 1H), 4.33 (q, $J = 7.1$ Hz, 2H), 3.81 (s, 2H), 2.89-2.95 (m, 1H), 2.59-2.71 (m, 2H), 2.19-2.26 (m 1H), 1.79-1.86 (m 2H), 1.35 (t, $J = 7.0$ Hz, 3H), 1.03 (d, $J = 6.1$ Hz, 3H); ^{13}C NMR [100 MHz, CDCl_3] δ 166.1, 166.0, 146.7, 134.3, 131.0, 129.9 (2C), 129.5 (2C), 127.4, 127.0, 112.5, 60.7, 38.72, 32.6, 31.3, 29.4, 26.3, 21.6, 14.6; HRMS (ESI) $[\text{M}+\text{H}]^+$, calc'd for $\text{C}_{20}\text{H}_{24}\text{NO}_3\text{S}_2$ 390.11921, found 390.11874; IR (solid ATR): 3217, 2952, 2916, 2164, 2036, 1655, 1561, 1519, 1473, 1437, 1383, 1324, 1291, 1274, 1232, 1190, 1109, 1069, 1028, 992, 927, 880, 779, 752, 736, 693 cm^{-1} ; HPLC purity: >95% $t_{\text{R}} = 1.293$ min. (95% MeOH/Water with 0.1% formic acid, isocratic, 1.0 mL/min.); $t_{\text{R}} = 1.190$ min. (95% MeCN/Water with 0.1% formic acid, isocratic, 1.0 mL/min.).

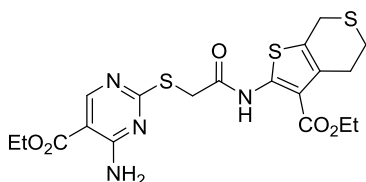


ethyl 6-methyl-2-(2-(pyridin-2-ylthio)acetamido)-4,5,6,7-tetrahydrobenzo[b]thiophene-3-carboxylate (1794-13). Compound **1794-13** was prepared according to procedure H using compound **21b** (0.3 g, 0.8 mmol) and pyridine-2-thiol (0.09 g, 0.8 mmol). The crude material was recrystallized in absolute ethanol to afford the title compound as an off-white solid (0.0989 g, 32%). ^1H NMR [400 MHz, CDCl_3] δ 11.94 (br s, 1H), 8.45 (dt, $J = 1.5, 4.7$ Hz, 1H), 7.43 (td, $J = 1.8, 7.6$ Hz, 1H), 7.19 (d, $J = 1.8$ Hz, 1H), 6.92-6.95 (m, 1H), 4.22 (q, $J = 7.1$ Hz, 2H), 4.00 (s, 2H), 2.80-2.85 (m, 1H), 2.51-2.65 (m, 2H), 2.13-2.19 (m, 1H), 1.72-1.79 (m, 2H), 1.27 (t, $J = 7.0$ Hz, 4H), 0.97 (d, $J = 6.1$ Hz, 3H); ^{13}C NMR [100 MHz, CDCl_3] δ 166.9, 165.9, 156.4, 150.1, 147.1, 136.4, 130.8, 126.9, 122.2, 120.2, 112.3, 60.4, 33.8, 32.6, 31.3, 29.4, 26.3, 21.6, 14.6; HRMS (ESI) $[\text{M}+\text{H}]^+$, calc'd for $\text{C}_{19}\text{H}_{23}\text{N}_2\text{O}_3\text{S}_2$ 391.11446, found 391.11406; IR (solid ATR): 3214, 2950, 2360, 2340, 1980, 1666, 1579, 1559, 1523, 1454, 1430, 1413, 1368, 1324, 1292, 1273, 1234, 1191, 1139, 1117, 1033, 988, 872, 783, 764, 717, 620 cm^{-1} ; HPLC purity: >95% $t_{\text{R}} = 1.140$ min. (95% MeOH/Water with 0.1% formic acid, isocratic, 1.0 mL/min.); $t_{\text{R}} = 1.130$ min. (95% MeCN/Water with 0.1% formic acid, isocratic, 1.0 mL/min.).



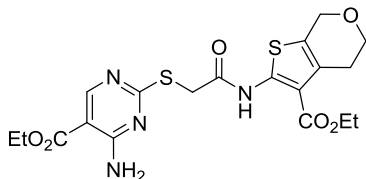
4-amino-2-((2-((3-(ethoxycarbonyl)-6-methyl-4,5,6,7-tetrahydrobenzo[b]thiophen-2-yl)amino)-2-oxoethyl)thio)pyrimidine-5-carboxylic acid (1794-14). Compound **1794-14** was prepared according to procedure H using compound **21b** (0.3 g, 0.8 mmol) and compound **24** (0.1 g, 0.8 mmol). The crude material was heated in absolute ethanol and then filtered while hot to afford the title compound as an off-white solid (0.235 g, 66%). ^1H NMR [400 MHz, $\text{DMSO}-d_6$] δ

13.25 (br s, 1H), 11.68 (s, 1H), 8.60 (s, 1H), 7.97 (br s, 1H), 7.86 (br s, 1H), 4.25 (q, $J = 7.1$ Hz, 2H), 4.07 (s, 2H), 2.80-2.84 (m, 1H), 2.69 (dd, $J = 4.6, 16.2$ Hz, 1H), 2.55-2.58 (m, 1H), 2.15 (dd, $J = 9.8, 15.9$ Hz, 1H), 1.75-1.78 (m, 2H), 1.26 (t, $J = 7.0$ Hz, 4H), 0.98 (d, $J = 6.1$ Hz, 3H); ^{13}C NMR [100 MHz, DMSO- d_6] δ 172.0, 167.4, 166.0, 164.9, 161.9, 159.1, 145.9, 130.1, 126.0, 111.5, 101.8, 60.4, 34.0, 31.7, 30.5, 28.6, 25.6, 21.1, 14.1; HRMS (ESI) $[\text{M}+\text{H}]^+$, calc'd for $\text{C}_{19}\text{H}_{23}\text{NO}_3\text{S}_2$ 451.11044, found 451.10981; IR (solid ATR): 3432, 3390, 3220, 2947, 2361, 2340, 2036, 1669, 1609, 1561, 1525, 1433, 1409, 1382, 1343, 1326, 1295, 1273, 1227, 1184, 1139, 1118, 1029, 974, 888, 809, 782, 764, 721, 688 cm^{-1} ; HPLC purity: >95% $t_{\text{R}} = 1.671$ min. (85% MeOH/Water with 0.1% formic acid, isocratic, 1.0 mL/min.); $t_{\text{R}} = 1.225$ min. (75% MeCN/Water with 0.1% formic acid, isocratic, 1.0 mL/min.).

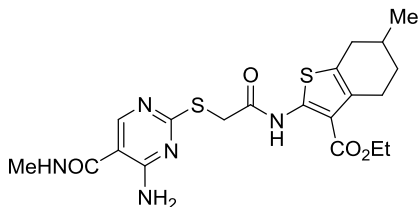


ethyl 4-amino-2-((2-((3-(ethoxycarbonyl)-4,7-dihydro-5H-thieno[2,3-c]thiopyran-2-yl)amino)-2-oxoethyl)thio)pyrimidine-5-carboxylate (1794-16). Compound **1794-16** was prepared according to procedure H using compound **21d** (0.3 g, 0.8 mmol) and ethyl 4-amino-2-mercaptopyrimidine-5-carboxylate (0.2 g, 0.8 mmol). The crude material was heated in absolute ethanol and then filtered while hot to afford the title compound as a light brown solid (0.308 g, 82%). ^1H NMR [400 MHz, CDCl_3] δ 11.90 (br s, 1H), 8.72 (s, 1H), 7.94 (br s, 1H), 6.55 (br s, 1H), 4.34 (q, $J = 7.2$ Hz, 2H), 4.33 (q, $J = 7.2$ Hz, 2H), 3.93 (s, 2H), 3.70 (s, 2H), 3.06 (t, $J = 6.0$ Hz, 2H), 2.89 (t, $J = 5.7$ Hz, 2H), 1.38 (t, $J = 7.1$ Hz, 3H), 1.37 (t, $J = 7.0$ Hz, 3H); ^{13}C NMR [100 MHz, CDCl_3] δ 173.8, 166.7, 166.5, 166.2, 162.6, 159.6, 147.1, 130.7, 123.5, 112.7, 101.9, 61.3, 61.0, 35.0, 28.3, 26.5, 25.4, 14.5, 14.4; HRMS (ESI) $[\text{M}+\text{H}]^+$, calc'd for $\text{C}_{19}\text{H}_{23}\text{N}_4\text{O}_5\text{S}_3$ 483.08251, found 483.08280; IR (solid ATR): 3408, 3226, 2986, 2360, 1697, 1670, 1636, 1572, 1522, 1478, 1424, 1362, 1324, 1301, 1245, 1202, 1157, 1123, 1095, 1045, 1018, 965, 890, 783,

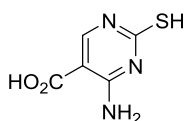
755, 709, 616 cm^{-1} ; HPLC purity: >95% $t_R = 1.649$ min. (85% MeOH/Water with 0.1% formic acid, isocratic, 1.0 mL/min.); $t_R = 1.656$ min. (75% MeCN/Water with 0.1% formic acid, isocratic, 1.0 mL/min.).



ethyl 4-amino-2-((2-((3-(ethoxycarbonyl)-4,7-dihydro-5H-thieno[2,3-c]pyran-2-yl)amino)-2-oxoethyl)thio)pyrimidine-5-carboxylate (1794-17). Compound **1794-17** was prepared according to procedure H using compound **21e** (0.3 g, 0.8 mmol) and ethyl 4-amino-2-mercaptopyrimidine-5-carboxylate (0.2 g, 0.8 mmol). The crude material was heated in absolute ethanol and then filtered while hot to afford the title compound as a light brown solid (0.315 g, 82%). ^1H NMR [400 MHz, CDCl_3] δ 11.85 (br s, 1H), 8.73 (s, 1H), 7.94 (br s, 1H), 6.58 (br s, 1H), 4.69 (br s, 2H), 4.34 (q, $J = 7.2$ Hz, 2H), 4.33 (q, $J = 7.2$ Hz, 2H), 3.92 (app. t, $J = 5.4$ Hz, 4H), 2.86 (t, $J = 5.4$ Hz, 2H), 1.39 (t, $J = 7.0$ Hz, 3H), 1.37 (t, $J = 7.1$ Hz, 3H); ^{13}C NMR [100 MHz, CDCl_3] δ 173.8, 166.7, 166.5, 166.2, 162.6, 159.6, 148.1, 128.8, 125.0, 112.0, 101.9, 65.2, 64.8, 61.3, 61.0, 34.9, 27.2, 14.5, 14.4.; HRMS (ESI) $[\text{M}+\text{H}]^+$, calc'd for $\text{C}_{19}\text{H}_{23}\text{N}_4\text{O}_6\text{S}_2$ 467.10535, found 467.10544; IR (solid ATR): 3398, 3222, 2985, 2832, 2360, 2340, 1698, 1670, 1640, 1573, 1524, 1479, 1439, 1362, 1325, 1295, 1253, 1200, 1158, 112, 1092, 1046, 1022, 967, 892, 869, 781, 754, 711, 670 cm^{-1} ; HPLC purity: >95% $t_R = 1.133$ min. (85% MeOH/Water with 0.1% formic acid, isocratic, 1.0 mL/min.); $t_R = 1.157$ min. (75% MeCN/Water with 0.1% formic acid, isocratic, 1.0 mL/min.).

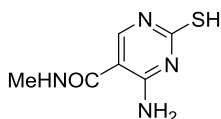


ethyl 2-(2-((5-acetamido-4-aminopyrimidin-2-yl)thio)acetamido)-6-methyl-4,5,6,7-tetrahydrobenzo[b]thiophene-3-carboxylate (1794-18). Compound **1794-18** was prepared according to procedure H using compound **21b** (0.3 g, 0.8 mmol) and compound **25** (0.1 g, 0.8 mmol). The crude material was heated in absolute ethanol and then filtered while hot to afford the title compound as a white solid (0.307 g, 81%). ^1H NMR [400 MHz, $\text{DMSO-}d_6$] δ 11.66 (br s, 1H), 8.46-8.49 (m, 2H), 8.19 (br s, 1H), 7.73 (br s, 1H), 4.26 (q, $J = 7.0$ Hz, 2H), 4.08 (s, 2H), 2.82-2.86 (m, 1H), 2.73 (d, $J = 4.3$ Hz, 3H), 2.64-2.69 (m, 1H), 2.57-2.59 (m, 1H), 2.14-2.20 (m, 1H), 1.78 (m, 2H), 1.27 (t, $J = 7.0$ Hz, 4H), 0.99 (d, $J = 6.4$ Hz, 3H); ^{13}C NMR [100 MHz, $\text{DMSO-}d_6$] δ 169.9, 166.2, 166.1, 164.9, 161.6, 155.0, 146.0, 130.2, 125.9, 111.4, 105.0, 60.4, 34.1, 31.7, 30.5, 28.7, 25.9, 25.6, 21.1, 14.1; HRMS (ESI) $[\text{M}+\text{H}]^+$, calc'd for $\text{C}_{20}\text{H}_{26}\text{N}_5\text{O}_4\text{S}_2$ 464.14207, found 464.14175; IR (solid ATR): 3427, 3391, 3340, 3262, 2946, 1641, 1600, 1572, 1556, 1521, 1475, 1439, 1407, 1382, 1324, 1280, 1236, 1206, 1150, 1033, 993, 954, 871, 820, 802, 783, 755, 718, 620 cm^{-1} ; HPLC purity: >95% $t_{\text{R}} = 1.571$ min. (85% MeOH/Water with 0.1% formic acid, isocratic, 1.0 mL/min.); $t_{\text{R}} = 1.369$ min. (75% MeCN/Water with 0.1% formic acid, isocratic, 1.0 mL/min.).

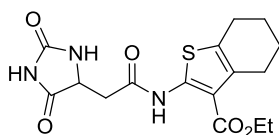


4-amino-2-mercaptopyrimidine-5-carboxylic acid (24). A mixture of 10% aqueous KOH (10.0 mL) and ethyl 4-amino-2-mercaptopyrimidine-5-carboxylate (0.5 g, 2.3 mmol) was refluxed for 30 minutes. The reaction mixture was acidified with 1M aqueous HCl (pH 2-3). The precipitate was filtered and washed with water. The crude off-white solid (0.394 g, quant.) was carried on

without further purification. HRMS (ESI) $[M+H]^+$, calc'd for $C_5H_6N_3O_2S$ 172.01752, found 172.01725.

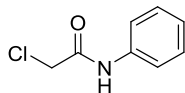


4-amino-2-mercapto-*N*-methylpyrimidine-5-carboxamide (25). A suspension of ethyl 4-amino-2-mercaptopyrimidine-5-carboxylate (0.5 g, 2.5 mmol) in methylamine 40% in water (20.0 mL, 258 mmol) was heated in a sealed tube at 100 °C for 5 hours. The reaction mixture was evaporated under reduced pressure, and water was added to the residue. The crude white solid (0.286 g, 62%) was carried on without further purification. 1H NMR [400 MHz, $DMSO-d_6$] δ 12.52 (br s, 1H), 8.53 (br s, 1H), 8.43 (d, $J = 4.7$ Hz, 1H), 8.27 (br s, 1H), 8.05 (s, 1H), 2.68 (d, $J = 4.7$ Hz, 3H); ^{13}C NMR [100 MHz, $DMSO-d_6$] δ 179.4, 165.2, 160.3, 143.5, 100.1, 25.8; HRMS (ESI) $[M+H]^+$, calc'd for $C_6H_9N_4OS$ 185.04916, found 185.04921.

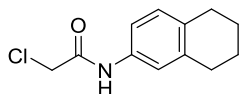


ethyl 2-(2-(2,5-dioxoimidazolidin-4-yl)acetamido)-4,5,6,7-tetrahydrobenzo[*b*]thiophene-3-carboxylate (1794-26). A mixture of 2-(2,5-dioxoimidazolidin-4-yl)acetic acid (0.8 g, 5.0 mmol) and thionyl chloride (0.7 mL, 10.0 mmol) in dioxane (3.0 mL) was heated under reflux for 30 minutes. The reaction mixture was cooled and then treated with 10.0 mL of hexanes. The precipitate was separated by filtration and carried on without further purification. A solution of the crude acid chloride (0.9 g, 5.0 mmol) dissolved in dioxane (5.0 mL) was added to a solution of compound **11c** (1.1 g, 5.0 mmol) and TEA (0.5 mL, 3.5 mmol) dissolved in dioxane (5.0 mL). The reaction suspension was heated to 100 °C for 30 minutes. The reaction was cooled to room temperature and then treated with 50.0 mL of water. The precipitate was filtered and then rinsed several times with DCM to afford the title compound as a light yellow solid (0.142 g, 8%). 1H NMR [400 MHz, $DMSO-d_6$] δ 10.99 (s, 1H), 10.67 (s, 1H), 7.90 (s, 1H), 4.34-4.31 (m, 1H), 4.28

(q, $J = 7.1$ Hz, 2H), 3.01-2.89 (m, 2H), 2.72-2.66 (m, 2H), 2.61-2.55 (m, 2H), 1.76-1.67 (m, 4H), 1.31 (t, $J = 7.1$ Hz, 3H); ^{13}C NMR [100 MHz, DMSO- d_6] δ 175.3, 166.4, 164.8, 157.6, 145.5, 130.4, 126.2, 111.6, 60.4, 54.4, 37.4, 25.8, 23.7, 22.5, 22.3, 14.1; HRMS (ESI) $[\text{M}+\text{H}]^+$, calc'd for $\text{C}_{16}\text{H}_{20}\text{N}_3\text{O}_5\text{S}$ 366.11182, found 366.11172; HPLC purity: >95% $t_{\text{R}} = 1.357$ min. (75-95% MeOH/Water with 0.1% formic acid, gradient over 5 minutes, 1.0 mL/min.).

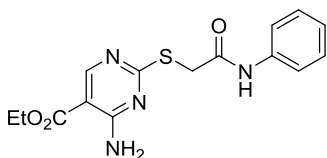


2-chloro-*N*-phenylacetamide (29). To a solution of aniline (0.3 mL, 3.0 mmol) dissolved in DCM (20.0 mL) was added TEA (0.4 mL, 3.0 mmol). The reaction was chilled to 0 °C then added 2-chloroacetyl chloride (0.2 mL, 3.00 mmol). The reaction was warmed to room temperature and allowed to stir for 16 hours. The reaction was quenched with 1M aqueous HCl and further diluted with water. The mixture was extracted with DCM, washed with brine, and dried over MgSO_4 . The crude off-white solid (0.509 g, quant.) was carried on without further purification. ^1H NMR [400 MHz, CDCl_3] δ 8.30 (br s, 1H), 7.55 (d, $J = 7.3$ Hz, 2H), 7.37, (t, $J = 7.9$ Hz, 2H), 7.18 (t, $J = 7.5$ Hz, 1H), 4.19 (s, 2H); ^{13}C NMR [100 MHz, CDCl_3] δ 164.0, 136.8, 129.3 (2C), 125.4, 120.3 (2C), 43.1; HRMS (ESI) $[\text{M}+\text{H}]^+$, calc'd for $\text{C}_8\text{H}_9\text{ClNO}$ 170.03672, found 170.03693.

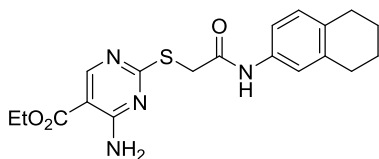


2-chloro-*N*-(5,6,7,8-tetrahydronaphthalen-2-yl)acetamide (30). To a solution of 5,6,7,8-tetrahydronaphthalen-2-amine (0.4 g, 3.0 mmol) dissolved in DCM (20.0 mL) was added TEA (0.4 mL, 3.0 mmol). The reaction was chilled to 0 °C then added 2-chloroacetyl chloride (0.2 mL, 3.00 mmol). The reaction was warmed to room temperature and allowed to stir for 16 hours. The reaction was quenched with 1M aqueous HCl and further diluted with water. The mixture was extracted with DCM, washed with brine, and dried over MgSO_4 . The crude brown solid (0.615 g, 92%) was carried on without further purification. ^1H NMR [400 MHz, CDCl_3] δ 8.11

(br s, 1H), 7.18 (d, $J = 3.1$ Hz, 1H), 7.14 (dd, $J = 2.3, 8.1$ Hz, 1H), 6.95 (d, $J = 7.9$ Hz, 1H), 4.08 (s, 2H), 2.65-2.67 (m, 4H), 1.70 (quintet, $J = 3.3$ Hz, 4H); ^{13}C NMR [100 MHz, CDCl_3] δ 164.0, 138.2, 134.6, 134.1, 129.8, 120.9, 117.9, 43.1, 29.6, 29.1, 23.3, 23.2; HRMS (ESI) $[\text{M}+\text{H}]^+$, calc'd for $\text{C}_{12}\text{H}_{15}\text{ClNO}$ 224.08367, found 224.08398.



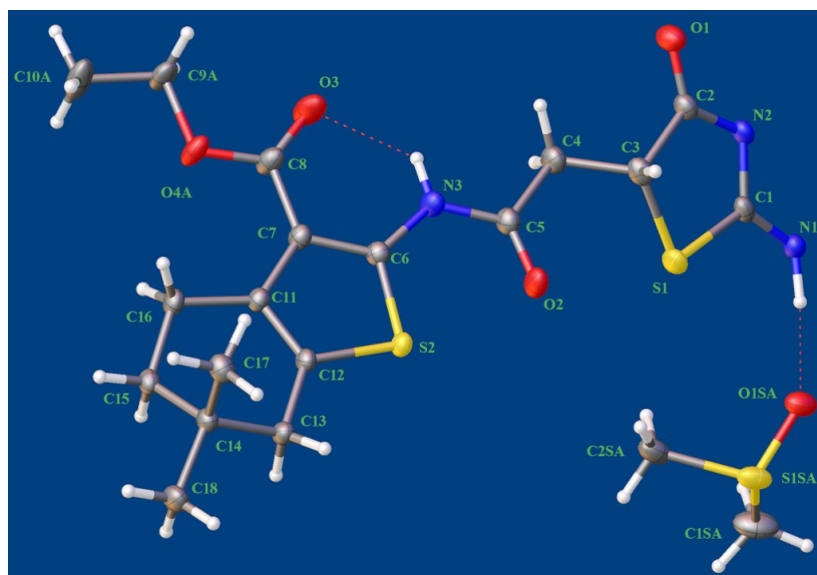
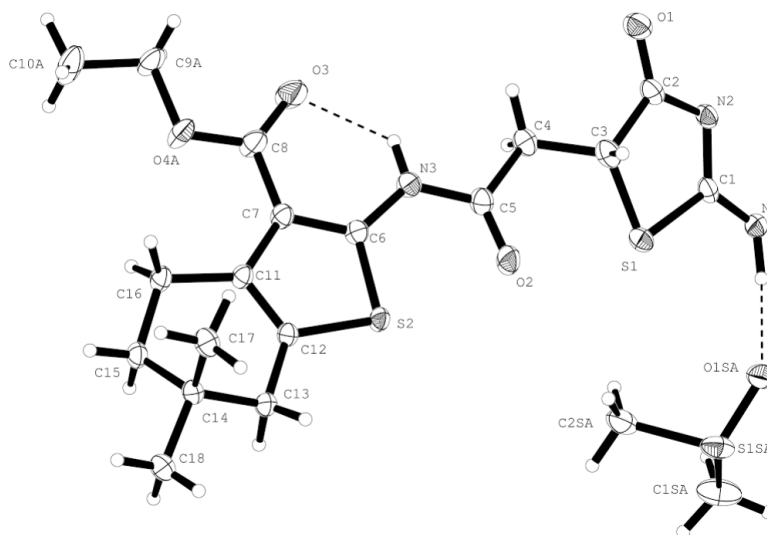
ethyl 4-amino-2-((2-oxo-2-(phenylamino)ethyl)thio)pyrimidine-5-carboxylate (1794-10). To a suspension of ethyl 4-amino-2-mercaptopyrimidine-5-carboxylate (0.1 g, 0.6 mmol) in a 1:1 ratio of water (3.0 mL) and EtOH (3.0 mL) was added sodium carbonate (0.1 g, 0.9 mmol). The reaction was allowed to stir for 30 minutes before adding compound **29** (0.1 g, 0.6 mmol). The reaction was heated to 50 °C where it stirred for 16 hours. The reaction mixture was poured over 1M aqueous HCl (20.0 mL) in crushed ice. The crude solid obtained by vacuum filtration was purified by flash column chromatography (ISCO, 4 g silica gel, 0-50% EtOAc-Hexanes over 15 minutes) to afford the title compound as a white solid (0.136 g, 68%). ^1H NMR [400 MHz, CDCl_3] δ 9.24 (br s, 1H), 8.69 (s, 1H), 7.91 (s, 1H), 7.39 (d, $J = 7.6$ Hz, 2H), 7.21 (t, $J = 7.9$ Hz, 2H), 7.00 (t, $J = 7.3$ Hz, 1H), 5.94 (br s, 1H), 4.30 (q, $J = 7.1$ Hz, 2H), 3.77 (s, 2H), 1.33 (t, $J = 7.2$ Hz, 3H); ^{13}C NMR [100 MHz, CDCl_3] δ 174.2, 167.5, 166.0, 162.0, 159.1, 138.1, 129.2 (2C), 124.5, 119.9 (2C), 102.5, 61.5, 35.6, 14.4; HRMS (ESI) $[\text{M}+\text{H}]^+$, calc'd for $\text{C}_{15}\text{H}_{17}\text{N}_4\text{O}_3\text{S}$ 333.10159, found 333.10202; IR (solid ATR): 3406, 3267, 3129, 2978, 2360, 2165, 1691, 1667, 1632, 1602, 1566, 1535, 1498, 1467, 1442, 1366, 1316, 1242, 1206, 1171, 1100, 962, 906, 880, 863, 803, 755, 714, 691, 672 cm^{-1} ; HPLC purity: >95% $t_{\text{R}} = 1.278$ min. (85% MeOH/Water with 0.1% formic acid, isocratic, 1.0 mL/min.); $t_{\text{R}} = 0.650$ min. (75% MeCN/Water with 0.1% formic acid, isocratic, 1.0 mL/min.).



ethyl 4-amino-2-((2-oxo-2-((5,6,7,8-tetrahydronaphthalen-2-yl)amino)ethyl)thio)pyrimidine-5-carboxylate (1794-11). To a suspension of ethyl 4-amino-2-mercaptopyrimidine-5-carboxylate (0.2 g, 1.3 mmol) in a 1:1 ratio of water (5.0 mL) and EtOH (5.0 mL) was added sodium carbonate (0.2 g, 2.0 mmol). The reaction was allowed to stir for 30 minutes before adding compound **30** (0.2 g, 0.9 mmol). The reaction was heated to 50 °C where it stirred for 72 hours. The solvent was removed under vacuum and DMF was added to assist in solubility. The reaction was heated to 50 °C for 16 hours. The suspension was dissolved in EtOAc and washed with water and brine. The organic extracts were dried over anhydrous MgSO₄ and concentrated. The crude material was purified by flash column chromatography (ISCO, 12 g silica gel, 0-35% EtOAc-Hexanes over 20 minutes) to afford the title compound as an off-white solid (0.197 g, 60%). ¹H NMR [400 MHz, CDCl₃] δ 9.07 (br s, 1H), 8.76 (s, 1H), 7.97 (br s, 1H), 7.23 (d, *J* = 1.5 Hz, 1H), 7.11 (dd, *J* = 1.9 Hz, 7.9 Hz, 1H), 6.97 (d, *J* = 8.2 Hz, 1H), 5.96 (br s, 1H), 4.37 (q, *J* = 7.1 Hz, 2H), 3.84 (s, 2H), 2.70-2.72 (m, 4H), 1.74-1.77 (m, 4H), 1.40 (t, *J* = 7.0 Hz, 3H); ¹³C NMR [100 MHz, CDCl₃] δ 174.2, 167.2, 166.1, 162.1, 159.2, 138.0, 135.3, 133.6, 129.7, 120.6, 117.6, 102.4, 61.5, 35.6, 29.7, 29.1, 23.4, 23.3, 14.5; HRMS (ESI) [M+H]⁺, calc'd for C₁₉H₂₃N₄O₃S 387.14854, found 387.14788; IR (solid ATR): 3414, 3275, 3136, 2928, 2361, 1691, 1658, 1632, 1567, 1529, 1464, 1418, 1366, 1308, 1244, 1211, 1192, 1172, 1099, 996, 962, 907, 871, 831, 802, 761, 671 cm⁻¹; HPLC purity: >95% *t*_R = 1.020 min. (85% MeOH/Water with 0.1% formic acid, isocratic, 1.0 mL/min.); *t*_R = 0.980 min. (75% MeCN/Water with 0.1% formic acid, isocratic, 1.0 mL/min.).

1.6.2 Crystal Structure Data

Compound **1794-20** X-ray Data (Dr. John Bacsá, Emory X-ray Crystallography Center, Department of Chemistry)



Crystal data for **1794-20** $C_{20}H_{28}N_3O_5S_3$, $M = 486.63$, colourless needle, $0.662 \times 0.162 \times 0.156$ mm³, Triclinic, space group $P -1$ (No. 2), $V = 1188.59(9)$ Å³, $Z = 2$, $D_c = 1.360$ g/cm³, $F_{000} = 514$, Bruker APEX-II CCD, CuK α radiation, $\lambda = 1.54184$ Å, $T = 173$ K, $2\theta_{max} = 139.0^\circ$, 16104 reflections collected, 6309 unique ($R_{int} = 0.0618$). Final $Goof = 1.043$, $R1 = 0.0464$, $wR2 = 0.1240$, R indices based on 5638 reflections with $I > 2\sigma(I)$ (refinement on F^2), 352

parameters, 38 restraints. Lp and absorption corrections applied, $\mu = 3.158 \text{ mm}^{-1}$.

Table 1. Crystal data and structure refinement for twin5_FIN.

Identification code	twin5	
Empirical formula	C ₂₀ H ₂₈ N ₃ O ₅ S ₃	
Formula weight	486.63	
Temperature	173 K	
Wavelength	1.54184 Å	
Crystal system	Triclinic	
Space group	P -1	
Unit cell dimensions	a = 5.6270(2) Å	$\alpha = 88.030(3)^\circ$
	b = 10.3897(4) Å	$\beta = 82.954(3)^\circ$
	c = 20.5153(10) Å	$\gamma = 87.388(4)^\circ$
Volume	1188.59(9) Å ³	
Z	2	
Density (calculated)	1.360 Mg/m ³	
Absorption coefficient	3.158 mm ⁻¹	
F(000)	514	
Crystal size	0.662 x 0.162 x 0.156 mm ³	
Theta range for data collection	4.26 to 69.49°.	
Index ranges	-6 ≤ h ≤ 6, -12 ≤ k ≤ 12, 0 ≤ l ≤ 24	
Reflections collected	16104	
Independent reflections	6309 [R(int) = 0.0618]	
Completeness to theta = 69.49°	94.3 %	
Absorption correction	Semi-empirical from equivalents	
Max. and min. transmission	0.753215 and 0.53685	
Refinement method	Full-matrix least-squares on F ²	
Data / restraints / parameters	6309 / 38 / 352	
Goodness-of-fit on F ²	1.043	
Final R indices [I > 2σ(I)]	R1 = 0.0464, wR2 = 0.1240	
R indices (all data)	R1 = 0.0518, wR2 = 0.1287	
Largest diff. peak and hole	0.497 and -0.382 e.Å ⁻³	

Table 2. Atomic coordinates ($\times 10^4$) and equivalent isotropic displacement parameters ($\text{\AA}^2 \times 10^3$) for twin5_FIN. U(eq) is defined as one third of the trace of the orthogonalized U_{ij} tensor.

	x	y	z	U(eq)
S(1)	9628(1)	4944(1)	1340(1)	39(1)
S(2)	2400(1)	6562(1)	3313(1)	30(1)
O(1)	13312(3)	7974(2)	1002(1)	48(1)
O(2)	6429(3)	6051(2)	2453(1)	50(1)
O(3)	3456(4)	10577(2)	2402(1)	68(1)
O(4A)	167(4)	11169(2)	3051(1)	46(1)
N(1)	12246(3)	3931(2)	295(1)	36(1)
N(2)	13169(3)	5986(2)	561(1)	33(1)
N(3)	5062(3)	8118(2)	2435(1)	37(1)
C(1)	11888(3)	4938(2)	665(1)	32(1)
C(2)	12474(4)	6903(2)	1011(1)	36(1)
C(3)	10527(4)	6500(2)	1565(1)	38(1)
C(4)	8502(4)	7504(2)	1664(1)	41(1)
C(5)	6608(4)	7140(2)	2221(1)	36(1)
C(6)	3081(4)	7998(2)	2902(1)	31(1)
C(7)	1452(4)	8986(2)	3095(1)	32(1)
C(8)	1791(5)	10287(2)	2804(1)	44(1)
C(9A)	446(7)	12468(3)	2756(2)	51(1)
C(10A)	-1633(9)	13252(4)	3058(2)	70(1)
C(11)	-391(4)	8563(2)	3596(1)	29(1)
C(12)	-87(4)	7296(2)	3763(1)	29(1)
C(13)	-1594(4)	6556(2)	4287(1)	34(1)
C(14)	-2991(3)	7494(2)	4780(1)	32(1)
C(15)	-4183(4)	8556(2)	4383(1)	33(1)
C(16)	-2438(4)	9373(2)	3938(1)	34(1)
C(17)	-1298(4)	8070(2)	5213(1)	40(1)
C(18)	-4907(4)	6759(2)	5218(1)	47(1)
O(4B)	-266(13)	10989(8)	2925(6)	46(1)
C(9B)	-790(30)	12287(8)	2658(6)	51(1)
C(10B)	330(30)	13260(12)	3014(6)	57(5)
S(1SA)	7731(2)	1245(1)	1239(1)	46(1)

O(1SA)	10084(7)	1781(5)	943(3)	47(1)
C(1SA)	6389(10)	567(5)	594(2)	70(2)
C(2SA)	5645(7)	2575(4)	1361(3)	53(2)
S(1SB)	8335(3)	806(2)	1054(1)	39(1)
O(1SB)	10503(12)	1582(9)	828(6)	59(3)
C(1SB)	7895(13)	-154(6)	382(3)	54(2)
C(2SB)	5827(10)	1902(8)	1025(4)	63(3)

Table 3. Bond lengths [Å] and angles [°] for twin5_FIN.

S(1)-C(1)	1.762(2)
S(1)-C(3)	1.807(2)
S(2)-C(6)	1.724(2)
S(2)-C(12)	1.740(2)
S(1SA)-C(1SA)	1.782(5)
S(1SA)-C(2SA)	1.776(4)
S(1SA)-O(1SA)	1.509(5)
S(1SB)-C(1SB)	1.777(7)
S(1SB)-O(1SB)	1.510(8)
S(1SB)-C(2SB)	1.778(7)
O(1)-C(2)	1.227(3)
O(2)-C(5)	1.215(3)
O(3)-C(8)	1.211(3)
O(4A)-C(8)	1.332(3)
O(4A)-C(9A)	1.467(4)
O(4B)-C(9B)	1.469(13)
O(4B)-C(8)	1.341(8)
N(1)-C(1)	1.307(3)
N(2)-C(2)	1.360(3)
N(2)-C(1)	1.330(3)
N(3)-C(5)	1.355(3)
N(3)-C(6)	1.385(3)
N(1)-H(1)	0.953(18)
N(3)-H(3A)	0.8600
C(2)-C(3)	1.540(3)
C(3)-C(4)	1.509(3)
C(4)-C(5)	1.515(3)
C(6)-C(7)	1.380(3)
C(7)-C(11)	1.440(3)
C(7)-C(8)	1.470(3)
C(9A)-C(10A)	1.479(6)
C(9B)-C(10B)	1.475(18)
C(11)-C(12)	1.357(3)
C(11)-C(16)	1.510(3)

C(12)-C(13)	1.499(3)
C(13)-C(14)	1.548(3)
C(14)-C(18)	1.530(3)
C(14)-C(15)	1.529(3)
C(14)-C(17)	1.532(3)
C(15)-C(16)	1.523(3)
C(3)-H(3)	1.02(3)
C(4)-H(4A)	1.01(3)
C(4)-H(4B)	1.01(3)
C(9A)-H(9AB)	0.9700
C(9A)-H(9AA)	0.9700
C(9B)-H(9BA)	0.9700
C(9B)-H(9BB)	0.9700
C(10A)-H(10A)	0.9600
C(10A)-H(10B)	0.9600
C(10A)-H(10C)	0.9600
C(10B)-H(10F)	0.9600
C(10B)-H(10E)	0.9600
C(10B)-H(10D)	0.9600
C(13)-H(13B)	0.9700
C(13)-H(13A)	0.9700
C(15)-H(15B)	0.9700
C(15)-H(15A)	0.9700
C(16)-H(16B)	0.9700
C(16)-H(16A)	0.9700
C(17)-H(17A)	0.9600
C(17)-H(17C)	0.9600
C(17)-H(17B)	0.9600
C(18)-H(18A)	0.9600
C(18)-H(18B)	0.9600
C(18)-H(18C)	0.9600
C(1SA)-H(1SF)	0.9600
C(1SA)-H(1SD)	0.9600
C(1SA)-H(1SE)	0.9600
C(2SA)-H(2SD)	0.9600
C(2SA)-H(2SE)	0.9600

C(2SA)-H(2SF)	0.9600
C(1SB)-H(1SA)	0.9600
C(1SB)-H(1SB)	0.9600
C(1SB)-H(1SC)	0.9600
C(2SB)-H(2SA)	0.9600
C(2SB)-H(2SB)	0.9600
C(2SB)-H(2SC)	0.9600
C(1)-S(1)-C(3)	90.07(10)
C(6)-S(2)-C(12)	90.86(10)
C(1SA)-S(1SA)-C(2SA)	96.0(2)
O(1SA)-S(1SA)-C(1SA)	107.8(3)
O(1SA)-S(1SA)-C(2SA)	106.9(3)
C(1SB)-S(1SB)-C(2SB)	98.4(4)
O(1SB)-S(1SB)-C(2SB)	105.4(4)
O(1SB)-S(1SB)-C(1SB)	106.1(5)
C(8)-O(4A)-C(9A)	114.8(2)
C(8)-O(4B)-C(9B)	126.6(9)
C(1)-N(2)-C(2)	112.43(17)
C(5)-N(3)-C(6)	125.32(19)
C(1)-N(1)-H(1)	123.1(16)
C(6)-N(3)-H(3A)	117.00
C(5)-N(3)-H(3A)	117.00
N(1)-C(1)-N(2)	123.13(18)
S(1)-C(1)-N(2)	116.90(15)
S(1)-C(1)-N(1)	119.97(15)
N(2)-C(2)-C(3)	114.96(18)
O(1)-C(2)-N(2)	124.7(2)
O(1)-C(2)-C(3)	120.38(19)
S(1)-C(3)-C(4)	114.25(16)
S(1)-C(3)-C(2)	105.26(14)
C(2)-C(3)-C(4)	111.84(17)
C(3)-C(4)-C(5)	112.47(18)
O(2)-C(5)-N(3)	121.9(2)
N(3)-C(5)-C(4)	114.89(18)
O(2)-C(5)-C(4)	123.2(2)
N(3)-C(6)-C(7)	125.03(19)

S(2)-C(6)-N(3)	122.59(16)
S(2)-C(6)-C(7)	112.38(16)
C(6)-C(7)-C(11)	111.89(18)
C(6)-C(7)-C(8)	119.6(2)
C(8)-C(7)-C(11)	128.5(2)
O(3)-C(8)-C(7)	124.4(2)
O(3)-C(8)-O(4A)	121.5(2)
O(4B)-C(8)-C(7)	108.9(4)
O(4A)-C(8)-C(7)	114.0(2)
O(3)-C(8)-O(4B)	124.8(5)
O(4A)-C(9A)-C(10A)	105.7(3)
O(4B)-C(9B)-C(10B)	110.2(11)
C(7)-C(11)-C(12)	112.18(19)
C(12)-C(11)-C(16)	120.64(19)
C(7)-C(11)-C(16)	127.15(18)
C(11)-C(12)-C(13)	126.5(2)
S(2)-C(12)-C(13)	120.82(15)
S(2)-C(12)-C(11)	112.67(16)
C(12)-C(13)-C(14)	110.07(17)
C(13)-C(14)-C(15)	107.57(17)
C(13)-C(14)-C(17)	110.65(16)
C(13)-C(14)-C(18)	109.09(17)
C(15)-C(14)-C(17)	110.59(17)
C(15)-C(14)-C(18)	109.82(16)
C(17)-C(14)-C(18)	109.10(18)
C(14)-C(15)-C(16)	114.46(18)
C(11)-C(16)-C(15)	111.85(17)
C(2)-C(3)-H(3)	109.1(14)
S(1)-C(3)-H(3)	108.0(12)
C(4)-C(3)-H(3)	108.3(13)
H(4A)-C(4)-H(4B)	105(2)
C(3)-C(4)-H(4B)	109.3(16)
C(3)-C(4)-H(4A)	112.4(14)
C(5)-C(4)-H(4B)	112.1(16)
C(5)-C(4)-H(4A)	105.1(16)
O(4A)-C(9A)-H(9AA)	111.00

C(10A)-C(9A)-H(9AB)	111.00
C(10A)-C(9A)-H(9AA)	111.00
H(9AA)-C(9A)-H(9AB)	109.00
O(4A)-C(9A)-H(9AB)	111.00
O(4B)-C(9B)-H(9BB)	110.00
C(10B)-C(9B)-H(9BA)	109.00
O(4B)-C(9B)-H(9BA)	110.00
H(9BA)-C(9B)-H(9BB)	108.00
C(10B)-C(9B)-H(9BB)	110.00
C(9A)-C(10A)-H(10A)	109.00
H(10A)-C(10A)-H(10B)	110.00
C(9A)-C(10A)-H(10C)	110.00
C(9A)-C(10A)-H(10B)	109.00
H(10A)-C(10A)-H(10C)	109.00
H(10B)-C(10A)-H(10C)	109.00
H(10D)-C(10B)-H(10E)	110.00
C(9B)-C(10B)-H(10F)	109.00
H(10E)-C(10B)-H(10F)	109.00
H(10D)-C(10B)-H(10F)	109.00
C(9B)-C(10B)-H(10E)	110.00
C(9B)-C(10B)-H(10D)	110.00
C(14)-C(13)-H(13A)	110.00
C(12)-C(13)-H(13B)	110.00
H(13A)-C(13)-H(13B)	108.00
C(14)-C(13)-H(13B)	110.00
C(12)-C(13)-H(13A)	110.00
C(16)-C(15)-H(15B)	109.00
C(14)-C(15)-H(15A)	109.00
H(15A)-C(15)-H(15B)	108.00
C(16)-C(15)-H(15A)	109.00
C(14)-C(15)-H(15B)	109.00
H(16A)-C(16)-H(16B)	108.00
C(11)-C(16)-H(16B)	109.00
C(11)-C(16)-H(16A)	109.00
C(15)-C(16)-H(16A)	109.00
C(15)-C(16)-H(16B)	109.00

H(17A)-C(17)-H(17B)	110.00
C(14)-C(17)-H(17C)	109.00
H(17A)-C(17)-H(17C)	109.00
H(17B)-C(17)-H(17C)	109.00
C(14)-C(17)-H(17A)	109.00
C(14)-C(17)-H(17B)	109.00
H(18B)-C(18)-H(18C)	109.00
C(14)-C(18)-H(18A)	109.00
H(18A)-C(18)-H(18C)	109.00
H(18A)-C(18)-H(18B)	109.00
C(14)-C(18)-H(18B)	110.00
C(14)-C(18)-H(18C)	109.00
S(1SA)-C(1SA)-H(1SE)	109.00
H(1SD)-C(1SA)-H(1SF)	109.00
S(1SA)-C(1SA)-H(1SF)	109.00
H(1SD)-C(1SA)-H(1SE)	110.00
S(1SA)-C(1SA)-H(1SD)	109.00
H(1SE)-C(1SA)-H(1SF)	109.00
S(1SA)-C(2SA)-H(2SF)	109.00
H(2SD)-C(2SA)-H(2SF)	109.00
H(2SE)-C(2SA)-H(2SF)	109.00
H(2SD)-C(2SA)-H(2SE)	109.00
S(1SA)-C(2SA)-H(2SD)	110.00
S(1SA)-C(2SA)-H(2SE)	109.00
S(1SB)-C(1SB)-H(1SA)	109.00
S(1SB)-C(1SB)-H(1SB)	109.00
S(1SB)-C(1SB)-H(1SC)	110.00
H(1SA)-C(1SB)-H(1SB)	109.00
H(1SA)-C(1SB)-H(1SC)	109.00
H(1SB)-C(1SB)-H(1SC)	109.00
S(1SB)-C(2SB)-H(2SA)	109.00
S(1SB)-C(2SB)-H(2SB)	109.00
S(1SB)-C(2SB)-H(2SC)	109.00
H(2SA)-C(2SB)-H(2SB)	110.00
H(2SA)-C(2SB)-H(2SC)	109.00
H(2SB)-C(2SB)-H(2SC)	109.00

Table 4. Anisotropic displacement parameters ($\text{\AA}^2 \times 10^3$) for twin5_FIN. The anisotropic displacement factor exponent takes the form: $-2\pi^2 [h^2 a^{*2} U^{11} + \dots + 2 h k a^* b^* U^{12}]$

	U^{11}	U^{22}	U^{33}	U^{23}	U^{13}	U^{12}
S(1)	37(1)	42(1)	35(1)	5(1)	13(1)	-2(1)
S(2)	33(1)	27(1)	28(1)	-4(1)	3(1)	3(1)
O(1)	46(1)	47(1)	49(1)	-7(1)	8(1)	-10(1)
O(2)	51(1)	42(1)	49(1)	3(1)	21(1)	10(1)
O(3)	91(1)	41(1)	61(1)	12(1)	33(1)	2(1)
O(4A)	75(1)	26(1)	33(1)	2(1)	7(1)	12(1)
N(1)	33(1)	33(1)	40(1)	3(1)	5(1)	1(1)
N(2)	28(1)	37(1)	31(1)	4(1)	6(1)	0(1)
N(3)	43(1)	35(1)	30(1)	-1(1)	8(1)	0(1)
C(1)	24(1)	41(1)	29(1)	7(1)	3(1)	6(1)
C(2)	30(1)	44(1)	32(1)	2(1)	3(1)	-1(1)
C(3)	35(1)	49(1)	27(1)	1(1)	1(1)	0(1)
C(4)	38(1)	45(1)	37(1)	-3(1)	8(1)	0(1)
C(5)	37(1)	40(1)	31(1)	-5(1)	2(1)	1(1)
C(6)	35(1)	32(1)	26(1)	-4(1)	0(1)	-1(1)
C(7)	38(1)	30(1)	27(1)	-3(1)	1(1)	2(1)
C(8)	63(2)	32(1)	34(1)	2(1)	9(1)	3(1)
C(9A)	72(3)	29(2)	46(2)	13(1)	11(2)	10(2)
C(10A)	96(3)	51(2)	51(2)	19(2)	18(2)	35(2)
C(11)	33(1)	28(1)	27(1)	-4(1)	-1(1)	2(1)
C(12)	29(1)	29(1)	29(1)	-6(1)	2(1)	1(1)
C(13)	34(1)	29(1)	38(1)	-2(1)	5(1)	0(1)
C(14)	29(1)	33(1)	33(1)	-4(1)	3(1)	1(1)
C(15)	29(1)	34(1)	37(1)	-9(1)	-1(1)	3(1)
C(16)	37(1)	31(1)	33(1)	-6(1)	1(1)	6(1)
C(17)	36(1)	50(1)	34(1)	-4(1)	-2(1)	0(1)
C(18)	39(1)	45(1)	50(1)	-1(1)	14(1)	-3(1)
O(4B)	75(1)	26(1)	33(1)	2(1)	7(1)	12(1)
C(9B)	72(3)	29(2)	46(2)	13(1)	11(2)	10(2)
C(10B)	79(10)	46(8)	42(7)	5(6)	-4(7)	14(8)
S(1SA)	47(1)	47(1)	46(1)	17(1)	-12(1)	-19(1)

O(1SA)41(2)	46(3)	56(2)	10(2)	-12(2)	-13(2)
C(1SA)77(3)	77(4)	62(3)	5(3)	-23(3)	-42(3)
C(2SA)37(2)	59(3)	63(3)	24(2)	-7(2)	-13(2)
S(1SB)30(1)	40(1)	45(1)	10(1)	-3(1)	-2(1)
O(1SB)38(3)	44(4)	94(7)	8(4)	-6(3)	-16(3)
C(1SB)58(4)	65(5)	41(3)	13(3)	-9(3)	-34(4)
C(2SB)37(3)	75(6)	70(5)	24(4)	5(3)	18(4)

Table 5. Hydrogen coordinates ($\times 10^4$) and isotropic displacement parameters ($\text{\AA}^2 \times 10^3$) for twin5_FIN.

	x	y	z	U(eq)
H(3)	11270(40)	6380(20)	1992(14)	45
H(3A)	5332	8874	2266	44
H(4A)	7620(50)	7630(20)	1267(14)	49
H(4B)	9180(50)	8370(30)	1728(14)	49
H(1)	11480(40)	3139(15)	402(14)	58
H(9AA)	450	12452	2283	61
H(9AB)	1934	12816	2850	61
H(13A)	-578	5965	4517	41
H(13B)	-2714	6056	4088	41
H(15A)	-5239	8162	4114	40
H(15B)	-5165	9117	4685	40
H(16A)	-3288	9830	3611	41
H(16B)	-1802	10008	4198	41
H(17A)	-622	7396	5473	60
H(17B)	-2176	8689	5496	60
H(17C)	-35	8488	4939	60
H(18A)	-5981	6401	4950	70
H(18B)	-5791	7338	5523	70
H(18C)	-4153	6076	5456	70
H(10A)	-1552	14118	2880	105
H(10B)	-1608	13259	3525	105
H(10C)	-3088	12889	2965	105
H(9BA)	-2513	12459	2701	61
H(9BB)	-187	12339	2194	61
H(10D)	-177	13164	3476	68
H(10E)	-134	14107	2862	68
H(10F)	2045	13140	2935	68
H(1SD)	4758	379	748	105
H(1SE)	7262	-213	458	105
H(1SF)	6425	1170	228	105

H(2SD)	5753	3121	972	80
H(2SE)	6001	3057	1726	80
H(2SF)	4052	2267	1452	80
H(1SA)	6447	-612	487	81
H(1SB)	9229	-759	297	81
H(1SC)	7770	390	-1	81
H(2SA)	5933	2335	602	94
H(2SB)	5815	2524	1361	94
H(2SC)	4377	1437	1096	94

Table 6. Torsion angles [°] for twin5_FIN.

C(3)-S(1)-C(1)-N(1)	176.28(17)
C(3)-S(1)-C(1)-N(2)	-3.43(16)
C(1)-S(1)-C(3)-C(2)	5.16(15)
C(1)-S(1)-C(3)-C(4)	128.23(16)
C(6)-S(2)-C(12)-C(11)	1.09(18)
C(12)-S(2)-C(6)-C(7)	-0.89(17)
C(6)-S(2)-C(12)-C(13)	-176.90(18)
C(12)-S(2)-C(6)-N(3)	178.80(19)
C(8)-O(4A)-C(9A)-C(10A)	175.3(3)
C(9A)-O(4A)-C(8)-C(7)	-178.8(2)
C(9A)-O(4A)-C(8)-O(3)	5.2(4)
C(2)-N(2)-C(1)-S(1)	0.0(2)
C(1)-N(2)-C(2)-O(1)	-176.7(2)
C(1)-N(2)-C(2)-C(3)	4.5(3)
C(2)-N(2)-C(1)-N(1)	-179.74(19)
C(5)-N(3)-C(6)-S(2)	3.5(3)
C(5)-N(3)-C(6)-C(7)	-176.9(2)
C(6)-N(3)-C(5)-C(4)	174.82(19)
C(6)-N(3)-C(5)-O(2)	-3.4(3)
N(2)-C(2)-C(3)-C(4)	-131.2(2)
N(2)-C(2)-C(3)-S(1)	-6.6(2)
O(1)-C(2)-C(3)-S(1)	174.55(18)
O(1)-C(2)-C(3)-C(4)	49.9(3)
C(2)-C(3)-C(4)-C(5)	-178.27(18)
S(1)-C(3)-C(4)-C(5)	62.3(2)
C(3)-C(4)-C(5)-N(3)	165.11(19)
C(3)-C(4)-C(5)-O(2)	-16.7(3)
N(3)-C(6)-C(7)-C(8)	-1.0(3)
N(3)-C(6)-C(7)-C(11)	-179.18(19)
S(2)-C(6)-C(7)-C(11)	0.5(2)
S(2)-C(6)-C(7)-C(8)	178.69(17)
C(6)-C(7)-C(11)-C(16)	178.5(2)
C(6)-C(7)-C(8)-O(3)	-1.2(4)
C(6)-C(7)-C(11)-C(12)	0.3(3)

C(6)-C(7)-C(8)-O(4A)	-177.1(2)
C(8)-C(7)-C(11)-C(12)	-177.7(2)
C(8)-C(7)-C(11)-C(16)	0.5(4)
C(11)-C(7)-C(8)-O(4A)	0.8(4)
C(11)-C(7)-C(8)-O(3)	176.7(2)
C(7)-C(11)-C(12)-C(13)	176.9(2)
C(16)-C(11)-C(12)-S(2)	-179.28(16)
C(7)-C(11)-C(16)-C(15)	173.5(2)
C(12)-C(11)-C(16)-C(15)	-8.5(3)
C(16)-C(11)-C(12)-C(13)	-1.4(3)
C(7)-C(11)-C(12)-S(2)	-1.0(2)
S(2)-C(12)-C(13)-C(14)	157.72(15)
C(11)-C(12)-C(13)-C(14)	-20.0(3)
C(12)-C(13)-C(14)-C(15)	48.7(2)
C(12)-C(13)-C(14)-C(17)	-72.2(2)
C(12)-C(13)-C(14)-C(18)	167.75(18)
C(13)-C(14)-C(15)-C(16)	-62.6(2)
C(17)-C(14)-C(15)-C(16)	58.3(2)
C(18)-C(14)-C(15)-C(16)	178.78(17)
C(14)-C(15)-C(16)-C(11)	41.5(2)

Symmetry transformations used to generate equivalent atoms:

Table 7. Hydrogen bonds for twin5_FIN [\AA and $^\circ$].

D-H...A	d(D-H)	d(H...A)	d(D...A)	$\angle(\text{DHA})$
N(1)-H(1)...O(1SA)	0.953(18)	1.90(2)	2.808(6)	158(2)
N(3)-H(3A)...O(3)	0.8600	2.0300	2.672(3)	131.00
C(3)-H(3)...S(2)#1	1.02(3)	2.87(3)	3.864(2)	164.6(17)
C(4)-H(4A)...O(1)#2	1.01(3)	2.56(3)	3.378(3)	139(2)
C(2SA)-H(2SF)...O(3)#30.9600		2.5800	3.109(6)	115.00
C(10A)-H(10A)...O(2)#40.9600		2.4500	3.314(5)	149.00
C(15)-H(15A)...S(2)#2	0.9700	2.8600	3.810(2)	168.00

Symmetry transformations used to generate equivalent atoms:

#1 _____ +1_
 #2 _____ -1_
 #3 _____
 #4 _____ -1_1_

1.7 Biology Experimental Detail

1.7.1 In Vitro Antagonism Assay (Dr. Stephen Traynelis Laboratory, Emory School of Medicine, Department of Pharmacology)

Expression of glutamate receptors in *Xenopus laevis* oocytes

All protocols involving the use of animals were approved by the Emory University IACUC. RNA was synthesized from linearized template cDNA for rat glutamate receptor subunits according to manufacturer specifications (Ambion). Quality of synthesized cRNA was assessed by gel electrophoresis, and quantity was estimated by spectroscopy and gel electrophoresis. Stage V and VI oocytes were surgically removed from the ovaries of large, well-fed and healthy *Xenopus laevis* anesthetized with 3-amino-benzoic acid ethyl ester (1-3 g/L) as previously described. Clusters of isolated oocytes were incubated with 292 U/mL Worthington (Freehold,

NJ) type IV collagenase or 1.3 mg/mL collagenase (Life Technologies, Gaithersburg, MD; 17018–029) for 2 hr in Ca^{2+} -free solution comprised of (in mM) NaCl, 1 KCl, 2.4 NaHCO_3 , 0.82 MgSO_4 , 10 HEPES, with slow agitation to remove the follicular cell layer. Oocytes were then washed extensively in the same solution and maintained in Barth's solution comprised of (in mM) 88 NaCl, 1 KCl, 2.4 NaHCO_3 , 10 HEPES, 0.82 MgSO_4 , 0.33 $\text{Ca}(\text{NO}_3)_2$, and 0.91 CaCl_2 and supplemented with 100 $\mu\text{g}/\text{mL}$ gentamycin, 10 $\mu\text{g}/\text{mL}$ streptomycin, and 10 $\mu\text{g}/\text{mL}$ penicillin. Oocytes were manually defolliculated and injected within 24 hrs of isolation with 3-5 ng of GluN1-1a (hereafter GluN1) subunit and 7-10 ng of GluN2 subunit in a 50 nL volume, or 5-10 ng in 50 nL of AMPA or kainate receptor cRNAs, and incubated in Barth's solution at 15°C for 1–7 d. Glass injection pipettes had tip sizes ranging from 10-20 microns, and were backfilled with mineral oil.

Two electrode voltage clamp recording from *Xenopus laevis* oocytes

Two electrode voltage clamp recordings were made 2–7 days post-injection as previously described. Oocytes were placed in a dual-track plexiglass recording chamber with a single perfusion line that splits in a Y-configuration to perfuse two oocytes. Dual recordings were made at room temperature (23 °C) using two Warner OC725B or OC725C two electrode voltage clamp amplifiers, arranged as recommended by the manufacturer. Glass microelectrodes (1-10 M Ω) were filled with 300 mM KCl (voltage electrode) or 3 M KCl (current electrode). The bath clamps communicated across silver chloride wires placed into each side of the recording chamber, both of which were assumed to be at a reference potential of 0 mV. Oocytes were perfused with a solution comprised of (in mM) 90 NaCl, 1 KCl, 10 HEPES, and 0.5 BaCl_2 ; pH was adjusted to 7.4 or 7.6 by addition of 1 M NaOH. Oocytes expressing GluNR/GluN2A were pre-incubated before recording in recording solution supplemented with 50 μM BAPTA-AM at room temperature. Oocytes were recorded under voltage clamp at -40 mV. Final concentrations for control application of glutamate (50-100 μM) plus glycine (30 μM) to oocytes expressing NMDA receptors were achieved by dilution from 100 and 30-100 mM stock solutions,

respectively. In addition, 10 μM final EDTA was obtained by adding a 1:1000 dilution of 10 mM EDTA, in order to chelate contaminant divalent ions such as extracellular Zn^{2+} . Homomeric GluA1 AMPA receptors were activated by 100 μM glutamate. Homomeric GluK6 kainate receptors were incubated in concanavalin A (10 μM) for 5 minutes, and activated by 100 μM glutamate. Concentration-response curves for experimental compounds acting on NMDA receptors were obtained by applying in successive fashion a maximally effective concentration of glutamate/glycine, followed by glutamate/glycine plus variable concentrations of experimental compounds. Concentration-response curves consisting of 5 to 8 concentrations were obtained in this manner. The baseline leak current at -40 mV was measured before and after recording, and the full recording linearly corrected for any change in leak current. Oocytes with glutamate-evoked responses smaller than 50 nA were not included in the analysis. The level of inhibition produced by experimental compounds was expressed as a percent of the initial glutamate response, and averaged together across oocytes from a single frog. Each experiment consisted of recordings from 3 to 10 oocytes obtained from a single frog. Results from >3 experiments using oocytes from 3 different frogs were pooled, and the percent responses at antagonist concentrations for each oocyte were fitted by the equation,

$$\text{Percent Response} = (100 - \text{minimum}) / (1 + ([\text{conc}] / IC_{50})^{nH}) + \text{minimum}$$

where *minimum* is the residual percent response in saturating concentration of the experimental compounds, IC_{50} is the concentration of antagonist that causes half of the achievable inhibition, and nH is a slope factor describing steepness of the inhibition curve. Minimum was constrained to be greater than or equal to 0.

1.7.2 Patch Clamp Recordings from Cerebellar Granule Cells (Dr. Stephen Traynelis Laboratory, Emory School of Medicine, Department of Pharmacology)

Primary culture of cerebellar granule cells was made from rat pups with age of P6-8 as described previously (Traynelis and Cull-Candy, 1991). Whole-cell voltage clamp recordings

were performed at -70 mV using electrodes with open tip resistances between 6-8 M Ω when filled with internal solution containing the following (in mM): 110 D-gluconic acid, 110 CsOH, 30 CsCl, 5 HEPES, 4 NaCl, 0.5 CaCl₂, 2 MgCl₂, 5 BAPTA, 2 Na₂ATP, and 0.3 NaGTP (pH 7.35 with CsOH). The extracellular recording solution was applied using a base solution comprised of (in mM): 150 NaCl, 10 HEPES, 3 KCl, 0.5 CaCl₂, 0.01 EDTA (pH 7.6 with NaOH). Rapid solution exchange was achieved using a two-barrel theta-glass pipet manipulated by a piezoelectric translator (whole-cell 10-90% solution exchange times were ~4 ms).

1.7.3 Lactate Dehydrogenase Assay (Dr. Stephen Traynelis Laboratory, Emory School of Medicine, Department of Pharmacology)

Primary hippocampus cultures were prepared from rat pups, P0-P1. On the sixth day *in vitro*, the cells were treated by replacing the media in each well with HBSS (Hank's balanced salt solution) containing 1.8 μ M CaCl₂, 2.5 μ M glucose and 10 mM HEPES, in addition to the specified test compounds or control. Treatments lasted one hour, at which point the media was replaced with typical culture media. After twenty four hours, the concentration of LDH in the culture media was determined, similarly to Koh and Choi, 1987, by adding 0.25 mL of treated media to 0.75 mL of the assay buffer (0.75 mM NADH, 4.6 μ M sodium pyruvate, 100 mM K₂PO₄, at a pH of 7.5). The mixture's absorbance of 340 nm was recorded for 45 minutes at 20 second intervals for each well. The slope of the absorbance readings was used as an approximation of the enzymatic activity of the individual wells and compared to controls.

Part 2:

Part 2: Discovery of Novel Tetrahydroisoquinoline (THIQ)-Based CXCR4 Antagonists and Conformational Analysis of Structurally Similar CXCR4 Antagonists

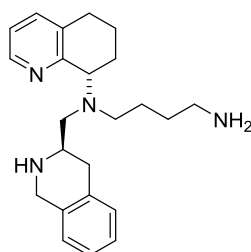
CHAPTER 2

Discovery of Novel Tetrahydroisoquinoline (THIQ)-Based CXCR4 Antagonists

2.1 Statement of Purpose

The G protein-coupled receptor (GPCR) CXCR4 has attracted significant attention over the past few years. This receptor partners with its natural chemokine ligand, CXCL12, and thus is connected to a divergent set of signaling pathways ranging from chemotaxis and cell survival to gene transcription and proliferation. These downstream signaling events govern a variety of cellular responses that are often selectively manipulated by various carcinomas to promote invasion, metastasis, and tumor longevity at the expense of the host. From a historical perspective, however, CXCR4 first drew attention due to its role in mediating HIV infection of T-cells by serving as a co-receptor for viral envelope protein gp120. Consequently, CXCR4 antagonists are heavily pursued for their potential to attenuate autoimmune diseases, cancer, and AIDS.

For the past several years, our laboratory has devoted efforts to identify novel small molecule CXCR4 antagonists that interfere with the chemokine signaling pathway and attenuate HIV infection. Recent research efforts have led to the discovery of a series of novel and potent CXCR4 antagonists that contain a 1,2,3,4-tetrahydroisoquinoline (THIQ) ring (Figure 2.1). The study presented herein aims to identify more potent analogues with improved pharmacokinetic properties. Additionally, our objective is to reveal requirements for binding through structure activity relationship (SAR) investigations.



ECXC00947

Figure 2.1 Structure of Potent CXCR4 Antagonist Developed in the Liotta Laboratory.

2.2 Introduction and Background

2.2.1 Chemokines and Chemokine Receptors

Chemokines belong to a family of small secreted proteins (molecular weight 8-10 kDa) that bind to the chemokine receptor subfamily of G protein-coupled receptors (GPCRs). They have traditionally been divided into four major groups (C, CC, CXC, and CX₃C) on the basis of the number and spacing of conserved cysteine residues within the amino (*N*)-termini of their protein sequences (Figure 2.2).⁶⁷ Functionally, chemokines are classified as being “homeostatic” or “inflammatory” based on their pivotal role in directing immune cell migration. A handful of chemokines exhibit characteristics of both categories, whereas homeostatic chemokines are expressed by certain cell types. Homeostatic chemokines direct the fate of mobilized cells during routine tissue maintenance and development and are key players in the regulation of lymphocyte trafficking and functional compartmentalization of lymphoid organs. In contrast, inflammatory chemokines mobilize cells to the site of infection and are secreted under conditions of cellular duress brought on by pro-inflammatory stimuli such as IL-1, TNF α , or viruses.

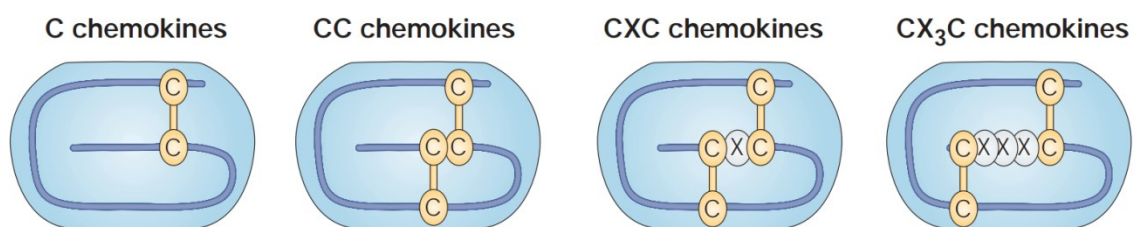


Figure 2.2 Family of Chemokine Receptors.⁶⁸

To date, approximately fifty chemokines have been identified with varying degrees of sequence homology.^{69,70} However, almost all chemokines, regardless of family, share a similar monomeric structure. Disulfide linkages between the four highly conserved cysteine residues (two residues in the case of C-chemokines) stabilize the tertiary protein structural motif common amongst all chemokines. The unstructured *N*-terminus is followed by the C, CC, CXC, or CX₃C

motif and connected *via* an exposed 10-20 residue *N-loop* to the highly structured core consisting of a single turn 3_{10} helix, three antiparallel β -strands, and a C-terminal α -helix (Figure 2.3).^{71,72} In addition to binding their receptors, soluble chemokines bind *via* their C-terminal α -helix to glycosaminoglycans (GAGs) on the surface of endothelial cells. This interaction not only serves as an anchor under the strong shear flow conditions in the blood vessels, but it also forms an immobilized chemotactic gradient, which directs passing immune cells toward the source of chemokine secretion.

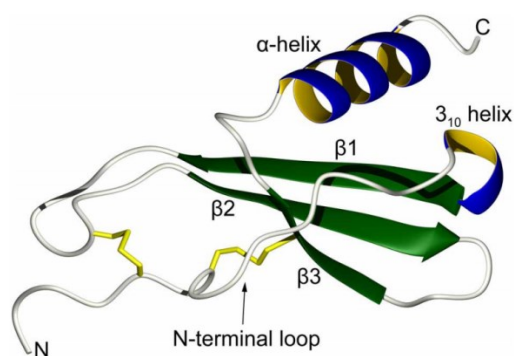


Figure 2.3 Topology of a Typical Chemokine⁷³

Chemokine receptors are characterized by a collection of seven-transmembrane (7TM) alpha helices that couple to peripheral G proteins associated with the inner leaflet of the plasma membrane that trigger numerous signaling cascades within the cell. While the majority of chemokine receptors bind to a variety of chemokines, some receptors are highly specific. The nineteen known chemokine receptors are categorized according to the subclass of chemokine ligands they bind, with one C, ten CC, seven CXC, and one CX3C chemokine-binding receptors (Figure 2.4).⁷⁴ Chemokine receptors share many common structural features; they are composed of approximately 340-370 amino acids that are divided into a short and acidic extracellular *N*-terminus, seven helical transmembrane domains (comprised of three intracellular and three extracellular loops), and a short intracellular C-terminal tail containing serine and threonine

residues that become phosphorylated upon ligand binding to the receptor. The unstructured *N*-terminal domain of the chemokine receptor imparts ligand specificity, while the C-terminal end interacts with a G protein. All chemokine receptors signal at least through heterotrimeric G proteins (primarily $G\alpha_i$ -coupled), with the exception of CXCR7, which is biased toward β -arrestin-mediated signaling.

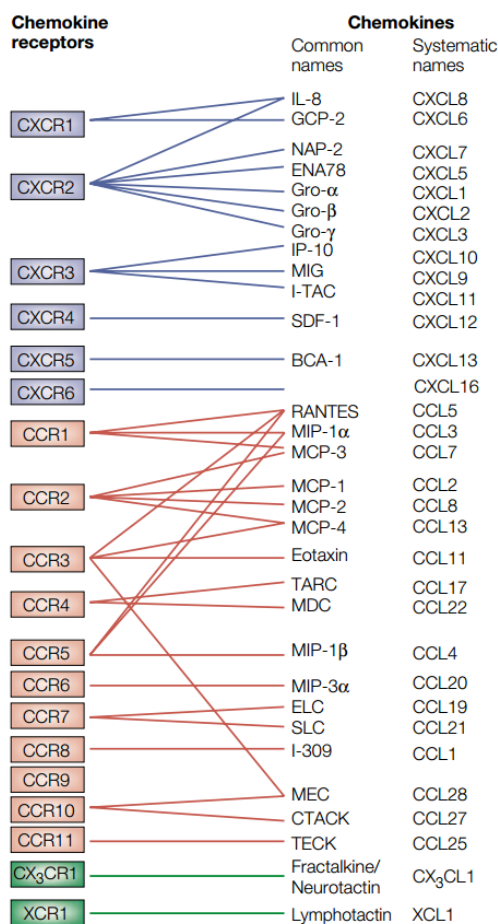


Figure 2.4 Chemokine Receptors and Their Ligands⁷⁴

The complexity of the chemokine network has increased with accumulating evidence for receptor dimerization. Studies have indicated that GPCRs can assemble into transient homo- and/or heteromeric complexes. The combinatorial assembly of different receptors and signaling

molecules increases variability among receptor subtypes and serves as a mechanism to increase both specificity and sensitivity to a given ligand while broadening the scope for varied and complex signaling responses.⁶⁷

2.2.2 *CXCR4 and its Ligand CXCL12*

The CXC chemokine receptor type 4 (CXCR4) is an integral membrane protein that belongs to the class A family of GPCRs.⁷⁵ Functional receptor is expressed on a variety of tissues and cell types, including leukocyte subpopulations,⁷⁶ hematopoietic progenitor cells, and non-hematopoietic cells like endothelial and epithelial cells. The receptor was originally cloned by a number of groups as an orphan chemokine receptor and was initially given the name LESTR or fusin. Upon the discovery that the CXC motif chemokine ligand 12 (CXCL12) was the biological ligand for LESTR/fusin, the receptor was renamed CXCR4.

CXCL12, also referred to as stromal cell-derived factor 1 (SDF-1), is the only natural ligand known to bind CXCR4.⁷⁷⁻⁷⁹ Like most chemokines, CXCL12 binds to another receptor, namely CXCR7. This homeostatic chemokine is expressed by both lymphoid (bone marrow, spleen, and thymus) and non-lymphoid (stomach, kidney, liver, lung, brain, and heart) organs. CXCL12 functions primarily as a chemoattractant to hematopoietic stem cells (HSC) where it is integral to the retention and homing of these cells in the bone marrow microenvironment.⁸⁰⁻⁸² The importance of CXCL12 and CXCR4 in growth and development was demonstrated in gene knockout experiments in mice.⁷⁴ CXCR4 and CXCL12 knockouts were embryonic lethal. These genetic disruptions resulted in compromised hematopoiesis revealed as a defect in the trafficking of HSC from the fetal liver to the embryonic bone marrow. Additionally, defects in heart and brain development and vascularization were observed.

Prior to 2010, structural information regarding CXCR4 was largely based on homology models constructed from other known GPCR crystal structures. However, in late 2010, Stevens and coworkers reported five independent crystal structures of CXCR4 bound to a small molecule

antagonist (**IT1t**) and a cyclic peptide (**CVX15**) antagonist at 2.5 Å to 3.9 Å resolution, respectively.⁸³ The homodimer structures revealed an interface with helices V and VI with implications for their involvement in regulating signaling (Figure 2.5). The location and shape of the ligand binding sites differed from other GPCRs in that they remained closer to the extracellular surface. The crystal structures have provided important clues about the interactions between CXCR4 and CXCL12. Likewise, several chemokine structures have also been determined *via* nuclear magnetic resonance (NMR) spectroscopy or X-ray crystallography, including CXCL12. These receptor and ligand “blueprints” have provided opportunities for researchers to implement structure-based drug design programs in lieu of the therapeutic implications of targeting the CXCR4/CXCL12 axis (*vide infra*).

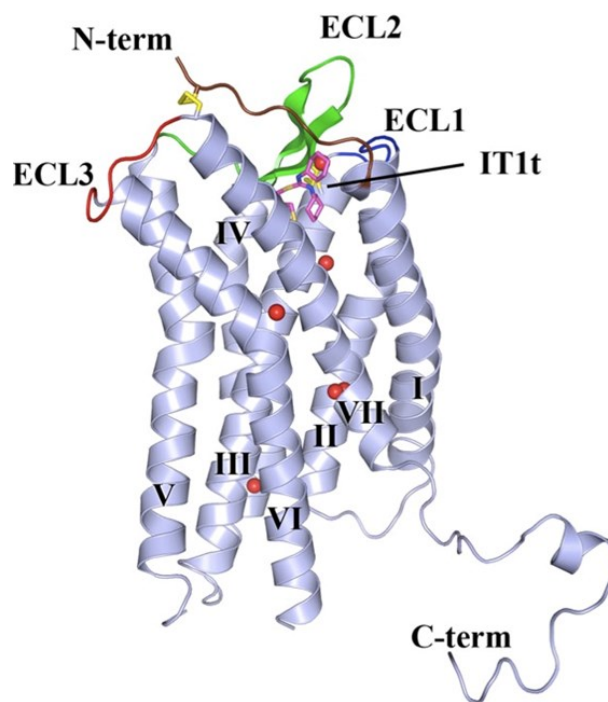


Figure 2.5 Cartoon Representation of CXCR4 Structure.⁸³

2.2.3 CXCR4/CXCL12 Signaling

The interaction of CXCL12 with CXCR4 (and all other chemokines with their receptors) is generally considered to occur through a two-step process (Figure 2.6).⁷⁷ In the first step, CXCL12 binds with its core region and *N-loop* (binding domain) to the *N*-terminus and extracellular loops (ECLs) of the receptor where it is anchored to the extracellular side of CXCR4. The flexible *N*-terminus of CXCL12 is positioned in such a way that it interacts with a second site formed by parts of the ECLs and transmembrane (TM) helices. This “fly casting” mechanism triggers conformational changes that result in receptor activation.

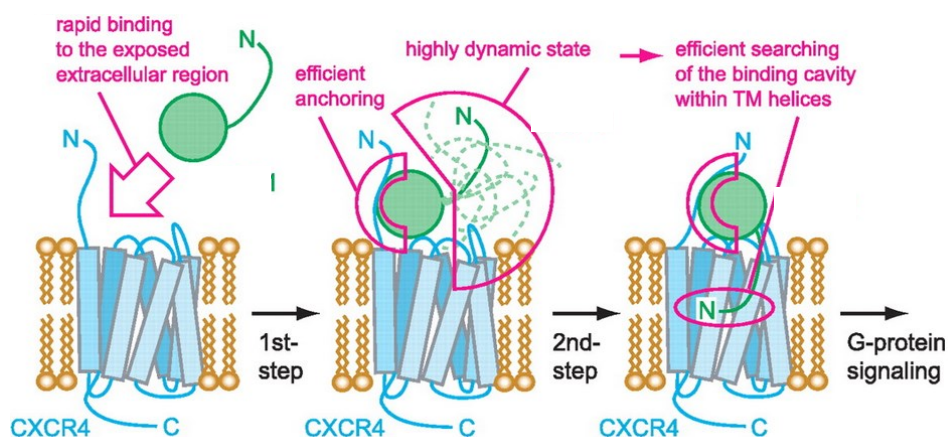


Figure 2.6 Proposed Two-Step Mechanism for CXCL12 and CXCR4 Binding.⁷⁷

Activation of CXCR4 by CXCL12 stimulates various downstream signaling pathways resulting in a number of physiological responses, such as chemotaxis,^{78,84} cell survival and proliferation,^{85,86} intracellular calcium flux,⁸⁷ and gene transcription (Figure 2.7).⁸⁸ Similar to other GPCRs, CXCR4 is complexed with an intracellular $\alpha\beta\gamma$ -trimeric G protein anchored to the inner surface of the cell membrane. In its basal state, the G protein binds guanosine diphosphate (GDP). Upon ligand binding and activation, GDP is released and replaced by guanosine

triphosphate (GTP). This causes the trimer to disassociate to a $G\alpha$ monomer bound to GTP and a $G\beta\gamma$ dimer. The signal is transmitted to an effector protein through its interaction with the GTP-bound α -subunit. The activated $G\alpha_i$ protein inhibits the cyclic adenosine monophosphate (cAMP)-dependent pathway by blocking adenylate cyclase activity. While it was originally believed that CXCR4 was limited to $G\alpha_i$ signaling, recent data has suggested that it can couple to other $G\alpha$ proteins such as $G\alpha_q$, $G\alpha_o$, and $G\alpha_s$.⁸⁹

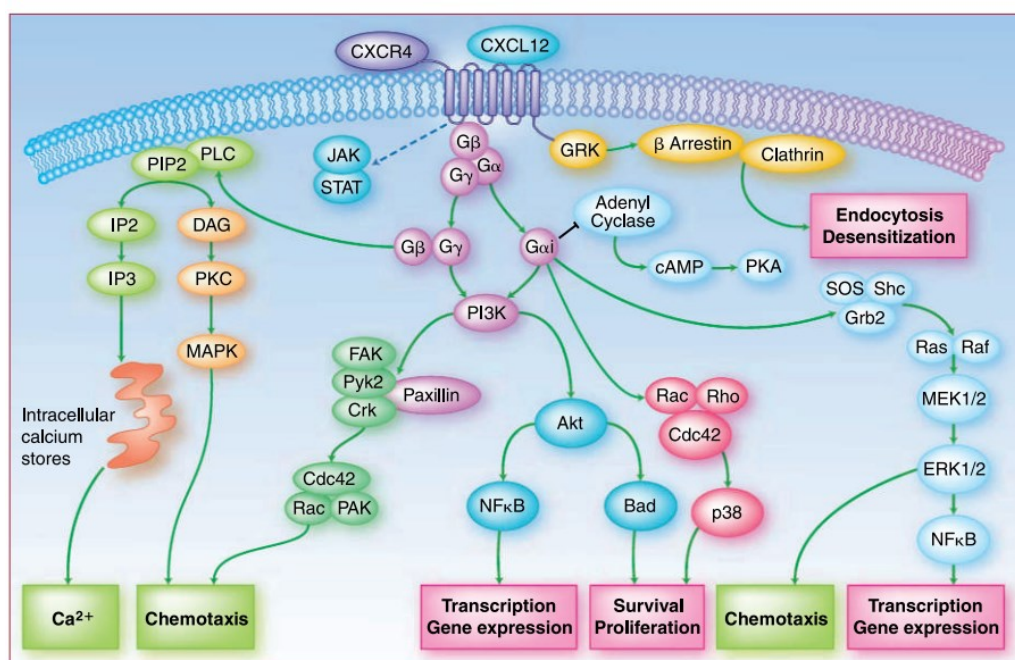


Figure 2.7 CXCR4 Signaling Pathway.⁸⁹

2.2.4 Therapeutic Rationale for Targeting CXCR4 or CXCR4/CXCL12 Axis

Human Immunodeficiency Virus (HIV)

In 1998, CXCR4 was discovered as one of the coreceptors utilized by the T-lymphocyte tropic (X4) strains of HIV-1 in order to gain entry into target cells, a key step of virus replication.⁹⁰ As illustrated in Figure 2.8, the cellular entry of HIV requires the sequential interaction of the viral envelope glycoprotein gp120 with CD4 receptor and a co-receptor protein CC chemokine

receptor type 5 (CCR5) or CXCR4 located on the surface of the host cell.⁹¹ The initial binding event between gp120 and the CD4 receptor at the cell membrane leads to critical conformational changes that facilitate the molecular recognition of the coreceptor by the V3 loop fragment of gp120. The interaction between gp120 and either CCR5 or CXCR4 induces additional conformational changes within the gp120/gp41 trimer that trigger the insertion of a fusion peptide into the cell membrane of the target cells. Following the fusion event, the viral core containing the HIV genome enters the cytoplasm of the cell where it begins the multi-stepped replication process.

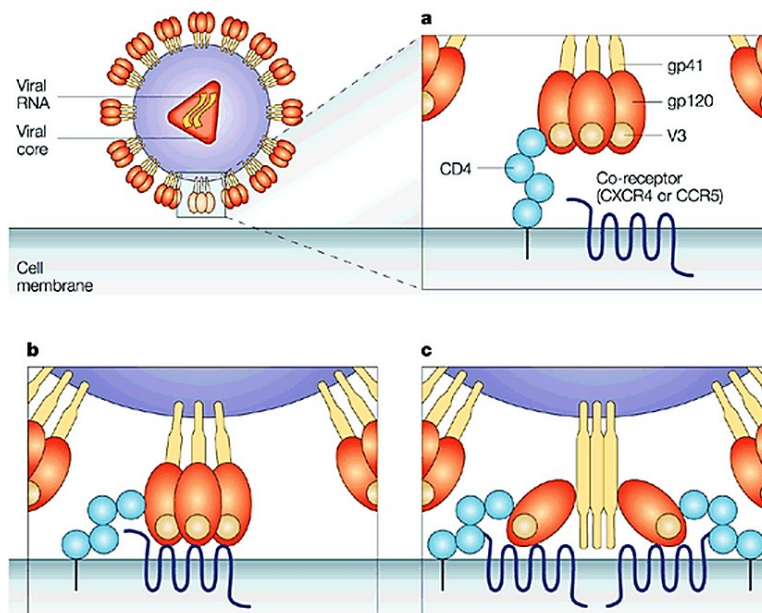
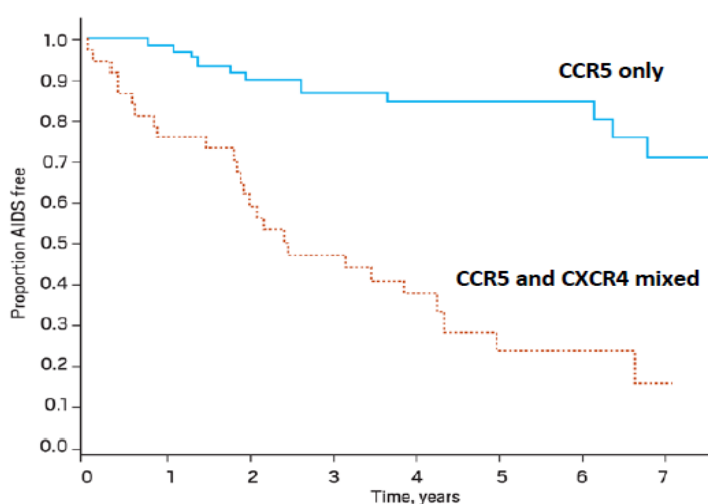


Figure 2.8 Mechanism of HIV-1 Cell Entry.⁹¹

M-macrophage tropic (R5) strains that use CCR5 as the entry coreceptor predominate during the early stages of viral infection.⁹² However, in 50-60% of infected individuals, X4 strains emerge within an average of five years. X4-tropic virus is associated with a more pronounced depletion of CD4⁺ T cells than R5 virus. The virus has a wider range of susceptible target cells due to broad expression pattern of CXCR4 in comparison to the 15-30% expression of

CCR5 on CD4⁺ T cells. The phenotypic switch from R5 to X4 is thought to arise from an X4/R5 intermediate strain capable of using both the CCR5 and CXCR4 receptor. Consequently, this switch is clinically characterized by accelerated depletion of CD4⁺ T cells and rapid progression to acquired immune deficiency syndrome (AIDS) (Graph 1.1), thus highlighting the importance of therapeutic strategies that target X4 viral strains.

Graph 2.1 Clinical Progression to AIDS: R5 vs. Dual/Mixed Tropic Virus.⁹²



Kaplan-Meier curves for clinical progression to AIDS ($P < 0.001$).

Stem Cell Mobilization

HSCs are multipotent stem cells which give rise to blood-forming cells from the myeloid (monocytes and macrophages, neutrophils, basophils, eosinophils, erythrocytes, dendritic cells) and lymphoid (T-cells, B-cells, NK-cells) lineages.^{81,93} Mature blood cells are derived from HSCs and formed through intermediates termed hematopoietic progenitor cells (HPCs). At various stages of differentiation, hematopoietic cells are held within their main site of production, the bone marrow (BM). Movement of HSCs and HPCs between BM and peripheral blood at steady-state conditions is at very low frequency. HPCs are retained in the marrow by the interaction of CXCL12 with CXCR4 (Figure 2.9).

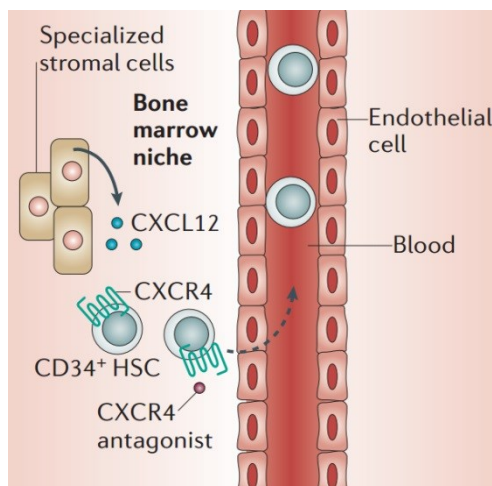


Figure 2.9 Hematopoietic Stem Cell (HSC) Niche in Bone Marrow (BM).⁹⁴

The observation that the number of circulating HSCs increased in patients recovering from chemotherapy led to the first autologous hematopoietic stem cell transplantation using mobilized peripheral blood stem cells.^{82,95} The ability of the transplanted stem cells to home to the BM and regenerate normal hematopoiesis has proven useful in the treatment of diseases that damage or destroy the bone marrow, including relapsed Hodgkin lymphoma, recurrent, chemosensitive non-Hodgkin lymphoma, and multiple myeloma.

Due to the low frequency of circulating HSCs, immediately following high-dose chemotherapy or other myeloablative conditions, patients are commonly given a hematopoietic growth factor. Granulocyte colony-stimulating factor (G-CSF) is the gold-standard used to mobilize HSCs/HPCs for transplantation. However, its use has been shown to result in broad individual variability in circulating cell numbers and has been associated with untoward side effects that are amplified due to repeated dosing that is frequently required.

While treatment with G-CSF mobilizes stem cells and neutrophils and reduces retention signals in the BM by lowering levels of CXCL12, highly selective CXCR4 antagonists have been shown to strongly reduce retention signals specifically for hematopoietic cells. Phase III clinical studies with the CXCR4 antagonist, **AMD3100**, showed that the drug strongly synergized with

G-CSF.^{93,96-98} Additionally, the drug combination increased the mobilization of stem cells and neutrophils to a greater capacity than G-CSF treatment alone.

Cancer and Metastasis

Over the past several years, the involvement of chemokines and their receptors in cancer has been firmly established. Specifically, expression of CXCR4 transcripts and/or protein has been reported in over 23 different types of cancer, where it is commonly overexpressed in leukemia, breast, lung, prostate, ovarian, and colorectal cancers.^{78,84,85,89,99} Data suggest that CXCR4 responsive cancer cells preferentially migrate toward organ sites with abundant CXCL12 in a gradient-dependent manner, thus correlating the expression of CXCR4 with cancer invasiveness.

The complex process of tumor growth and metastasis requires many steps for primary tumor development and establishment of secondary tumors. The steps include 1) survival and growth of the primary tumor 2) detachment of tumor cells from the primary growth 3) intravasation into blood or lymphatic vessels 4) migration and transport through the body 5) extravasation and colonization in a new site of the body and 6) survival, proliferation, and angiogenesis of the metastasized cells. The role of CXCL12 and CXCR4 in cancer can be divided into three general categories which contribute to one or more of the aforementioned processes: provide directional cues for migration/metastasis, shape the tumor microenvironment, and present survival and/or growth signals. Consequently, therapeutics that block the CXCR4/CXCL12 interaction or inhibit downstream intracellular signaling have become an increasingly high priority in cancer research.

2.2.5 Clinically Relevant CXCR4 Antagonists

Given the key role of chemokine receptors in the HIV infection, pathogenesis of autoimmune and inflammatory diseases, and cancer it is not surprising that CXCR4 has rapidly gained attention during the last decade by both academia and the pharmaceutical industry in the quest to develop drugs to treat such diseases. In general, CXCR4 antagonists can be divided into three categories: peptide antagonists,^{100,101} *pseudo-peptide* antagonists, and non-peptide (small

molecule) CXCR4 antagonists.^{102–104} Peptide CXCR4 antagonists were initially designed to mimic CXCL12. However, the poor pharmacokinetic (PK) profile of peptide antagonists like **T140**^{72,105,106} (Figure 2.10) provoked interest in *pseudo*-peptide CXCR4 antagonists exemplified by **KRH-1636**.^{107–109}

The discovery elucidating CXCR4 as a coreceptor used along with CD4 by X4 HIV-1 strains for cellular entry catalyzed the deluge of research in this field. This seminal finding coincided with elucidation of the mechanism of the anti-HIV-1 bicyclam **AMD3100** (Figure 2.10). At physiological pH, **AMD3100** carries an overall charge of +4, where each cyclam ring is doubly charged and can adopt a stable *trans*-III *R,R,S,S* type conformation with respect to the four nitrogen atoms. **AMD3100** was the first CXCR4 antagonist to enter clinical trials as an X4 HIV-1 entry inhibitor, but was eventually withdrawn from Phase II clinical trials due to cardiotoxicity observed with administration of high doses.¹¹⁰ However, an unexpected observation was made during pharmacokinetic studies with single dose intravenous **AMD3100** administration. The drug was shown to mobilize various white blood cells, including hematopoietic (CD34⁺) cells.⁸² Through further clinical investigations, the compound was subsequently approved by the FDA for use in mobilizing HSCs for autologous transplants in patients with non-Hodgkin lymphoma and multiple myeloma.

The unique biological properties of the CXCR4/CXCL12 signaling axis and additional research with **AMD3100** prompted a surge in research efforts to identify other small molecule CXCR4 antagonists. Systematic efforts to replace the cyclam rings of **AMD3100** with moieties that retained basic character (with reduced overall charge) and reduced the molecular weight resulted in a series of compounds exemplified by **AMD11070** (Figure 2.10).¹¹⁰ Three structural modifications were shown to be effective replacements for the cyclam pharmacophore: 1) a chiral tetrahydroquinoline (THQ) piece, 2) a basic heterocycle, and 3) a butyl amine chain. **AMD11070** was the first oral CXCR4 antagonist to enter the clinic and advance to phase II clinical trials.

Although **AMD11070** was withdrawn from clinical trials due to liver toxicity, this small molecule paved the way for other discovery efforts, which produced preclinical leads, such as the hybrid-piperazine (**GSK812397**) and isothiourea (**IT1t**) compounds.

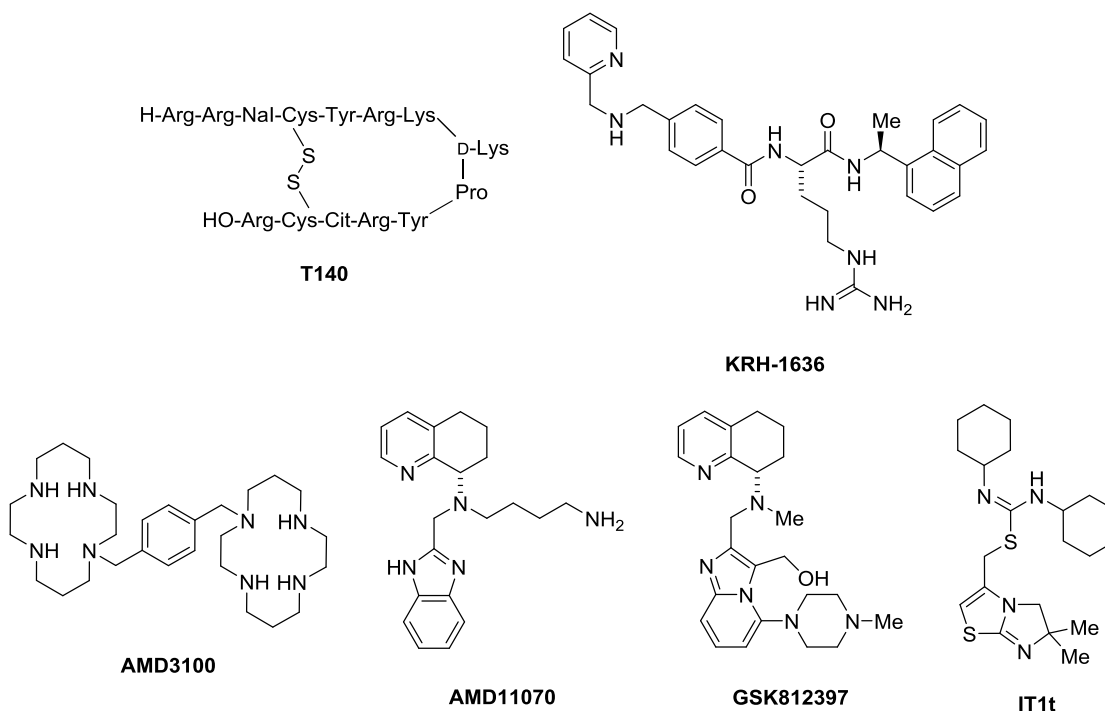


Figure 2.10 Structures of Selected CXCR4 Antagonists.

2.2.6 Rationale for THIQ-Based CXCR4 Antagonists

In light of the development of **AMD11070** as an oral HIV treatment, our initial focus was on replacement of the benzimidazole moiety. We hypothesized that this subunit was the likely source of CYP450 isozyme (3A4, 2D6) inhibition observed with this compound.⁸⁷ We proposed that this molecule represented a generalized scaffold which could be optimized based on its reported HIV-1 potency and oral bioavailability. This hypothesis was tested by Lawrence Wilson, Ph.D., a senior scientist in the Liotta lab who synthesized compounds containing prolines (**1**), fused phenyl piperidines (**2**), piperazines (**3**), and derivatives thereof as replacements to the

benzimidazole (Figure 2.11). In all examples, the (*S*)-tetrahydroquinoline (THQ) headpiece from the 11070 series was retained due to observed benefits for CXCR4 potency.¹¹¹

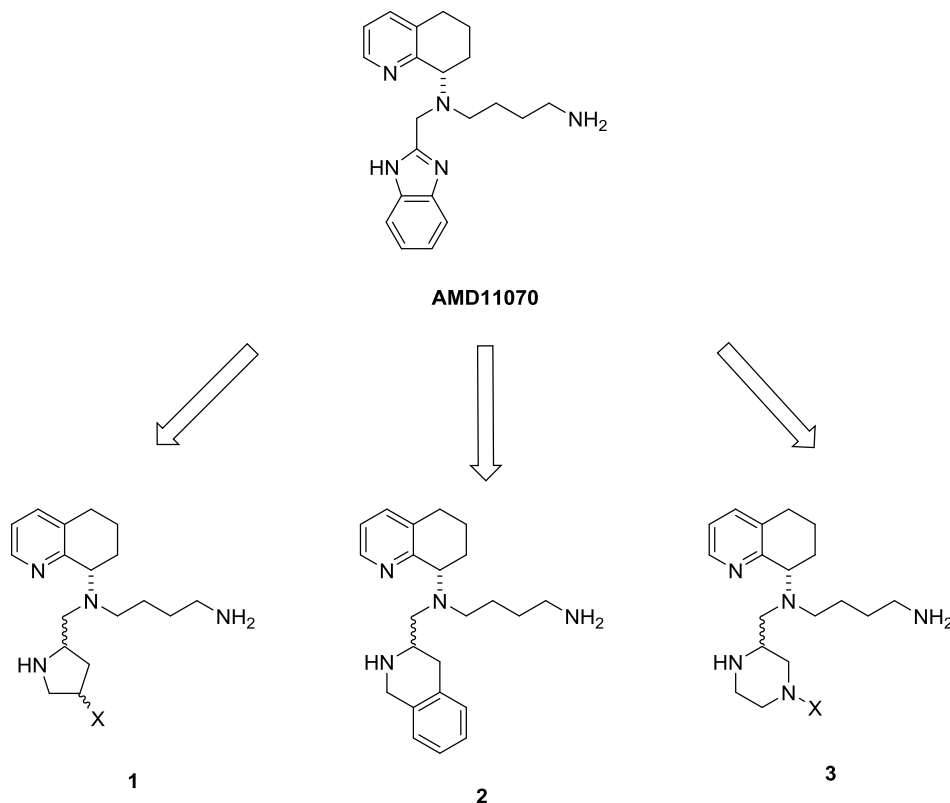


Figure 2.11 Initial Hit-to-Lead Efforts.

In general, the fused phenyl piperidines (**2**) and piperazines (**3**) showed antagonist effects at CXCR4 in an HIV infectivity assay, with comparable potencies to the 11070 series. However, initial modifications made to the proline-containing compounds resulted in inactivity, potentially indicating the necessity of a larger heterocycle at this position. Subsequent separation and testing of compound diastereomers showed that the (*S,R*)-THIQ isomer (**ECXC00947**) was more potent than the (*S,S*)-THIQ isomer (**4**). Likewise, both of these compounds exhibited greater potency than both piperazine diastereomers **5** and **6** (Figure 2.12).

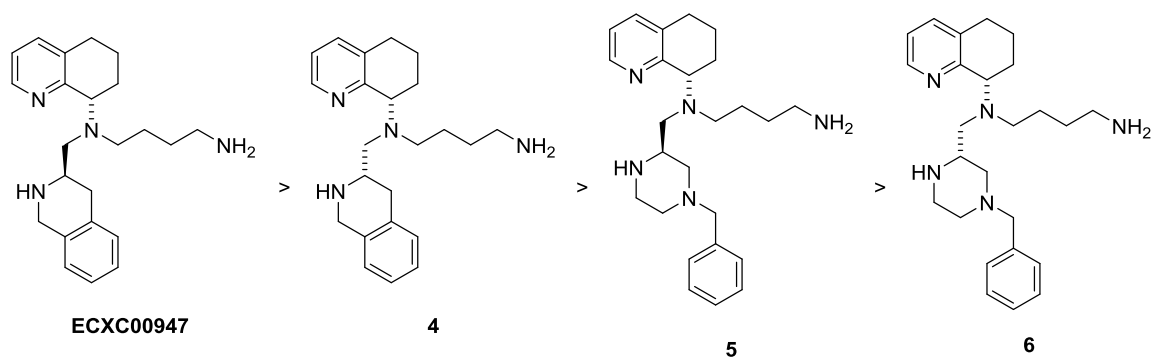
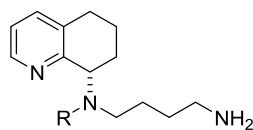


Figure 2.12 Conclusions on Initial Hit-to-Lead Efforts.

On account of the above results, Huanyu Zhao, Ph.D. in the Liotta group synthesized a series of piperidine compounds in which the isomeric heterocycle and additional stereogenic center were variable.⁸⁷ We opted to pursue the isomeric fused phenyl piperidines because these substructures are commonly found in many drug-like compounds and GPCR ligands. A viral attachment assay with HIV-1_{IIIB} in CCR5/CXCR4-expressing HeLa-CD4-LTR- β -gal (MAGI) cells was initially used to measure each compound's ability to block potential viral entry, as well as cellular toxicological properties (Table 2.1).⁸⁷

Table 2.1 MAGI Assay Results for Series of Piperidine Compounds.

Compound ID	R	MAGI HIV-1 _{III} B IC ₅₀ (μM) [†]	MAGI HIV-1 _{III} B TC ₅₀ (μM) [†]
7-(R)^a 8-(S)^a		>30 >30	>30 >30
ECXC00947-(R)^b 4-(S)^b		0.005 1.4	>10 >10
9-(R)^b 10-(S)^b		0.25 0.45	>30 >30
11-(R)^c		1.1	>30
12-(R)^c		0.01	5.8

[†]All assays were performed in duplicate. Compounds synthesized by ^aHuanyu Zhao, Ph.D, ^bLawrence Wilson, Ph.D., ^cAnthony Prosser.

Both the location of fusion of the aromatic ring and compound stereochemistry had a strong impact on potency. The action of the THQ and THIQ moieties indicated that a combination of phenyl ring placement and nitrogen atom basicity is important for activity. Interestingly, in the case of compounds **7** and **8**, they showed no effect against viral entry in the MAGI assay up to 30 μM, highlighting the importance of a basic heterocycle. In comparison, THIQ compounds **ECXC00947**, **4**, and **9-12** exhibited a range of antiviral potencies. However, both the presence and site of the phenyl ring fusion to the piperidine ring had a dramatic effect on potency.

Piperidine **11** which contained no phenyl ring fusion demonstrated diminished potency in the MAGI assay. Meanwhile, the distal ring (*R*)-isomer **ECXC00947** was measured to be 50-500-fold more potent than the isomeric compounds (**9** and **10**) with the phenyl ring adjacent to the extending carbon. Interestingly, extension of the phenyl ring to the naphthyl moiety as in THIQ analogue (**12**) did not significantly alter its antiviral activity. This suggests that these compounds bind in a region that may be able to accommodate additional substitutions and extensions to the THIQ ring. The stereochemistry at the attachment point on the THIQ ring had a significant effect on compound potency. The respective isomers with the (*R*) configuration at the THIQ ring chiral center (**ECXC00947** and **9**) represented the most potent analogues. Compound **ECXC00947** was shown to be greater than 100-fold more potent than the compounds bearing the opposite stereochemistry (**4** and **10**). Consequently, compound **ECXC00947** was chosen for additional medicinal chemistry and biological studies (data not included).⁸⁷

The structural similarity between the two scaffolds (**AMD11070** and **ECXC00947**) prompted our group to further examine the subtleties between the benzimidazole and THIQ series. Early investigations included conservative and independent modifications to the nitrogen atom of the THIQ ring and the butylamine of the side chain. While exploring the SAR around the THIQ series, we were interested in determining if any of the modifications published for the 11070 series of compounds could be used in our optimization efforts toward a more potent THIQ analogue. Several concepts were addressed throughout our medicinal chemistry efforts around THIQ **ECXC00947**:

- 1) Can a more robust and cost-effective route toward THIQ analogues be developed?
- 2) What is the role of the butylamine nitrogen in receptor binding?
- 3) What modifications will improve compound bioavailability and retain potency?

2.2.7 Rationale for Masking the Basicity of the Butylamine Nitrogen

Initial pharmacokinetic studies conducted with compound **ECXC00947** indicated that the molecule was poorly absorbed upon oral administration to rats. Therefore, the primary goals of the SAR study (described in section 2.4.1) were to identify compounds more potent than the current lead (**ECXC00947**), while increasing overall lipophilicity toward a more bioavailable molecule.

Lipophilicity is a physical property described as the ability of a compound to dissolve in an organic phase (typically lipids, oils, or non-polar solvents) that is immiscible with water. An increasing body of literature has emerged highlighting the importance of lipophilicity on biological processes of drug action such as absorption, distribution, metabolism, excretion, and toxicity (ADMET).¹¹² However, if a compound is too lipophilic, it might be insoluble in aqueous media (for example gastrointestinal fluid or blood). Likewise, the compound could bind too strongly to plasma proteins thus reducing the concentration of free drug in the blood to a level that could potentially prevent production of the desired effect. Additionally, a very lipophilic drug could also accumulate in lipid bilayers which could cause toxicity due to high drug levels or prohibit its access to target cells.

Simple partition experiments or computational methods can be used to model lipophilicity. Experimentally, a sample compound in an octanol/aqueous mixture is equilibrated over a set period of time. Once the resulting emulsion is separated, the concentration of drug in each layer is measured and used to calculate the partition coefficient (P) represented as $\log_{10}P$ or $\log P$ (Figure 2.13). In contrast, the distribution coefficient (D) or $\log D$ is the ratio of the sum of the concentrations of all forms of the compound (ionized and un-ionized) in the two phases. For $\log D$ measurements, the aqueous phase is buffered such that the pH is not significantly perturbed by introduction of the compound (Figure 2.13). The majority of literature devoted to the impact of lipophilicity on drug properties has been based on calculated values ($\text{clog}P$ and $\text{clog}D$) rather than measured data. Several different computational methods have been made available for

prediction of both partition and distribution coefficients. The reliability of these calculated values is dependent on the accuracy of the pK_a calculations for each drug. Nonetheless, the vast majority of members in the medicinal chemistry community agree that the optimal range of lipophilicity falls within the narrow range of $\log D$ between 1 and 3.

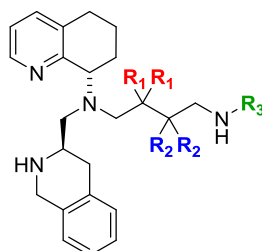
$$X_{\text{aqueous}} \xrightleftharpoons{P} X_{\text{octanol}}$$

$$\log P_{\text{octanol/water}} = \log \left(\frac{[\text{drug}]_{\text{octanol}}}{[\text{drug}]_{\text{un-ionized water}}} \right)$$

$$\log D_{\text{octanol/water}} = \log \left(\frac{[\text{drug}]_{\text{octanol}}}{[\text{drug}]_{\text{un-ionized water}} + [\text{drug}]_{\text{ionized water}}} \right)$$

Figure 2.13 Equations for Octanol/Water Partition and Distribution Coefficients.

Given our understanding of lipophilicity and its connection to absorption, we believed that the poor oral absorption observed with the lead compound (**ECXC00947**) was reflective of its negative $\log D$ value calculated at physiological pH 7.4. According to pK_a calculations, I hypothesized that if the primary amine was largely responsible for the low $\text{clog}D$, then masking the basicity of that nitrogen should increase $\text{clog}D$ values and provide compounds that exhibit more favorable physical properties. I initially set out to test this hypothesis through the design and synthesis of compounds (see section 2.3.3) with varied pK_a values calculated for the side chain nitrogen (Table 2.2).

Table 2.2 Calculated p*K*_a Values for Side Chain Nitrogen.

Compound ID	R ₁	R ₂	R ₃	Calculated p <i>K</i> _a (X-NH ₃ ⁺)	clog <i>D</i> (pH 7.4)
13	H	H		N/A	1.16
14	H	H		N/A	0.92
15	H	H		N/A	1.80
16	H	F	H	7.0	1.52
17	F	H	H	9.5	-0.22
ECXC00947	H	H	H	10.4	-0.65
18	H	H		13.6	-1.25

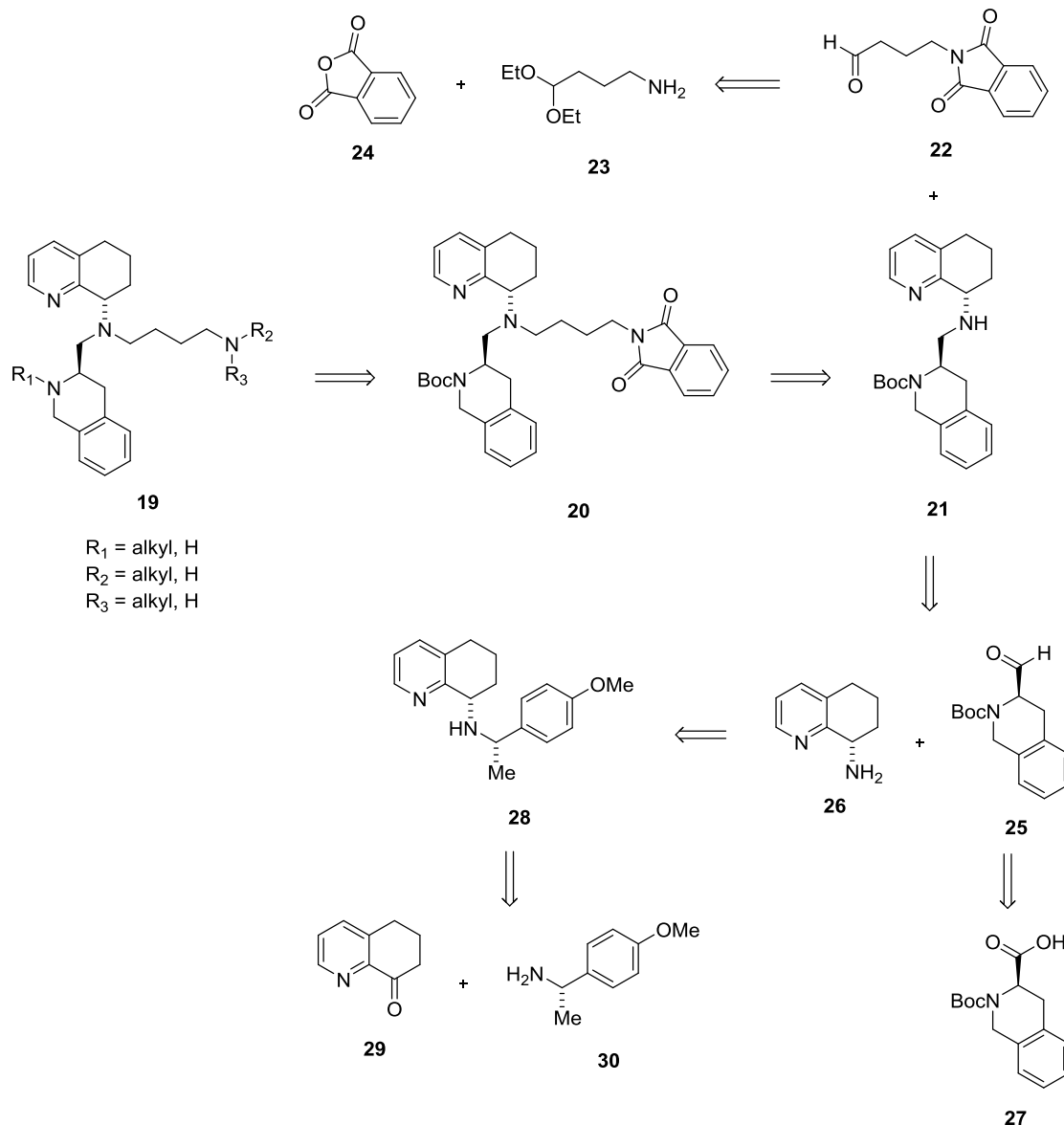
N/A = not applicable

Compounds with an acylated nitrogen (**13-15**) would remove all possibilities of a positive charge at this position. Urea **14** and dimethylurea **15** were chosen as targets so that basicity and/or steric volume at the position of interest could be altered, but H-bond donors and acceptors could be retained. Unsurprisingly, the clog*D* values predicted for these compounds were positive numbers and larger than the value predicted for **ECXC00947**. Meanwhile, the difluoro-containing compounds (**16-17**) would serve to decrease the basic character of the primary amine through induction. The compound with the fluorine atoms closest to the primary nitrogen had a predicted clog*D* value greater than the compound with fluorine atoms positioned one more methylene unit removed. The inverse trend was observed for calculated p*K*_a values.

2.3 Synthesis of THIQ Analogues

2.3.1 Retrosynthetic Analysis Toward THIQ Analogues

The general synthetic plan toward a variety of THIQ analogues was based on reductive aminations to attach several key fragments summarized in Scheme 2.1.⁸⁷ It was envisaged that target compounds **19** with substitutions at the THIQ nitrogen, the butylamine nitrogen, or at both positions would come from the orthogonally protected advanced intermediate **20**. This molecule could be formed through a reductive amination between the secondary amine half-scaffold (**21**) and phthalimide protected aminobutyraldehyde **22**. Moving further along the retrosynthetic path, aldehyde **22** was imagined to come from condensation of amine **23** onto phthalic anhydride (**24**). Meanwhile, the half-scaffold intermediate (**21**) could arise from the reductive amination with aminoaldehyde **25** and THQ amine **26**, which could be traced back to the amino acid derivative **27** and chiral amine **28**, respectively. According to procedures described for the **11070** series, the protected chiral amine fragment (**28**) was expected to come from another reductive amination between the commercially available ketone (**29**) and chiral directing group (**30**).

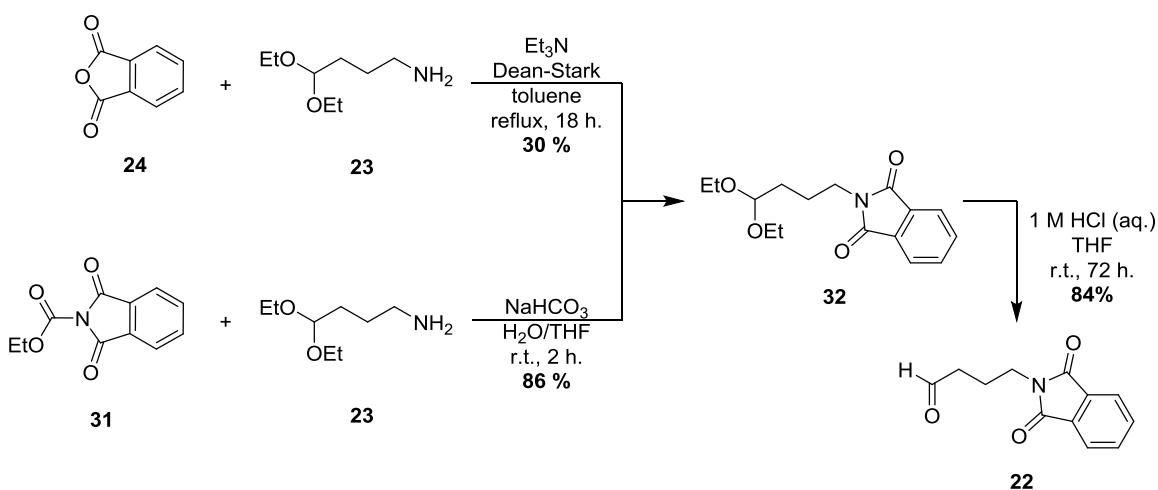


Scheme 2.1 Retrosynthetic of THIQ Analogues.

2.3.2 Optimization of Synthetic Routes Toward Analogues

A number of THIQ analogues were synthesized according to the retrosynthetic scheme discussed above. In order to gain access to a large number of diverse molecules, we were interested in optimizing reactions toward a few key intermediates. Additionally, we investigated cost-effective routes that would afford large quantities of enantiopure starting materials.

Shortly after I joined the CXCR4 project, I focused my efforts on addressing problem spots in our synthetic routes. Prior to my work, the side chain aldehyde (**22**) had been synthesized using phthalic anhydride (**24**) and 4-aminobutyraldehyde diethyl acetal (**23**) as illustrated in Scheme 2.2.¹¹³ While the reaction shown only represents a single attempt, the poor yield obtained was consistent with the results from additional experiments conducted by several other group members. In order to drive the sluggish reaction to completion, refluxing conditions with a Dean-Stark trap were necessary to remove water formed during the reaction.

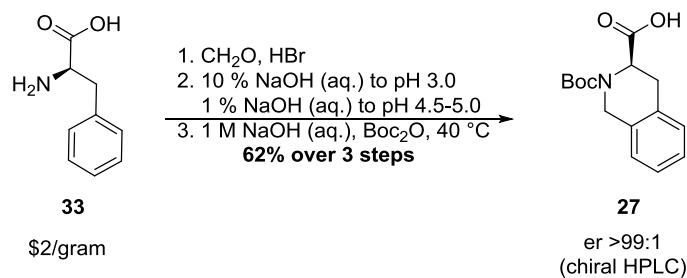


Scheme 2.2 Optimization of Aminoaldehyde Synthesis.

When phthalic anhydride (**24**) was replaced with *N*-carbethoxyphthalimide (**31**), the rapid reaction provided diethylacetal **32** which could be isolated from the urethane byproduct in high yield.¹¹⁴ We suspected that solvent polarity and the identity of the leaving group played an important role in this reaction. The polar solvent in the second reaction may have helped solvate or stabilize the charge generated in the tetrahedral intermediate. The reduced reaction time and improved product yield allowed for rapid scale-up of more than 40 g of the desired aldehyde (**22**) upon hydrolysis of diethylacetal **32**.

Our early SAR studies showed that the THIQ moiety was a suitable replacement for the benzimidazole ring found in **AMD11070**. However, the THIQ ring introduced another stereogenic center to the molecule that generated a pair of diastereomers. As discussed in section 2.2.6, the (*R*)-THIQ diastereomer (**ECXC00947**) was more than 100-fold more potent than the (*S*)-THIQ diastereomer (**4**). Based on this data, we knew that it would be important to access starting material with the appropriate configuration. During our initial hit-to-lead studies, we purchased the Boc protected (*R*)-THIQ carboxylic acid (**27**, Scheme 2.1) from a commercial vendor for nearly \$100/g. Upon further analysis of this material by chiral HPLC, we found that the material we had been purchasing was an 80:20 mixture of the (*R*)-enantiomer and the (*S*)-enantiomer, respectively. We decided to pursue more cost-effective synthetic routes that would provide a large quantity of the starting material with an enantiomeric ratio (er) >95:5.

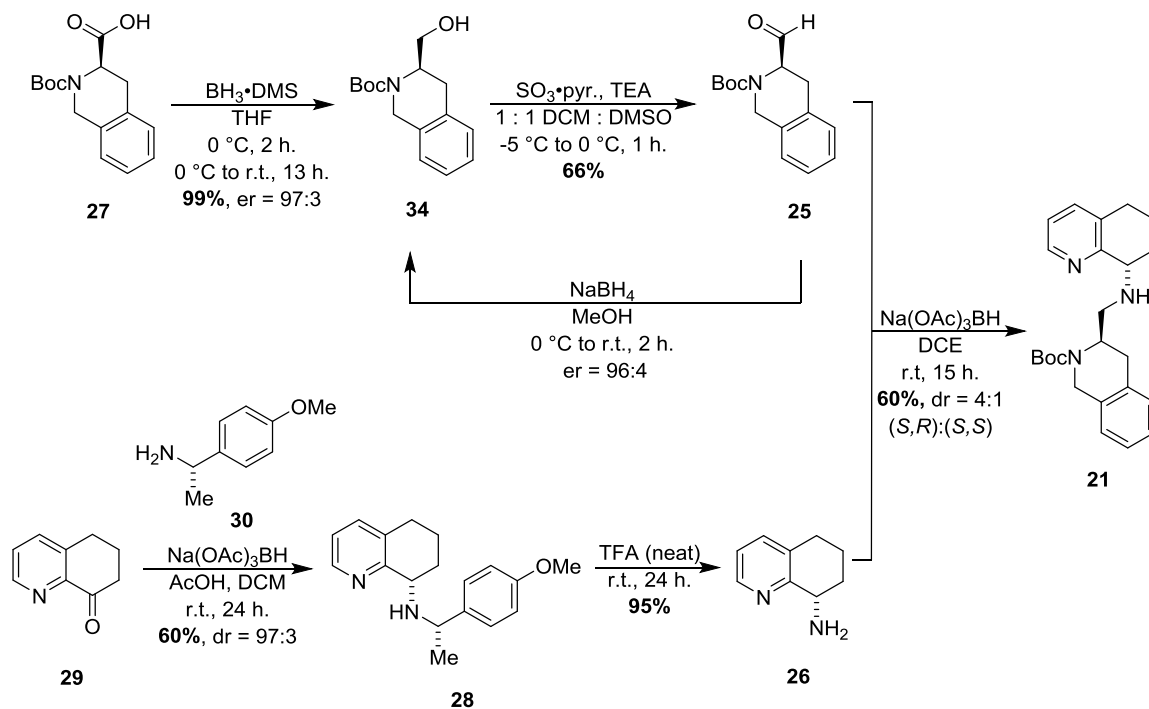
Fortunately, the synthesis of carboxylic acid **27** was achieved in three short steps that required no column chromatography or purification (Scheme 2.3).^{114,115} Briefly, commercially available D-Phe **33** (purchased for approximately \$2/g) was treated with formaldehyde (37 wt. % in water) and HBr (48 wt. % in water). The THIQ HBr salt formed in the Pictet Spengler reaction was filtered and basified with aqueous NaOH to provide the free base. Finally, reaction with Boc anhydride afforded the protected (*R*)-THIQ carboxylic acid (**27**) in a 62% yield over three steps. The enantiomeric ratio of solid was determined to be >99:1 by chiral HPLC. The cyclization reaction not only provided several grams of starting material for our medicinal chemistry studies, but it also served as a potential path toward substituted THIQ analogues that might be accessed using various amino acid derivatives.



Scheme 2.3 Synthesis of (*R*)-THIQ Carboxylic Acid from a Commercial Amino Acid.

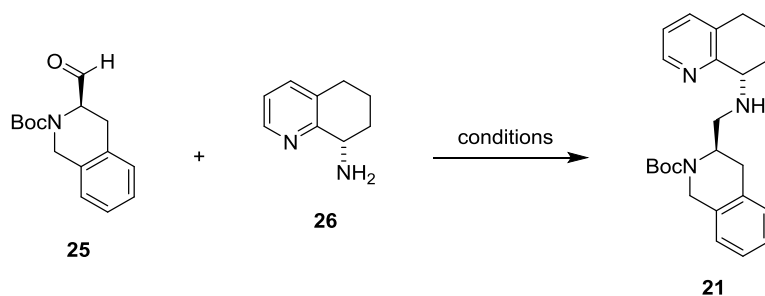
2.3.3 Forward Synthesis of THIQ Analogues

With the starting material obtained from the reactions discussed above, we were able to generate the half-scaffold amine intermediate (**21**) according to the synthesis illustrated in Scheme 2.4.^{87,116,117} Borane dimethyl sulfide reduction of (*R*)-THIQ carboxylic acid **27** provided amino alcohol **34** in good yield with little to no racemization detected by chiral HPLC. The Parikh-Doering oxidation afforded aldehyde **25**. An aliquot of this material was reduced back to the alcohol to check if the oxidation conditions promoted racemization. Gratifyingly, the crude aldehyde exhibited no appreciable racemization. Due to the instability of this material and its susceptibility to epimerization, we opted to carry this material forward without column chromatography. Reductive amination with aminoaldehyde **25** and chiral amine **26** (synthesized according to the two step procedure described for the 11070 series of compounds) furnished the half-scaffold secondary amine (**21**) as a 4:1 mixture of inseparable diastereomers.



Scheme 2.4 Synthesis of Half-Scaffold Amine Intermediate.

We attributed the diminished diastereomeric ratio to imine-enamine tautomerization that proceeded during the reductive amination reaction. In addition, we hypothesized that trace acetic acid from the reducing agent could have catalyzed imine formation, while the polar solvent (DCE) may have shifted the equilibrium toward the enamine. Likewise, we considered using a stronger reducing agent that would rapidly convert the imine to the desired product. While sodium triacetoxyborohydride is typically the reagent of choice for reductive aminations due to its mild reactivity and non-toxic byproducts, the reaction was attempted with a stronger reducing agent, specifically, sodium cyanoborohydride, as shown in Scheme 2.5.



Reductant	Solvent	Reductant Addition	dr [†] (<i>S,R</i>):(<i>S,S</i>)
Na(OAc) ₃ BH	DCE	pre-stir 25 and 26 for 30 minutes	4:1
Na(OAc) ₃ BH	DCE	immediately	7:1
Na(OAc) ₃ BH	DCM	immediately	10:1
Na(OAc) ₃ BH ^a	THF	immediately	4:1
Na(OAc) ₃ BH ^a	Toluene	immediately	2:1
NaBH ₃ CN ^a	DCE	immediately	10:1
NaBH ₃ CN	MeOH	immediately	14:1*

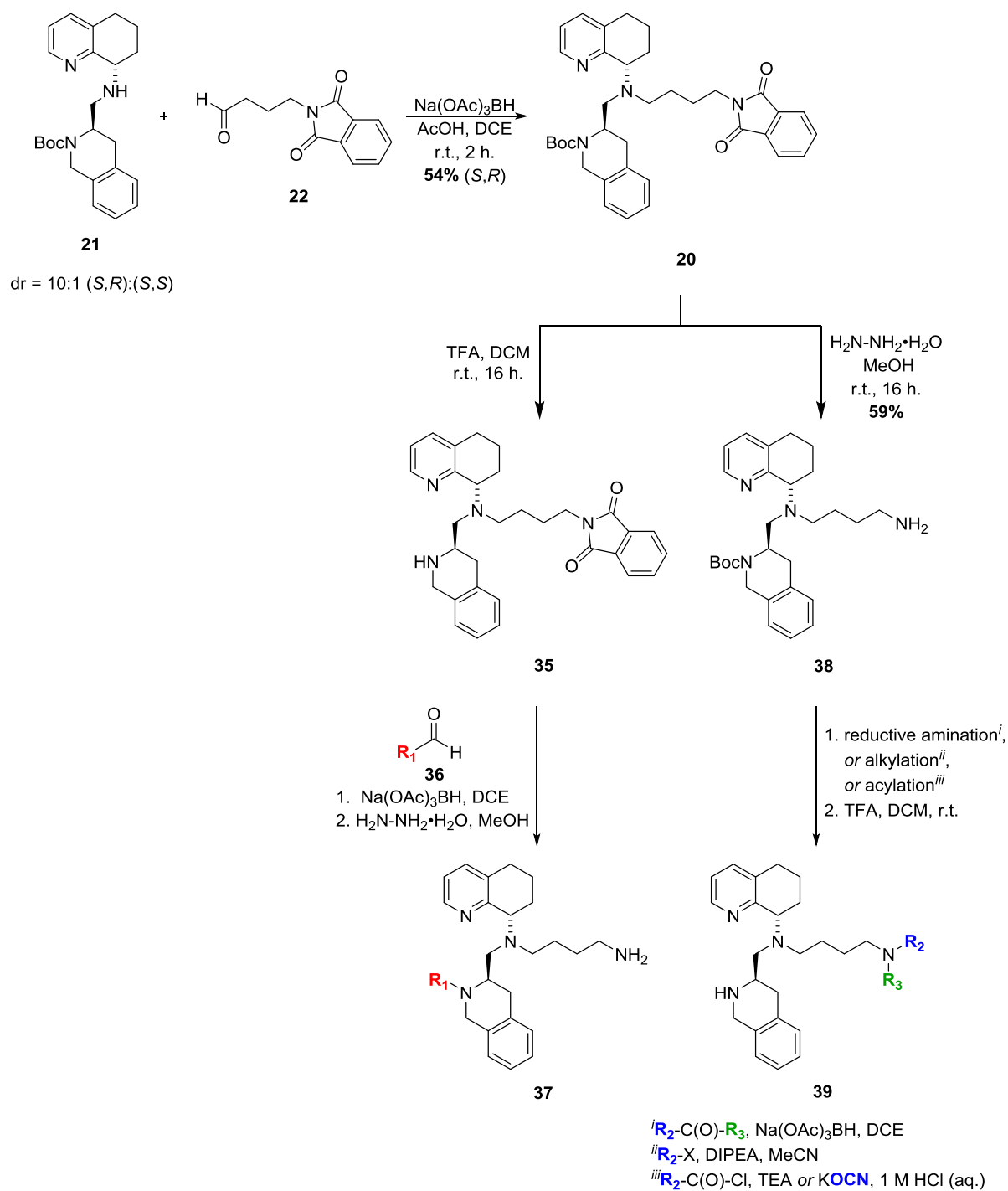
[†]Diastereomeric ratios were calculated using LC-MS. ^aReactions were carried out by Anthony Prosser. *Low reaction yield, significant reduction of aldehyde to alcohol.

Scheme 2.5 Examples of Reductive Amination Conditions.

It was clear that the indirect reductive amination procedure where the imine was formed prior to the addition of sodium triacetoxyborohydride was detrimental to the diastereomeric ratio. However, the ratio was increased in favor of the desired diastereomer when the reductant was directly added to the reaction. While the switch to DCM as the solvent did not result in drastic changes, we were pleased to observe an improvement in the ratio. Nonpolar solvents negatively impacted the ratio of diastereomers formed. This was attributed to poor solubility of the reductant in these solvents. Finally, use of a stronger reductant, sodium cyanoborohydride, resulted in diastereomeric ratios comparable or better than those observed with sodium triacetoxyborohydride. However, in both examples a portion of aldehyde **25** was reduced to the alcohol. The example with MeOH resulted in a high diastereomeric ratio (14:1), but suffered from significant reduction of the aldehyde to the alcohol and very low conversion to product, potentially due to poor aldehyde solubility in the reaction solvent.

The results obtained from the reaction screening conditions highlighted the necessity of modifying the alkylation procedure. Moving forward, three important changes were made to improve the diastereomeric ratio: 1) the reducing agent was carefully stored to exclude moisture (new reagent was used whenever possible, old reagent was disposed of) 2) reactions were carried out in DCM (dry solvent was obtained from solvent purification system) 3) sodium triacetoxyborohydride was added immediately following the addition of aldehyde.

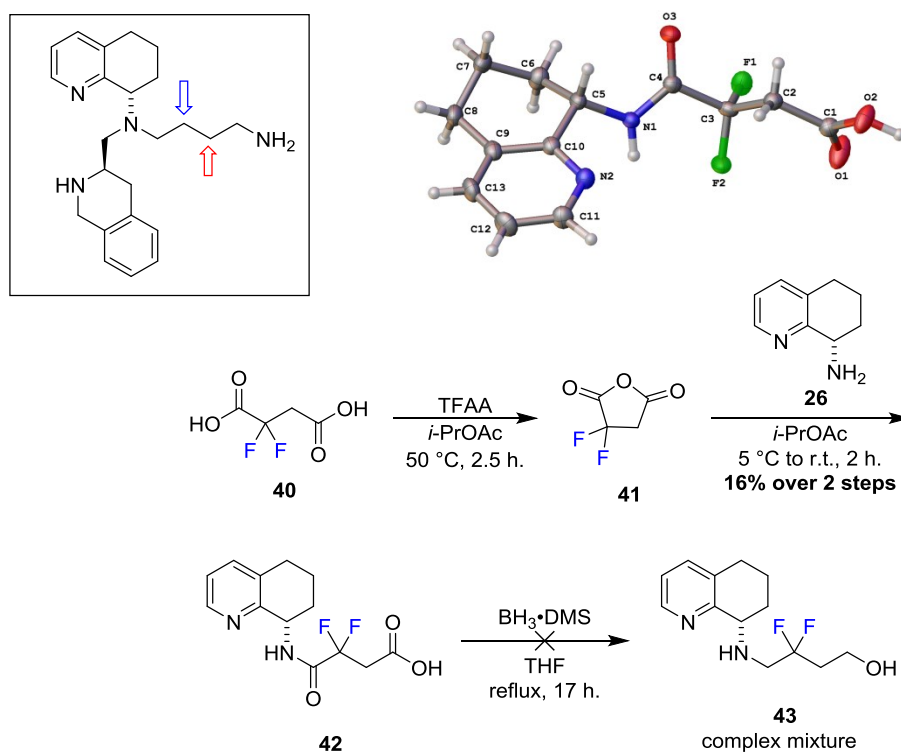
Despite improvements in the ratio of diastereomers obtained, their separation in subsequent steps was necessary (Scheme 2.6). Fortunately, once the phthalimide side chain was attached, the diastereomers could be separated by column chromatography. With the orthogonally protected material in hand (**20**), various analogues could be synthesized. For compounds that contained substituents on the THIQ nitrogen, they first required Boc deprotection with TFA to provide compound **35**. The nitrogen atom could be alkylated *via* a reductive amination with the appropriate aldehyde (**36**). Finally, removal of the phthalimide protecting group with hydrazine hydrate furnished compounds like **37**. In order to access compounds with substitutions to the butylamine nitrogen, the phthalimide moiety was removed from compound **20**. Depending on the desired attachment, either a reductive amination, alkylation, acylation was executed following by Boc deprotection to provide compounds like **39**.



Scheme 2.6 Divergent Route Toward THIQ Analogues.

Two difluoro-containing analogues were proposed (see discussion in section 2.1.7) in an effort to improve the pharmacological and physical properties of the series. We hypothesized that by attenuating the basicity of the butylamine, we could increase the lipophilicity of the THIQ-based

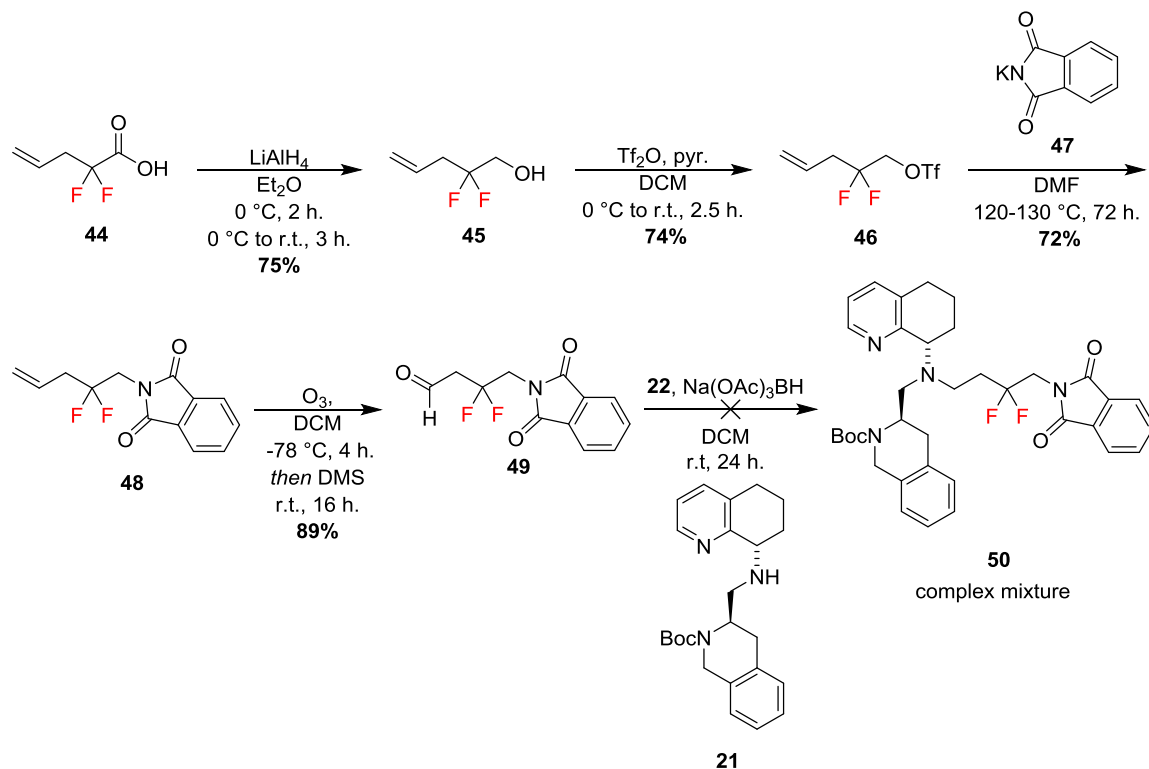
compounds. While the difluoro-containing analogues would have provided additional information regarding basicity and its relationship to potency, all synthetic attempts to generate these molecules were unsuccessful. Schemes 2.7 and 2.8 highlight a few of the unfruitful routes toward these compounds.



Scheme 2.7 Attempted Synthesis of Difluoro Analogue.

Treatment of 2,2-difluorsuccinic acid (**40**) with trifluoroacetic anhydride (TFAA) provided cyclic anhydride **41**.¹¹⁸ Nucleophilic ring-opening by chiral amine **26** exclusively formed the α -difluoroamide regioisomer (**42**) as confirmed by X-ray crystallography, albeit in very low yield presumably due to the volatility of previous intermediates, residual reactive reagents from crude reaction mixtures, and loss of the zwitterion product during work-up (Scheme 2.7). Unfortunately, an attempt to reduce both the amide group and the carboxylic acid by refluxing with borane dimethyl sulfide complex resulted in a complex mixture of starting material, partially

reduced compound, a trace amount of the desired product (**43**), and other unidentifiable byproducts.



Scheme 2.8 Synthetic Route to Difluoro Regioisomer.

The second difluoro-containing compound can also be accessed from the route illustrated in Scheme 2.7 by making a few changes to the reaction order sequence. However, the difficulty we encountered with volatile intermediates and poor reaction yields caused us to investigate a different route toward compound **50** (Scheme 2.8). Reduction of 2,2-difluoropent-4-enoic acid (**44**) with lithium aluminum hydride provided alcohol **45**.¹¹⁹ Conversion to the triflate (**46**) followed by displacement with potassium phthalimide (**47**) afforded the nitrogen protected difluoropentene (**48**).¹²⁰ Ozonolysis of alkene **48** generated the aldehyde fragment (**49**) for the alkylation step. However, reaction with the half-scaffold amine (**21**) resulted in several byproducts and less than 10% of the desired product (**50**). According to LC-MS traces and ¹⁹F

NMR, it appeared that a majority of the material represented the vinyl fluoride elimination byproduct. On account of the challenges we experienced in the synthesis of the fluorinated analogues, we decided to discontinue efforts toward these molecules and to pursue molecular models to better understand our current antagonists.

2.4 Results and Discussion

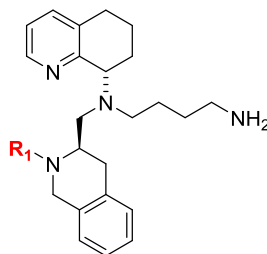
2.4.1 Structure Activity Relationship of THIQ Analogues

The SAR of the THIQ series of compounds was elucidated using the biological data generated from two different assays: 1) blockade of HIV-1_{IIIB} attachment *via* the CXCR4 receptor in MAGI cells 2) inhibition of CXCL12-induced calcium flux/release in Chem-1 cells. All compounds were subjected to both agonist and antagonist modes within the calcium flux assay. None of the compounds tested showed agonist activity at CXCR4, yet achieved complete blockade of CXCL12-induced calcium flux with various potencies. The collaboration of CXCR4 project members from the Liotta laboratory resulted in several novel CXCR4 antagonists. In general, the compounds revealed a range of potencies and divergent SAR.

As illustrated in Table 2.3, substitution at the THIQ nitrogen with either H-bond acceptors or aliphatic moieties resulted in a slight drop in potency (2–10-fold) in the MAGI assay when compared to **ECXC00947**. However, the 5-fluoro-2-pyridyl compound (**57**) suffered a 20-fold loss of activity. While the list is not comprehensive, the selected entries highlight the major trends observed for the series. Although we hypothesized that various heterocycles would increase potency through H-bond interactions with the receptor, we found that the bulky appendages actually decreased potency to a greater degree than small substituents. A similar trend was observed with data from the calcium flux assay, however, the effect was much more pronounced. In comparison to **ECXC00947**, compounds **51-58** demonstrated a 10–100-fold decrease in their ability to block CXCL12-induced calcium flux. Specifically, molecules containing cyclic moieties (**53**, **55**, **58**) were approximately 100-fold less active than

ECXC00947 in the calcium flux assay versus only 10-fold less active in the MAGI assay. Compounds **51** and **52** with methyl and isopropyl attachments, respectively, did not exhibit as large a difference in activity between the two assays. Overall, the trend emphasized the importance of an H-bond donor at the THIQ nitrogen and the need to retain basicity.

Table 2.3 Effect of THIQ Nitrogen Atom Substitutions on Viral Attachment and Calcium Flux.



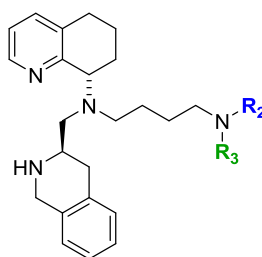
Compound ID	R ₁	MAGI HIV-1 _{III} B IC ₅₀ (μM) ^{†,‡}	Ca ²⁺ Flux IC ₅₀ (μM) [‡]
ECXC-00947 ^a	H	0.005	0.003
51 ^b	Me	0.02	0.039
52 ^b	<i>i</i> -Pr	0.03	0.14
53 ^b		0.03 (TC ₅₀ = 6.9)	0.23
54 ^b		0.06 (TC ₅₀ = 3.4)	0.1
55 ^b		0.07 (TC ₅₀ = 4.5)	0.65
56 ^b		0.06	0.06
57 ^b		0.1 (TC ₅₀ = 33.6)	0.14
58 ^b		0.08	0.57

[†]All compounds had TC₅₀ values >10 μM. [‡]All assays were run in duplicate. Compounds were synthesized by ^aLawrence Wilson, Ph.D., ^bValarie Truax.

Modifications to the butylamine nitrogen also provided interesting details regarding structural requirements for potent inhibition (Table 2.4). Alkylation of the side chain amine with simple

groups such as dimethyl substituents (**59**) and an isopropyl group (**60**) retained potent activity in both assays. However, to our surprise, the 2-pyridyl compounds (**62**, **63**) and carbamide derivatives (**13-15**) were 25–85-fold less potent than compound **ECXC00947** in the MAGI assay.⁸⁷ However, the majority of these compounds remained equipotent in blocking CXCL12-induced calcium flux.

Table 2.4 Effect of Butylamine Nitrogen Substitutions on Viral Attachment and Calcium Flux.



Compound ID	R ₂	R ₃	MAGI HIV-1 _{III} B IC ₅₀ (μM) ^{†,‡}	Ca ²⁺ Flux IC ₅₀ (μM) [‡]
ECXC00947 ^a	H	H	0.005	0.003
59 ^b	Me	Me	0.03	0.008
60 ^b	<i>i</i> -Pr	H	0.04	0.007
61 ^b		H	0.01 (TC ₅₀ = 4.1)	0.007
62 ^a		H	0.12	0.001
63 ^b		H	0.13 (TC ₅₀ = 6.9)	0.16
13		H	0.29	0.004
14		H	0.21	0.003
15		H	0.42	0.18
18		H	0.007	0.003

[†]All compounds had TC₅₀ values >10 μM. [‡]All assays were run in duplicate. Compounds were synthesized by ^aLawrence Wilson, Ph.D., ^bValarie Truax.

The results signified that basicity and the steric environment of the butylamine nitrogen could be critical for anti-HIV activity, but not for the disruption of CXCL12-mediated receptor signaling since nearly all substitution patterns (with the exception of dimethyl urea **15**) resulted in potent inhibition of calcium flux. This hypothesis was further supported by the data obtained for guanidine **18**. This strongly basic arginine mimic exhibited the same potent activity observed with lysine mimic **ECXC00947**. While the complete nature of the differences discussed above was not initially understood, we developed computational models (*vide infra*) that attempted to explain this phenomenon through proposed receptor interactions. Taken together with the THIQ nitrogen substitution effects, the results are significant and novel with regard to antagonist design.

2.4.2 Interpretation of Biological Data Through Molecular Modeling

We undertook a computational docking study in order to better understand the preliminary SAR and to develop a working hypothesis on how our compounds interact with the receptor. Using the recently reported CXCR4 crystal structure, a postdoctoral chemist in our laboratory, Bryan Cox, Ph.D., developed a computational model of **ECXC00947** bound to CXCR4 (further details discussed in Chapter 3). Compound **ECXC00947** was docked into the CVX15 peptide-bound form of the receptor (PDB ID 3OE0) based on the hypothesis that the THIQ-based compounds act as peptide mimetics. Depicted in Figure 2.14 is a pose of **ECXC00947** where the bottom nitrogen forms an electrostatic interaction with Glu288 and the butylamine interacts with Asp171 *via* a salt bridge. Meanwhile, the top THQ ring is buried in a hydrophobic pocket about Arg188 near the site of the naphthylalanine ring from the CVX15 peptide.

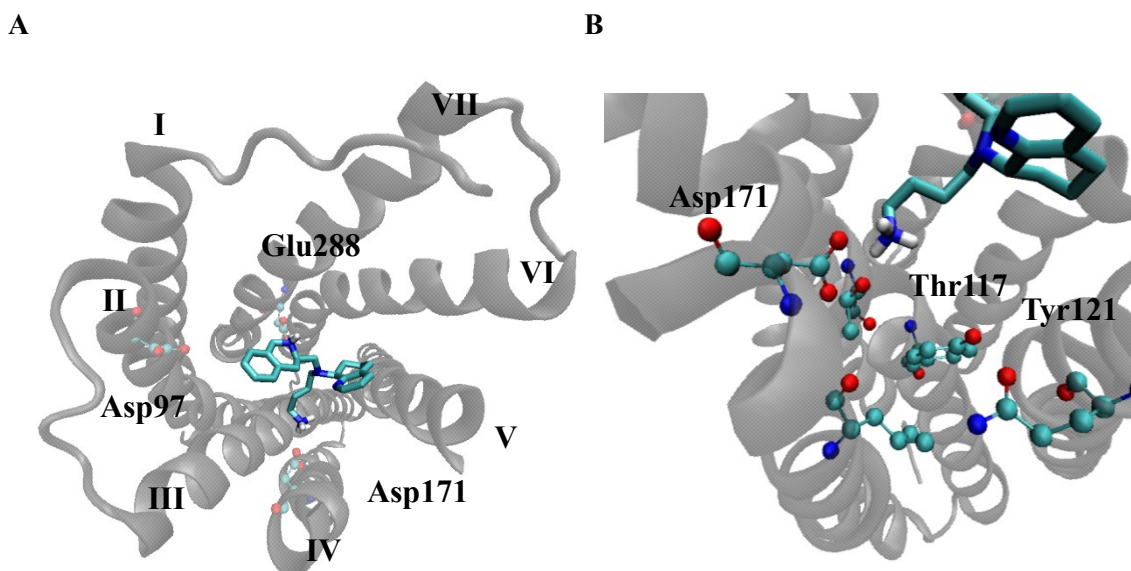


Figure 2.14 Proposed Bioactive Pose of **ECXC-00947** (blue tube) Docked into CXCR4:CVX15 Crystal Structure (grey ribbon). Interactions between compound **ECXC00947** and key residues are highlighted: **A**) D97 (Helix II), D171 (Helix IV), E288 (Helix VII) and **B**) T117 (Helix III), Y121 (Helix III).

We were optimistic that docking urea **14** into the same crystal structure mentioned above would shed light on the biological data with regard to its bias toward inhibition of receptor signaling over blockade of viral attachment. Shown in Figure 2.15 is the proposed bioactive pose of compound **14**. The compound appeared to adopt a conformation very similar to **ECXC00947**, with the exception of the butyl side chain. Specific differences were apparent in the contacts the urea moiety was shown to make with the receptor. Therefore, we concluded that if Asp171 is critical for viral entry, then compounds that do not interact with this residue will be less active in the MAGI assay.

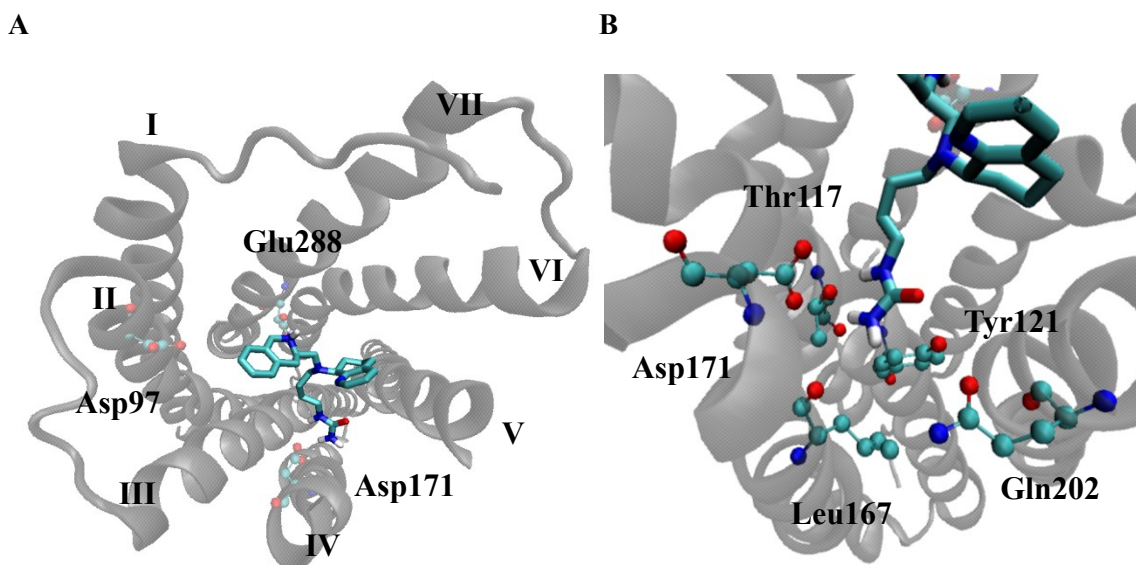


Figure 2.15 Proposed Bioactive Pose of **14** (blue tube) Docked into CXCR4:CVX15 Crystal Structure (grey ribbon). Interactions between compound **14** and key residues are highlighted: **A**) D171 (Helix IV), E288 (Helix VII) and **B**) T117 (Helix III), Y121 (Helix III), Q202 (Helix V).

2.4.3 *In Vitro* Analysis of Drug Efflux and Permeability

Assessing and understanding the ADMET properties of candidate compounds is critical to successful drug discovery. One of the most important properties of oral compounds is absorption. While drugs that target surface receptors do not require access to the inside of target cells, they may have to cross membrane barriers depending on the route and point of administration. For oral medications, the compounds must survive encounters with low pH environments and numerous gastrointestinal secretions. Additionally, absorption of oral drugs involves transport across the lipoidal membranes of epithelial cells lining the GI tract. This absorption can occur through passive diffusion or by active carrier transport mechanisms.

A large number of the drug candidate failures from development programs have been attributed to undesirable pharmacokinetic properties like poor absorption. Therefore, it is of no surprise that cellular permeability and lipophilicity are drug characteristics that are now being considered much earlier in the drug discovery process. Assays that estimate the ability of

potential drug compounds to cross the intestinal epithelium have been widely used in academic laboratories and in the pharmaceutical industry.

An established *in vitro* model system for measuring drug absorption uses the Caco-2 cell line, an immortalized, heterogeneous cell line derived from a human colorectal adenocarcinoma. These cells resemble intestinal epithelial cells in that they form a polarized monolayer with a well-defined brush border on the apical surface and intercellular junctions. The assays works by introducing the test compound to either the upper (apical, A) or lower (basolateral, B) chamber to measure permeability as illustrated in Figure 2.16. Samples are taken from the opposite chamber at various time intervals in order to measure the amount of compound that crossed the cell monolayer. The permeability coefficient (P_{app}) is calculated in the absorptive ($A \rightarrow B$) and secretive ($B \rightarrow A$) directions (Figure 2.17).

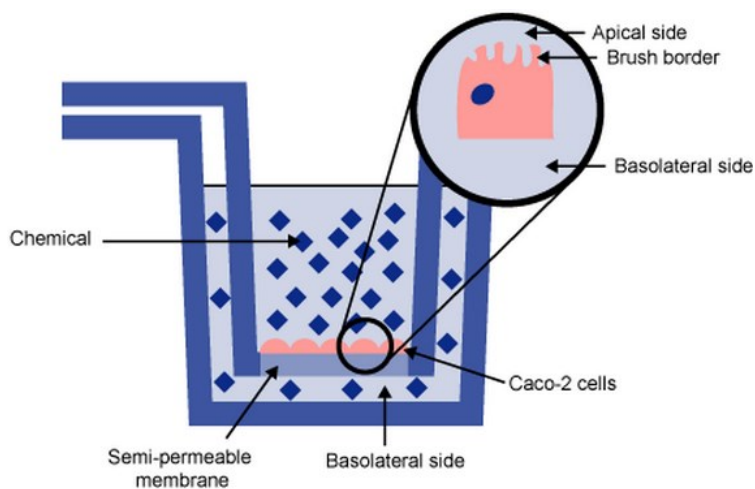


Figure 2.16 Diagram of the Caco-2 Permeability Assay.¹²¹

$$P_{\text{app}} = \left(\frac{\frac{dQ}{dt}}{C_o \times A} \right)$$

$\frac{dQ}{dt}$ = rate of drug permeation across cells

C_o = donor compartment concentration at time zero

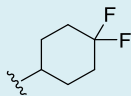
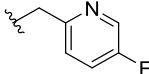
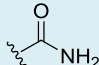
A = area of cell monolayer

Figure 2.17 Equation Used to Calculate Permeability Coefficient (P_{app}).

Although the acetylated compounds (**13-15**, Table 2.4) were less potent than the lead compound (**ECXC00947**) in the MAGI assay, they did display potent inhibition of CXCL12-induced calcium flux. Therefore, the urea compound (**14**) and a number of other molecules from the series were selected for permeability testing by the Caco-2 assay (for brevity, only compounds **ECXC00947**, **60**, **61**, **63** and **14** are represented in Table 2.5). Specifically, we were interested in whether or not the pharmacokinetic properties of **14** and **ECXC00947** determined *in vitro* were reflective of their calculated $\log D$ values (0.92 and -0.65, respectively).

All compounds were classified as having low permeability, with the exception of fluoropyridyl **63**. The high permeability of this compound could explain the toxicity observed in the MAGI assay (Table 2.4). Specifically, we speculated that this compound could have entered cells and activated death pathways. However, this possibility was not explored further. Additionally, the large efflux ratios indicated that these compounds underwent active efflux potentially mediated by permeability glycoprotein (P-gp). Compound **ECXC00947** did not appear to undergo significant efflux. Unfortunately, the increased lipophilicity predicted for the urea-containing compound (**14**) did not seem to translate to improved absorption. While its predicted $\log D$ was positive (0.92) and larger than that of the lead compound (-0.65), the value did not fall within the proposed optimal range of 1-3. This could explain the disparity in the predicted absorption and the permeability classification determined by the assay.

Table 2.5 Caco-2 Permeability Data for Selected THIQ Analogues.

Compound ID	R ₂	R ₃	P _{app} (10 ⁻⁶ cm/s)		Efflux Ratio	Permeability Classification [†]	Significant Efflux [‡]
			A → B	B → A			
ECXC00947 ^a	H	H	<0.47	0.94	>2	low	no
60^b	<i>i</i> -Pr	H	0.61	15.9	26	low	yes
61^b		H	0.23	17.3	75	low	yes
63^b		H	1.15	28.4	25	high	yes
14		H	0.19	6.7	35	low	yes

[†](P_{app} A → B) < 1.0 x 10⁻⁶ cm/s: low; (P_{app} A → B) ≥ 1.0 x 10⁻⁶ cm/s: high. [‡] Efflux ratio > 3.0 and (P_{app} B → A) ≥ 1.0 x 10⁻⁶ cm/s. Compounds were synthesized by ^aLawrence Wilson, Ph.D., ^bValarie Truax.

2.5 Conclusions

Chemokine receptors have attracted increasing attention as potential drug targets. More specifically, CXCR4 has been heavily pursued by medicinal chemistry programs due to its involvement in many disease states, including several immunodeficiency disorders and more than 23 different types of cancer. However, the development of CXCR4 antagonists has been hindered by a lack of drugs with oral bioavailability or by compounds that cause toxicity due to undesired off-target activity. Throughout this study, we were interested in identifying potent CXCR4 antagonists that might address the issues discussed above.

In summary, a novel series of potent CXCR4 antagonists was identified through a hit-to-lead effort focused on benzimidazole replacements. The series makes use of a GPCR chemotype containing a chiral linkage that may exploit unique and critical contacts with amino acid residues in the receptor. Additionally, the chiral (*R*)-THIQ scaffold has provided several compounds with intriguing biological selectivity.

The chemical routes employed at the inception of the project were acceptable for synthesizing a handful of THIQ-based compounds. However, as several new analogues were proposed, we were interested in arriving at a more cost-effective and efficient synthetic approach. By changing

the starting material used in the synthesis of the butylamine side chain (**22**, Scheme 2.2), the reaction time was reduced to 2 hours, and the product yield was significantly improved. Likewise, I was able to rapidly generate over 50 g of enantiopure (*R*)-THIQ carboxylic acid starting material (**27**, Scheme 2.3) in just a few steps from the inexpensive unnatural amino acid, D-phenylalanine. These reaction improvements expedited the synthesis of several analogues that were important for SAR development.

Initial modifications to the THIQ nitrogen and butylamine side chain provided clues regarding the types of interactions necessary for tight binding to the receptor. We hypothesized that acylated compounds (**13-15**) that masked the basicity of the side chain nitrogen would be potent in both assays and have improved physical properties. Unfortunately, they were less active in the viral attachment assay when compared to our lead compound (**ECXC00947**). Interestingly, they retained potency against CXCL12-induced calcium flux. Comparison of the poses modeled in the CXCR4:CVX15 crystal structure highlighted different residues interacting with urea **14** and **ECXC00947**. It remains to be seen whether or not this difference is substantial enough to account for the discrepancy in anti-HIV activity between these two compounds.

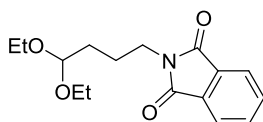
Several compounds were analyzed *in vitro* by the Caco-2 assay to assess their potential for *in vivo* absorption. According to *clogD* predictions, we expected the urea-containing compound (**14**) to perform better than the lead molecule (**ECXC00947**). However, both compounds were classified by low permeability. Additionally, only compound (**ECXC00947**) demonstrated no significant efflux in the Caco-2 assay.

Taken together, the data have provided valuable insight for the prospective design of CXCR4 antagonists with unique properties. More specifically, the results indicate that rational design may lead to compounds that block X4-tropic HIV entry and do not interfere with CXCL12-based receptor signaling or provide more potent antagonists of the CXCR4/CXCL12 axis with potential utility in stem cell mobilization and cancer treatment.

2.6 Chemistry Experimental Detail

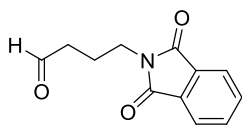
2.6.1 Synthetic Chemistry Experimental Detail

All reagents were obtained from commercial suppliers and used without further purification unless specified otherwise. Reaction progress was monitored by thin layer chromatography (TLC) on pre-coated glass plates (silica gel 60 F254, 0.25 mm) or liquid chromatography-mass spectrometry (LC-MS) using an analytical column (Agilent, ZORBAX Eclipse XDB-C18, 50 x 4.6 mm, 3.5 μm). When noted, flash chromatography was performed manually or on a Teledyne ISCO Combiflash Companion with prepackaged Teledyne Redisep or Silicycle disposable normal phase or amine functionalized silica columns. Proton and carbon NMR spectra were recorded on an INOVA-400 (400 MHz), VNMRS 400 (400 MHz), INOVA-600 (600 MHz), or Unity-600 (600 MHz). All chemical shifts are reported in parts per million and referenced to the residual solvent peak. Mass spectra were performed by the Emory University Mass Spectroscopy Center on either a VG 70-S Nier Johnson or JEOL instrument. Final compound purity was established through high-performance liquid chromatography (HPLC) on a Agilent 1200 Series system using an analytical column (Agilent, ZORBAX Eclipse XDB-C18, 50 x 4.6 mm, 3.5 μm) and a mixture of either water and MeOH or water and MeCN as the mobile phase both with constant 0.1% v/v formic acid at a flow rate of 1.0 mL/min.). Enantiopurity was determined by chiral HPLC on an Agilent 1200 Series system with a ChiralPak AD-RH column (150 mm x 4.6 mm, 5 μm) and a mixture of water and MeCN as the mobile phase with constant 0.1% v/v formic acid at a flow rate of 1.0 mL/min.).

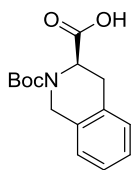


2-(4,4-diethoxybutyl)isoindoline-1,3-dione (32). Deionized water (116 mL) and THF (116 mL) were added to a 1000 mL round bottom flask. To the solvent were added sodium bicarbonate (13.0 g, 155 mmol) and 4-aminobutyraldehyde diethyl acetal (26.8 mL, 155 mmol). To this

mixture was added *N*-carbethoxyphthalimide (35.7 g, 163 mmol). The reaction was kept at room temperature for 2 hours. The reaction mixture was diluted with EtOAc (200 mL) and washed with brine. The organic phase was separated, and the aqueous layer was extracted with EtOAc (200 mL). The organic layers were combined, washed with brine, and dried over anhydrous MgSO₄. The solvent was removed *in vacuo* yielding a colorless oil. The crude material was purified by flash column chromatography (300 g silica gel, 20% EtOAc-Hexanes) to afford the title compound as a clear oil (39.0 g, 86%). ¹H NMR [400 MHz, CDCl₃] δ 7.94-7.74 (m, 2H), 7.74-7.54 (m, 2H), 4.51 (t, *J* = 5.6 Hz, 1H), 3.71 (t, *J* = 7.1 Hz, 2H), 3.63 (dq, *J* = 7.1, 9.4 Hz, 2H), 3.48 (dq, *J* = 7.1, 9.4 Hz, 2H), 1.83-1.71 (m, 2H), 1.70-1.59 (m, 2H), 1.18 (t, *J* = 7.1 Hz, 6H); ¹³C NMR [100 MHz, CDCl₃] δ 168.5 (2C), 134.0 (2C), 132.3 (2C), 123.3 (2C), 102.6, 61.4 (2C), 37.9, 31.1, 24.2, 15.5 (2C).

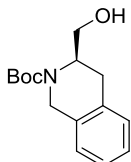


4-(1,3-dioxisoindolin-2-yl)butanal (22). To a solution of compound 33 (2.8 g, 9.5 mmol) dissolved in THF (9.0 mL) was added 1 M HCl (2.7 mL, 2.7 mmol). After 72 hours, the reaction was quenched with careful addition of saturated aqueous NaHCO₃. The solvent was removed and the residue was diluted with EtOAc (50 mL). The organic phase was washed with brine and dried over anhydrous MgSO₄. The crude material was purified by flash column chromatography (ISCO, 40 g silica gel, 0-40% EtOAc-Hexanes over 22 minutes) to afford the title compound as an oil that solidified upon standing to a white solid (1.70 g, 84%). ¹H NMR [400 MHz, CDCl₃] δ 9.76 (d, *J* = 1.2 Hz, 1 H), 7.83 (dd, *J* = 3.1, 5.4 Hz, 2H), 7.71 (dd, *J* = 3.0, 5.3 Hz, 2H), 3.73 (t, *J* = 6.8 Hz, 2H), 2.53 (td, *J* = 1.1, 7.3 Hz, 2H), 2.01 (pentet, *J* = 7.0 Hz, 2H); ¹³C NMR [100 MHz, CDCl₃] δ 201.1, 168.5 (2C), 134.2 (2C), 132.2(2C), 123.5 (2C), 41.3, 37.3, 21.3; HRMS (ESI) [M+H]⁺, calc'd for C₁₂H₁₂NO₃ 218.08117, found 218.08144.

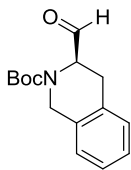


(R)-2-(tert-butoxycarbonyl)-1,2,3,4-tetrahydroisoquinoline-3-carboxylic acid (27). Step 1: Synthesis of (R)-1,2,3,4-tetrahydroisoquinoline-3-carboxylic acid hydrobromide. A slurry containing D-phenylalanine (20.0 g, 121 mmol) and 48 wt. % HBr in water (96.0 mL, 848 mmol) was heated to 40 °C. To the slurry was added 37 wt. % formaldehyde in water (18.0 mL, 242 mmol) at a rate of 1 mL/min. The reaction was then heated to 85 °C for 12 hours. The reaction was cooled to room temperature where it stirred for 6 hours. The resulting white precipitate was collected by filtration, rinsed with EtOH, and dried under high vacuum. The crude white solid (23.8 g, 76%) was carried on without further purification. Step 2: Synthesis of (R)-1,2,3,4-tetrahydroisoquinoline-3-carboxylic acid. The HBr salt from step 1 (15.0 g, 58.1 mmol) was stirred in water (6.0 mL) and treated with 10% aqueous NaOH solution to a pH of 3. The solution was further basified with 1% aqueous NaOH solution to a pH of 4.5-5. The resulting slurry was filtered, rinsed with water, and dried. The crude white solid (9.30 g, 91%) was carried on without further purification. HRMS (ESI) $[M+H]^+$, calc'd for $C_{10}H_{12}NO_2$ 178.08626, found 178.08626. Step 3: To a suspension of the free base from step 2 (9.3 g, 52.7 mmol) in dioxane (150 mL) was added 1 M NaOH (211 mL, 211 mmol) and di-*tert*-butyl dicarbonate (24.5 mL, 105 mmol). The resulting mixture was stirred at room temperature for 12 hours before being concentrated. To the residue was added EtOAc (500 mL). The reaction was acidified to pH = 2.0 with 6 M HCl. The organic layer was washed with brine and water. The organic layer dried over anhydrous $MgSO_4$, filtered, and concentrated. The crude white solid (13.4 g, 92%) was carried on without further purification. 1H NMR [400 MHz, $CDCl_3$] (1:1 mixture of rotamers due to restricted rotation) δ 9.78 (br s, 1H), 7.06-7.25 (m, 4H), 5.13 (dd, $J = 3.2, 6.2$ Hz, 0.5 H), 4.75 (app. t, $J = 5.5$ Hz, 0.5H), 4.69 (dd, $J = 16.3, 8.1$ Hz, 1H), 4.48 (app. t, $J = 16.7$ Hz, 1H), 3.30-3.22 (m, 0.5H), 3.21-3.10 (m, 1.5H), 1.52 (s, 4.5H), 1.41 (s, 4.5H); ^{13}C NMR [100 MHz, $CDCl_3$]

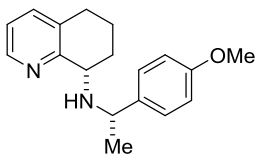
δ 178.0, 177.2, 155.9, 155.0, 134.0, 132.9, 132.1, 131.8, 128.7, 128.0, 127.2, 127.1, 127.0, 126.9, 126.6, 126.4, 81.2, 54.3, 52.5, 44.7, 44.1, 31.5, 31.0, 28.6, 28.4; HRMS (ESI) $[M-H]^-$, calc'd for $C_{16}H_{18}NO_4$ 276.12413, found 276.12394; $[\alpha]_D = -9.5^\circ$ (c 1.03, $CHCl_3$); HPLC chirality: er >99:1 (*R*)-enantiomer $t_R = 7.450$ min., (*S*)-enantiomer $t_R = 7.941$ min. (30-60-80% MeCN/Water with 0.1% formic acid, gradient over 20 minutes, 1.0 mL/min.).



***tert*-butyl (*R*)-3-(hydroxymethyl)-3,4-dihydroisoquinoline-2(*1H*)-carboxylate (34).** A solution of compound **27** (7.0 g, 25.2 mmol) in dry THF (50.0 mL) was cooled to 0 °C. A solution of 2.0 M borane dimethyl sulfide in THF (25.2 mL, 50.5 mmol) was slowly added to the reaction mixture. The reaction was kept at 0 °C for 2 hours until being warmed to room temperature where it stirred for 13 hours. The mixture was cooled to 0 °C before slowly adding MeOH (70 mL) and allowed to warm to room temperature where it stirred for 2 hours. The solvent was removed by rotary evaporation. To the light yellow oil was added EtOAc (100 mL) and water (50 mL). The organic phase was removed. The aqueous layer was extracted with EtOAc (50 mL). The organic extracts were combined and washed with saturated aqueous $NaHCO_3$ and brine. The organic layer was dried over $MgSO_4$ and concentrated. The crude light yellow oil (6.59 g, 99%) was carried on without further purification. 1H NMR [600 MHz, $CDCl_3$] δ 7.22-7.18 (m, 2H), 7.18-7.14 (m, 1H), 7.14-7.11 (m, 1H), 4.89-4.61 (m, 1H), 4.60-4.39 (m, 1H), 4.32 (d, $J = 16.4$ Hz, 1H), 3.61-3.38 (m, 2H), 3.04 (dd, $J = 15.8, 6.0$ Hz, 1H), 2.81 (s, 1H), 1.51 (s, 9H); HRMS (ESI) $[M+H]^+$, calc'd for $C_{15}H_{21}NO_3$ 264.15942, found 264.15959; HPLC chirality: er >97:3 (*R*)-enantiomer $t_R = 5.348$ min., (*S*)-enantiomer $t_R = 4.924$ min. (50-80% MeCN/Water with 0.1% formic acid, gradient over 10 minutes, 1.0 mL/min.).

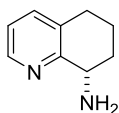


tert-butyl (R)-3-formyl-3,4-dihydroisoquinoline-2(1H)-carboxylate (25). A solution of compound **34** (2.0 g, 7.6 mmol) and TEA (3.2 mL, 22.8 mmol) dissolved in DCM (22.0 mL) was cooled to -5 °C. To the reaction mixture was added SO₃-pyridine complex (3.6 g, 22.8 mmol) dissolved in DMSO (22.0 mL, 319.0 mmol). The reaction was held at 0 °C for 1 hour. The reaction mixture was quenched with saturated aqueous NaHCO₃ and extracted with diethyl ether (3x). Organics were washed with brine, dried over Na₂SO₄, filtered, and concentrated by rotary evaporation to a yellow oil. The crude material was purified by flash column chromatography (ISCO, 40 g silica gel, 0-15% EtOAc-Hexanes over 15 minutes) to afford the title compound as a colorless oil (1.28 g, 65%). ¹H NMR [400 MHz, CDCl₃] (1:1 mixture of rotamers due to restricted rotation) δ 9.52 (s, 0.5H), 9.47 (s, 0.5H), 7.25-7.07 (m, 4H), 4.84 (dd, *J* = 6.4, 3.7 Hz, 0.5H), 4.70 (d, *J* = 16.1 Hz, 1H), 4.58 (d, *J* = 16.4 Hz, 1H), 4.46 (app. t, *J* = 5.4 Hz, 0.5H), 3.26 (dd, *J* = 15.9, 3.8 Hz, 0.5H), 3.10 (m, 1.5H), 1.54 (s, 4.5H), 1.46 (s, 4.5H); ¹³C NMR [100 MHz, CDCl₃] δ 201.3, 200.7, 155.8, 155.0, 134.3, 133.3, 132.5, 132.1, 128.6, 127.9, 127.5, 127.3, 127.2, 127.1, 126.6, 126.5, 81.5, 81.2, 60.7, 59.4, 45.2, 44.5, 29.5, 28.6, 28.5.



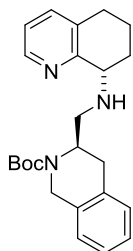
(S)-N-((S)-1-(4-methoxyphenyl)ethyl)-5,6,7,8-tetrahydroquinolin-8-amine (28). A solution of (S)-1-(4-methoxyphenyl)ethanamine (48.8 mL, 331 mmol) and 6,7-dihydroquinolin-8(5H)-one (44.2 g, 301 mmol) in DCM (700 mL) was added acetic acid (0.17 mL, 3.0 mmol) followed by sodium triacetoxyborohydride (89.0 g, 421.0 mmol) in one portion. The reaction was allowed to stir at room temperature. After 20 minutes, a slight exotherm was observed (20.2-31.7 °C). At this time, the reaction flask was chilled in a cold water bath until the temperature dropped. The

reaction was allowed to stir at room temperature for 24 hours. Solid NaHCO₃ (80.0 g) was added followed by water (500 mL). The reaction mixture was allowed to stir at room temperature for 30 minutes before being transferred to a separatory funnel. The aqueous layer was extracted with DCM (3x). The organics were dried over MgSO₄ and concentrated to a brown oil. The crude material was purified by flash column chromatography (120 g silica gel, 50-70-100% EtOAc-Hexanes). The resulting brown-yellow oil was dried on high vacuum (79 g). The material was triturated in cold hexanes to afford the title compound as a light yellow solid (50.5 g, 60%). Only one diastereomer was observed by NMR. ¹H NMR [400 MHz, CDCl₃] δ 8.42 (ddd, *J* = 4.7, 1.8, 0.8 Hz, 1H), 7.41-7.30 (m, 3H), 7.06 (dd, *J* = 7.7, 4.7 Hz, 1H), 6.91-6.83 (m, 2H), 4.05 (q, *J* = 6.6 Hz, 1H), 3.84 (dd, *J* = 7.7, 5.2 Hz, 1H), 3.81 (s, 3H), 2.82-2.62 (m, 3H), 1.84 (dq, *J* = 13.0, 5.5, 2.6 Hz, 1H), 1.74 (dddd, *J* = 13.0, 7.7, 5.3, 2.4, 1.0 Hz, 1H), 1.65-1.55 (m, 1H), 1.55-1.47 (m, 1H), 1.45 (d, *J* = 6.5 Hz, 3H); ¹³C NMR [150 MHz, CDCl₃] δ 158.4, 158.3, 146.9, 139.9, 137.0, 132.5, 127.9 (2C), 121.9, 113.7 (2C), 58.3, 57.7, 55.4, 30.3, 28.9, 25.0, 19.6; HRMS (ESI) [M+H]⁺, calc'd for C₁₈H₂₃N₂O 283.18049, found 283.18044.

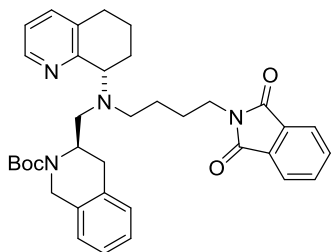


(S)-5,6,7,8-tetrahydroquinolin-8-amine (26). A mixture of compound **28** (5.9 g, 20.8 mmol) and TFA (16.0 mL, 208.0 mmol) stirred at ambient temperature for 24 hours. The reaction was diluted with EtOAc (100 mL) and water (100 mL). The organic layer was extracted with water (4 x 40 mL). The water layer was basified with solid NaOH pellets (pH 12-14) and extracted with DCM (3 x 100 mL). The organic extracts were combined, dried over Na₂SO₄, and concentrated by rotary evaporation. The crude light brown oil (2.84 g, 95%) was carried on without further purification. ¹H NMR [400 MHz, CDCl₃] δ 8.33 (d, *J* = 3.1 Hz, 1H), 7.32-7.24 (m, 1H), 6.98 (ddd, *J* = 7.7, 4.5, 2.8 Hz, 1H), 3.93 (app. t, *J* = 6.5, 6.5 Hz, 1H), 2.81-2.61 (m, 2H), 2.19-2.05 (m, 1H), 1.87 (s, 3H), 1.78-1.56 (m, 2H); ¹³C NMR [100 MHz, CDCl₃] δ 159.7, 147.1, 136.7,

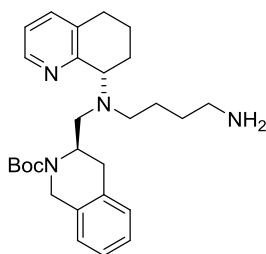
131.6, 121.7, 51.5, 32.1, 29.1, 20.0; HRMS (ESI) $[M+H]^+$, calc'd for $C_9H_{13}N_2$ 149.10732, found 149.10736.



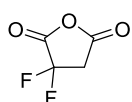
tert-butyl (R)-3-(((S)-5,6,7,8-tetrahydroquinolin-8-yl)amino)methyl)-3,4-dihydroisoquinoline-2(1H)-carboxylate (21). To a solution of amine **26** (0.7 g, 4.6 mmol) dissolved in DCE (19.0 mL) was added sodium triacetoxyborohydride (1.2 g, 5.7 mmol) immediately followed by aldehyde **25** (1.0 g, 3.8 mmol) dissolved in dichloroethane (19.0 mL). The reaction was allowed to stir at room temperature for 15 hours. The mixture was quenched with saturated aqueous $NaHCO_3$ and extracted with DCM (3x). The organic layer was dried over Na_2SO_4 , filtered and concentrated by rotary evaporation to a golden brown oil (~2.0 g). The crude material was purified by flash column chromatography (ISCO, 80 g silica gel, 0-5% DCM-MeOH over 20 minutes) to afford the title compound as a brown oil (0.908 g, 60%, dr = 4:1 by LC-MS). 1H NMR [400 MHz, $CDCl_3$] (reported as a mixture of diastereomers) δ 8.38 (s, 1H), 7.36 (d, $J = 7.7$ Hz, 1H), 7.21-7.02 (m, 5H), 4.90-4.72 (m, 1H), 4.71-4.44 (m, 1H), 4.29 (d, $J = 16.9$ Hz, 1H), 3.81- 3.65 (m, 1H), 3.14-2.92 (m, 2H), 2.84-2.68 (m, 3H), 2.58 (t, $J = 10.1$ Hz, 1H), 2.00-1.91 (m, 2H), 1.73-1.59 (m, 2H), 1.51 (s, 9H), 1.44 (br s, 1H); HRMS (ESI) $[M+H]^+$, calc'd $C_{24}H_{32}N_3O_2$ 394.24890, found 394.24894.



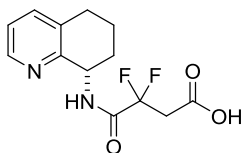
tert-butyl (R)-3-(((4-(1,3-dioxisoindolin-2-yl)butyl)((S)-5,6,7,8-tetrahydroquinolin-8-yl)amino)methyl)-3,4-dihydroisoquinoline-2(1H)-carboxylate (20). To a solution of amine **21** (1.2 g, 3.0 mmol) in dry DCE (10.0 mL) was added aldehyde **22** (1.0 g, 4.5 mmol) and acetic acid (0.17 mL, 3.0 mmol). Immediately following, was added sodium triacetoxyborohydride (1.0 g, 4.5 mmol) in one portion. The reaction was allowed to stir at room temperature for 2 hours and then was quenched with saturated aqueous NaHCO₃ (pH 9). The aqueous phase was extracted with DCM (3x), dried over Na₂SO₄, filtered, and concentrated by rotary evaporation to a light brown oil. The crude material was purified by flash column chromatography (ISCO, 80 g silica gel, 0-10% EtOAc-Hexanes over 10 minutes, then 10% EtOAc for 3 minutes, 10-17% EtOAc over 4 minutes) to afford the title compound as an off-white foam (1.01 g, 54%). ¹H NMR [600 MHz, CDCl₃] δ 8.32 (d, *J* = 16.2 Hz, 1H), 7.84-7.81 (m, 2H), 7.71-7.68 (m, 2H), 7.21 (d, *J* = 7.8 Hz, 1H), 7.09-7.06 (m, 3H), 7.01-6.98 (m, 1H), 6.95-6.92 (m, 1H), 4.64 (d, *J* = 16.8 Hz, 1H), 4.12 (d, *J* = 16.8 Hz, 1H), 3.59-3.53 (m, 2H), 2.98-2.91 (m, 2H), 2.78-2.53 (m, 5H), 2.42-2.40 (m, 1H), 2.05-2.01 (m, 2H), 1.93 (br s, 1H), 1.74-1.63 (m, 5H), 1.49 (s, 9H), 1.37-1.33 (m, 2H); ¹³C NMR [150 MHz, CDCl₃] δ 168.4, 158.2, 155.1, 146.8, 136.3, 134.0, 133.8, 133.3, 132.2, 129.4, 129.0, 126.3, 126.1, 125.9, 123.1, 121.3, 79.7, 61.6, 55.3, 51.1, 49.6, 43.2, 38.0, 30.5, 29.1, 28.6, 27.1, 26.4, 21.3; HRMS (ESI) [M+H]⁺, calc'd C₃₆H₄₃N₂O₄ 595.32788, found 595.32808.



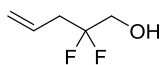
tert-butyl (R)-3-(((4-aminobutyl)((S)-5,6,7,8-tetrahydroquinolin-8-yl)amino)methyl)-3,4-dihydroisoquinoline-2(1H)-carboxylate (38). Compound **20** (0.8 g, 1.4 mmol) was dissolved in MeOH (7.0 mL) followed by the addition of 24% aqueous solution of hydrazine hydrate (2.2 mL, 10.7 mmol). The reaction was allowed to stir at room temperature for 24 hours. The solvent was removed and DCM was added to the resulting residue. The organic layer was washed with 0.5 M aqueous NaOH, and the aqueous layer was discarded. To the organic layer was added 1 M aqueous HCl (pH 3). The organic layer was extracted twice with 1 M aqueous HCl and then discarded. The aqueous layer was treated with solid NaOH to bring the pH to 12-13. The aqueous layer was extracted with DCM (3x). The combined organic extracts were dried over Na₂SO₄, filtered, and concentrated. The crude yellow, amorphous foam (0.400 g, 60%) was carried on without further purification. HRMS (ESI) [M+H]⁺, calc'd C₂₈H₄₁N₄O₂ 465.32240, found 465.32226.



3,3-difluorodihydrofuran-2,5-dione (41). To a solution of 2,2-difluorosuccinic acid (0.5 g, 3.3 mmol) in *i*-PrOAc (6.5 mL) was added TFAA (0.6 mL, 3.9 mmol) in one portion at room temperature. The reaction stirred at 50 °C for 2.5 hours. A small aliquot of the reaction mixture was added to MeOH. Analysis of the aliquot by LC-MS showed the methyl ester (with remaining starting material) indicative of the anhydride adduct. The reaction material was carried on immediately to next reaction without concentrating or purifying.

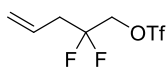


(S)-3,3-difluoro-4-oxo-4-((5,6,7,8-tetrahydroquinolin-8-yl)amino)butanoic acid (42). To a flask containing compound **41** (0.4 g, 3.3 mmol) held at 5 °C, was added dropwise amine **26** (0.5 g, 3.3 mmol) dissolved in *i*-PrOAc (1.0 mL). While adding the amine, the reaction temperature was kept below 20 °C. Following the addition, the reaction was allowed to warm to room temperature where it stirred for 2 hours. The mixture was quenched with water and added saturated aqueous NaHCO₃ to pH 8-9. The organic layer was separated. The aqueous layer was acidified with 5N HCl to pH 1 and extracted with *i*-PrOAc. All three layers were analyzed by LC-MS and found to contain the desired product (presumably due to formation of the zwitterion). All extraction flasks were retained and sat exposed to air. After evaporating for 5 days at room temperature, the acidic aqueous layer contained a significant amount of pink needle crystals. The crystals were filtered and rinsed with water to afford the title compound (0.204 g, 16%). A sample was submitted to the Emory X-ray Crystallography Center, Department of Chemistry where the crystal structure was solved by Dr. John Bacsa (see section 2.6.2). ¹H NMR [600 MHz, DMSO-*d*₆] δ 12.83 (s, 1H), 8.95 (d, *J* = 8.0 Hz, 1H), 8.38 (dd, *J* = 4.7, 1.5 Hz, 1H), 7.52 (dd, *J* = 7.7, 1.6 Hz, 1H), 7.21 (dd, *J* = 7.7, 4.6 Hz, 1H), 4.93 (td, *J* = 7.6, 5.6 Hz, 1H), 3.32- 3.10 (m, 2H), 2.85-2.68 (m, 2H), 1.99 (dtd, *J* = 12.9, 6.8, 5.3, 2.9 Hz, 1H), 1.95-1.80 (m, 2H), 1.74 (dtd, *J* = 12.7, 7.1, 6.4, 3.5 Hz, 1H).

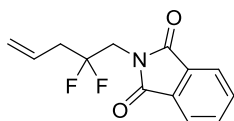


2,2-difluoropent-4-en-1-ol (45). To a flask containing 1 M LiAlH₄ in diethyl ether (26.5 mL, 26.5 mmol) at 0 °C was slowly added a solution of 2,2-difluoropent-4-enoic acid (1.0 mL, 8.8 mmol) in dry diethyl ether (4.0 mL). The reaction stirred at 0 °C for 2 hours before being warmed to room temperature over 3 hours. The mixture was cooled to 0 °C and was added

dropwise 1.0 mL of water followed by 1.0 mL of a 15% aqueous NaOH solution. Finally, 3.0 mL of water was added. The slurry stirred for 1 hour at room temperature and was then filtered over a pad of Celite. The filtrate was washed with water (18 mL), and the organic phase was dried over MgSO₄. The solvent was carefully removed at room temperature. The crude clear oil (1.62 g, 75%) was carried on without further purification. ¹H NMR [400 MHz, CDCl₃] δ 5.81 (ddt, *J* = 16.8, 10.3, 7.2 Hz, 1H), 5.32-5.25 (m, 1H), 5.25-5.21 (m, 1H), 3.73 (td, *J* = 12.8, 6.1 Hz, 2H), 2.71 (tdt, *J* = 16.3, 7.2, 1.3 Hz, 2H), 2.49 (t, *J* = 6.8 Hz, 1H); ¹³C NMR [100 MHz, CDCl₃] 121.8 (t, *J*_{C-F} = 242.7 Hz), 120.9, 120.9, 63.7 (t, *J*_{C-F} = 31.3 Hz), 38.2 (t, *J*_{C-F} = 24.7 Hz).

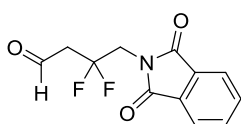


2,2-difluoropent-4-en-1-yl trifluoromethanesulfonate (46). To a solution of compound **45** (0.6 g, 5.2 mmol) and pyridine (0.5 mL, 5.7 mmol) in DCM (4.0 mL) cooled to 0 °C was added dropwise a solution of triflic anhydride (1.0 mL, 5.7 mmol) dissolved in dry DCM (2.0 mL). After addition was complete (25 minutes), the reaction stirred at room temperature for 2 hours. The mixture was cooled to 0 °C and then quenched with water (8.0 mL). The aqueous layer was extracted with DCM (3x). The combined organics were washed with water and dried over MgSO₄. The solvent was carefully removed on the rotary evaporator. The crude brown oil (1.01 g, 74%) was carried on without further purification. ¹H NMR [400 MHz, CDCl₃] δ 5.78 (ddt, *J* = 17.4, 10.4, 7.2 Hz, 1H), 5.39-5.33 (m, 2H), 4.52 (t, *J* = 11.2 Hz, 2H), 2.77 (tdt, *J* = 15.8, 7.2, 1.2 Hz, 2H); ¹⁹F NMR [400 MHz, CDCl₃] δ -75.20 (s), -106.69 (tt, *J* = 15.9, 11.2 Hz).

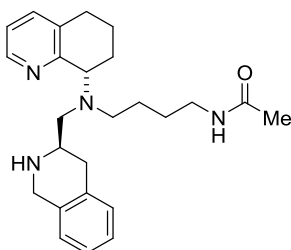


2-(2,2-difluoropent-4-en-1-yl)isoindoline-1,3-dione (48). A suspension of compound **46** (1.0 g, 3.8 mmol) and potassium phthalimide (0.9 g, 5.0 mmol) in dry DMF (9.0 mL) was heated under at 120-130 °C for 72 hours. The reaction was cooled to room temperature and quenched with water (20 mL). The mixture was extracted with diethyl ether (4 x 15 mL). The combined

extracts were washed with 1 M aqueous NaOH (3 x 3 mL) and water (3 x 10 mL), dried over MgSO₄, and concentrated by rotary evaporation. The crude light yellow solid (0.696 g, 72%) was carried on without further purification. ¹H NMR [400 MHz, CDCl₃] δ 7.91 (dd, *J* = 5.5, 3.1 Hz, 2H), 7.77 (dd, *J* = 5.5, 3.0 Hz, 2H), 5.89 (ddt, *J* = 17.3, 10.2, 7.1 Hz, 1H), 5.41-5.16 (m, 2H), 4.08 (t, *J* = 13.7 Hz, 2H), 2.72 (tdt, *J* = 16.2, 7.0, 1.3 Hz, 2H); ¹⁹F NMR [400 MHz, CDCl₃] δ -102.32 (tt, *J* = 16.2, 13.6 Hz); HRMS (ESI) [M+H]⁺, calc'd for C₁₃H₁₂F₂NO₂ 252.08306, found 252.08308.

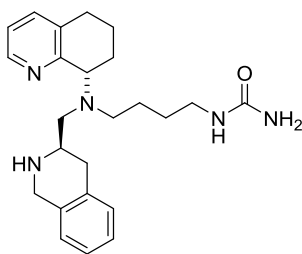


4-(1,3-dioxoisindolin-2-yl)-3,3-difluorobutanal (49). A solution of compound **48** (0.4 g, 1.6 mmol) in dry DCM (8.0 mL) was ozonized (voltage: 3-4, control: 50% ozone output) at -78 °C until 10 minutes after the appearance of a blue coloration (30 minutes). Immediately following, dimethyl sulfide (0.5 mL, 6.4 mmol) was added, and reaction mixture was allowed to stir at room temperature for 19 hours. The reaction was washed with saturated aqueous NaHCO₃ (2x) and water (2x), dried over anhydrous MgSO₄, and concentrated by rotary evaporation. The crude light yellow oil (0.360 g, 89%) was carried on without further purification. ¹H NMR [400 MHz, CDCl₃] δ 9.83 (p, *J* = 1.9 Hz, 1H), 7.97-7.84 (m, 2H), 7.84-7.68 (m, 2H), 4.22 (t, *J* = 13.0 Hz, 2H), 3.05 (td, *J* = 16.6, 2.0 Hz, 2H); ¹⁹F NMR [400 MHz, CDCl₃] δ -98.75 (tt, *J* = 16.7, 13.0, 1.7 Hz).



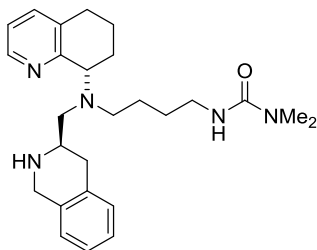
N-(4-(((*R*)-1,2,3,4-tetrahydroisoquinolin-3-yl)methyl)((*S*)-5,6,7,8-tetrahydroquinolin-8-yl)amino)butyl)acetamide (13). Step 1: Synthesis of *tert*-butyl (*R*)-3-(((4-acetamidobutyl)((*S*)-

5,6,7,8-tetrahydroquinolin-8-yl)amino)methyl)-3,4-dihydroisoquinoline-2(1*H*)-carboxylate. To a stirred solution of compound **38** (0.2 g, 0.5 mmol) in DCM (5.0 mL) was added TEA (0.11 mL, 0.8 mmol). The solution was cooled to 0 °C before adding freshly distilled acetyl chloride (0.040 mL, 0.6 mmol). The reaction was warmed to room temperature where it stirred for 4 hours. The reaction was quenched with 1 M aqueous HCl and extracted with DCM. The organic layer was washed with brine, dried over anhydrous MgSO₄, and concentrated under vacuum. The crude white amorphous foam (0.3 g, 98%) was carried on without further purification. HRMS (ESI) [M+H]⁺, calc'd for C₃₀H₄₃N₄O₃ 507.33297, found 507.33316. Step 2: To a solution of the material from step 1 (0.3 g, 0.5 mmol) dissolved in DCM (3.6 mL) was added TFA (1.2 mL). The reaction stirred at room temperature for 5 hours. It was diluted with DCM and made basic with 1 M aqueous NaOH. The organic layer was separated, and the aqueous layer was extracted with DCM (2 x 25 mL). The combined organic layers were washed with water, dried over anhydrous MgSO₄, and concentrated to an off-white foam. The crude material was purified by gravity column (10 g silica gel, 90:10 DCM-MeOH then 90:10 DCM-MeOH with 1% v/v NH₄OH) to afford the title compound as an off-white amorphous foam (0.0450 g, 22%). ¹H NMR [400 MHz, CDCl₃] δ 8.43 (dd, *J* = 1.4, 4.7 Hz, 1H), 7.32 (d, *J* = 6.7 Hz, 1H), 7.08-6.96 (m, 5H), 6.69 (br s, 1H), 4.05 (dd, *J* = 6.4, 9.5 Hz, 1H), 3.97 (d, *J* = 15.0 Hz, 1H), 3.68 (d, *J* = 15.0 Hz, 1H), 3.33-3.19 (m, 2H), 3.01 (dd, *J* = 2.7, 13.1 Hz, 1H), 2.93 (br s, 1H), 2.88-2.84 (m, 1H), 2.87-2.73 (m, 1H), 2.69 (br s, 1H), 2.65-2.57 (m, 3H), 2.43-2.37 (m, 2H), 2.10-1.92 (m, 3H), 1.88 (s, 3H), 1.76-1.52 (m, 5H); ¹³C NMR [100 MHz, CDCl₃] δ 170.6, 158.7, 146.9, 136.9, 135.6, 134.6, 134.2, 129.2, 126.6, 126.1, 125.7, 121.8, 61.5, 57.6, 54.2, 52.2, 48.6, 39.7, 34.0, 29.7, 27.3, 27.0, 26.7, 23.3, 22.2; HRMS (ESI) [M+H]⁺, calc'd for C₂₅H₃₅N₄O 407.28054, found 407.28162; HPLC purity: >95% *t*_R = 1.166 min. (25-95% MeOH/Water with 0.1% formic acid, gradient over 3 minutes, 1.0 mL/min.).



1-(4-(((*R*)-1,2,3,4-tetrahydroisoquinolin-3-yl)methyl)((*S*)-5,6,7,8-tetrahydroquinolin-8-yl)amino)butyl)urea (14). Step 1: Synthesis of *tert*-butyl (*R*)-3-(((*S*)-5,6,7,8-tetrahydroquinolin-8-yl)(4-ureidobutyl)amino)methyl)-3,4-dihydroisoquinoline-2(*1H*)-carboxylate. A stirred solution of compound **38** (0.2 g, 0.4 mmol) in 1 M aqueous HCl (0.3 mL, 0.3 mmol) and water (3.0 mL) was treated with potassium cyanate (0.1 g, 1.7 mmol). The mixture was stirred at room temperature for 14 hours. The reaction was diluted with DCM. Additional 1 M aqueous HCl was added to remove residual starting material. The aqueous layer was extracted with DCM and then concentrated at reduced pressure. The crude off-white amorphous foam (0.2 g, 94%) was carried on without further purification. HRMS (ESI) $[M+H]^+$, calc'd for $C_{29}H_{42}N_5O_3$ 508.32822, found 508.32850. Step 2: To a solution of the material from step 1 (0.2 g, 0.3 mmol) dissolved in DCM (1.5 mL) was added TFA (0.5 mL). The reaction stirred at room temperature for 1.5 hours. It was diluted with DCM and made basic with 1 M aqueous NaOH. The organic layer was separated, and the aqueous layer was extracted with DCM (2 x 25 mL). The combined organic layers were washed with water, dried over anhydrous $MgSO_4$, and concentrated to an off-white foam. The crude material was purified by gravity column (4 g silica gel, 90:10 DCM-MeOH with 1% v/v NH_4OH) to afford the title compound as an off-white amorphous foam (0.0590 g, 45%). 1H NMR [400 MHz, $CDCl_3$] δ 8.43 (dd, $J = 1.2, 4.9$ Hz, 1H), 7.36-7.28 (m, 1H), 7.10-7.03 (m, 3H), 7.02-6.98 (m, 1H), 6.97-6.93 (m, 1H), 6.32 (br s, 1H), 4.93 (s, 2H), 4.04 (dd, $J = 6.2, 9.5$ Hz, 1H), 3.91 (d, $J = 15.2$ Hz, 1H), 3.52 (d, $J = 15.2$ Hz, 1H), 3.23-3.12 (m, 4H), 3.04-2.97 (m, 1H), 2.80-2.55 (m, 4H), 2.51-2.35 (m, 3H), 2.07-1.86 (m, 3H), 1.75-1.48 (m, 5H); ^{13}C NMR [100 MHz, $CDCl_3$] δ 159.9, 158.4, 146.9, 137.1 135.3, 134.4, 134.2, 129.2, 126.6, 126.2, 125.8, 121.9,

61.6, 57.3, 53.9, 52.0, 48.2, 40.3, 33.8, 29.7, 26.9, 26.7, 25.8, 22.1; HRMS (ESI) $[M+H]^+$, calc'd for $C_{24}H_{34}N_5O$ 408.27579, found 408.27590; HPLC purity: >95% $t_R = 0.596$ min. (50-95% MeOH/Water with 0.1% formic acid, gradient over 3 minutes, 1.0 mL/min.).

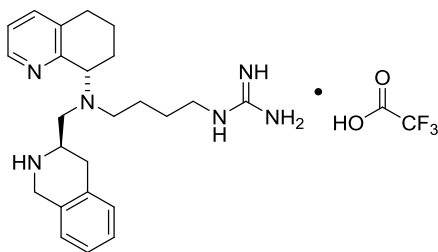


1,1-dimethyl-3-(4-(((*R*)-1,2,3,4-tetrahydroisoquinolin-3-yl)methyl)((*S*)-5,6,7,8-

tetrahydroquinolin-8-yl)amino)butyl)urea (15). Step 1: Synthesis of *tert*-butyl (*R*)-3-(((4-(3,3-dimethylureido)butyl)((*S*)-5,6,7,8-tetrahydroquinolin-8-yl)amino)methyl)-3,4-

dihydroisoquinoline-2(*H*)-carboxylate. To a stirred solution of compound **38** (0.2 g, 0.3 mmol) in DCM (5.0 mL) was added TEA (0.072 mL, 0.5 mmol). The solution was cooled to 0 °C before adding dimethylcarbamic chloride (0.035 mL, 0.4 mmol). The reaction was warmed to room temperature where it stirred for 24 hours. The reaction was quenched with 1 M aqueous HCl and extracted with DCM. The organic layer was washed with brine, dried over anhydrous $MgSO_4$, and concentrated under vacuum. The crude white amorphous foam (0.2 g, 98%) was carried on without further purification. HRMS (ESI) $[M+H]^+$, calc'd for $C_{31}H_{46}N_5O_3$ 536.35952, found 536.36011. Step 2: To a solution of the material from step 1 (0.1 g, 0.2 mmol) dissolved in DCM (5.0 mL) was added TFA (0.2 mL). The reaction stirred at room temperature for 14 hours. It was diluted with DCM and made basic with 1 M aqueous NaOH. The organic layer was separated, and the aqueous layer was extracted with DCM (2 x 25 mL). The combined organic layers were washed with water, dried over anhydrous $MgSO_4$, and concentrated to an off-white foam. The crude material was purified by preparative TLC (500 micron silica gel in 80:20 DCM-MeOH with 2% v/v NH_4OH) to afford the title compound as a white amorphous foam (0.0490 g, 57%). 1H NMR [400 MHz, $CDCl_3$] δ 8.43 (d, $J = 4.3$ Hz, 1H), 7.32 (d, $J = 7.0$ Hz,

1H), 7.09-6.99 (m, 5H), 4.54 (app. t, $J = 5.0$ Hz, 1H), 4.09-4.02 (m, 2H), 3.88 (d, $J = 15.0$ Hz, 1H), 3.24-3.22 (m, 2H), 3.03-2.97 (m, 2H), 2.86 (s, 6H), 2.81-2.59 (m, 6H), 2.48-2.35 (m, 2H), 2.08-2.05 (m, 1H), 2.00-1.94 (m, 1H), 1.91-1.85 (m, 1H), 1.74-1.65 (m, 1H), 1.56-1.54 (m, 4H); ^{13}C NMR [100 MHz, CDCl_3] δ 158.9, 158.7, 146.9, 136.7, 135.6, 134.8, 134.1, 129.2, 126.6, 126.1, 125.7, 121.6, 61.6, 57.8, 54.2, 52.5, 48.7, 41.1, 36.4, 36.3, 33.9, 29.6, 28.9, 28.3, 27.2, 22.2; HRMS (ESI) $[\text{M}+\text{H}]^+$, calc'd for $\text{C}_{26}\text{H}_{38}\text{N}_5\text{O}$ 436.30709, found 436.30740; HPLC purity: >95% $t_{\text{R}} = 1.385$ min. (25-95% MeOH/Water with 0.1% formic acid, gradient over 3 minutes, 1.0 mL/min.).



1-(4-(((R)-1,2,3,4-tetrahydroisoquinolin-3-yl)methyl)((S)-5,6,7,8-tetrahydroquinolin-8-yl)amino)butyl)guanidine, trifluoroacetic acid (18). Step 1: Synthesis of *tert*-butyl (*R*)-3-(8-(((*tert*-butoxycarbonyl)amino)-12,12-dimethyl-10-oxo-2-((*S*)-5,6,7,8-tetrahydroquinolin-8-yl)-11-oxa-2,7,9-triazatridec-8-en-1-yl)-3,4-dihydroisoquinoline-2(*1H*)-carboxylate. To a solution of compound **38** (0.4 g, 0.8 mmol) and DIPEA (0.4 mL, 2.4 mmol) in dry MeCN (8.0 mL) at 0 °C was added *tert*-butyl (((*tert*-butoxycarbonyl)imino)(1H-pyrazol-1-yl)methyl)carbamate (0.3 g, 0.9 mmol). The reaction was allowed to stir at room temperature for 1 hour. The reaction mixture was concentrated by rotary evaporation. The residue was taken up in EtOAc and washed with saturated aqueous NaHCO_3 and brine. The organic layer was dried over Na_2SO_4 , filtered, and concentrated to a light brown oil. The crude material was purified by flash column chromatography (ISCO, 12 g silica gel, 0-50% EtOAc-Hexanes over 12 minutes) to afford the title compound as a white amorphous foam (0.404 g, 73%). ^1H NMR [600 MHz, CDCl_3] δ 11.51 (s, 1H), 8.43-8.32 (m, 1H), 8.27 (app. t, $J = 5.1$ Hz, 1H), 7.27-7.24 (m, 1H), 7.16-6.90 (m, 5H),

4.66 (d, $J = 16.8$ Hz, 1H), 4.38 (s, 1H), 4.17 (d, $J = 17.0$ Hz, 1H), 4.01-3.80 (m, 1H), 3.40-3.26 (m, 2H), 3.20-2.90 (m, 2H), 2.86-2.53 (m, 5H), 2.46-2.33 (m, 1H), 2.07-1.88 (m, 2H), 1.80-1.52 (m, 4H), 1.51 (s, 9H), 1.50 (s, 9H), 1.50 (s, 9H), 1.41-1.32 (m, 2H); HRMS (ESI) $[M+H]^+$, calc'd for $C_{39}H_{59}N_6O_6$ 707.44906, found 707.44954. Step 2: To a solution of the material from step 1 (0.4 g, 0.6 mmol) in DCM (2.8 mL) was added TFA (2.8 mL). The reaction stirred at room temperature for 4 hours before being concentrated. To the residue was added water (5 mL), solid $NaHCO_3$, and solid NaCl. The aqueous layer was extracted with chloroform (3 x 50 mL). The organic extracts were combined, dried over Na_2SO_4 , filtered, and concentrated to a light brown foam (~0.3 g). A portion of the crude material (0.079 g) was purified by flash column chromatography (ISCO, 4.5 g amine functionalized silica gel, 0-10% MeOH-DCM over 22 minutes) to afford the title compound as an off-white solid (0.0310 g). 1H NMR [400 MHz, $CDCl_3$] δ 8.43 (dd, $J = 4.6, 1.4$ Hz, 1H), 8.30 (br s, 1H), 7.64 (br s, 3H), 7.38-7.32 (m, 1H), 7.13 (dd, $J = 7.7, 4.7$ Hz, 1H), 7.11-7.03 (m, 2H), 7.03-6.97 (m, 1H), 6.96-6.90 (m, 1H), 4.04 (dd, $J = 9.3, 6.9$ Hz, 1H), 3.81 (d, $J = 15.4$ Hz, 1H), 3.32-3.18 (m, 3H), 2.91-2.64 (m, 6H), 2.64-2.50 (m, 2H), 2.48-2.29 (m, 3H), 2.15-1.96 (m, 2H), 1.97-1.83 (m, 2H), 1.80-1.60 (m, 4H); ^{13}C NMR [100 MHz, $CDCl_3$] δ 157.8, 157.7, 146.9, 137.6, 135.0, 134.4, 133.9, 129.1, 126.6, 126.3, 126.0, 122.4, 60.9, 56.9, 53.2, 51.7, 47.9, 41.6, 34.1, 29.8, 25.9, 24.9, 23.2, 22.1; ^{19}F NMR [400 MHz, $CDCl_3$] δ -75.99 (s); IR (solid ATR): 3154, 2934, 1668, 1496, 1446, 1426, 1317, 1199, 1176, 1130, 747, 720 cm^{-1} .

2.6.2 Crystal Structure Data

Compound 42 X-ray Data (Dr. John Bacsá, Emory X-ray Crystallography Center, Department of Chemistry).

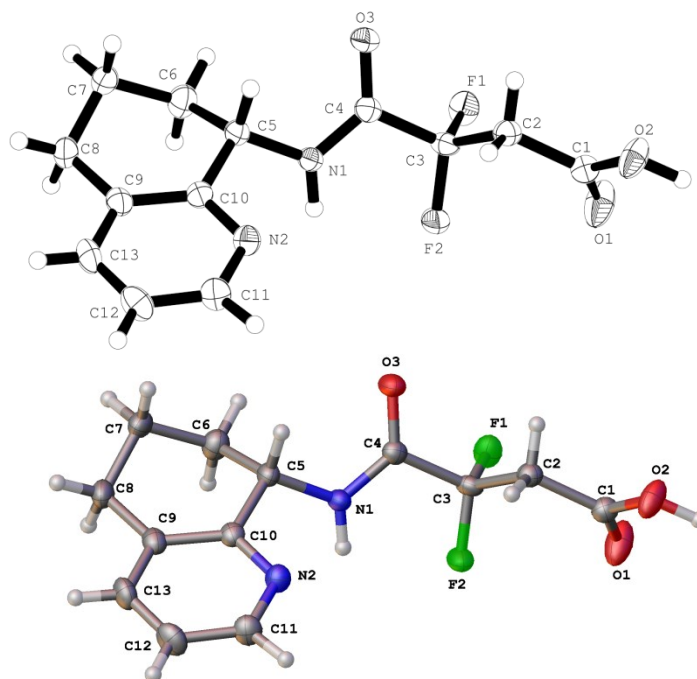


Table 1. Crystal data and structure refinement.

Empirical formula	$C_{13}H_{14}F_2N_2O_3$
Formula weight	284.26
Temperature	173(2) K
Wavelength	0.71073 Å
Crystal system	Orthorhombic
Space group	P 21 21 21
Unit cell dimensions	$a = 5.0769(11)$ Å $\alpha = 90^\circ$
	$b = 13.010(3)$ Å $\beta = 90^\circ$
	$c = 19.286(4)$ Å $\gamma = 90^\circ$
Volume	$1273.9(5)$ Å ³
Z	4
Density (calculated)	1.482 Mg/m ³
Absorption coefficient	0.125 mm ⁻¹
F(000)	592
Crystal size	$0.747 \times 0.17 \times 0.15$ mm ³
Theta range for data collection	1.89 to 30.21°
Index ranges	$-7 \leq h \leq 7$, $-16 \leq k \leq 18$, $-27 \leq l \leq 20$

Reflections collected	15938
Independent reflections	3756 [R(int) = 0.0300]
Completeness to theta = 30.21°	99.2 %
Absorption correction	Semi-empirical from equivalents
Max. and min. transmission	0.8374 and 0.6859
Refinement method	Full-matrix least-squares on F ²
Data / restraints / parameters	3756 / 0 / 237
Goodness-of-fit on F ²	1.045
Final R indices [I>2sigma(I)]	R1 = 0.0436, wR2 = 0.1129
R indices (all data)	R1 = 0.0451, wR2 = 0.1151
Absolute structure parameter	-0.1(2)
Largest diff. peak and hole	0.504 and -0.291 e.Å ⁻³

Table 2. Atomic coordinates ($\times 10^4$) and equivalent isotropic displacement parameters ($\text{\AA}^2 \times 10^3$). U(eq) is defined as one third of the trace of the orthogonalized U^{ij} tensor.

Atom	x	y	z	U(eq)
F(1)	5969(2)	5102(1)	3840(1)	29(1)
F(2)	9599(2)	5671(1)	4308(1)	27(1)
O(1)	7355(3)	7279(1)	3490(1)	44(1)
O(2)	4942(3)	8262(1)	4190(1)	36(1)
O(3)	4218(2)	4570(1)	5172(1)	29(1)
N(1)	8618(2)	4537(1)	5391(1)	19(1)
N(2)	11189(2)	5153(1)	6600(1)	22(1)
C(1)	6105(3)	7401(1)	4012(1)	23(1)
C(2)	5631(2)	6578(1)	4553(1)	20(1)
C(3)	6959(2)	5558(1)	4423(1)	19(1)
C(4)	6491(2)	4820(1)	5036(1)	19(1)
C(5)	8328(2)	3911(1)	6015(1)	19(1)
C(6)	8229(3)	2764(1)	5844(1)	28(1)
C(7)	8160(3)	2128(1)	6506(1)	26(1)
C(8)	10709(3)	2278(1)	6904(1)	27(1)
C(9)	11465(3)	3398(1)	6978(1)	22(1)
C(10)	10440(2)	4163(1)	6545(1)	19(1)
C(11)	12990(3)	5414(1)	7078(1)	27(1)
C(12)	14065(3)	4710(1)	7536(1)	30(1)
C(12)	14065(3)	4710(1)	7536(1)	30(1)
C(13)	13259(3)	3696(1)	7486(1)	28(1)
F(1)	5969(2)	5102(1)	3840(1)	29(1)
F(2)	9599(2)	5671(1)	4308(1)	27(1)

O(1)	7355(3)	7279(1)	3490(1)	44(1)
O(2)	4942(3)	8262(1)	4190(1)	36(1)
O(3)	4218(2)	4570(1)	5172(1)	29(1)
N(1)	8618(2)	4537(1)	5391(1)	19(1)

Table 3. Bond lengths [Å].

F(1)-C(3)	1.3657(14)
F(2)-C(3)	1.3667(13)
O(1)-C(1)	1.2005(18)
O(2)-C(1)	1.3116(17)
O(3)-C(4)	1.2273(14)
O(2)-H(2)	0.85(3)
N(1)-C(4)	1.3299(15)
N(1)-C(5)	1.4614(16)
N(2)-C(11)	1.3412(18)
N(2)-C(10)	1.3480(16)
N(1)-H(1)	0.89(2)
C(1)-C(2)	1.5144(17)
C(2)-C(3)	1.5096(17)
C(3)-C(4)	1.5414(16)
C(5)-C(10)	1.5165(16)
C(5)-C(6)	1.5294(18)
C(6)-C(7)	1.5218(19)
C(7)-C(8)	1.517(2)
C(8)-C(9)	1.5127(18)
C(9)-C(10)	1.4004(17)
C(9)-C(13)	1.392(2)
C(11)-C(12)	1.384(2)
C(12)-C(13)	1.385(2)
C(2)-H(2A)	0.93(2)
C(2)-H(2B)	0.93(2)
C(5)-H(5)	0.97(2)
C(6)-H(6A)	0.98(2)
C(6)-H(6B)	0.99(2)
C(7)-H(7A)	0.965(19)
C(7)-H(7B)	0.97(2)
C(8)-H(8A)	0.95(2)
C(8)-H(8B)	0.97(3)
C(11)-H(11)	0.97(2)
C(12)-H(12)	0.94(3)
C(13)-H(13)	0.90(3)

Table 4 Bond Angles [°].

C(1)-O(2)-H(2)	113(2)
C(4)-N(1)-C(5)	119.74(9)
C(10)-N(2)-C(11)	119.24(10)
C(4)-N(1)-H(1)	123.3(13)
C(5)-N(1)-H(1)	116.9(13)
O(2)-C(1)-C(2)	110.63(11)
O(1)-C(1)-C(2)	124.60(12)
O(1)-C(1)-O(2)	124.77(12)
C(1)-C(2)-C(3)	115.87(10)
F(1)-C(3)-F(2)	105.90(9)
F(1)-C(3)-C(2)	110.71(9)
C(2)-C(3)-C(4)	110.51(9)
F(1)-C(3)-C(4)	107.76(9)
F(2)-C(3)-C(2)	111.73(9)
F(2)-C(3)-C(4)	110.06(9)
O(3)-C(4)-N(1)	125.48(11)
O(3)-C(4)-C(3)	118.28(10)
N(1)-C(4)-C(3)	116.21(9)
C(6)-C(5)-C(10)	112.28(10)
N(1)-C(5)-C(6)	111.70(10)
N(1)-C(5)-C(10)	111.30(9)
C(5)-C(6)-C(7)	110.50(11)
C(6)-C(7)-C(8)	109.55(12)
C(7)-C(8)-C(9)	112.86(11)
C(8)-C(9)-C(10)	122.22(12)
C(8)-C(9)-C(13)	120.06(12)
C(10)-C(9)-C(13)	117.71(11)
C(5)-C(10)-C(9)	120.77(11)
N(2)-C(10)-C(5)	117.36(10)
N(2)-C(10)-C(9)	121.80(10)
N(2)-C(11)-C(12)	122.70(12)
C(11)-C(12)-C(13)	117.96(13)
C(9)-C(13)-C(12)	120.53(13)
C(1)-C(2)-H(2A)	109.5(12)
C(1)-C(2)-H(2B)	108.8(13)
C(3)-C(2)-H(2A)	107.0(12)
C(3)-C(2)-H(2B)	109.0(13)
H(2A)-C(2)-H(2B)	106.2(17)
N(1)-C(5)-H(5)	107.6(11)
C(6)-C(5)-H(5)	104.6(12)
C(10)-C(5)-H(5)	109.1(11)
C(5)-C(6)-H(6A)	109.9(15)
C(5)-C(6)-H(6B)	107.9(14)
C(7)-C(6)-H(6A)	111.2(14)
C(7)-C(6)-H(6B)	107.5(13)
H(6A)-C(6)-H(6B)	109.8(19)
C(6)-C(7)-H(7A)	109.0(11)
C(6)-C(7)-H(7B)	110.1(12)

C(8)-C(7)-H(7A)	109.8(11)
C(8)-C(7)-H(7B)	109.8(12)
H(7A)-C(7)-H(7B)	108.6(17)
C(7)-C(8)-H(8A)	109.4(14)
C(7)-C(8)-H(8B)	116.1(18)
C(9)-C(8)-H(8A)	104.7(14)
C(9)-C(8)-H(8B)	110.5(16)
H(8A)-C(8)-H(8B)	102(2)
N(2)-C(11)-H(11)	114.8(12)
C(12)-C(11)-H(11)	122.5(12)
C(11)-C(12)-H(12)	120.0(15)
C(13)-C(12)-H(12)	122.1(15)
C(9)-C(13)-H(13)	123.4(17)
C(12)-C(13)-H(13)	115.9(18)

Table 5. Anisotropic displacement parameters ($\text{\AA}^2 \times 10^3$). The anisotropic displacement factor exponent takes the form: $-2\pi^2 [h^2 a^{*2} U^{11} + \dots + 2 h k a^* b^* U^{12}]$.

Atom	U^{11}	U^{22}	U^{33}	U^{23}	U^{13}	U^{12}
F(1)	41(1)	24(1)	21(1)	-2(1)	-6(1)	-2(1)
F(2)	17(1)	34(1)	29(1)	10(1)	4(1)	2(1)
O(1)	65(1)	31(1)	35(1)	10(1)	24(1)	16(1)
O(2)	52(1)	20(1)	36(1)	7(1)	22(1)	8(1)
O(3)	16(1)	36(1)	34(1)	12(1)	-1(1)	-1(1)
N(1)	16(1)	22(1)	19(1)	4(1)	0(1)	-1(1)
N(2)	26(1)	21(1)	19(1)	0(1)	-3(1)	2(1)
C(1)	26(1)	20(1)	22(1)	1(1)	1(1)	1(1)
C(2)	21(1)	19(1)	21(1)	2(1)	2(1)	1(1)
C(3)	17(1)	21(1)	18(1)	1(1)	-1(1)	0(1)
C(4)	18(1)	19(1)	20(1)	2(1)	-1(1)	1(1)
C(5)	19(1)	19(1)	20(1)	4(1)	-1(1)	0(1)
C(6)	38(1)	19(1)	26(1)	2(1)	-3(1)	-2(1)
C(7)	25(1)	21(1)	33(1)	7(1)	0(1)	0(1)
C(8)	25(1)	21(1)	35(1)	9(1)	-1(1)	3(1)
C(9)	22(1)	22(1)	22(1)	4(1)	1(1)	4(1)
C(10)	19(1)	21(1)	16(1)	2(1)	0(1)	2(1)
C(11)	33(1)	25(1)	23(1)	-3(1)	-6(1)	2(1)
C(12)	35(1)	34(1)	22(1)	-2(1)	-9(1)	4(1)
C(13)	30(1)	32(1)	22(1)	4(1)	-6(1)	7(1)

Table 6. Hydrogen coordinates ($\times 10^4$) and isotropic displacement parameters ($\text{\AA}^2 \times 10^3$).

Atom	x	y	z	U(eq)
H(1)	10240(40)	4711(15)	5270(11)	28(5)
H(2)	5160(60)	8740(20)	3899(16)	60(8)
H(2A)	3840(40)	6450(15)	4589(10)	28(5)
H(2B)	6160(40)	6826(16)	4983(11)	30(5)
H(5)	6620(40)	4060(15)	6212(9)	23(4)
H(6A)	6700(50)	2617(19)	5550(11)	38(5)
H(6B)	9870(50)	2584(19)	5594(11)	39(6)
H(7A)	6690(40)	2349(15)	6786(9)	23(4)
H(7B)	7930(40)	1407(16)	6396(10)	29(5)
H(8A)	12120(50)	1977(17)	6653(11)	37(5)
H(8B)	10830(60)	1930(20)	7347(14)	59(7)
H(11)	13470(40)	6132(16)	7080(10)	29(5)
H(12)	15300(50)	4927(19)	7868(14)	46(6)
H(13)	14060(60)	3250(20)	7775(13)	52(7)

Table 7. Torsion angles [$^\circ$].

C(5)-N(1)-C(4)-O(3)	-2.84(18)
C(5)-N(1)-C(4)-C(3)	174.79(10)
C(4)-N(1)-C(5)-C(6)	86.45(13)
C(4)-N(1)-C(5)-C(10)	-147.17(10)
C(11)-N(2)-C(10)-C(5)	177.86(11)
C(11)-N(2)-C(10)-C(9)	0.88(17)
C(10)-N(2)-C(11)-C(12)	-2.2(2)
O(1)-C(1)-C(2)-C(3)	2.9(2)
O(2)-C(1)-C(2)-C(3)	-177.72(11)
C(1)-C(2)-C(3)-F(1)	-64.99(12)
C(1)-C(2)-C(3)-F(2)	52.79(13)
C(1)-C(2)-C(3)-C(4)	175.69(10)
F(1)-C(3)-C(4)-O(3)	-59.13(13)
F(1)-C(3)-C(4)-N(1)	123.07(10)
F(2)-C(3)-C(4)-O(3)	-174.17(10)
F(2)-C(3)-C(4)-N(1)	8.03(14)
C(2)-C(3)-C(4)-O(3)	61.96(13)
C(2)-C(3)-C(4)-N(1)	-115.85(11)
N(1)-C(5)-C(6)-C(7)	175.23(11)
C(10)-C(5)-C(6)-C(7)	49.39(14)
N(1)-C(5)-C(10)-N(2)	36.79(13)
N(1)-C(5)-C(10)-C(9)	-146.19(11)
C(6)-C(5)-C(10)-N(2)	162.85(10)
C(6)-C(5)-C(10)-C(9)	-20.13(15)
C(5)-C(6)-C(7)-C(8)	-64.50(14)

C(6)-C(7)-C(8)-C(9)	48.15(15)
C(7)-C(8)-C(9)-C(10)	-19.56(19)
C(7)-C(8)-C(9)-C(13)	161.18(13)
C(8)-C(9)-C(10)-N(2)	-177.84(12)
C(8)-C(9)-C(10)-C(5)	5.27(19)
C(13)-C(9)-C(10)-N(2)	1.43(19)
C(13)-C(9)-C(10)-C(5)	-175.46(11)
C(8)-C(9)-C(13)-C(12)	176.75(13)
C(10)-C(9)-C(13)-C(12)	-2.5(2)
N(2)-C(11)-C(12)-C(13)	1.0(2)
C(11)-C(12)-C(13)-C(9)	1.4(2)

Table 8. Hydrogen bonds [\AA and $^\circ$].

D-H...A	d(D-H)	d(H...A)	d(D...A)	$\angle(\text{DHA})$
N(1)-H(1)...F(2)	0.89(2)	2.26(2)	2.6047(14)	102.9(15)
N(1)-H(1)...O(3)#1	0.89(2)	2.04(2)	2.8745(15)	157.5(18)
O(2)-H(2)...N(2)#2	0.85(3)	1.81(3)	2.6413(16)	168(3)
C(5)-H(5)...O(3)	0.97(2)	2.439(18)	2.7807(16)	100.4(12)

Symmetry transformations used to generate equivalent atom:

#1 $1+x, y, z$ #2 $1/2+x, 3/2-y, 1-z$

2.7 Biology Experimental Detail

2.7.1 MAGI Antiviral Assay with HIV-1_{IIIB} (Southern Research Institute, Frederick, MD)

Cell Preparation

MAGI-CCR5/CXCR4 cells (obtained from the NIH AIDS Research and Reference Reagent Program) were passaged in T-75 flasks prior to use in the antiviral assay. MAGI-CCR5/CXCR4 cells were derived from HeLa-CD4-LTR- β -gal cells. The cells have been engineered to express high levels of CD4 and CXCR4 and contain one copy of the HIV-1 LTR promoter driving expression of the β -galactosidase gene upon HIV-1 Tat transactivation. On the day preceding the assay, the cells were plated at 1×10^4 well and incubated at 37°C overnight. Total cell and viability quantification was performed using a hemacytometer and trypan blue exclusion. Cell viability was greater than 95% for the cells utilized in the assay.

Virus Preparation

The virus used for testing was the CXCR4-tropic strain HIV-1_{III_B}. This virus was obtained from the NIH AIDS Research and Reference Reagent Program and was grown in Ghost Hi5/MAGI-CCR5/CXCR4 co-cultures for the production of stock virus pools. For each assay, a pre-titered aliquot of virus was removed from the freezer (-80 °C) and allowed to thaw slowly to room temperature in a biological safety cabinet. The virus was re-suspended and diluted into tissue culture medium such that the amount of virus added to each well in a volume of 50 µL was approximately ten TCID₅₀/well (~0.001 TCID₅₀/cell).

Assay Setup

Compounds were evaluated at one or two concentrations (for initial screening) or in dose-response at six concentrations (triplicate wells/concentration). On the day of assay setup, compound dilutions were prepared at two-times (2x) the final required concentrations. Media used for plating the cells the day before assay setup was aspirated from the plates and replaced with 50 µL of the 2x compounds, followed by the addition of 50 µL of virus, which diluted the compounds to the final 1x concentrations. Cell control wells (cells only) and virus control wells (cells plus virus) were included on each assay plate. Identical uninfected assay plates (virus replaced with media) were prepared for parallel cytotoxicity testing. The cultures were incubated for 48 hours or 6 days (depending on compound or client requirements) after which antiviral efficacy was measured as the inhibition of β-galactosidase reporter expression, and cytotoxicity was monitored by MTS staining.

β-galactosidase Chemiluminescent Endpoint Analysis

A chemiluminescent endpoint was used to determine the extent of β-galactosidase expression as a measure of HIV-1 infection of the cells. Upon HIV-1 attachment and entry into the MAGI-CXCR4 cells, HIV-1 Tat transactivates the LTR dependent β-galactosidase enzyme to express higher than normal levels of β-galactosidase. Thus there is a direct relationship between the level of HIV-1 infection and the level of β-galactosidase detected in the cells. At 48 hours or 6 days post infection, plates were aspirated, and PBS was added to each well. Gal-screen reagent

(Tropix, Bedford, MA) was then added per the manufacturer's instructions for chemiluminescent detection of β -galactosidase activity and incubated at room temperature for 90 minutes. The resulting chemiluminescence signal was then read using a Microbeta Trilux luminescence reader (PerkinElmer/Wallac).

MTS Staining for Cell Viability

At assay termination, the cytotoxicity assay plates were stained with the soluble tetrazolium-based dye MTS (CellTiter Reagent, Promega) to determine cell viability and quantify compound toxicity. MTS is metabolized by the mitochondrial enzymes of metabolically active cells to yield a soluble formazan product, allowing the rapid quantitative analysis of cell viability and compound cytotoxicity. The MTS is a stable solution that does not require preparation before use. At termination of the assay, 15 μ L of MTS reagent was added per well. The microtiter plates were then incubated for 1.5-2 hours at 37 $^{\circ}$ C; the incubation interval was chosen based on empirically determined times for optimal dye reduction. The plates were read spectrophotometrically at 490/650 nm with a Molecular Devices Vmax plate reader.

Data Analysis

Percent inhibition of virus replication and percent cell viability at each concentration were calculated using an in-house computer program. For dose-response testing, IC_{50} (50% inhibition of virus replication), IC_{90} (90% inhibition of virus replication), TC_{50} (50% cytotoxicity), and therapeutic index values ($TI = TC_{50}/IC_{50}$; also referred to as Antiviral Index or AI) were provided. Raw data for both antiviral activity and cytotoxicity with analyzed/tabulated data were provided in a printout summarizing the individual compound activity. An IC_{50} of 2-5 nM was obtained for **AMD3100**.

2.7.2 Calcium Flux Assay (Millipore, Inc. St. Charles, MO)

CXCR4-expressing Chem-1 cells were loaded with Fluo-4, washed, and pre-incubated with the indicated concentrations of test compounds for 10 minutes. Calcium flux in response to 5 nM

recombinant human CXCL12 was determined on a Molecular Devices Flex Station. An EC₅₀ for calcium mobilization by CXCL12 of ~ 4 nM with signal/noise at ligand E_{max} = 542, Z' = 0.82 with CXCL12 at the EC₅₀. An IC₅₀ of 57 nM was obtained for **AMD3100**.

2.7.3 Caco-2 Permeability Assay (*Absorption Systems, Exton, PA*)

Cell monolayers were grown to confluence on collagen-coated, microporous, polycarbonate membranes in 12-well Costar Transwell® plates. The permeability assay buffer was Hanks Balanced Salt Solution containing 10 mM HEPES and 15 mM glucose at a pH of 7.4. The buffer in the receiver chamber also contained 1% bovine serum albumin. The dosing solution concentration was 5 μM test compound in the assay buffer. Cell monolayers were dosed on the apical side (A-to-B) or basolateral side (B-to-A) and incubated at 37 °C with 5% CO₂ in a humidified incubator. Samples were taken from the donor and receiver chambers at 120 minutes. Each determination was performed in duplicate. The co-dosed lucifer yellow flux was also measured for each monolayer to ensure no damage was inflicted to the cell monolayers during the flux period. All samples were assayed by LC-MS/MS using electrospray ionization. The apparent permeability, P_{app}, and percent recovery were calculated as follows:

$$P_{app} = (dC_r / dt) \times V_r / (A \times C_A)$$

$$\text{Percent Recovery} = 100 \times ((V_r \times C_r^{\text{final}}) + (V_d \times C_d^{\text{final}})) / (V_d \times C_N)$$

Where, dC_r / dt is the slope of the cumulative concentration in the receiver compartment versus time in μM s⁻¹; V_r is the volume of the receiver compartment in cm³; V_d is the volume of the donor compartment in cm³; A is the area of the insert (1.13 cm² for 12-well Transwell®); C_A is the average of the nominal dosing concentration and the measured 120 minute donor concentration in μM; C_N is the nominal concentration of the dosing solution in μM; C_r^{final} is the cumulative receiver concentration in μM at the end of the incubation period; C_d^{final} is the concentration of the donor in μM at the end of the incubation period.

CHAPTER 3

Conformational Analysis of Structurally Similar CXCR4 Antagonists

3.1 Statement of Purpose

In collaboration with colleagues in pharmacology, biology, and medicine, our laboratory has devoted efforts toward the discovery of novel therapeutic agents against cancer, viruses, inflammation and neuronal disorders. One drug target of present interest to our laboratory is CXCR4 (discussed in chapter 2). Compelling evidence has highlighted the role of this receptor in HIV-1 infection, stem cell trafficking, and cancer/tumor metastasis. Consequently, our objective has been to design and synthesize small molecule CXCR4 antagonists that block HIV infection and/or tumor metastasis *in vivo* by hindering CXCR4 function.

The recent report of CXCR4 X-ray structures in complex with two antagonists has raised enthusiasm for deeper understanding of receptor function and the requirements for ligand binding. Five variants of the CXCR4 receptor were solved by engineering T4 lysozyme in a loop between transmembrane helices V and VI on the cytoplasmic side of the GPCR. In addition to these structures, several different classes of well-characterized CXCR4 antagonists and corresponding SAR data have also been published (Figure 3.1). By analyzing the plethora of data surrounding these compounds, we have developed a much greater appreciation for the complexity of molecular pharmacology as it relates to CXCR4. Furthermore, the knowledge gained from the studies described herein has guided and advanced our drug discovery program.

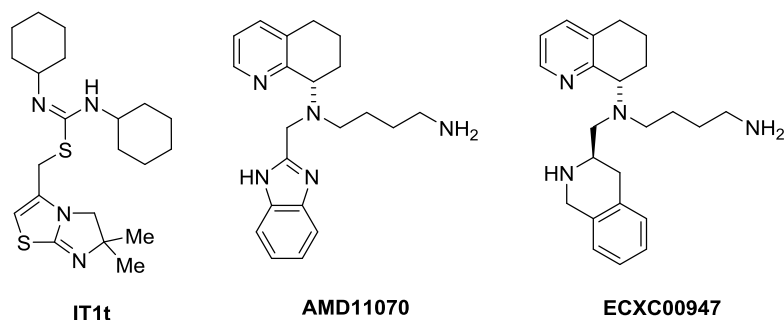


Figure 3.1 Structures of CXCR4 Antagonists used in Computational and Experimental Studies.

3.2 Introduction and Background

3.2.1 History of Medicine and Drug Discovery

Natural substances obtained from plants and animals have been used to treat mankind's diseases for many centuries. During the Middle Ages, exotic substances like mercury and sulfur were used as disinfectants and to combat diseases, such as syphilis. However, the majority of these efforts resulted in harmful side effects or fatality because of lack of knowledge of drug action. Quinine, a natural compound isolated from the bark of the cinchona tree, first appeared in therapeutics in the early 1600s, and continued to be used for several centuries as a malarial treatment.¹²² In the latter part of the nineteenth century, salicylic acid was isolated from bark of the Willow tree and used as an antipyretic. Its use led to the first synthetically prepared pharmaceutical, aspirin. The drug was recognized as the universal pain reliever in the early 1900s and continues to be utilized in most of the world today. Throughout the history of medicine, biologically active substances ranging from arsenic to morphine, some of which now known to be highly toxic or addictive, have been used to treat human illnesses.

The substances that were used during these times reflected the state of medical knowledge. Empirical data that was generated on accident served as the most valuable asset in the treatment of disease. However, ancient physicians like Galen and Sushruta made major contributions toward the advancement of medicine. Specifically, their documented cases of trial and error derived from patients increased our understanding of the human body and of medical therapies. However, lack of knowledge regarding the scientific basis of disease limited the means of rationally and systematically discovering new therapeutics. Instead, serendipity and traditional folk wisdom passed down over the years set the foundation for the earliest forms of disease control.

It was not until the 19th and 20th centuries that drug discovery could be executed in a more logical manner. Major advancements in both chemistry and biology would revolutionize the medical field. The field of modern organic chemistry formally began in 1828 upon discovery by Fredrich Wöhler that urea could be synthesized using simple inorganic substances like ammonium cyanate. The finding was of great historical significance because it dispelled the mainstream belief at the time that organic matter possessed a “vital force” inherent to all things living and could only be synthesized by living organisms. The field was further developed through the formulation of structural theory in the late 19th century by Cooper, Kekulé, Kolbe, Perkin, and others. This framework enabled the elucidation of the precise atom arrangements of biologically active compounds. Consequently, this knowledge aided in the design of synthetic routes toward these molecules. These experiments provided the impetus to synthesize non-natural molecules of practical interest thus launching the field of synthetic organic chemistry. Meanwhile, several other discoveries transformed the field of biology. The germ theory of disease established by Louis Pasteur and the concept of chemoreceptors as selective binding sites for chemotherapeutic agents introduced by Paul Ehrlich both opened the door to a deeper understanding of receptor function.¹²³ In 1905, J. N. Langley reported that receptors operated as “switches” that could be blocked or activated by antagonists or agonists, respectively.

With these breakthroughs and advances, rational drug discovery began to take shape. The collaboration of chemists and biologists resulted in hundreds of molecules that were tested for efficacy against various diseases. In turn, information garnered from biological testing was translated into modifications to starting compounds according structure activity relationships. The investigations led to many medical landmarks including the discovery of insulin, the development of sulfa drugs treat infections, the serendipitous discovery of the natural antibiotic, penicillin, by Alexander Fleming,¹²⁴ and the isolation of anti-tubercular aminoglycoside, streptomycin, from *Streptomyces griseus* by Salman Waksman.¹²⁵

3.2.2 Structure-based Drug Design

As X-ray crystal structures of protein-ligand complexes began to emerge in the 1970s and 1980s, the potential of rational drug discovery became increasingly clear. These investigations led to a concept known today as “structure-based drug design” (SBDD). This technique is typically used in the design of novel, small molecules that fit in macromolecular binding pockets. The approach relies on the three-dimensional (3-D) structure of a protein target, preferably bound to a ligand that is used as a starting point for further modifications and improvement of drug properties. The structure and bioactive conformation of known ligands, as well as accurate and detailed information regarding the structural and chemical characteristics of the protein target are critical components of SBDD. The structures enable researchers to view how a particular molecule or group of molecules interacts with the target. Additionally, the structures may indicate which target features can be exploited through *de novo* design. While the majority of 3-D protein structures are obtained from X-ray crystallography and electron diffraction, several are also acquired by solution and solid state nuclear magnetic resonance (NMR).

Analysis of these structures is accomplished using a number of computational tools including homology models, molecular dynamics, pharmacophore development, and ligand docking.¹²⁶ While the former two are resource intensive and time-consuming methods used primarily to study protein function and mechanism, the later techniques have been used in high-throughput virtual screens of large databases to identify new compounds that bind the target protein. Consequently, these tools have been instrumental in identifying/optimizing lead compounds and guiding the direction of research projects, especially during the early stages of drug discovery.

3.2.3 Conformation and Drug Design

An understanding of the structure and properties of biologically active molecules are fundamental components of rational drug design. The vast majority of pharmaceutical agents are

flexible molecules that bind to and modulate the activity of proteins.¹²⁷ A flexible compound binds to a target or receptor in a single conformation. However, the protein must either pay an energy penalty for converting the conformations of the molecule in solution to the bound conformation, or it must extract from solution a conformer that closely resembles the bound molecule.¹²⁸ Since the molecule loses degrees of freedom upon binding, the penalty is almost entirely entropic. It has been estimated that approximately 2 kcal/mol of strain energy must be expended by a ligand for protein binding.¹²⁸

Academic researchers and scientists in the pharmaceutical industry have devoted significant efforts to determining the conformations of protein-bound molecules. Scientists have rationalized that armed with information regarding a bound conformation, medicinal chemists can make structural modifications that “lock” the molecule into that orientation.¹²⁷ It has been hypothesized that by constraining the molecule in a favorable conformation prior to binding, the entropic penalty can be circumvented.

Having access to X-ray crystal structures of every drug bound to all of the important protein targets would be incredibly useful, but it is not feasible or realistic. While crystal structures depicting protein-bound drugs can be found in the literature, they are limited in number due to the numerous challenges associated with protein crystallization and determination. In addition, X-ray structures provide a static snapshot of ligand binding that likely obscure protein motion. Fortunately, several examples have now shown that a molecule’s bioactive conformation is almost identical to one among several found in solution. Therefore, it is clear that knowledge regarding the conformations of a drug-like, flexible molecule found in solution is powerful and can greatly benefit rational design programs.

3.2.4 Tools for Conformational Analysis

NMR Spectroscopy

Since its development in 1946 by research groups at Stanford and Harvard, NMR spectroscopy has become a mainstay technique used in many different scientific fields. Early on, NMR spectroscopy was primarily used in the routine structure determination of organic molecules. Today, it continues to make large contributions to the structural elucidation of complex natural products.¹²⁹ More recently, NMR has been utilized to determine the structure of proteins.¹³⁰ It has also found utility in the medical field through its manifestation to Magnetic Resonance Imaging (MRI), a technique that has revolutionized diagnostic medicine.¹³¹ Therefore, it is of no surprise that five Nobel prizes have been awarded to the researchers whose work was instrumental in the development and application of NMR spectroscopy.

NMR spectroscopy is a powerful technique that has been used to provide stereochemical information regarding the configuration of chiral centers in various molecules. Additionally, its usefulness in determining conformation has distinguished NMR from many other techniques. Such experiments are possible because NMR spectroscopy provides two important variables related to conformation: 1) coupling constants and 2) interproton distances.

Proton-proton coupling constants, $J_{\text{H-H}}$, can be used to derive the dihedral angles about chemical bonds. The torsional angle is calculated using the Karplus equation^{132,133} shown below:

$$J(\phi) = A \cos^2\phi + B \cos\phi + C$$

where J is the 3J coupling constant, ϕ is the dihedral angle, and A , B , and C are empirically derived parameters whose values are dependent on the atoms and substituents involved. The second important variable provides the distance between two protons. These values can be acquired through the two-dimensional (2-D) technique called Nuclear Overhauser Effect Spectroscopy (NOESY) that maps protons separated in space by less than 5 Å. This combination of dihedral bond angles and interproton distances defines the molecular conformation.

However, there is a fundamental problem associated conformational analysis by NMR. More specifically, this is due to the relative populations of equilibrating conformations in solution that are governed by their relative free energies in solution. The relation between free energy and equilibrium constant is central to this situation:

$$\Delta G = -RT \ln K$$

where ΔG is the free energy difference, R is the gas constant, T is the temperature and K is the equilibrium constant. From this equation, it is clear that a small difference in free energy has a significant impact on the equilibrium constant since K is exponentially dependent on ΔG . For example, if a molecule exists in only two conformations in solution with a free energy difference between them of only 2 kcal/mol, the lower energy conformation would exist to the extent of 97%, while the higher energy one would be 3%. If the energy difference between the two were 4 kcal/mol, the lower energy conformer would exist to the extent of 99.9%, and the higher energy conformer would be virtually non-existent. Unfortunately, conformers that exist less than 2-3% in solution cannot be detected by most NMR instruments due to insufficient signal generated by such small concentrations.

Kinetics also serves as a limitation to determining conformations using NMR. The rotational barriers between conformations (ΔG^\ddagger) are typically very small (2-5 kcal/mol) compared to the amount of thermal energy present at room temperature (approximately 20 kcal/mol).¹³⁴ The large amount of thermal energy present at room temperature allows for rapid conformational interconversion (Figure 3.2). The time scale in which NMR spectroscopy operates is on the order of tens of milliseconds. However, conformational interconversion occurs much faster, typically on the order of tens of microseconds or less. The coupling constants and interproton distances determined from NMR spectroscopy represent the average values for these variables. Therefore, using this average data to assign a single structure is inherently flawed.

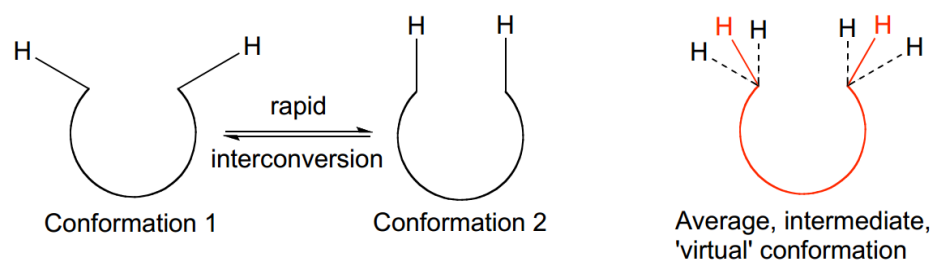


Figure 3.2 Pictorial Representation of Rapid Conformational Interconversion that Takes Place on the NMR Time Scale.

In theory it is possible to “freeze out” these motions at extremely low temperatures, however line broadening is typically observed in these experiments (Figure 3.3). For molecules with a rotational barrier equal to 10 kcal/mol, distinct conformer signals can only be observed by NMR at $-100\text{ }^{\circ}\text{C}$. However, a majority of molecules have rotational barriers of only a few kcal/mol and thus attempts to observe separate conformer signals would be futile. The sharp and well-defined resonances from NMR experiments conducted at room temperature do not necessarily indicate lack of conformational interconversion. Rather, it may mean that this process is fast compared to the experimental time scale.

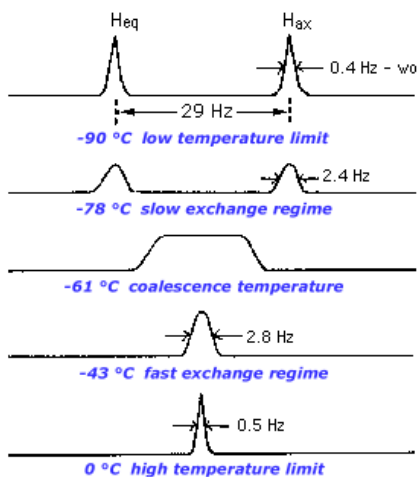


Figure 3.3 NMR Spectrum of Cyclohexane- d_{11} Illustrating the Effect of Temperature on Conformational Exchange.¹³⁵

Molecular Mechanics

Advances in computation over the last several years have given rise to several theoretical methods that have been widely used in studies pertaining to the conformations of organic compounds. One of the most influential and commonly used methods is molecular mechanics. Molecular mechanics methods use classical mechanics to predict the energy of a molecule as a function of its conformation. More specifically, collections of equations and experimentally-derived parameters called force fields are used to calculate the potential energy of a molecule.

Molecular mechanics assumes that the steric energy of a molecule arises from a set of specific interactions within a molecule. These interactions include the stretching or compressing of bonds beyond their equilibrium lengths and angles, torsional effects of twisting about single bonds, van der Waals forces of attraction or repulsion between atoms, and the electrostatic interactions between partial charges in a molecule due to bond polarity. The contribution of each of these interactions is quantified using potential function models that express the energy of the interaction as a function of distance, angle, or charge. The total steric energy of a molecule can be written as a sum of the energies of the interactions:

$$E_{\text{total}} = E_{\text{stretch}} + E_{\text{bend}} + E_{\text{torsion}} + E_{\text{vdW}} + E_{\text{electrostatic}}$$

The bond stretching, bending, and torsion interactions are classified as bonded interactions because the atoms involved must be directly bonded to one another or bonded to a common atom. In contrast, van der Waals and electrostatic interactions exist between non-bonded atoms.

All the potential functions discussed above involve a force constant or interaction constant. While these constants should theoretically be available from quantum mechanical calculations, it is necessary to derive them empirically due to the approximate nature of the equations. Experimental parameters are often incorporated to augment the equations and facilitate accurate reproductions of molecular geometries and energies for a number of well-characterized compounds. Because these constants are used to determine the structures of new molecules, their

accuracy is critical to molecular mechanics calculations. As such, a number of different force fields have been developed over the years including MM2, MM3, AMBER, MMFF, and OPLS. Each of these force fields involves careful parameterization of the equations based on data obtained from experiment and high-level quantum mechanics calculations. The central idea of molecular mechanics is that the force field constants are internally transferrable and can be applied to a wide variety of molecules.

Although molecular mechanics relies on data from experimentally characterized molecules, there are a few limitations to the method that are worth noting. This parametric method is used as an interpolative technique, rather than an extrapolative one and must not stray too far from known chemistry. Consequently, new molecules with unusual bonding are rarely amenable to modeling, and require alternative analysis with full quantum mechanical treatment of the system. In addition, molecular properties such as stereoelectronic effects, aromaticity, hyperconjugation, and frontier orbital interactions which require knowledge of the electron distribution within a molecule require quantum mechanical methods such as molecular orbital theory. Finally, molecular mechanics parameters are available only for certain types of bonds and functional groups.

Comparing the energies of two different isomers that were calculated from the same force field is acceptable. However, energies calculated using different force fields cannot be compared due to potential differences in force field parameterization. Further complication arises from that fact that some force fields have a tendency to generate questionable, high-energy structures. However, in general, lack of a solid reference standard severely constrains the assignment of theoretically generated structures as low or high in energy since the assignment depends strictly on the method used and its associated parameters. Accordingly, different methods may provide divergent results. Unfortunately, no single best set of force constants is available on account of structural diversity.

3.2.5 *NMR Analysis of Molecular Flexibility In Solution (NAMFIS)*

Fortunately, a few of the key limitations discussed in the previous section have been addressed by a hybrid technique that combines both NMR spectroscopy and molecular mechanics. NAMFIS which stands for NMR Analysis of Molecular Flexibility In Solution, was developed in 1995 by Cicero and co-workers at the University of Rome in Italy.¹³⁶ The overall objective is to compare the thoroughly enumerated conformations with the average NMR data to generate a dataset that replicates the Boltzmann population of the conformers in solution.

NAMFIS requires the input of two sets of variables: 1) the average coupling constants and average distances from 2-D NMR and 2) the set of conformations computed through the conformational search. The deconvolution method calculates the distances and coupling constants for all of the theoretical structures. The coupling constants are calculated by NAMFIS using a highly parameterized version of the Karplus equation, Haasnoot-Altona.¹³³ The parameters of this equation account for the influence of electronic effects contributed by substituents and substituent orientation with respect to particular protons.

The NAMFIS method varies the mole fractions of the theoretical conformations, calculates the resulting coupling constants and distances, and compares these weighted parameters to the corresponding experimental data. The goodness-of-fit for the calculated and average experimental parameters is expressed as the Sum of Squared Differences (SSD), a statistical measure of fit between data sets. By definition, the “best-fit” solution would be one for which the SSD is smallest, where the accompanying mole fractions would represent the ideal ensemble of conformations in solution.

Unlike other methods that constrain a single structure or structural family to fit the geometric NMR data, NAMFIS varies the mole fraction of each structure from a comprehensive conformational search and fits the resulting ensemble to the NMR data until a best fit for the entire dataset is obtained. In doing so, the method derives a Boltzmann conformer population in solution. In addition, by performing a geometric fit of the two datasets and considering the

implicit energies from the NMR data, NAMFIS bypasses ambiguities in locating low-energy conformations of flexible, polar molecules that result from incomplete sampling of conformational space and inadequate representation of solvation. NAMFIS is a powerful tool that can tease out a small number of individual conformations from average NMR data and serves as a useful alternative to purely theoretical methods for investigating molecular conformations. Several examples from our laboratory (including those underscored in this study) and others attest to the utility of this technique.^{137–140}

3.3 Conformational Analysis of CXCR4 Antagonists

3.3.1 Introduction

Three different CXCR4 antagonists were chosen for our computational and experimental studies (Figure 3.1). The first investigation involved an isothioureia-containing compound (**IT1t**) that was co-crystallized with CXCR4. The structure of **IT1t** bound to the protein was solved at 2.5 Å resolution.⁸³ Prior to the 2010 publication disclosing the atomic coordinates of the protein-ligand complex, a community-wide GPCR docking competition was held in which 25 teams across the world made an effort to predict the docking pose of **IT1t** to CXCR4. Interestingly, all of the predictions differed from the X-ray poses of **IT1t** by RMS deviations of 2–4 Å. On account of these results, we decided to reevaluate the bound structure of **IT1t** in the context of a comparative analysis of predicted binding conformations, a new solvate of the ligand in the solid state, and NMR analysis of conformations in solution. We were optimistic that these studies would be informative and potentially provide insights into docking newly-conceived ligands into the expansive CXCR4 receptor binding pocket.

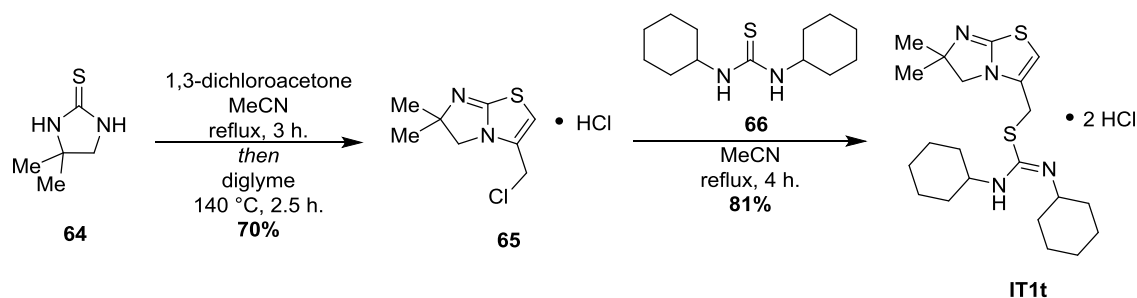
The second ligand we pursued was **AMD11070** due to the large amount of structural and pharmacological data surrounding this compound (see chapter 2 for additional information regarding this antagonist). Additionally, we were interested in predicting interactions between the ligand and CXCR4 according to site-directed mutagenesis data⁸⁶ and published SAR data in

order to gain a better understanding how our structurally-related THIQ-series of compounds might bind.⁸⁷ Molecular modeling experiments executed by postdoctoral scientist, Bryan Cox, Ph.D., and graduate student, Anthony Prosser, provided a model for the bioactive conformation of **AMD11070**. In order to link the proposed binding pose to an experimental structure, **AMD11070** was synthesized and utilized in conformational analysis studies.

Finally, we applied the information acquired from the studies with **AMD11070** to our series of THIQ analogues. A model was constructed around our lead compound, **ECXC00947**, to explain the biological data discussed in chapter 2. Solution NMR experiments were performed with **ECXC00947** to identify a conformation that supported our docked pose. The synthesis of **ECXC00947** was carried out by Lawrence Wilson, Ph.D., according to the route disclosed in chapter 2.

3.3.2 Synthesis of CXCR4 Antagonists for Computational Studies

The synthesis of **IT1t** commenced with mono-thioalkylation of 4,4-dimethylimidazolidine-2-thione (**64**) using 1,3-dichloroacetone (Scheme 3.1).¹⁴¹ Exposing this intermediate to high temperature allowed for regioselective addition of the unhindered nitrogen to the carbonyl group and subsequent dehydration to afford 5,5-fused heterocycle **65** in good yield. Exclusive formation of the regioisomer with the geminal methyl groups at C-6 was subsequently confirmed by X-ray analysis of the crystalline final compound. Treatment of chloride **65** with 1,3-dicyclohexylurea (**66**) furnished the isothiourea (**IT1t**) HCl salt. Crystallization of this material from absolute ethanol provided a sample for X-ray crystallography analysis that confirmed the structure (Figure 3.4).



Scheme 3.1 Synthesis of **IT1t**.

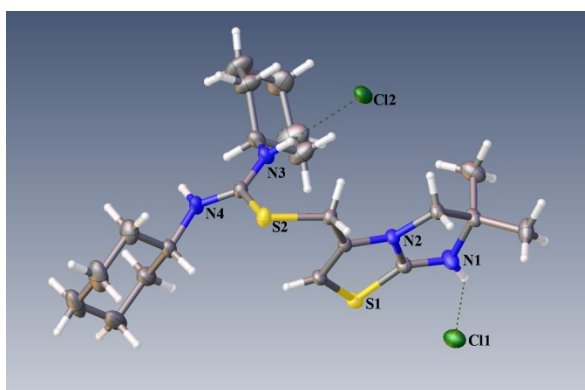
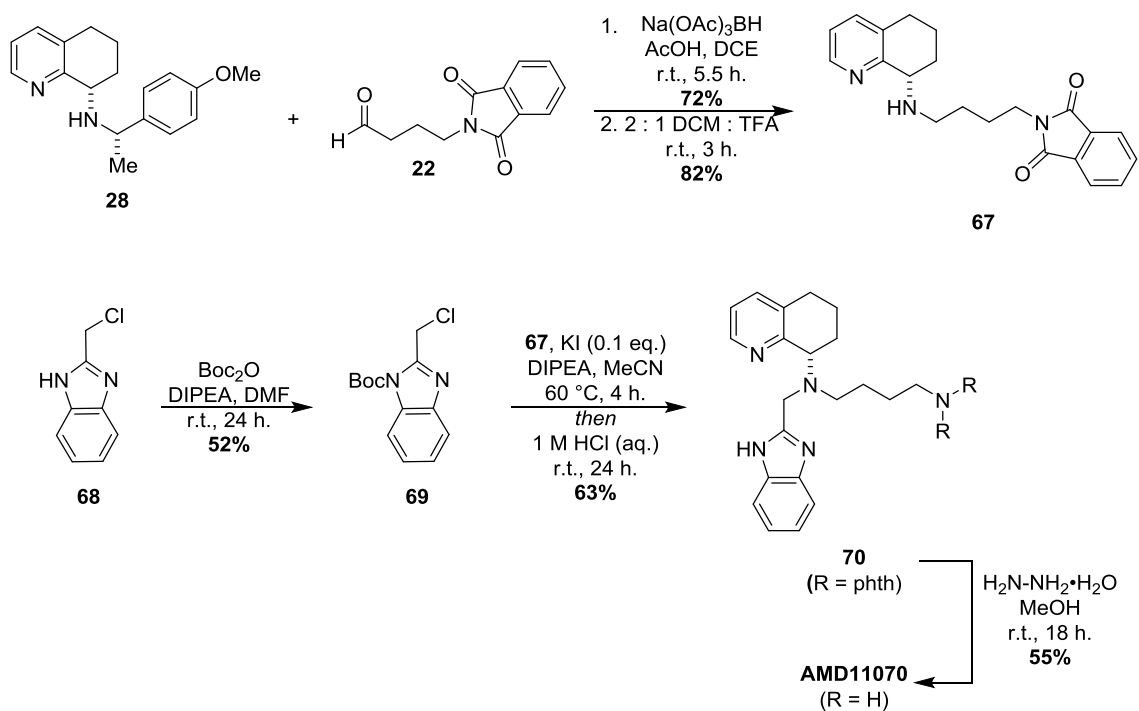


Figure 3.4 Crystal Structure of **IT1t**.

The second set of experiments was conducted using another well-known CXCR4 antagonist, **AMD11070**. According to literature procedures previously described,¹¹¹ the synthesis of **AMD11070** began with alkylation of the THQ fragment (Scheme 3.2). The secondary amine (**67**) was generated in two steps starting with reductive amination between amine **28** and side chain aldehyde **22** (the synthesis of compounds **28** and **22** is described in chapter 2), followed by deprotection of the *p*-methoxybenzyl protecting group using TFA. A simple Boc protection of 2-(chloromethyl)benzimidazole (**68**) furnished the aryl chloride fragment (**69**) that was used in an alkylation reaction with secondary amine fragment **67** to provide the mono-protected amine (**70**) upon subsequent acid-mediated deprotection. Finally, removal of the phthalimide protecting group with hydrazine hydrate afforded **AMD11070**.



Scheme 3.2 Synthesis of **AMD11070**.

3.3.3 Results and Discussion

Conformational Analysis of IT1t

Upon further analysis of the crystal structure with **IT1t** bound to CXCR4, several important observations were made. As illustrated in Figure 3.5, the crystal structure depicts **IT1t** as a dication. The pK_a values of 9.6 and 8.0 reported in an earlier publication were consistent with double protonation in the crystal lattice of the solvated ligand. However, examination of the ligand surroundings revealed a considerable number of short intra- and intermolecular contacts.

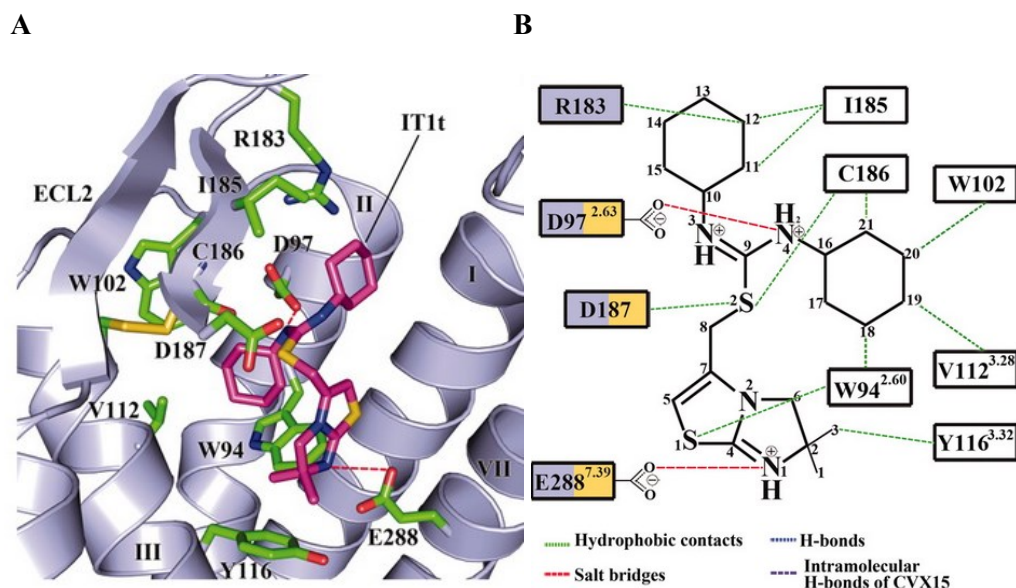


Figure 3.5 Cartoon Representation of Crystal Structure with **IT1t** (magenta) Bound to CXCR4 and Schematic Representation of Selected Interactions between CXCR4 and **IT1t**. **A**) Shown in green stick representation are the receptor residues involved in the ligand interactions. **B**) Reported mutations that have been shown to decrease HIV-1 infectivity and to disrupt CXCL12 binding and signaling are represented with blue and yellow, squares, respectively.⁸³

Five short intramolecular separations between ligand atoms were evident: an H-S distance of 2.6 Å (vdW 3.0 Å), H-C of 2.6 Å (vdW 2.9 Å), and H-H of 1.8, 2.0 and 2.1 Å (vdW 2.4 Å). Interestingly, one of the latter short contacts represented by an N-H hydrogen of the isothioureia group was eclipsed with the axial hydrogen of the ipso carbon on the adjacent cyclohexyl ring. In addition, the torsion angle (HN-C-NH) measured 146°, which strongly disagreed with the expected angle of 180°. From an intermolecular prospective, five rather short contacts were observed. The contacts include: H-HC(Trp94) of 1.79 Å, CH-OOC(Asp97) of 2.07 Å, H-H(Ala98) of 1.87 Å, CH-O=C(Cys186) of 2.37 Å, and S-HC(Asp287) of 2.80 Å. While adjustment of the structures by constrained refinement alleviated the short intermolecular contacts (by separating a few of the binding pocket residues from the ligand) and corrected the HN-C-NH torsion angle in **IT1t** to 164°, the other short intramolecular contacts remained (data not shown).

Several reports have revealed that docking **IT1t** back into the crystal structure does not reproduce the pose from the X-ray, unless the molecule is rigidly docked.¹⁴² Application of these same procedures in our hands delivered the same results. Therefore, taken together with the short contacts described above, we wanted to identify another conformation that could occupy the X-ray electron density and resolve steric interferences. Ana Alcaraz, Ph.D., a computational chemist from our laboratory, attempted this task. Using a method developed by OpenEye called AFITT, she was able to refine the CXCR4 ligand in the binding pocket.

Upon location of potential ligand density regions, the small molecule was fit to the space resulting in three conformations. The top ranked form flipped the cyclohexyl groups by 180° to relieve both intra- and intermolecular short contacts and adjusted the torsion from 141° to -176°. The second ranked pose also flipped the cyclohexyl groups and normalized the torsions. However, one of the rings adopted a high energy twist boat conformation. The third pose flipped the hetero-bicyclic ring, placing the germinal methyl groups at C-6 in a completely different protein environment. Depicted in Figure 3.6 is the superposition of the most favorable AFITT structure (pink) and the structure of **IT1t** from the crystal structure (blue) contained within the X-ray electron density (gray mesh). While both conformations fit the electron density equally well, with a heavy-atom RMSD of 1.0 Å, the AFITT structure relieved considerable internal strain as discussed above.

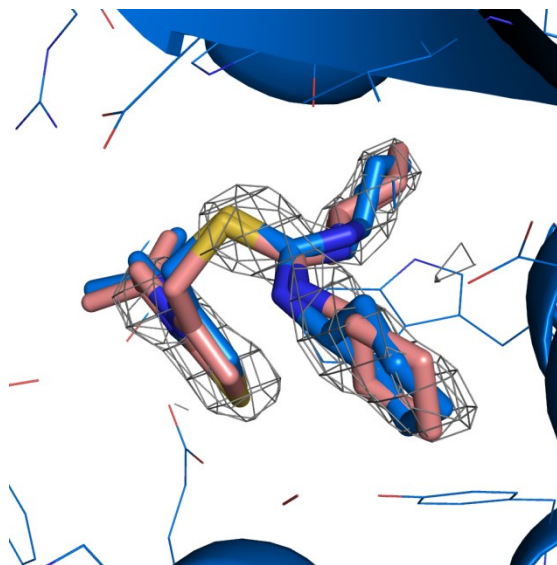


Figure 3.6 Overlay of AFITT Structure (pink) with **IT1t** (blue) from the Crystal Structure within the X-ray Electron Density (gray mesh).

Four different conformations of **IT1t** were compared (two structures of **IT1t** that originated from the published the crystal structure, **YUGQOH**, and the structure obtained from crystals grown in our laboratory, **CCDC 974559**; the CXCR4 protein-ligand complex; and the AFITT refinement). Each of the structures presented the cyclohexyl rings in the equatorial conformation and a planar hetero-bicyclic ring. The structures were individually aligned by heavy-atom matching to the **IT1t** structure derived from the protein complex. The low RMSD of the AFITT structure (0.4 Å) highlighted the overall similarity of these two forms. However, the RMSD values for both **YUGQOH** and **CCDC 974559** small molecule crystal structures were 5-6 fold larger (2.3 and 2.0 Å, respectively) due to significant deviations in the location of the cyclohexyl rings. By contrast, alignment of the independently determined small molecule crystal structures with one another yielded a diminutive RMSD of 0.5 Å. Further inspection of the two structures revealed that, apart from small conformational variations, the major difference between them was that **YUGQOH** showed a hydrogen bond between a single isothioureia N-H hydrogen atom and a water molecule that was absent in **CCDC 974559**.

The next question we sought to answer was whether or not the low energy AFITT conformation could be found in solution. To address this question, we began with a 50,000-step Monte Carlo Mixed-Mode (MCMM) conformational search. The search was performed on the doubly charged structure of **IT1t** in three different force fields (AMBER*, MMFFs, and OPLS-2005). Using enhanced torsion sampling and a 30 kJ/mol energy cutoff, a total of 3,379 conformations were generated (1,375 in AMBER*, 962 in MMFFs, and 1,042 in OPLS-2005). With respect to conformation of the cyclohexyl groups, there were two important outcomes worth noting. First, the OPLS-2005 force field was the only molecular mechanics protocol that provided a global minimum structure where both cyclohexyl rings adopted the chair conformation with the amine attachments in the equatorial position. The other two force fields predicted structures with chair conformations; however the amine substituents were in the axial position. This finding suggested that the molecular mechanics parameters in the latter force fields applied to the charged iminocyclohexanes biased the structures in favor axial conformations. Second, all three force fields generated many structures with non-chair cyclohexyl ring conformations. These results highlighted the limitations to using purely theoretical methods as discussed in section 3.2.

Next, a combination of 1-D and 2-D NMR experiments was executed with **IT1t** to assign all of the compound's proton and carbon peaks. However substantial overlap in the alkyl region of the spectrum prohibited exact assignments for all of the protons on the cyclohexyl rings. Data from a 2-D COSY experiment assisted in the relative assignments of a few of these protons. Unfortunately, with these limited assignments, only four NOE-derived distances could be used in the NAMFIS analysis. Application of the NAMFIS protocol using a subset of conformers from the complete search and the NMR-derived distances provided four conformations with populations of 13-58% and a SSD of 0.

Heavy-atom RMSDs relative to the AFITT structure fell at $< 2.5 \text{ \AA}$. When docked rigidly into the receptor, the most populated structure, NAMFIS-1 (RMSD = 0.9 \AA), demonstrated a good

binding fit and made hydrogen bond contacts with Asp97 and Glu288 that corresponded to important interactions found in the crystal structure (Figure 3.5). We were pleased that a NAMFIS-derived conformation (NAMFIS-1) matched closely the AFITT structure. In addition, the relative energy of this AMBER* conformation was within 3 kcal/mol of the corresponding global minimum. Had it been possible to derive additional NOE distances for **IT1t** in solution, we surmise that an even better match to the AFITT structure would have been derived by the NAMFIS treatment.

Conformational Analysis of **AMD11070**

At this point, we shifted our attention to another CXCR4 antagonist, namely **AMD11070**. As discussed in chapter 2, this small molecule was the first oral compound to enter the clinic. Several reports have been published regarding the synthesis, SAR, and biological data associated with this compound. Likewise, this structure served as the basis for our medicinal chemistry efforts outlined in the previous chapter. Therefore, we wanted to better understand how this molecule interacted with CXR4 so that we might form new hypotheses for our structurally-related class of THIQ compounds.

Two chemists from our laboratory (Bryan Cox, Ph.D., and Tony Prosser) engaged in the development of GPCR binding models for our CXCR4 antagonist program.¹⁴³ Their studies focused on forms of the receptor provided in the two crystal structures of CXCR4 with **IT1t** and **CVX15** (see chapter 2). Although initial considerations for small molecule modeling found the **IT1t** binding site attractive, other studies mentioned above demonstrated the difficulty in reproducing the bound conformation of **IT1t**. Inspection of the CXCR4 crystal structures revealed clear differences in residues important for small molecule binding. These observations implied a need to examine the differences in more detail in order to generate insights that went beyond the results of constrained docking.

Docking small molecule antagonists into the structure of CXCR4 complexed to **IT1t**, resulted in poses that lacked critical interactions identified by site-directed mutagenesis.¹⁴³ Consequently,

we hypothesized that some small molecules might interact more favorably in the CVX15-bound form of the receptor and served as peptidomimetics. This hypothesis was tested by comparing conformational variations in the binding sites of each crystal structure used in docking studies. Previously reported site-directed mutagenesis data for **AMD11070** supported molecular interactions with CXCR4, despite the absence of a crystal structure with it bound to the ligand.

Docking **AMD11070** into the CXCR4:CVX15 peptide crystal structure provided a pose that accommodated all interactions identified by site-directed mutagenesis (Figure 3.7A). However, similar results were not obtained by docking **AMD11070** into the CXCR4:IT1t crystal structure (Figure 3.7B). Only the top scoring pose from the CXCR4:CVX15 model displayed a strong interaction with Asp171.

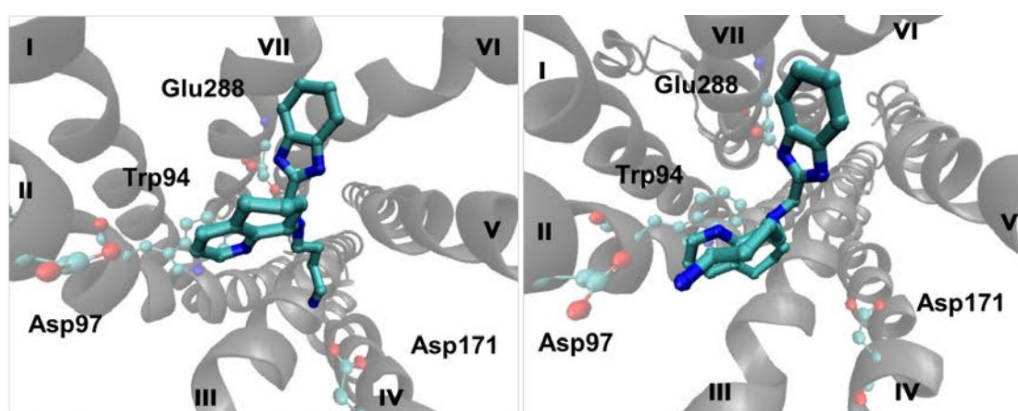


Figure 3.7 Top Pose of **AMD11070** (blue) Docked into **A**) CXCR4:CVX15 Peptide Crystal Structure (gray) **B**) CXCR4:IT1t Crystal Structure (gray). Highlighted are the key amino acid residues for AMD11070 based on site-directed mutagenesis data.

In the pose from the CXCR4:CVX15 model, the protonated butyl amine engages in a tight electrostatic interaction with Asp171 and also forms hydrogen bond interactions with the alcohol on Thr117 and the backbone carbonyl of His113. Additionally, the benzimidazole nitrogen donates a hydrogen bond to Glu288. The THQ ring forms two weak interactions. Measurements show that an aromatic carbon is 3.6 Å from the carboxyl oxygen on Asp97. Furthermore, the

dihedral angle between the aromatic C-H on **AMD11070** with the C-O on Asp97 is 140°. Taken together, these parameters describe a weak C-H···O hydrogen bond. The aromatic ring also forms a hydrophobic interaction with Trp94, where ring centroids are off-set just enough to avoid a π - π stacking interaction. In our pose, the butylamine side chain adopts a single gauche conformation between C2-C3 at the relatively low energy cost of ~0.8 kcal/mol.

A single-point quantum chemical calculation at the B3LYP/6-31G* level of theory in an implicit water solvent model revealed that the **AMD11070** pose from the CXCR4:CVX15 crystal structure is 8.1 kcal/mol lower in energy than the best **AMD11070** pose from the CXCR4:IT1t crystal structure (data not shown). These observations suggest that docking **AMD11070** into the CXCR4:CVX15 structure yielded a satisfying representation of the bioactive pose that matched mutagenesis results and captured a low-energy ligand conformation.

The bioactive pose of **AMD11070** was compared with experimentally determined conformations. The crystal structure of the **AMD11070** free-base overlays reasonably well with the bioactive pose of **AMD11070** with a Tanimoto shape score of 0.64 (Figure 3.8A). In general, the orientations of the three substituents are shared between the two conformations, with a few significant differences. Comparison of the bioactive and small molecule crystal conformers shows a slight rotation about the benzimidazole ring. Likewise, the THQ ring is rotated nearly 180° in the small molecule crystal structure relative to the bioactive pose. While the crystal form shows the butylamine chain in an extended conformation, the bioactive pose depicts a single gauche twist.

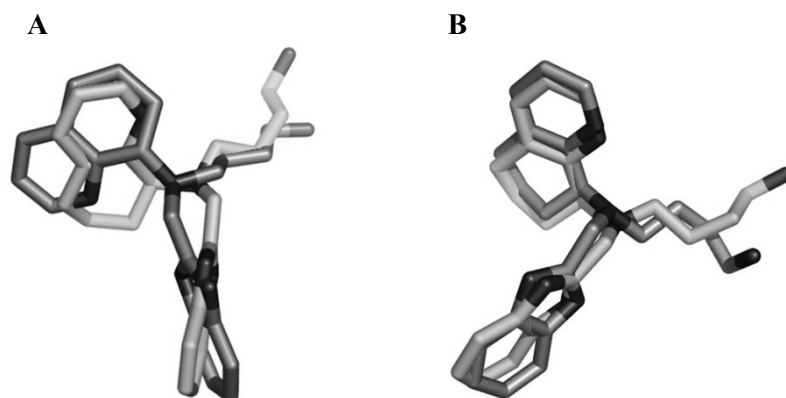


Figure 3.8 Comparison of the Bioactive Pose of **AMD11070** from the CXCR4:CVX15 Crystal Structure (light gray) with **A**) the **AMD11070** Small Molecule Crystal Structure (dark gray) and **B**) NAMFIS-3 (dark gray). Tanimoto Shape scores were determined for **A**) 0.64 and **B**) 0.79.¹⁴³

Solution conformers of **AMD11070** were obtained by the NMR NAMFIS method. Input for this analysis consisted of a “complete set” of *in silico* generated conformers and the distance scaled NOE cross-peaks. Thus, an exhaustive *in silico* search for **AMD11070** yielded a total of 10,755 conformations (4,397 in AMBER*, 2,861 in MMFFs, and 3,497 in OPLS-2005). In addition, 2-D NOESY analysis of the CXCR4 antagonist furnished 31 NOE cross-peaks that were converted to interproton distances using an *o*-phenyl NOE cross peak and its known distance as an internal ruler (Figure 3.9).

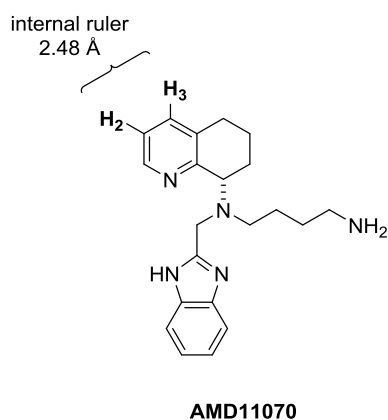


Figure 3.9 Structure of **AMD11070** and Internal Ruler Used to Derive the Interproton Distances.

Treatment by NAMFIS provided 13 conformers of **AMD11070** with populations ranging from 0.6-24.6%. Gratifyingly, the SSD (56) for the output indicated a satisfying quality of fit. Of the 13 conformers, two solution conformers of **AMD11070** presented high Tanimoto shape scores of 0.71 when overlaid with the free-base crystal structure (Figure 3.10). Notably, the conformers orient the THQ ring in the same way as the small molecule crystal structure. This result supports the proposition that the solution ensemble of **AMD11070** conformers contain the small molecule X-ray form.

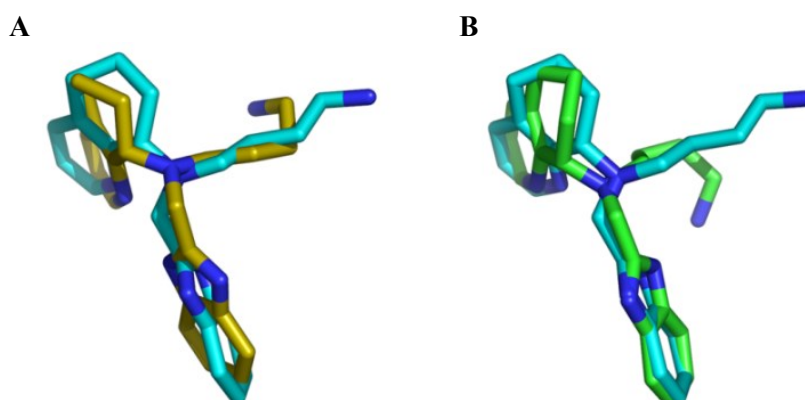


Figure 3.10 Alignment of the **AMD11070** Small Molecule X-ray Structure (blue) with **A**) NAMFIS-4 (yellow) and **B**) NAMFIS-9 (green).¹⁴³

Alignment of the 13 NAMFIS-derived conformers to the bioactive pose of **AMD11070** revealed that the NAMFIS-3 conformer (14.3%) is nearly identical to our proposed structure, exhibiting a Tanimoto shape score of 0.79 (Figure 3.8B). The THQ and benzimidazole rings of this conformer align faithfully with those of the bioactive pose. As illustrated in Figure 3.8B, the main difference between the **AMD11070** bioactive pose and this solution conformer lies in the orientation of the butyl amine side chain: the bioactive pose exhibits one gauche twist, while the NAMFIS-3 conformer contains two gauche twists. The outcome of these studies demonstrated that the empirically-derived conformer pool contained structures that are similar to both the small

molecule X-ray structure and the most favorable docked ligand in the CXCR4:CVX15 binding site. More importantly, its presence in solution validates the docked **AMD11070** structure as a viable low-energy binding conformation. Furthermore, the data supports the notion that the peptide crystal structure should be considered as a potential receptor model for other small molecule CXCR4 antagonists.

Conformational Analysis of **ECXC00947**

Our next objective was to apply the results obtained from the experiments with **AMD11070** to the lead compound from our THIQ-based series of antagonists. We began the computational docking study using both available crystal structures—CXCR4 in complex with the small molecule, **IT1t** and the CVX15 peptide-bound form of the receptor. Based on the outcome of exercises with **AMD11070**, we hypothesized that our lead molecule would also exhibit a pose biased for the CXCR4:CVX15 structure and make similar interactions.

Docking **ECXC00947** into the CXCR4:IT1t model yielded a pose where both heterocyclic rings occupied the minor binding pocket (Figure 3.11A). The THQ ring is buried in a hydrophobic pocket and π -stacks with Trp94. The nitrogen in the THIQ ring forms an electrostatic interaction with Asp97 (Figure 3.11B). Meanwhile, the butylamine forms an electrostatic interaction with Glu288.

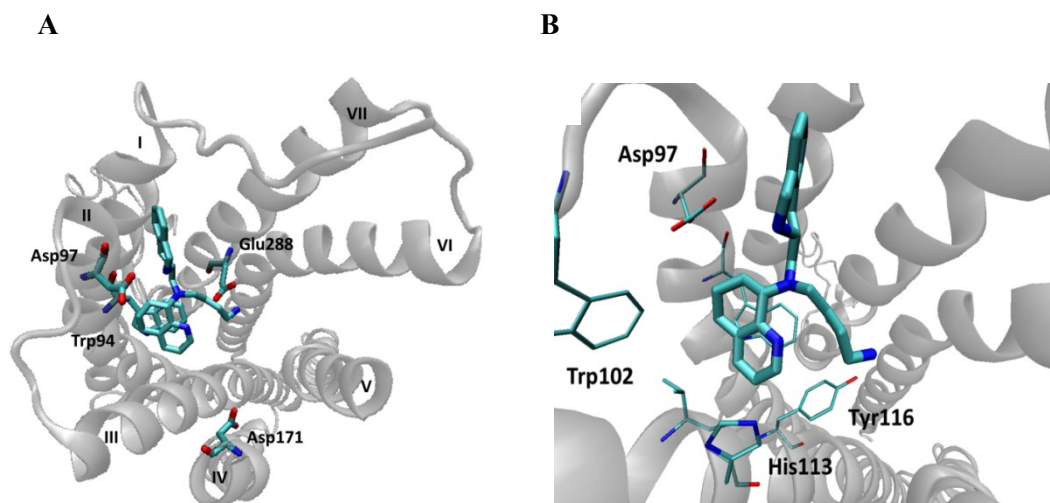


Figure 3.11 Model of **ECXC00947** Binding to CXCR4 Derived from the CXCR4:IT1t Small Molecule Crystal Structure (PDB 3ODU). Image **B** portrays the interactions of the THIQ ring with CXCR4 residues. Highlighted in both images are residues important for binding of a similar small molecule, **AMD11070**.

When the same molecule was docked into CXCR4:CVX15 model, a unique pose was established (Figure 3.12A). Similar to the first example, the top THQ moiety is buried in a hydrophobic pocket. However, in this pose, the heterocyclic ring is positioned about Arg188 near the site of the naphthylalanine ring from the CVX15 peptide (Figure 3.12B). Additionally, the THIQ nitrogen from the bottom portion of the molecule forms an electrostatic interaction with Glu288, while the butylamine interacts Asp171.

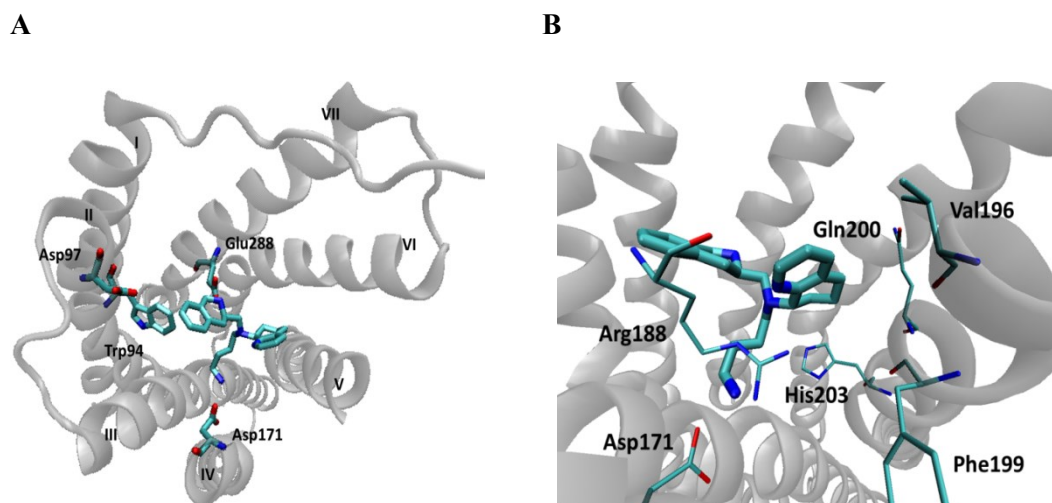


Figure 3.12 Model of **ECXC00947** Binding to CXCR4 Derived from the CXCR4:CVX15 Peptide Crystal Structure (PDB 3OE0). Image **B** portrays the interactions of the THQ ring with CXCR4 residues. Highlighted in both images are residues important for binding of a similar small molecule, **AMD11070**.

In order to determine which model predicted the most accurate pose, we again set out to determine the conformations of **ECXC00947** in solution by NMR spectroscopy and computational modeling techniques. Complete proton and carbon assignments were made for compound **ECXC00947** using 1-D and 2-D NMR experiments such as $^1\text{H}/^{13}\text{C}$ and COSY/HMBC, respectively. Likewise, 22 interproton distances were calculated from 2-D NOESY data according to the same internal ruler used for **AMD11070** (see Figure 3.9). A 100,000-step MCM conformational search conducted in three force fields (AMBER*, MMFFs, and OPLS-2005) provided a conformer pool believed to be complete due to delivery of the global minimum more than 25 times in each search. The NOE-derived distances and complete set of conformations were input into the NAMFIS program. Deconvolution of the solution structures resulted in 9 conformers in populations ranging from 0.9-38.4%. The high fit quality of these structures to the input data was indicated by a low SSD of 9.

Overlay of the NAMFIS-derived structures to the bioactive conformation predicted for each model, demonstrates that the pose of **ECXC00947** from the CXCR4:CVX15 crystal structure is

the predominant conformer in solution. Depicted in Figure 3.13 are the NAMFIS conformers that exhibit the best fit to the poses from each model. While both NAMFIS conformers seem to fit quite well to the predicted poses, the CXCR4:CVX15 model produced a lower heavy-atom RMSD (0.7 vs. 1.4 Å).

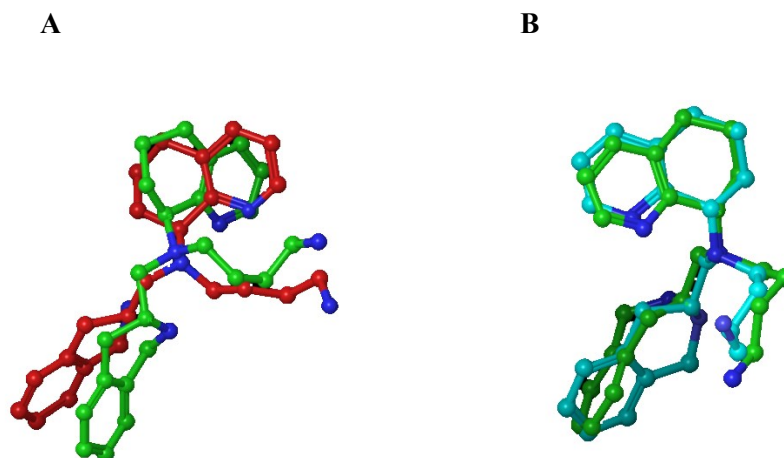
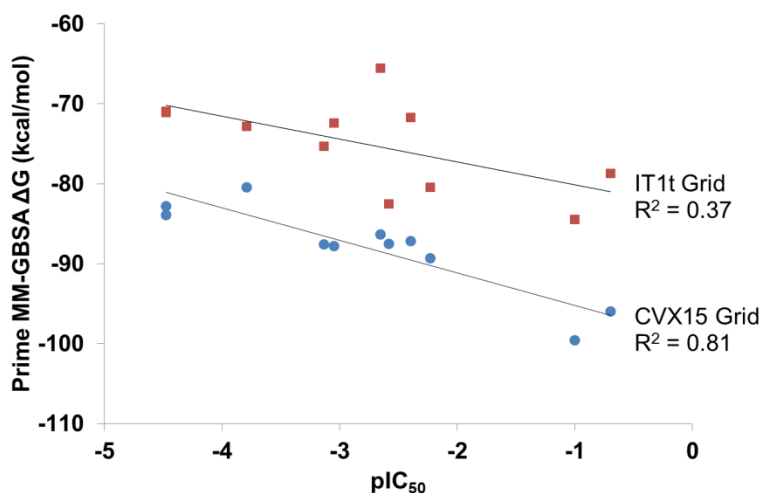


Figure 3.13 Overlay of NAMFIS Conformer (green) with Best Fit to Poses Derived from **A)** CXCR4:IT1t Model (red) and **B)** CXCR4:CVX15 Model (blue). **A)** NAMFIS-9 (0.9%) with a heavy-atom RMSD of 1.4 Å; **B)** NAMFIS-1 (38.4%) with a heavy-atom RMSD of 0.7 Å.

Both model poses were supported by the presence of similar conformers found in solution. However, we wanted to further probe the differences between the two crystal structure models. Two receptor grids centered on the model poses discussed above were generated by Dr. Bryan Cox. A congeneric series of compounds similar to **ECXC00947** was docked into each of the grids and scored by MM-GBSA. The ΔG scores generated in each model for all compounds were compared to the anti-HIV activities (pIC_{50}) discussed in chapter 2. Models from both crystal structures correlated with antiviral activity, however superior correlation was observed with the CXCR4:CVX15 model (Graph 3.1). The combination of conformational analysis and the strong correlation of docking scores to the SAR data supported the peptide crystal structure model.

Subsequent molecular modeling exercises used exclusively the receptor grid constructed from the CXCR4:CVX15 model.

Graph 3.1 Comparison of Anti-HIV Activity (pIC_{50}) with Prime MM-GBSA Scores Derived from the CXCR4 Binding Models for a Congeneric Series of THIQ-based Compounds.



3.4 Design of Constrained Analogues

3.4.1 Introduction

Central to the practice of medicinal chemistry is an understanding of the thermodynamics associated with the events that govern molecular recognition. The non-covalent binding between a drug and protein is mediated by a number of interactions: ion-ion, dipole-dipole, hydrophobic, hydrogen bonding, and even shape complementarity. The strength of the binding equilibrium is determined using thermodynamic data that measures the contributions of each of these interactions. The probability of binding is typically favored with positive interactions of polar functional groups and the formation of hydrophobic contacts. In contrast, adverse factors for binding relate to the restriction of translational and vibrational energies upon formation of the complex. The consequence of ligand binding is a loss of conformational energy that is gained by

the surrounding environment (entropy). In order to overcome the entropic penalties of binding and to improve drug potency, a common strategy is to restrict a compound's conformational flexibility. Conceptually speaking, the strategy operates by the introduction of features such as steric bulk, unsaturation, and cyclized structures. Optimization of the free energy gained during the association of a ligand with its target by the relative spatial disposition of these functional groups can translate to receptor selectivity, increased potency, pharmacophore identification, and even metabolic stability.

The series of experimental and theoretical investigations discussed in section 3.3 provided important information not only about well-known CXCR4 antagonists from the literature, but also about our THIQ-based compounds. An interesting structural characteristic from the conformational analysis of both **AMD11070** and **ECXC00947** suggests that the butylamine side chain prefers to adopt non-linear conformations. Specifically, solution-based conformers and predicted bioactive poses exhibit one or more gauche twists within the chain. Several of the NAMFIS conformers demonstrate the high degree of flexibility in the side chain (Figure 3.14). We were interested in determining whether or not the gauche arrangement is required for binding. Furthermore, we hypothesized that restricting the side chain in a way that limits the number of possible conformations should allow for increased potency. Several different compounds were synthesized to test this hypothesis.

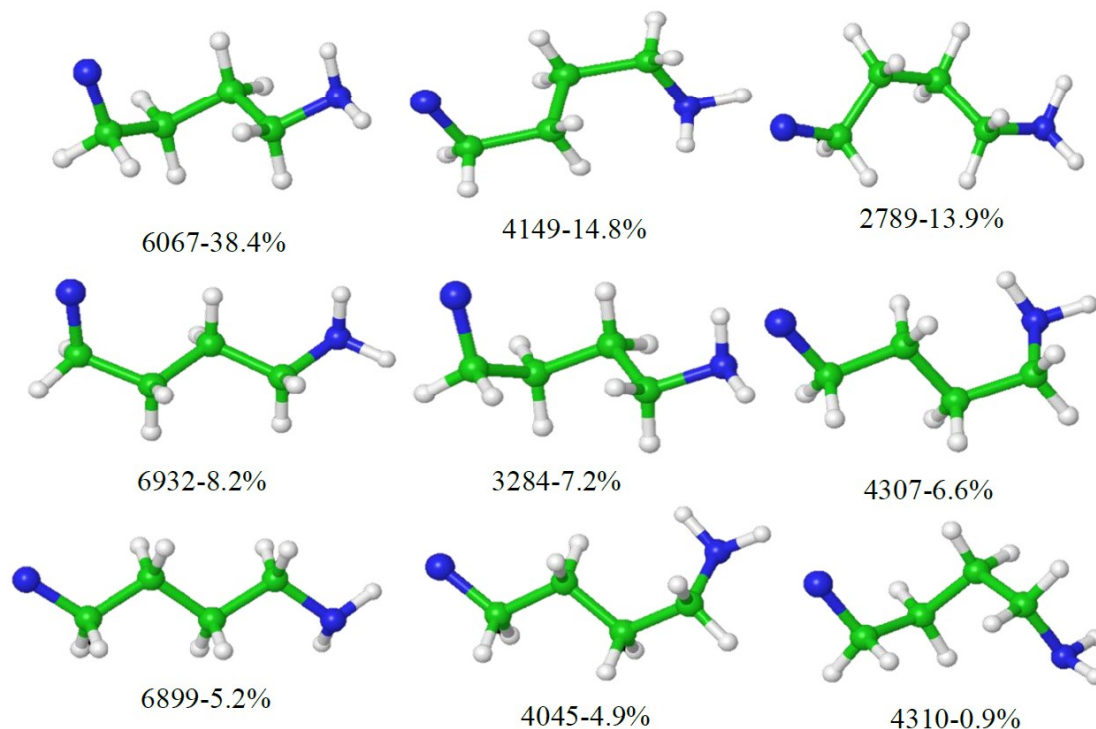


Figure 3.14 NAMFIS-derived Conformations of **ECXC00947** Butylamine Side Chain Represented as Fragments. The ball and stick fragments highlight the high degree of flexibility in the butylamine side chain. The blue ball on the left half of each fragment represents the nitrogen atom that attaches to the THIQ and THQ rings.

3.4.2 Synthesis of Constrained Analogues

A number of analogues were proposed for our studies regarding conformational pre-organization. Illustrated in Figure 3.15 is an overview of the planned target compounds. The synthesis of these THIQ-based analogues was accomplished using the routes discussed in chapter 2, with slight modifications.

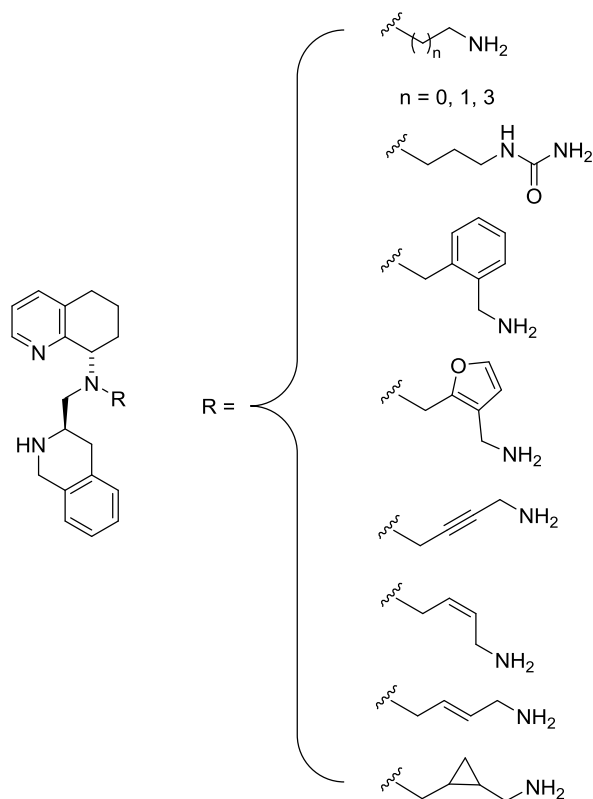
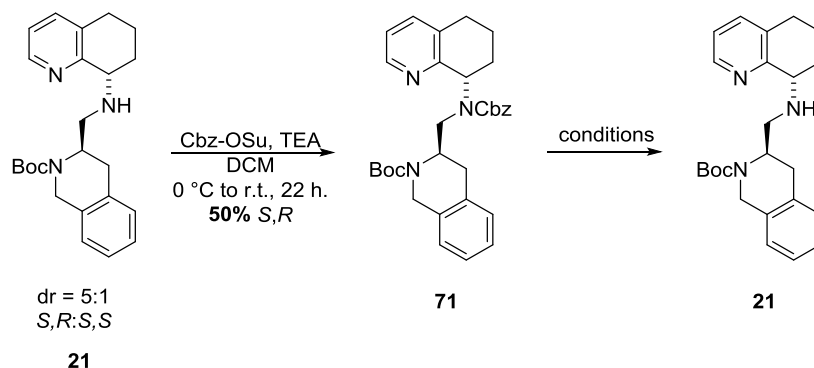


Figure 3.15 Target Compounds Designed to Probe the Effects of Conformational Flexibility.

In order to more rapidly access the compounds listed above, separation of the diastereomers was necessary prior to addition of the various side chains. Attempts to isolate only the desired diastereomer (*S,R*) of the half-scaffold amine intermediate were unsuccessful primarily due to streaking of the polar secondary amine during column chromatography. Ultimately, we decided to protect that nitrogen with a Cbz group to assist in purification and to potentially allow for better separation of the diastereomers. Gratifyingly, addition of the bulky protecting group changed the retention factors such that the diastereomers could easily be separated in less polar solvents like hexanes and ethyl acetate. With the desired diastereomer in hand, a number of the targets included above were synthesized.

Deprotection of the Cbz group proved challenging under standard hydrogenolysis conditions. Reactions carried out with palladium and activated charcoal under an atmosphere of hydrogen gas

or pressurized to 40 psi on the Parr Hydrogenator apparatus resulted in extremely low conversion percentages even after several days. I next looked to transfer hydrogenation conditions to cleave the carbamate. After experimenting with a few different sets of conditions and reagents, I found that the microwave-assisted reaction with 1,4-cyclohexadiene and palladium on carbon rapidly removed the Cbz group (Scheme 3.3). Furthermore, the product could be filtered and carried on to subsequent reactions.



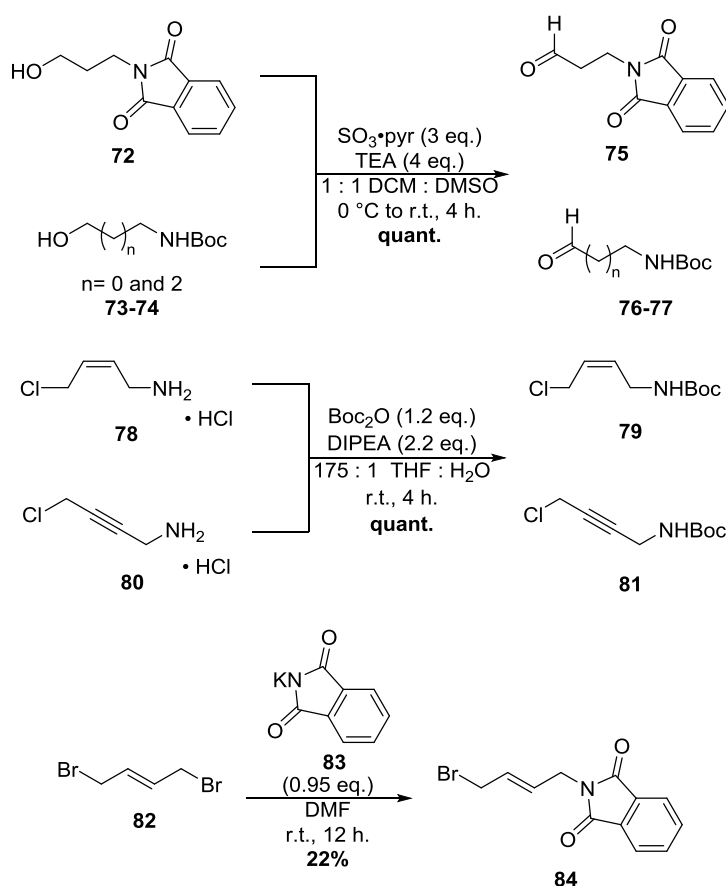
Reagent	Solvent	Additive	Temperature (°C)	Conversion (%)
10% Pd-C, H ₂ (40 psi)	EtOH	--	r.t.	<10 at 2 days
10% Pd-C, TES	10:1 MeOH:CHCl ₃	--	r.t.	15 at 3 h.
10% Pd-C, TES	10:1 MeOH CHCl ₃	xs AcOH	r.t.	<10 at 16 h.
10% Pd-C, cyclohexadiene	EtOH	--	r.t.	0 at 3 h.
10% Pd-C, cyclohexadiene	EtOH	xs AcOH	r.t.	56 at 16 h.
10% Pd-C, cyclohexadiene	EtOH	--	100 MW	72 at 5 min. 91 at 20 min. (74% isolated)

† Conversion percentages were calculated using LC-MS.

Scheme 3.3 Conditions Employed for Hydrogenolysis of Cbz Group.

The side chain fragments were either obtained from commercial vendors or prepared as the alkyl halide or aldehyde according to the reactions provided in Scheme 3.4. Parikh-Doering

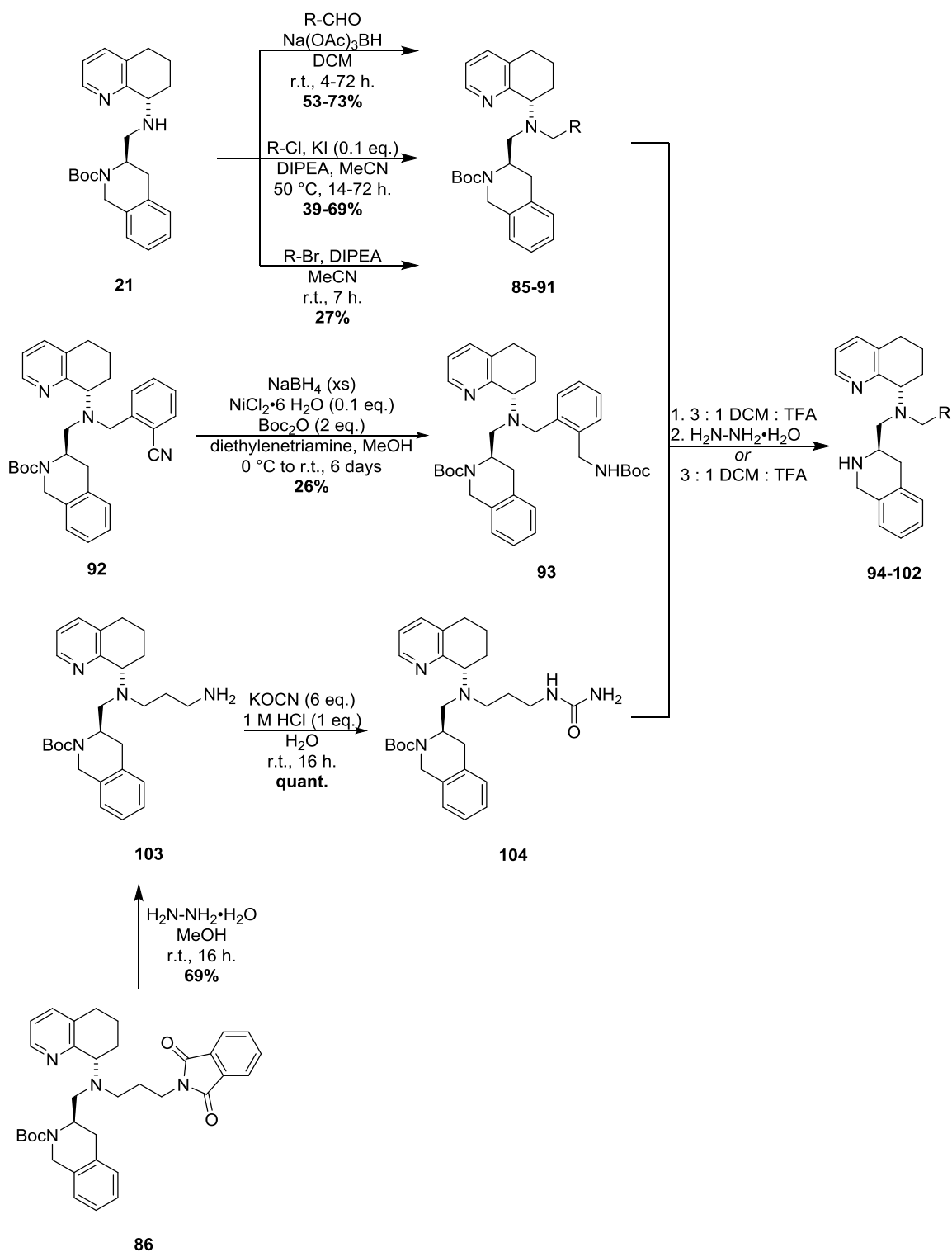
oxidation of the propyl and pentyl alcohols quantitatively provided the corresponding aldehydes (**75-77**). Protection of the *cis*-alkenyl amine (**78**) and the alkynyl amine (**80**) cleanly afforded the Boc protected chloride fragments (**79** and **81**, respectively). Finally, alkylation of (*E*)-1,4-dibromobut-2-ene (**82**) with less than one equivalent of potassium phthalimide furnished the protected (*E*)-alkenyl bromide fragment (**84**).



Scheme 3.4 Synthesis of Side Chain Fragments.

Through a combination of reductive aminations and alkylations the constrained fragments were attached to the half-scaffold amine (**21**) (Scheme 3.5). In the case of aryl nitrile **92**, a nickel-mediated reduction followed by trapping of the resultant amine with Boc anhydride provided protected intermediate **93**. Synthesis of the propyl urea-containing analogue was

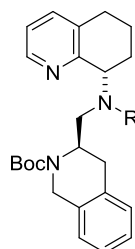
executed by first deprotecting the phthalimide **86** with hydrazine hydrate, and then treating the primary amine with potassium isocyanate under acidic conditions to provide urea **104**. Finally, complete deprotection provided the series of analogues that were submitted for testing.



Scheme 3.5 Complete Synthesis of Conformationally Restrained Analogues.

3.4.3 Results and Discussion

According to our hypothesis that was generated based on the molecular modeling and NMR experiments described in section 3.4.2, we expected a few of these compounds to be equipotent or more potent than the lead THIQ compound (**ECXC00947**). Specifically, we predicted that the (*Z*)-alkene side chain **98** could adopt a conformation most similar to the pose from the CXCR4:CVX15 model. Furthermore, this conformational pre-organization was expected to result in antiviral activity comparable to compound **ECXC00947**. The biological data for this series of analogues is summarized in Table 3.1.

Table 3.1 Effect of Conformational Restraints on Biological Activity.

Compound ID	R ₁	MAGI HIV-1 _{III} B IC ₅₀ (μM) ^{†,‡}	Ca ²⁺ Flux IC ₅₀ (μM) [‡]
ECXC00947 ^a		0.005	0.003
94		6.18	1.40
95		0.38	0.004
96		0.17	0.001
102		0.23	0.001
99		0.11	0.015
100		0.03	0.001
98		0.006	0.001
101		0.004	0.0002
97		0.03	0.0002

[†]All compounds had TC₅₀ values >10 μM. [‡]All assays were run in duplicate. Compound was synthesized by ^aLawrence Wilson, Ph.D.

Alterations in chain length appeared to have significant effects. Based on our predicted pose, the compound with only two methylene units in the side chain (**94**) would not be able to make interactions with Asp171, a residue critical for viral infectivity. As such, the significant loss of potency observed with this compound provides evidence for this shortcoming. Both the three (**95**) and five (**96**) carbon chain compounds were less active than the four carbon chain molecule **ECXC00947** in the HIV assay. The data indicate that the primary amine makes important

contacts reflective of its spatial positioning within the binding pocket. Similar to the four carbon chain urea discussed in chapter 2, the urea-containing compound that is shortened by only one methylene unit (**102**) was not able to restore anti-viral activity by making contacts to critical residues with any of the three available heteroatoms. The importance of electrostatic interactions (*via* the protonatable nitrogen) with regard to activity was further supported by these compounds.

As predicted, the compound with a (*Z*)-alkene in the side chain (**98**) showed activity similar to the saturated compound **ECXC00947** in the MAGI assay. However, the (*E*)-alkene (**100**) was slightly less active with an $IC_{50} = 0.030 \mu\text{M}$. Additionally, the alkyne displayed even less activity. This suggests that the linear conformation about the alkyne prevents the primary nitrogen from making important contacts. The compounds with aryl rings bisecting the chain showed potencies similar to the (*Z*)-alkene isomer. The benzylamine compound (**101**) was slightly more active than our lead compound, **ECXC00947**. However, the furan-containing compound (**97**) had an $IC_{50} = 0.030 \mu\text{M}$.

The above compounds were also tested in the calcium flux assay. Interestingly, all but three compounds (**94**, **95**, and **99**) were more potent than the lead compound (**ECXC00947**). Furthermore, the benzylamine-containing (**101**) and the furan-containing (**97**) compounds demonstrated subnanomolar activities against CXCL12-induced calcium flux ($IC_{50} = 0.0002 \mu\text{M}$). Given these highly potent compounds, additional investigation is warranted to further determine the accuracy of our molecular models.

3.5 Conclusions

Since the dawn of humanity, nature has served as mankind's medicine cabinet. Countless number of natural substances have been extracted from plants and organisms found on land and in water to treat various illnesses and diseases. Advances in science, technology, engineering, and mathematics made it possible to discover and design drugs in a rational and logical manner. Furthermore, as protein structures became more available through X-ray crystallography and

NMR, the significance of molecular conformation became clear. Several experimental and theoretical tools have helped improve our understanding of conformation and the role it plays in binding interactions.

Release of the first CXCR4 crystal structures in late 2010 catalyzed a cornucopia of research aimed at discovering novel receptor antagonists. Its involvement in aberrant physiological processes and disease states made CXCR4 a target of many drug discovery campaigns. In an attempt to learn from molecules described in the literature and advance our medicinal chemistry project centering on CXCR4, we analyzed these structures by computational chemistry and NMR spectroscopy techniques. From our studies of **IT1t**, we found that the conformation portrayed in the small molecule-bound CXCR4 crystal structure had several unfavorable intra- and intermolecular interactions characterized mainly by close contacts and abnormal torsion angles. Using the X-ray electron density, we were able to identify a conformation that resolved these issues and that fit the experimental data.

Armed with this information, we undertook molecular modeling studies to propose the binding interactions between **AMD11070** and CXCR4, despite the absence of a ligand-bound crystal structure. Although it seemed unconventional to dock this ligand into the peptide crystal structure (CXCR4:CVX15) instead of the small molecule structure (CXCR4:IT1t), results from these exercises suggested that the former should be considered, especially for molecules that might behave as peptidomimetics. Likewise, application of the NAMFIS technique helped validate the pose from our model.

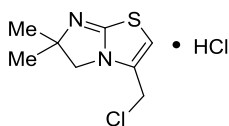
When this same technique was applied to our lead compound, **ECXC00947**, similar results were obtained. Using a model derived from the CXCR4:CVX15 crystal structure, we were able to generate a grid that was used to dock other THIQ-based compounds. Gratifyingly, the MM-GBSA scores from the docked structures correlated with the IC_{50} measurements from the MAGI assay. Upon further inspection of the predicted pose and the NAMFIS-derived solution conformations, we found that the butylamine side chain adopted a gauche conformation. We

hypothesized that designing molecules with limited flexibility about the side chain would lead to improvements in activity. Preliminary results from our synthetic efforts support the concept of conformational pre-organization as a means to increase potency. Studies with other conformationally restricted structures, namely the proposed cyclopropyl-containing molecules, should provide additional support for our hypothesis.

3.6 Chemistry Experimental Detail

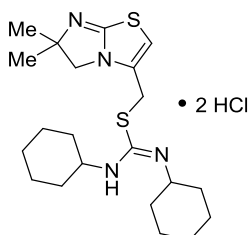
3.6.1 Synthetic Chemistry Experimental Detail

All reagents were obtained from commercial suppliers and used without further purification unless specified otherwise. Reaction progress was monitored by thin layer chromatography (TLC) on pre-coated glass plates (silica gel 60 F254, 0.25 mm) or liquid chromatography-mass spectrometry (LC-MS) using an analytical column (Agilent, ZORBAX Eclipse XDB-C18, 50 x 4.6 mm, 3.5 μ m). When noted, flash chromatography was performed manually or on a Teledyne ISCO Combiflash Companion with prepackaged Teledyne Redisep or Silicycle disposable normal phase or amine functionalized silica columns. Proton and carbon NMR spectra were recorded on an INOVA-400 (400 MHz), VNMRS 400 (400 MHz), INOVA-600 (600 MHz), or Unity-600 (600 MHz). All chemical shifts are reported in parts per million and referenced to the residual solvent peak. Mass spectra were performed by the Emory University Mass Spectroscopy Center on either a VG 70-S Nier Johnson or JEOL instrument.

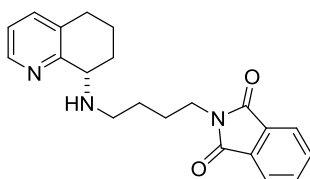


3-(chloromethyl)-6,6-dimethyl-5,6-dihydroimidazo[2,1-*b*]thiazole-2 HCl (65). To a mixture of 4,4-dimethylimidazolidine-2-thione (1.0 g, 7.5 mmol) in MeCN (15.0 mL) was added 1,3-dichloropropan-2-one (0.7 mL, 7.5 mmol). The reaction solution was heated to reflux for 3 hours. The reaction mixture was cooled, and the resulting white precipitate was filtered and

dried. The white solid (1.3 g) was re-suspended in 15 mL 2-methoxyethyl ether (diglyme) and heated to 140 °C for 2.5 hours. The reaction mixture was cooled to room temperature where it stirred overnight. The off-white solid was filtered and washed with ether. The crude off-white solid (1.31 g, 70%) was carried on without further purification.



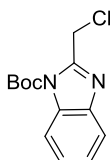
(6,6-dimethyl-5,6-dihydroimidazo[2,1-*b*]thiazol-3-yl)methyl **(*E*)-*N,N'*-**
dicyclohexylcarbamimidothioate (IT1t). A mixture of 1,3-dicyclohexylthiourea (0.5 g, 2.1 mmol) and compound **65** (1.0 g, 4.2 mmol) was refluxed in MeCN (20 mL) for 7 hours. While hot, the reaction mixture was filtered and rinsed with MeCN. The off-white precipitate (0.9 g) was dissolved in minimal MeOH (with heating) and added ether until flask became turbid. The flask was cooled to room temperature, and then was placed in freezer to assist in crystal formation. Upon scratching the glass of the flask, an off-white solid precipitated from the mixture. The precipitate was filtered and washed with ether to afford the title compound as an off-white solid (0.800 g, 81%). NMR assignments are included in section 3.6.2. HRMS (ESI) $[M+H]^+$ calc'd for $C_{21}H_{35}N_4S_2$ 407.22977, found 407.22930.



(*S*)-2-(4-((5,6,7,8-tetrahydroquinolin-8-yl)amino)butyl)isoindoline-1,3-dione (67). To a stirred mixture of amine **28** (1.00 g, 3.54 mmol), aldehyde **22** (1.15 g, 5.31 mmol), and AcOH (0.20 mL, 3.54 mmol) in DCE (12.0 mL) was added sodium triacetoxyborohydride (1.13 g, 5.31 mmol). The reaction was allowed to stir at room temperature for 5.5 hours. The reaction mixture was

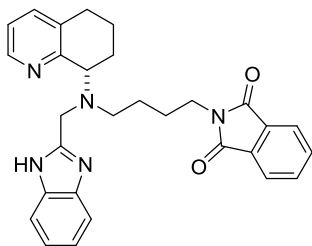
made basic (pH = 9) with saturated aqueous NaHCO₃. The aqueous layer was extracted with DCM (3 x 50 mL). The combined organics were washed with brine, dried over Na₂SO₄, and concentrated to a light brown/yellow oil (1.23 g). HRMS (ESI) [M+H]⁺ calc'd for C₃₀H₃₄N₃O₃ 484.25947; found 484.25981.

A solution of the yellow oil (1.21 g, 2.5 mmol) was stirred with a 1:2 mixture of TFA (1.0 mL, 13.0 mmol) and DCM (2 mL) at room temperature for 3 hours. The solvent was removed by rotary evaporation. The resulting brown/gray oil was diluted with water and EtOAc. The aqueous layer was basified with sat. aq. NaHCO₃ (pH = 9) and extracted with EtOAc (3x). The combined organic layers were concentrated to a brown oil. The oil was taken up in diethyl ether and 1M HCl was added to protonate the starting material. The ether layer was extracted with 1M HCl (2x). The aqueous layer was washed with ether (2x), basified with 15% NaOH (pH = 12), and extracted with DCM (4x). The organics were dried over Na₂SO₄, filtered, and concentrated to a light brown oil (0.718 g). HRMS (ESI) [M+H]⁺ calc'd for C₂₁H₂₄N₃O₂ 350.18630; found 350.18637.



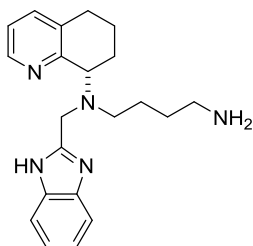
tert-butyl 2-(chloromethyl)-1H-benzo[d]imidazole-1-carboxylate (69). To a mixture of 2-(chloromethyl)-1H-benzo[d]imidazole (1.0 g, 6.0 mmol) and Boc anhydride (1.8 mL, 7.8 mmol) dissolved in dry DMF (12.0 mL) was added DIPEA (0.11 mL, 0.6 mmol). The reaction mixture was allowed to stir at room temperature overnight. The solvent was reduced to half on the rotary evaporator. The brown reaction mixture was diluted with EtOAc and washed with saturated aqueous NaHCO₃ (2x) and brine (2x). The organic layer was dried over anhydrous MgSO₄, filtered, and concentrated. The crude material was purified by flash column chromatography (ISCO, 25 g silica gel column, 0-15% EtOAc-Hexanes over 15 minutes) to afford the title compound as a colorless oil (0.830 g, 52%). ¹H NMR [400 MHz, CDCl₃] δ 8.00-7.96 (m, 1H),

7.77-7.74 (m, 1H), 7.43-7.34 (m, 2H), 5.07 (s, 2H), 1.74 (s, 9H); ^{13}C NMR [100 MHz, CDCl_3] δ 150.4, 148.3, 141.8, 133.5, 125.9, 124.8, 120.7, 115.3, 86.7, 39.8, 28.1; HRMS (ESI) $[\text{M}+\text{H}]^+$ calc'd for $\text{C}_{13}\text{H}_{16}\text{ClN}_2\text{O}_2$ 267.08948, found 267.08948.

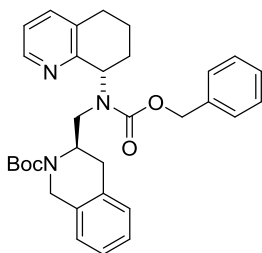


(S)-2-(4-(((1H-benzo[d]imidazol-2-yl)methyl)(5,6,7,8-tetrahydroquinolin-8-

yl)amino)butyl)isoindoline-1,3-dione (70). A mixture of compound **67** (0.72 g, 2.06 mmol), DIPEA (0.54 mL, 3.09 mmol), **69** (0.58 g, 2.16 mmol), and KI (0.034 g, 0.21 mmol) dissolved in dry MeCN (10.0 mL) was stirred at 60 °C for 4 hours. The reaction was cooled to room temperature and water (30 mL) and diethyl ether (50 mL) were added. The organic layer was washed with brine, dried over Na_2SO_4 , filtered, and concentrated to a brown oil. The oil was taken up in 1 M HCl (pH = 3-4) and diethyl ether. The acidic aqueous layer was stirred at room temperature for 24 hours. Toluene was added to the reaction mixture, and the pH was adjusted to 13 by addition of 10 M NaOH. The reaction mixture was filtered through a pad of celite, and the aqueous and organic phase were separated. The aqueous layer was extracted with toluene (2x). The combined organics were washed with 5% w/w aq. NaOH, dried over Na_2SO_4 , filtered, and concentrated to an off-white foam (0.625 g). Material was carried on without purification. HRMS (ESI) $[\text{M}+\text{H}]^+$ calc'd for $\text{C}_{29}\text{H}_{30}\text{N}_5\text{O}_2$ 480.23940, found 480.23910.

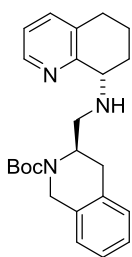


(S)-N¹-((1H-benzo[d]imidazol-2-yl)methyl)-N¹-(5,6,7,8-tetrahydroquinolin-8-yl)butane-1,4-diamine (AMD11070). To a solution of compound **70** (0.625 g, 1.30 mmol) in MeOH (6.0 mL) was added hydrazine hydrate (2.2 mL, 10.41 mmol) solution (24% in H₂O). The reaction was allowed to stir at room temperature overnight. The reaction mixture was concentrated and added DCM. The organic layer was washed with 0.5 M NaOH (to remove pthalhydrazide by-product). The aqueous layer was discarded. To the organic layer was added 1 M aqueous HCl (pH = 3). The organic layer was extracted twice with 1 M aqueous HCl. The organic layer was discarded. The acidic aqueous layer was stirred with decolorizing activated carbon for 1 hour at room temperature. The mixture was filtered, and DCM was added to the filtrate. The aqueous layer was treated with 4 M aqueous NaOH to bring pH to 13. The aqueous layer was extracted 2 times with DCM. The organics were combined, dried over Na₂SO₄, filtered, and concentrated to a light yellow oil that foamed under high vacuum (0.25 g). The crude material was purified by gravity column chromatography (8 g silica gel, pretreated with 95:5 DCM:MeOH with 2% concentrated NH₄OH and eluted with same solvent mixture). The resulting oil was taken up in DCM and washed with 0.5 M NaOH. The aqueous layer was extracted with DCM (3x). The organics were dried over Na₂SO₄, filtered, and concentrated to a foam (0.250 g, 55%). NMR assignments are included in section 3.6.2. HRMS (ESI) [M+H]⁺ calc'd for C₂₁H₂₈N₅ 350.23392, found 350.23399.

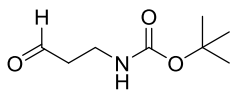


tert-butyl (R)-3-(((benzyloxy)carbonyl)((S)-5,6,7,8-tetrahydroquinolin-8-yl)amino)methyl)-3,4-dihydroisoquinoline-2(1H)-carboxylate (71). To a solution of compound **21** (11.0 g, 28.0 mmol) dissolved in dry DCM (140 mL) chilled to 0 °C was added TEA (6.6 mL, 47.5 mmol)

followed by OSu-Cbz (10.45 g, 41.9 mmol). The reaction mixture was warmed to room temperature where it stirred 2 days before removing the solvent under reduced pressure. The brown oil was dissolved in EtOAc and washed with 1M aq. HCl (3x). The organic layer was washed with brine, dried over Na₂SO₄, and concentrated to a brown oil (~16.5 g). The reaction mixture was purified by flash column chromatography (ISCO, 2 x 120 g silica gel column, 0-25% over 11 minutes, hold 25% for 5 minutes, 25%-50% over 8 minutes, hold 50% for 5 minutes EtOAc-hexanes) resulting in a white foam.

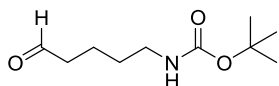


***tert*-butyl (R)-3-(((S)-5,6,7,8-tetrahydroquinolin-8-yl)amino)methyl)-3,4-dihydroisoquinoline-2(1H)-carboxylate (21)**. A solution of compound **71** (0.55 g, 1.042 mmol) in dry ethanol (4.0 mL) was added Pd/C (5 mg, 0.052 mmol) and cyclohexa-1,4-diene (0.59 mL, 6.25 mmol). The reaction mixture was heated in the microwave at 100 °C for 40 minutes. The reaction mixture was filtered over a pad of Celite, washed with DCM, and concentrated to an off-white/green foam (0.4 g). The material was carried on without further purification.

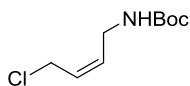


***tert*-butyl (3-oxopropyl)carbamate (76)**. A solution of *tert*-butyl (3-hydroxypropyl)carbamate **72** (0.30 mL, 1.76 mmol) and TEA (0.98 mL, 7.04 mmol) dissolved in DCM (6.0 mL) was cooled to 0 °C. To the reaction mixture was added SO₃-pyridine complex (0.840 g, 5.28 mmol) dissolved in DMSO (6.0 mL). The reaction was held at 0 °C for 1 hour and then allowed to warm to room temperature where it stirred for 3 hours. The reaction mixture was concentrated, quenched with sat. NaHCO₃, and extracted with ether (3x). The organic layer was washed with

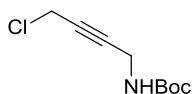
brine, dried over Na_2SO_4 , filtered, and concentrated a yellow oil (0.341 g). The crude material was carried on without further purification.



tert-butyl (5-oxopentyl)carbamate (77). A solution of *tert*-butyl (5-hydroxypentyl)carbamate **74** (0.30 mL, 1.47 mmol) and TEA (0.82 mL, 5.90 mmol) dissolved in DCM (6.0 mL) was cooled to 0 °C. To the reaction mixture was added SO_3 -pyridine complex (0.704 g, 4.42 mmol) dissolved in DMSO (6.0 mL). The reaction was held at 0 °C for 1 hour. The solvent was removed under rotary evaporation. To the residue was added sat. aq. NaHCO_3 , and the aqueous layer was extracted with ether (3x). The combined organic layers were washed with brine, dried over Na_2SO_4 , filtered and concentrated to a brown oil. The crude material was carried on to next step without further purification. The crude material was carried on without further purification.

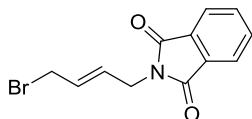


tert-butyl (Z)-(4-chlorobut-2-en-1-yl)carbamate (79). To a suspension of (Z)-4-chlorobut-2-en-1-amine hydrochloride **78** (0.500 g, 3.52 mmol) in THF (18.0 mL) and water (0.10 mL) was added DIPEA (1.4 mL, 7.75 mmol) followed by Boc anhydride (0.98 mL, 4.22 mmol). The resulting solution stirred at room temperature for 4 hours. The reaction was quenched with sat. aq. NaHCO_3 and extracted with ether (3x). The organics were washed with brine, dried over MgSO_4 , filtered, and concentrated to a clear oil that solidified upon standing. The crude material was carried on without further purification.

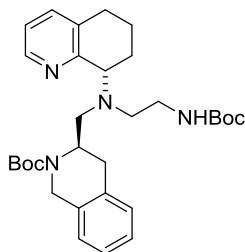


tert-butyl (4-chlorobut-2-yn-1-yl)carbamate (81). To a suspension of 4-chlorobut-2-yn-1-amine hydrochloride **80** (0.50 g, 3.57 mmol) in THF (18.0 mL) and water (0.10 mL) was added DIPEA (1.4 mL, 7.86 mmol) followed by Boc anhydride (0.99 mL, 4.29 mmol). The reaction was

allowed to stir at room temperature for 4 hours. The reaction was quenched with sat. aq. NaHCO_3 and extracted with ether (3x). The organics were washed with brine, dried over MgSO_4 , filtered, and concentrated to a light yellow oil. The crude material was carried on without further purification.

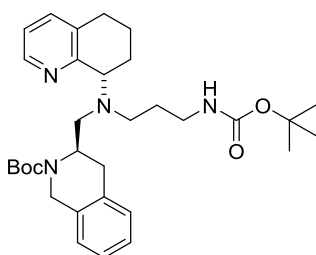


(E)-2-(4-bromobut-2-en-1-yl)isoindoline-1,3-dione (84). To a solution of (*E*)-1,4-dibromobut-2-ene (11.4 g, 53.3 mmol) in DMF (53.3 mL) was added potassium phthalimide (9.38 g, 50.6 mmol) as a suspension in DMF (50 mL). The reaction mixture was stirred at room temperature for 12 hours. The reaction was quenched with water, and the aq. layer was extracted with Et_2O (5 x 75 mL). The combined organic layers were washed with water (5 x 30 mL), and the solvent was removed under reduced pressure. The crude material was purified by flash column chromatography (9:1 to 2:1 hexanes- EtOAc) to obtain the title compound as a white solid.

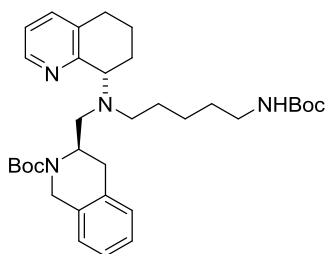


tert-butyl **(R)-3-(((2-((tert-butoxycarbonyl)amino)ethyl)((*S*)-5,6,7,8-tetrahydroquinolin-8-yl)amino)methyl)-3,4-dihydroisoquinoline-2(1*H*)-carboxylate (85).** To a mixture of compound **21** (0.366 g, 0.93 mmol) dissolved in 3.0 mL of DCM was added a solution of *tert*-butyl (2-oxoethyl)carbamate (0.14 mL, 0.93 mmol) in 2.0 mL of DCM. To the stirring mixture was added sodium triacetoxyborohydride (0.296 g, 1.40 mmol). The reaction stirred at room temperature overnight. An additional 0.5 eq (0.07 g) of aldehyde was added to reaction and allowed to stir for 1 hours. The reaction was quenched with sat. aq. NaHCO_3 and extracted with DCM (3x). The organic layer was washed with brine, dried over Na_2SO_4 , filtered, and concentrated to a

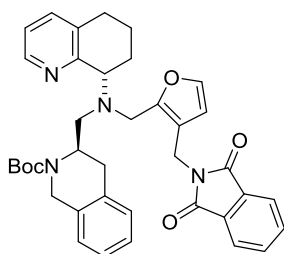
brown/orange oil (0.57 g). The crude material was purified by flash column chromatography (ISCO, 12 g silica gel, liquid load, 0-25% DCM-95:5 DCM/MeOH over 6 minutes, hold 3 minutes, 25-50% over 5 minutes, hold 3 minutes, 50-100% over 4 minutes, hold 4 minutes) resulting in an off-white foam (0.262 g, 53%). ^1H NMR [600 MHz, CDCl_3] δ 8.65-8.45 (m, 1H), 7.49-7.28 (m, 1H), 7.22-6.95 (m, 5H), 4.69-4.53 (m, 2H), 4.36 (dt, $J = 33.3, 14.6$ Hz, 2H), 4.17-3.99 (m, 1H), 3.33 (dd, $J = 39.0, 15.6$ Hz, 1H), 2.95 (dd, $J = 15.4, 5.5$ Hz, 1H), 2.86 (ddt, $J = 13.1, 6.7, 3.5$ Hz, 1H), 2.81-2.64 (m, 3H), 2.53 (dt, $J = 25.1, 11.6$ Hz, 1H), 2.45-2.15 (m, 4H), 2.09-1.96 (m, 1H), 1.83-1.57 (m, 2H), 1.56 (s, 18H).



tert-butyl (R)-3-(((3-((tert-butoxycarbonyl)amino)propyl)((S)-5,6,7,8-tetrahydroquinolin-8-yl)amino)methyl)-3,4-dihydroisoquinoline-2(1H)-carboxylate (86). To a mixture of compound **21** (0.206 g, 0.52 mmol) dissolved in 2.0 mL DCM was added a solution of compound **75** (0.091 g, 0.52 mmol) in 1.0 mL of DCM. To the stirring mixture was added sodium triacetoxyborohydride (0.166 g, 0.79 mmol). The reaction stirred at room temperature overnight and was quenched with sat. aq. NaHCO_3 and extracted with DCM (3 x). The organic layer was washed with brine, dried over Na_2SO_4 , filtered, and concentrated to a light brown oil (~0.3 g). The crude material was purified by flash column chromatography (ISCO, 12 g silica gel, liquid load, 0-50% DCM-95:5 DCM/MeOH over 15 minutes, then 100% 95:5 DCM/MeOH over 7 minutes) resulting in a white foam (0.211 g, 73%). HRMS (ESI) $[\text{M}+\text{H}]^+$ calc'd for $\text{C}_{32}\text{H}_{47}\text{N}_4\text{O}_4$ 551.35918, found 551.35903.

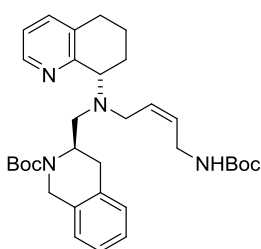


tert-butyl (R)-3-(((5-((tert-butoxycarbonyl)amino)pentyl)((S)-5,6,7,8-tetrahydroquinolin-8-yl)amino)methyl)-3,4-dihydroisoquinoline-2(1H)-carboxylate (87). To a mixture of compound **21** (0.150 g, 0.38 mmol) dissolved in 3.0 mL of DCM was added a solution of compound **77** (0.077 g, 0.38 mmol) in 2.0 mL of DCM. To the stirring mixture was added sodium triacetoxyborohydride (0.121 g, 0.57 mmol). The reaction stirred at room temperature for 48 hours. The reaction was quenched with sat. aq. NaHCO₃ and extracted with DCM (3 x). The combined organic layers were washed with brine, dried over Na₂SO₄, filtered, and concentrated to a brown/orange oil (0.225 g). The crude material was purified by flash column chromatography (ISCO, 12 g silica gel, liquid load, 0-25% DCM-95:5 DCM/MeOH over 11 minutes, hold 4 minutes, 25-50% over 6 minutes, hold 4 minutes, 50-100% over 4 minutes, hold 4 minutes) resulting in an off-white foam (0.155 g, 70%). HRMS (ESI) [M+H]⁺ calc'd for C₃₄H₅₁N₄O₄ 579.39048, found 579.39048.

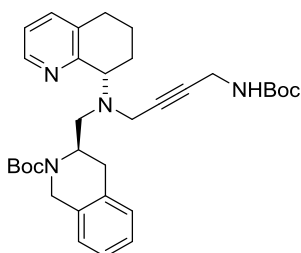


tert-butyl (R)-3-(((3-((1,3-dioxoisindolin-2-yl)methyl)furan-2-yl)methyl)((S)-5,6,7,8-tetrahydroquinolin-8-yl)amino)methyl)-3,4-dihydroisoquinoline-2(1H)-carboxylate (88). To a mixture of compound **21** (0.366 g, 0.93 mmol) dissolved in DCM (6.0 mL) was added 3-((1,3-dioxoisindolin-2-yl)methyl)furan-2-carbaldehyde (0.237 g, 0.93 mmol) immediately followed by sodium triacetoxyborohydride (0.296 g, 1.40 mmol). The reaction was allowed to stir at room

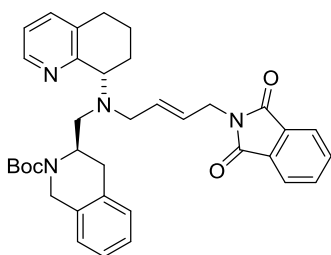
temperature overnight, and then was quenched with sat. aq. NaHCO₃ and extracted with DCM (3x). The organic layer was washed with brine, dried over Na₂SO₄, filtered, and concentrated to an off-white foam (~0.61 g). The crude material was purified by flash column chromatography (ISCO, 40 g silica gel, 0-35% EtOAc-Hexanes over 25 minutes) resulting in an off-white foam (0.400 g, 70%). HRMS (ESI) [M+H]⁺ calc'd for C₃₈H₄₁N₄O₅ 633.30715, found 633.30596.



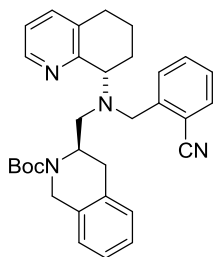
tert-butyl **(R)-3-((((Z)-4-((tert-butoxycarbonyl)amino)but-2-en-1-yl))((S)-5,6,7,8-tetrahydroquinolin-8-yl)amino)methyl)-3,4-dihydroisoquinoline-2(1H)-carboxylate (89)**. To a solution of compound **21** (0.298 g, 0.76 mmol) in 7.0 mL of MeCN was added DIPEA (0.20 mL, 1.14 mmol), and KI (0.013 g, 0.076 mmol). To the stirring mixture was added compound **79** (0.187 g, 0.91 mmol). The reaction mixture was heated to 50 °C where it stirred for 72 hours. The reaction was quenched with sat. aq. NaHCO₃ and extracted with DCM (3x). The organics were washed with brine, dried over Na₂SO₄, filtered, and concentrated to an off-white foam (0.43 g). The crude material was purified by flash column chromatography (ISCO, 12 g silica gel column, 0-25% EtOAc-Hexanes over 15 minutes) to give an off-white foam (0.312 g, 69%).



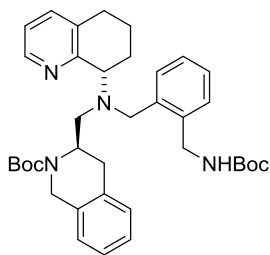
tert-butyl **(R)-3-(((4-((tert-butoxycarbonyl)amino)but-2-yn-1-yl)((S)-5,6,7,8-tetrahydroquinolin-8-yl)amino)methyl)-3,4-dihydroisoquinoline-2(1H)-carboxylate (90)**. To a solution of compound **21** (0.290 g, 0.74 mmol) in 5.0 mL MeCN was added DIPEA (0.19 mL, 1.11 mmol), and KI (0.012 g, 0.074 mmol). To the stirring mixture was added compound **81** (0.180 g, 0.88 mmol) dissolved in 2.0 mL of MeCN. The reaction mixture was heated to 50 °C where it stirred for 24 hours. The reaction was quenched with sat. aq. NaHCO₃ and extracted with DCM (3x). The combined organic layers were washed with brine, dried over Na₂SO₄, filtered, and concentrated to a brown foam. The crude material was purified by flash column chromatography (silica gel, 2:1 hexanes-EtOAc) to provide a white foam (0.160 g, 39%). HRMS (ESI) [M+H]⁺ calc'd for C₃₃H₄₅N₄O₄ 561.34353, found 561.34314.



tert-butyl **(R)-3-(((E)-4-(1,3-dioxisoindolin-2-yl)but-2-en-1-yl)((S)-5,6,7,8-tetrahydroquinolin-8-yl)amino)methyl)-3,4-dihydroisoquinoline-2(1H)-carboxylate (91)**. To a solution of compound **21** (0.4 g, 1.02 mmol) and DIPEA (0.27 mL, 1.53 mmol) dissolved in dry MeCN (6.0 mL) was added compound **84** (0.342 g, 1.22 mmol). The reaction was allowed to stir at room temperature for 7 hours. The solvent was removed at reduced pressure, and the residue was taken up in DCM. The organic layer was washed with brine, dried over Na₂SO₄, filtered, and concentrated to an off-white foam (0.633 g). The crude material was purified by flash column chromatography (silica gel, 3:1 EtOAc-hexanes) resulting in an off-white foam (0.164 g, 27%).

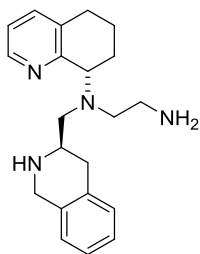


***tert*-butyl (R)-3-(((2-cyanobenzyl)((S)-5,6,7,8-tetrahydroquinolin-8-yl)amino)methyl)-3,4-dihydroisoquinoline-2(1H)-carboxylate (92).** To a mixture of compound **21** (0.298 g, 0.76 mmol) dissolved in DCM (6.0 mL) was added 2-formylbenzonitrile (0.099 g, 0.76 mmol) immediately followed by sodium triacetoxyborohydride (0.241 g, 1.14 mmol). The reaction was allowed to stir at room temperature for 4 hours. The reaction was quenched with sat. aq. NaHCO₃ and extracted with DCM. The organics were washed with brine, dried over NaSO₄, filtered, and concentrated to an off white foam (~0.36 g). The crude material was purified by flash column chromatography (ISCO, 24 g silica gel, 0-25% EtOAc-Hexanes over 15 minutes) resulting in an off white foam (0.246 g, 64%). HRMS (ESI) [M+H]⁺ calc'd for C₃₂H₄₇N₄O₄ 551.35918, found 551.35903.



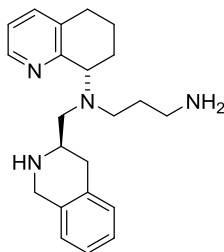
***tert*-butyl (R)-3-(((2-(((tert-butoxycarbonyl)amino)methyl)benzyl)((S)-5,6,7,8-tetrahydroquinolin-8-yl)amino)methyl)-3,4-dihydroisoquinoline-2(1H)-carboxylate (93).** To a solution of compound **92** (0.224 g, 0.44 mmol) dissolved in dry MeOH (4.4 mL) chilled to 0 °C were added Boc anhydride (0.21 mL, 0.88 mmol) and nickel(II)chloride hexahydrate (0.010 g, 0.044 mmol). Upon slow portioned addition of NaBH₄ (0.117 g, 3.09 mmol), the reaction mixture exothermed and effervesced to give a suspension with a fine black precipitate. The reaction was allowed to warm to room temperature. After 2 hours, the reaction mixture returned

to a light yellow color. Additional NaBH₄ (0.117 g, 3.09 mmol) was added, and the black suspension was allowed to stir over night. Additional NaBH₄ (0.117 g, 3.09 mmol) was added at room temperature, and the black suspension continued to stir for 48 hours. To the stirring suspension was added additional MeOH, followed by diethylenetriamine (0.048 mL, 0.44 mmol). The reaction stirred overnight before concentrating. The light grey oil was diluted with EtOAc and washed with sat. aq. NaHCO₃ (2x). The organic layer was washed with brine, dried over Na₂SO₄, and concentrated to an off-white foam (0.292 g). The crude material was purified by flash column chromatography (ISCO, 24 g silica gel, 0-25% EtOAc over 15 minutes) to give a clear oil (0.069 g, 26%) and starting material (0.079 g, 35% recovery).

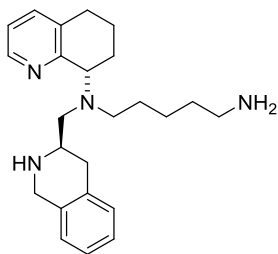


***N*¹-(((*R*)-1,2,3,4-tetrahydroisoquinolin-3-yl)methyl)-*N*¹-((*S*)-5,6,7,8-tetrahydroquinolin-8-yl)ethane-1,2-diamine (94).** A flask containing compound **85** (0.246 g, 0.46 mmol) in 3:1 DCM (2.4 mL) and TFA (0.8 mL) mixture was stirred at room temperature for 3 hours. The reaction was quenched with aq. sat. NaHCO₃. The aqueous layer was extracted with DCM (3x). The organic extracts were combined, dried over Na₂SO₄, filtered, and concentrated to an off-white foam (~0.15 g). The crude material was purified by flash column chromatography (silica gel, 9:1:0.1 DCM/MeOH/aq. NH₄OH) to obtain the title compound as an off-white foam (0.077 g, 50%). ¹H NMR [600 MHz, CDCl₃] δ 8.47 (dd, *J* = 4.8, 1.7 Hz, 1H), 7.41-7.33 (m, 1H), 7.10 (td, *J* = 7.2, 3.4 Hz, 3H), 7.04 (dd, *J* = 7.0, 2.1 Hz, 1H), 6.97 (d, *J* = 6.3 Hz, 1H), 5.51-5.02 (br s, 3H), 4.03 (d, *J* = 16.0 Hz, 1H), 3.99 (dd, *J* = 10.9, 5.9 Hz, 1H), 3.76 (d, *J* = 15.9 Hz, 1H), 3.11 (dd, *J* = 13.6, 3.5 Hz, 1H), 3.07-2.74 (m, 6H), 2.74-2.70 (m, 2H), 2.62 (dd, *J* = 13.5, 10.1 Hz, 1H), 2.50 (dd, *J* = 16.2, 10.1 Hz, 1H), 2.28-2.10 (m, 1H), 2.03 (dtt, *J* = 13.3, 5.3, 2.8 Hz, 1H), 1.86-1.78 (m,

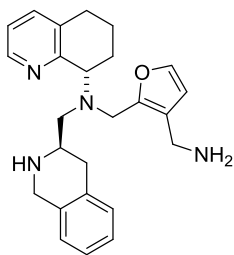
1H), 1.78-1.69 (m, 1H); ^{13}C NMR [150 MHz, CDCl_3] δ 159.0, 146.9, 136.8, 135.2, 134.6, 134.2, 129.3, 126.6, 126.2, 125.8, 121.6, 61.7, 59.2, 57.8, 54.2, 52.7, 48.4, 42.3, 33.6, 29.8, 29.6, 29.0, 24.7, 22.2; HRMS (ESI) $[\text{M}+\text{H}]^+$, calc'd for $\text{C}_{21}\text{H}_{29}\text{N}_4$ 337.23867, found 337.23886.



***N*¹-(((*R*)-1,2,3,4-tetrahydroisoquinolin-3-yl)methyl)-*N*¹-((*S*)-5,6,7,8-tetrahydroquinolin-8-yl)propane-1,3-diamine (95)**. A flask containing compound **86** (0.199 g, 0.36 mmol) in 3:1 DCM (2.4 mL) and TFA (0.8 mL) mixture was stirred at room temperature. After 4 hours, the reaction showed consumption of starting material. The reaction was quenched with aq. sat. NaHCO_3 . The aqueous layer was extracted with DCM (3x). The organic extracts were combined, dried over Na_2SO_4 , filtered, and concentrated to afford an off-white foam (~0.15 g). The material was purified by flash column chromatography (ISCO, 15.5 g amine functionalized gold column, 0-5% DCM-MeOH over 15 minutes). The fractions appeared to contain impurities, so the fractions were concentrated and the material (0.1 g) was repurified (ISCO, 4 g silica gel, 0-25% DCM-DCM/MeOH/ NH_4OH 80:20:2 over 9 minutes, hold 3 minutes, 25-50% over 5 minutes, hold 4 minutes, and 50-100% over 5 minutes, hold 3 minutes) resulting in a brown oil (0.065 g, 51%). ^1H NMR [600 MHz, CDCl_3] δ 8.45 (d, $J = 4.6$ Hz, 1H), 7.32 (d, $J = 7.6$ Hz, 1H), 7.10-6.99 (m, 5H), 4.08 (dd, $J = 10.2, 6.3$ Hz, 1H), 4.04 (d, $J = 15.0$ Hz, 1H), 3.91 (d, $J = 15.0$ Hz, 1H), 3.09 (dt, $J = 13.3, 6.7$ Hz, 1H), 2.94 (dd, $J = 13.2, 3.3$ Hz, 1H), 2.79-2.74 (m, 3H), 2.73-2.64 (m, 3H), 2.62 (dd, $J = 16.0, 3.6$ Hz, 1H), 2.47-2.26 (m, 3H), 2.09 (dddd, $J = 10.9, 8.0, 5.0, 2.2$ Hz, 2H), 1.99 (dh, $J = 12.9, 4.6, 4.0$ Hz, 2H), 1.90 (tdd, $J = 13.1, 10.2, 3.1$ Hz, 2H), 1.75-1.64 (m, 2H); ^{13}C NMR [150 MHz, CDCl_3] δ 156.8, 147.1, 138.2, 134.6, 134.2, 133.4, 129.5, 126.7, 126.5, 126.4, 122.7, 66.0, 58.4, 52.8, 51.8, 46.5, 40.0, 32.9, 29.9, 29.2, 26.2, 21.9.



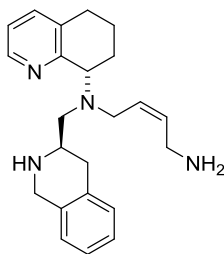
***N*¹-(((*R*)-1,2,3,4-tetrahydroisoquinolin-3-yl)methyl)-*N*¹-((*S*)-5,6,7,8-tetrahydroquinolin-8-yl)pentane-1,5-diamine (96).** A flask containing compound **87** (0.15 g, 0.26 mmol) in 3:1 DCM (2.4 mL) and TFA (0.8 mL) mixture was stirred at room temperature. After 3 hours, the starting material was completely consumed. The reaction was quenched with aq. sat. NaHCO₃. The aqueous layer was extracted with DCM (3x). The organic extracts were combined, dried over Na₂SO₄, filtered, and concentrated to a brown oil (~0.1 g). The crude material was purified by flash column chromatography (silica gel, 9:1:0.1 DCM/MeOH/NH₄OH) to obtain the title compound as a yellow oil (0.047g, 48%). ¹H NMR [600 MHz, CDCl₃] δ 8.45 (dd, *J* = 4.6, 1.6 Hz, 1H), 7.33 (dd, *J* = 7.6, 1.7 Hz, 1H), 7.20-6.91 (m, 5H), 4.17-4.04 (m, 2H), 3.92 (d, *J* = 15.0 Hz, 1H), 3.00 (ddd, *J* = 13.6, 6.9, 4.4 Hz, 2H), 2.78 (dtd, *J* = 16.6, 10.9, 6.5 Hz, 2H), 2.73-2.57 (m, 9H), 2.54-2.42 (m, 2H), 2.08 (dtd, *J* = 15.6, 5.3, 2.3 Hz, 1H), 1.98 (dtd, *J* = 13.4, 5.4, 3.3 Hz, 1H), 1.90 (tdd, *J* = 13.0, 10.1, 3.1 Hz, 1H), 1.77-1.67 (m, 1H), 1.59-1.42 (m, 4H), 1.42-1.28 (m, 2H); ¹³C NMR [150 MHz, CDCl₃] δ 159.0, 146.9, 136.8, 135.2, 134.6, 134.2, 129.3, 126.6, 126.2, 125.8, 121.6, 61.7, 59.2, 57.8, 54.2, 52.7, 48.4, 42.3, 33.6, 29.8, 29.6, 29.0, 24.7, 22.2; HRMS (ESI) [M+H]⁺ calc'd for C₂₄H₃₅N₄ 379.28562, found 379.28579.



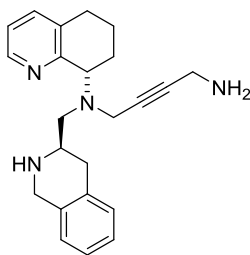
(*S*)-*N*-((3-(aminomethyl)furan-2-yl)methyl)-*N*-(((*R*)-1,2,3,4-tetrahydroisoquinolin-3-yl)methyl)-5,6,7,8-tetrahydroquinolin-8-amine (97). To a mixture of compound **88** (0.389 g,

0.62 mmol) dissolved in DCM (4.5 mL) was added TFA (1.5 mL). The reaction was allowed to stir at room temperature for 48 hours. The reaction was quenched with sat. aq. NaHCO₃ and extracted with DCM (3x). The combined organic layers were washed with brine, dried over Na₂SO₄, filtered, and concentrated to a dark brown foam (0.41 g). The material was passed through a plug of silica and eluted with 90:10:0.1 DCM/MeOH/NH₄OH resulting in a light brown foam (0.3 g). The material was carried on without further purification. HRMS (ESI) [M+H]⁺ calc'd for C₃₃H₃₃N₄O₃ 533.25472, found 533.25437.

To a solution of the light brown foam (0.3 g, 0.56 mmol) dissolved in MeOH (5.0 mL) was added hydrazine hydrate (0.8 mL, 3.78 mmol). The reaction was allowed to stir at room temperature overnight. The reaction mixture was concentrated to a yellow oil with white solid. The crude material was purified by flash column chromatography (ISCO, 12 g silica gel, solid loaded, 0-50% (90:10 DCM/MeOH 7 N NH₃ over 25 minutes) resulting in an off-white foam (0.035 g, 15%). ¹H NMR [600 MHz, CDCl₃] δ 8.47 (d, *J* = 4.6 Hz, 1H), 7.31 (d, *J* = 7.7 Hz, 1H), 7.25 (d, *J* = 5.3 Hz, 1H), 7.04 (dd, *J* = 8.0, 4.2 Hz, 3H), 6.96 (dt, *J* = 15.7, 3.9 Hz, 2H), 6.31 (s, 1H), 4.19 (d, *J* = 14.4 Hz, 1H), 4.00 (dd, *J* = 10.7, 6.5 Hz, 1H), 3.96 (d, *J* = 15.5 Hz, 2H), 3.87 (d, *J* = 14.4 Hz, 1H), 3.71 (d, *J* = 8.7 Hz, 3H), 3.11-2.90 (br s, 2H), 2.85 (d, *J* = 13.0 Hz, 1H), 2.73 (td, *J* = 11.8, 5.9 Hz, 1H), 2.63 (d, *J* = 16.5 Hz, 1H), 2.58-2.47 (m, 2H), 2.44 (dd, *J* = 12.5, 11.2 Hz, 1H), 2.34 (dd, *J* = 15.6, 10.2 Hz, 1H), 2.06 (dd, *J* = 12.8, 6.4 Hz, 1H), 1.95 (dt, *J* = 13.4, 4.4 Hz, 1H), 1.87 (q, *J* = 12.6, 12.1 Hz, 1H), 1.72-1.56 (m, 1H); ¹³C NMR [150 MHz, CDCl₃] δ 160.3, 156.0, 151.7, 146.8, 140.2, 138.0, 134.7, 133.2, 131.7, 129.1, 128.0, 127.7, 127.2, 126.0, 113.4, 65.3, 60.0, 50.9, 48.1, 46.1, 34.1, 33.1, 29.6, 29.1, 21.6; HRMS (ESI) [M+H]⁺ calc'd for C₂₅H₃₁N₄O 403.24924, found 403.24894.

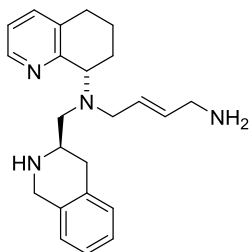


(Z)-N¹-(((R)-1,2,3,4-tetrahydroisoquinolin-3-yl)methyl)-N¹-((S)-5,6,7,8-tetrahydroquinolin-8-yl)but-2-ene-1,4-diamine (98). A solution of compound **89** (0.2 g, 0.36 mmol) in 3:1 DCM (2.4 mL) and TFA (0.8 mL) stirred at room temperature for 3 hours. Reaction mixture was quenched with sat. aq. NaHCO₃ and basified to pH = 12 with 15% aq. NaOH. The mixture was extracted with DCM, washed with brine, dried over Na₂SO₄, filtered, and concentrated to a brown oil (0.099 g). The crude material was purified by flash column chromatography (silica gel, 9:1:1 DCM/MeOH/NH₄OH) to give a light brown oil (0.0761 g, 59%). ¹H NMR [600 MHz, CDCl₃] δ 8.42 (d, *J* = 5.0 Hz, 1H), 7.29 (d, *J* = 7.3 Hz, 1H), 7.10-6.91 (m, 5H), 5.62 (app. q, *J* = 6.5 Hz, 2H), 4.07 (dd, *J* = 10.1, 6.5 Hz, 1H), 3.99 (d, *J* = 15.2 Hz, 1H), 3.82 (d, *J* = 15.0 Hz, 1H), 3.76 (dd, *J* = 14.2, 6.5 Hz, 1H), 3.40 (dd, *J* = 14.1, 6.1 Hz, 1H), 3.27 (ddd, *J* = 19.5, 14.4, 5.8 Hz, 2H), 2.80 (dd, *J* = 13.6, 3.0 Hz, 2H), 2.74 (dtd, *J* = 16.8, 11.2, 10.3, 5.4 Hz, 4H), 2.62 (dt, *J* = 16.3, 3.9 Hz, 1H), 2.58-2.54 (m, 1H), 2.38 (dd, *J* = 14.5, 10.5 Hz, 2H), 2.10-1.91 (m, 2H), 1.91-1.79 (m, 1H), 1.66 (tdt, *J* = 16.3, 12.4, 5.7 Hz, 1H); ¹³C NMR [150 MHz, CDCl₃] δ 158.1, 146.7, 136.8, 135.1, 134.2, 134.1, 131.5, 131.2, 129.1, 126.3, 126.0, 125.6, 121.6, 60.6, 57.2, 51.8, 50.3, 48.0, 38.0, 33.5, 29.3, 27.0, 21.9.



N¹-(((R)-1,2,3,4-tetrahydroisoquinolin-3-yl)methyl)-N¹-((S)-5,6,7,8-tetrahydroquinolin-8-yl)but-2-yne-1,4-diamine (99). A solution of compound **90** (0.160 g, 0.29 mmol) in 3:1 DCM

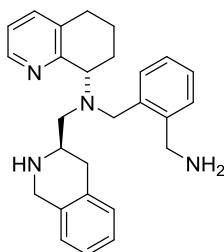
(2.4 mL) and TFA (0.8 mL) stirred at room temperature for 4 hours. The reaction mixture was quenched with sat. aq. NaHCO₃ and basified to pH = 12 with 15% aq. NaOH. The mixture was extracted with DCM (3x), washed with brine, dried over Na₂SO₄, filtered, and concentrated to a light brown solid (0.061 g). The crude material was purified by flash column chromatography (silica gel, 9:1:1 DCM/MeOH/NH₄OH) to give an orange/brown foam (0.036 g, 35%). ¹H NMR [600 MHz, CDCl₃] δ 8.40 (d, *J* = 4.3 Hz, 1H), 7.30 (d, *J* = 7.8 Hz, 1H), 7.13-6.92 (m, 5H), 4.27-4.09 (m, 1H), 3.97 (d, *J* = 15.1 Hz, 1H), 3.85 (d, *J* = 15.8 Hz, 2H), 3.56 (d, *J* = 17.0 Hz, 1H), 3.41 (s, 2H), 2.79 (ddd, *J* = 30.1, 20.3, 8.8 Hz, 3H), 2.62 (dd, *J* = 25.2, 16.3 Hz, 2H), 2.53-2.36 (m, 2H), 2.27 (br s, 3H), 2.11-2.05 (m, 1H), 1.97 (q, *J* = 13.0, 11.5 Hz, 2H), 1.69 (q, *J* = 16.3, 14.5 Hz, 1H); ¹³C NMR [150 MHz, CDCl₃] δ 160.7, 149.9, 148.8, 138.8, 137.0, 136.6, 132.2, 131.2, 128.9, 124.9, 123.8, 87.2, 82.7, 65.0, 58.9, 54.7, 53.8, 50.9, 45.8, 36.2, 34.4, 31.6, 23.8.



(*E*)-*N*¹-(((*R*)-1,2,3,4-tetrahydroisoquinolin-3-yl)methyl)-*N*¹-((*S*)-5,6,7,8-tetrahydroquinolin-8-yl)but-2-ene-1,4-diamine (100). To a solution of compound **91** (0.164 g, 0.28 mmol) dissolved in dry DCM (2.1 mL) was added TFA (0.7 mL). The reaction mixture stirred at room temperature for 4 hours. The reaction was quenched with sat. aq. NaHCO₃ and extracted with DCM (3x). The combined organic layers were washed with brine, dried over Na₂SO₄, filtered, and concentrated to an off-white foam (0.14 g). The crude material was carried on without further purification.

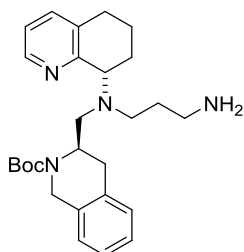
To a solution of the off-white foam (0.136 g, 0.28 mmol) dissolved in MeOH (3.0 mL) was added hydrazine hydrate (0.5 mL, 2.23 mmol). The reaction was allowed to stir at room temperature overnight before concentrating to a yellow oil with white solid. The crude material was purified

by flash column chromatography (ISCO, 12 g silica gel, solid loaded, 0-25% (80:20:2 DCM/MeOH/NH₄OH) and DCM over 25 minutes) resulting in an off-white foam (0.147 g, 99%). ¹H NMR [600 MHz, CDCl₃] δ 8.45 (dd, *J* = 4.8, 1.7 Hz, 1H), 7.32 (d, *J* = 7.9 Hz, 1H), 7.08-6.98 (m, 5H), 5.71 (qt, *J* = 15.6, 5.7 Hz, 2H), 4.10 (dd, *J* = 9.9, 6.3 Hz, 1H), 4.02 (d, *J* = 15.0 Hz, 1H), 3.83 (d, *J* = 14.9 Hz, 1H), 3.59 (dd, *J* = 14.2, 6.4 Hz, 1H), 3.29 (dd, *J* = 23.2, 5.3 Hz, 2H), 2.91 (dd, *J* = 13.2, 3.4 Hz, 1H), 2.76 (ddt, *J* = 14.0, 6.3, 3.6 Hz, 2H), 2.66 (dt, *J* = 16.7, 4.7 Hz, 1H), 2.61 (dd, *J* = 16.1, 3.7 Hz, 1H), 2.51-2.38 (m, 3H), 2.33 (br s, 3H), 2.07 (dddd, *J* = 15.8, 7.7, 4.8, 2.3 Hz, 1H), 1.98 (dh, *J* = 13.1, 4.6, 3.9 Hz, 1H), 1.94-1.87 (m, 1H), 1.70 (dddd, *J* = 24.6, 11.4, 5.0, 2.9 Hz, 1H); ¹³C NMR [150 MHz, CDCl₃] δ 158.8, 147.0, 136.7, 135.6, 134.8, 134.1, 133.2, 129.9, 129.3, 126.6, 126.1, 125.7, 121.6, 61.4, 57.2, 56.3, 52.2, 48.6, 43.9, 33.8, 29.6, 28.1, 22.0; HRMS (ESI) [M+H]⁺ calc'd for C₂₇H₃₉N₄O₂ 451.30675, found 451.30493.

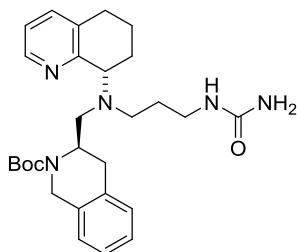


(S)-N-(2-(aminomethyl)benzyl)-N-(((R)-1,2,3,4-tetrahydroisoquinolin-3-yl)methyl)-5,6,7,8-tetrahydroquinolin-8-amine (101). To a solution of compound **93** (0.069 g, 0.11 mmol) in DCM (1.0 mL) was added TFA (0.3 mL). The reaction stirred at room temperature overnight. The reaction was quenched with sat. aq. NaHCO₃, and the pH was adjusted to 12 with NaOH. The reaction mixture was extracted with DCM (3x), washed with brine, dried over Na₂SO₄, and concentrated. The crude material was purified by flash column chromatography (silica gel, 90:10:0.1 DCM/MeOH/NH₄OH) to afford the title compound as a yellow oil (0.029 g, 62%). ¹H NMR [600 MHz, CDCl₃] δ 8.47 (dd, *J* = 10.0, 4.8 Hz, 1H), 7.38 (dd, *J* = 18.5, 7.6 Hz, 1H), 7.30 (d, *J* = 7.7 Hz, 2H), 7.19 (t, *J* = 7.4 Hz, 2H), 7.06-6.96 (m, 3H), 6.96-6.89 (m, 2H), 4.36-4.26 (m, 1H), 4.09 (d, *J* = 13.4 Hz, 1H), 3.98 (dd, *J* = 12.1, 6.7 Hz, 2H), 3.88 (dd, *J* = 20.3, 14.2 Hz, 2H),

3.57 (d, $J = 15.2$ Hz, 1H), 2.89-2.65 (m, 3H), 2.66-2.55 (m, 2H), 2.56-2.41 (m, 3H), 2.30 (dd, $J = 16.1, 9.0$ Hz, 1H), 2.18-2.07 (m, 1H), 1.95 (qd, $J = 10.5, 9.8, 3.9$ Hz, 2H), 1.61 (dtt, $J = 28.0, 12.0, 6.3$ Hz, 1H), 1.28-1.08 (m, 1H); ^{13}C NMR [150 MHz, CDCl_3] δ 162.8, 149.6, 149.4, 141.0, 139.8, 137.8, 136.9, 134.0, 133.4, 131.7, 130.7, 130.1, 129.6, 128.8, 128.6, 128.4, 124.6, 60.3, 59.5, 54.5, 49.8, 44.7, 36.0, 32.3, 32.0, 24.6, 24.3; HRMS (ESI) $[\text{M}+\text{H}]^+$ calc'd for $\text{C}_{27}\text{H}_{33}\text{N}_4$ 413.26997, found 413.26985.

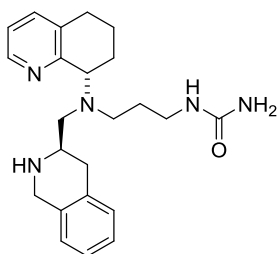


tert-butyl (R)-3-(((3-aminopropyl)((S)-5,6,7,8-tetrahydroquinolin-8-yl)amino)methyl)-3,4-dihydroisoquinoline-2(1H)-carboxylate (103). To a solution of compound **86** (0.274 g, 0.47 mmol) dissolved in MeOH (5.0 mL) was added hydrazine hydrate (0.8 mL, 3.77 mmol). The reaction was allowed to stir at room temperature overnight. The reaction mixture was concentrated to a yellow oil with white solid. The crude material was purified by flash column chromatography (ISCO, 12 g silica gel, solid loaded, 0-25% 80:20:2 DCM/MeOH/ NH_4OH and DCM over 25 minutes) resulting in an off-white foam (0.147 g, 69%). HRMS (ESI) $[\text{M}+\text{H}]^+$ calc'd for $\text{C}_{27}\text{H}_{39}\text{N}_4\text{O}_2$ 451.30675, found 451.30493.



tert-butyl (R)-3-(((S)-5,6,7,8-tetrahydroquinolin-8-yl)(3-ureidopropyl)amino)methyl)-3,4-dihydroisoquinoline-2(1H)-carboxylate (104). A stirred solution of compound **103** (0.147 g, 0.33 mmol) in 1 N HCl (0.3 mL, 0.33 mmol) and water (3.0 mL) was treated with potassium

cyanate (0.132 g, 1.63 mmol). The mixture was stirred at room temperature for 48 hours. The reaction mixture was diluted with DCM. To the aqueous layer was added additional 1 N HCl to remove residual starting amine. The aqueous layer was extracted with DCM. The organic layer was washed with brine, dried over Na₂SO₄, filtered, and concentrated to an off white foam (0.163 g). Crude material was carried on without further purification. HRMS (ESI) [M+H]⁺ calc'd for C₂₈H₄₀N₅O₃ 494.31257, found 494.31189.



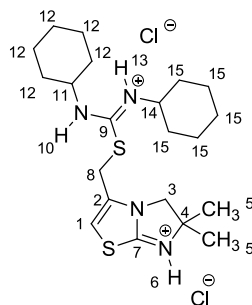
1-(3-(((*R*)-1,2,3,4-tetrahydroisoquinolin-3-yl)methyl)((*S*)-5,6,7,8-tetrahydroquinolin-8-yl)amino)propyl)urea (102). To a mixture of compound **104** (0.161 g, 0.33 mmol) dissolved in DCM (3.0 mL) was added TFA (1.0 mL). The reaction was allowed to stir at room temperature for 6 hours. The reaction was quenched with sat. aq. NaHCO₃ and extracted with DCM (3x). The combined organic layers were washed with brine, dried over Na₂SO₄, filtered, and concentrated to a light brown foam (0.122 g). The crude material was purified by flash column chromatography (ISCO, 12 g silica gel, 0-50% 90:10:0.1 DCM/MeOH/NH₄OH and DCM over 18 minutes) resulting in a white foam (0.057 g, 44%). ¹H NMR [600 MHz, CDCl₃] δ 8.44 (d, *J* = 3.8 Hz, 1H), 8.05 (br s, 1H), 7.39 (d, *J* = 7.6 Hz, 1H), 7.16-7.07 (m, 3H), 7.05 (d, *J* = 6.1 Hz, 1H), 6.97 (d, *J* = 6.4 Hz, 1H), 4.72 (s, 2H), 4.25 (dd, *J* = 9.7, 6.5 Hz, 1H), 3.95 (d, *J* = 15.6 Hz, 1H), 3.74 (d, *J* = 16.0 Hz, 1H), 3.70 (br s, 1H), 3.16 (t, *J* = 10.9 Hz, 1H), 2.96 (dt, *J* = 13.3, 4.2 Hz, 1H), 2.87-2.76 (m, 3H), 2.74 (t, *J* = 3.8 Hz, 1H), 2.74-2.60 (m, 1H), 2.51 (d, *J* = 7.6 Hz, 2H), 2.30 (t, *J* = 13.5 Hz, 1H), 2.14 (dd, *J* = 12.9, 6.7 Hz, 1H), 2.04 (dp, *J* = 13.0, 4.3 Hz, 1H), 1.89 (tdd, *J* = 12.7, 9.7, 3.0 Hz, 2H), 1.85-1.79 (m, 1H), 1.77-1.60 (m, 2H); ¹³C NMR [150 MHz, CDCl₃] δ 162.1, 160.4, 149.2, 139.9, 137.5, 136.8, 131.9, 128.8, 128.7, 128.3, 124.8, 62.3, 59.9, 56.1, 54.8 (2C), 50.7,

43.2, 36.4 (2C), 32.2, 29.2, 24.3; HRMS (ESI) $[M+H]^+$ calc'd for $C_{23}H_{32}N_5O$ 394.26014, found 394.26077.

3.6.2 NMR Experimental Detail

NMR experiments were performed on a Varian Unity Inova 600 equipped with either a 5 mm TRES-ZPGF (1H/13C/15N) probe or a 5 mm ID-ZPGF (1H/X) probe operating at 600 MHz (1H) and 150 (^{13}C). Both spectrometers use VNMR 6.1C software. For all 2-D experiments, the probe was tuned to the sample, and the 90° pulse width (1H pw90) was calibrated at a specific pulse power (tpwr) by identifying the 180° pulse which gave a null spectrum and dividing the result by two. The inversion recovery method was utilized to measure the spin-lattice relaxation times (T1) of the various 1H nuclei.

Averaged NMR Spectrum of **IT1t** **IT1t** was assigned by a combination of 2-D 1H and 1H - ^{13}C . Spectra were processed and analyzed using the MestReNova v8.0.2 software package. The NMR sample was prepared by dissolving 5.0 mg of **IT1t** in 0.6 mL of DMSO- d_6 (Cambridge Isotope Laboratories) and subsequently degassed and sealed. 1H and ^{13}C chemical shifts are reported in parts per million and referenced to the residual solvent peak. Due to peak overlap in the alkyl region of the spectrum, the cyclohexyl protons for each ring could not be definitively assigned. Data from the 2-D COSY experiment assisted in the relative assignments of a few cyclohexyl protons. The NOESY spectra was recorded at 300 ms in order to calculate the interproton distances from the cross-peak volumes using an internal calibration distance between the 1,3-diaxial protons of the ring namely, H-11 and H-12 of 2.60 Å. The relaxation delay (d1) was set to 6 s (~3 times the longest T1 of ~2.5 s), nt = 32, and ni = 256 (experiment time ~ 29 hours). The spectral assignments and the four NOE-derived distances are presented in Table 3.2 and Table 3.3.

Table 3.2 Spectral Assignments of **IT1t**.

Atom Number	¹ H	¹³ C
12/15	1.87-1.01 (m, 20H)	32.1, 31.0, 24.6, 24.5, 24.4
5	1.50 (s, 6H)	27.4
11	3.67 (app. s, 1H)	56.3
14	3.89 (app. s, 1H)	53.4
3	4.25 (s, 2H)	58.2
7	--	168.4
8	4.89 (s, 2H)	28.0
1	6.87 (s, 1H)	110.2
10	9.36 (br s, 1H)	--
13	9.87 (br s, 1H)	--
6	10.64 (br s, 1H)	--
2	--	131.4
4	--	69.3
9	--	160.1

Table 3.3 NOE-derived Distances for **IT1t**.

NOE Contact	Distance (Å)
3-8	2.34
1-8	3.44
3-5	2.58
11-12 (1,3-diaxial)	2.60*
14-15 (1,3-diaxial)	2.65

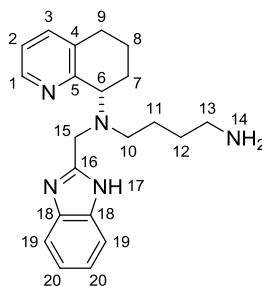
*Internal standard used to calculate distances.

Averaged NMR Spectrum of AMD11070 The chemical shifts were assigned to **AMD11070** by a combination of 2-D ¹H and ¹H-¹³C experiments. Spectra were processed and analyzed using the MestReNova v8.0.2 software package. The NMR sample was prepared by dissolving 11.0 mg of **AMD11070** in 0.8 mL of CDCl₃ (Cambridge Isotope Laboratories) and subsequently

degassed and sealed. ^1H chemical shifts provided in Table 3.4 are reported in parts per million and referenced to the residual solvent peak.

A NOESY spectrum was recorded at 300 ms mixing time. Interproton distances were calculated from cross-peak volumes using an internal calibration distance between H-2 and H-3 of 2.48 Å. The relaxation delay (d1) was set to 6 s (~3 times the longest T1 of ~2.5 s), nt = 16, and ni = 256 (experiment time ~ 14 hours). The 31 NOE-derived distances are presented in Table 3.5.

Table 3.4 Spectral Assignments of AMD11070.



Assignment	¹ H
1	8.60 (d, <i>J</i> = 4.3 Hz, 1H)
2	7.15 (dd, <i>J</i> = 7.6, 4.7 Hz, 1H)
3	7.42 (d, <i>J</i> = 7.6 Hz, 1H)
4	--
5	--
6	4.06 (dd, <i>J</i> = 9.7, 6.1 Hz, 1H)
7	2.21 (dddd, <i>J</i> = 10.4, 5.6, 4.4, 2.6, 1.4 Hz, 1H)
7'	1.92 (dddd, <i>J</i> = 12.9, 11.6, 9.9, 3.0 Hz, 1H)
8	1.70 (tdt, <i>J</i> = 13.5, 13.5, 8.6, 2.6, 2.6 Hz, 1H)
8'	2.08-2.01 (m, 1H)
9	2.74 (app. t, <i>J</i> = 3.9 Hz, 1H)
9'	2.85 (ddd, <i>J</i> = 16.1, 11.1, 4.9 Hz, 1H)
10	2.72 (dd, <i>J</i> = 7.8, 4.7 Hz, 1H)
10	2.57 (dt, <i>J</i> = 12.8, 7.5, 7.5 Hz, 1H)
11; 12	1.50-1.29 (m, 4H)
13	2.51 (app. t, <i>J</i> = 6.3 Hz, 2H)
14	not observed
15	4.10 (d, <i>J</i> = 16.7 Hz, 1H)
15	4.03 (d, <i>J</i> = 16.8 Hz, 1H)
16	--
17	not observed
18	--
19	7.65-7.54 (m, 2H)
20	7.22-7.18 (m, 1H)

^aDashed connectivity.

Table 3.5 NOE-derived Distances for **AMD11070**.

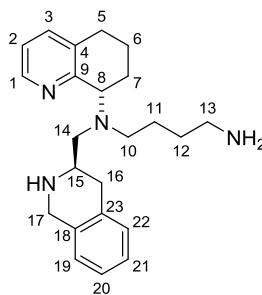
NOE Contacts	Distance (Å)
2-3	2.48*
3-9	2.88
3-9'	3.20
6-7'	3.13
6-8	2.79
6-10(K)	2.95
6-10(M)	3.74
6-11 or 12	2.92
6-15	2.51
7-7'	2.27
7'-15(G)	3.32
7'-15(H)	3.77
7-8	2.92
8-8'	2.07
8-9	3.34
8-10(K)	3.68
8'-9	3.23
8'-9'	3.25
8'-10(K)	3.56
9'-10(K)	2.00
10(K)-10(M)	2.18
10(K)-11 or 12	3.16
10(K)-11 or 12	3.40
10(K)-15(G)	3.74
10(K)-15(H)	3.50
10(M)-15(G)	3.63
11 or 12-15(H)	3.47
11 or 12-13	3.21
11 or 12-13	2.94
15(G)-15(H)	2.26
19-20	2.37

[†]Dashed connectivity. *Internal standard used to calculate distances.

Averaged NMR Spectrum of ECX00947 A sample for 1-D and 2-D NMR experiments was prepared by dissolving 5.0 mg of **ECXC00947** in 0.65 mL of CDCl₃ (Cambridge Isotope Laboratories) and subsequently degassed and sealed. In order to assist in structural proton assignments, an HMQC spectrum (nt = 48, ni = 256, experiment time ~15 hours) and a COSY spectrum (nt = 32, ni = 512, experiment time ~13 hours) was acquired. ¹H chemical shifts provided in Table 3.6 are reported in parts per million and referenced to the residual solvent peak.

A NOESY spectrum was recorded at 300 ms mixing time, which is expected to be in the linear range for small molecules. Interproton distances were calculated from cross-peak volumes using an internal calibration distance between H-2 and H-3 of 2.48 Å. The relaxation delay (d1) was set to 6 s (~3 times the longest T1 of ~2.5 s), nt = 32, and ni = 256 (experiment time = 29.5 hours). The 22 NOE-derived distances are presented in Table 3.7.

Table 3.6 Spectral Assignments of ECXC00947.



Atom Number	¹ H	¹³ C
1	8.46 (dd, <i>J</i> = 4.4, 0.9 Hz, 1H)	146.9
2	7.05-7.02 (m, 1H)	121.7
3	7.35-7.32 (m, 1H)	136.9
4	--	134.7
5 up	2.79 (m, 1H)	29.7
5 down	2.67 (app. dt, <i>J</i> = 16.8, 5.0, 5.0 Hz, 1H)	29.7
6 up	1.75-1.67 (m, 1H)	22.2
6 down	2.02-1.96 (m, 1H)	22.2
7 up	2.14-2.06 (m, 1H)	28.6
7 down	1.90 (dddd, <i>J</i> = 15.7, 13.0, 10.2, 3.1 Hz, 1H)	28.6
8 up	4.08 (dd, <i>J</i> = 9.6, 6.6 Hz, 1H)	62.0
9	--	158.8
10	3.02 (dt, <i>J</i> = 13.0, 5.8, 5.8 Hz, 1H)	54.6
10'	2.61-2.60 (m, 1H)	54.6
11	1.61-1.48 (m, 2H)	27.6
12	1.61-1.48 (m, 1H)	31.1
12'	1.48-1.40 (m, 1H)	31.1
13	2.76-2.74 (m, 2H)	42.2
14	2.98 (dd, <i>J</i> = 13.2, 3.2 Hz, 1H)	58.5
14'	2.38 (dd, <i>J</i> = 12.9, 10.5 Hz, 1H)	58.5
15 down	2.77-2.75 (m, 1H)	52.6
16 up	2.43 (dd, <i>J</i> = 15.9, 11.0 Hz, 1H)	34.0
16 down	2.63-2.61 (m, 1H)	34.0
17 up	4.07 (d, <i>J</i> = 15.1 Hz, 1H)	48.7
17 down	3.92 (d, <i>J</i> = 15.1 Hz, 1H)	48.7
18	--	135.7
19	7.09-7.08 (m, 1H)	126.2
20	7.08-7.07 (m, 1H)	125.8
21	7.02-7.01 (m, 1H)	126.6
22	7.03-7.07 (m, 1H)	129.3
23	--	134.3

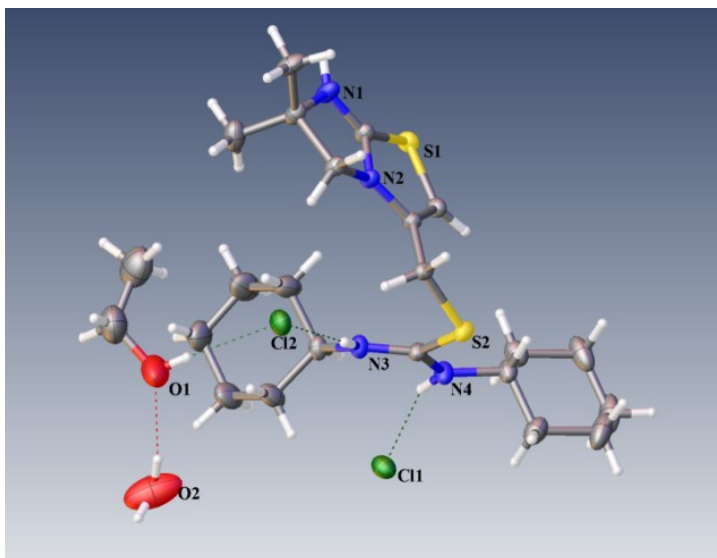
Table 3.7 NOE-derived Distances for **ECXC00947**.

NOE Contact	Distance (Å)
2-3	2.48*
5 down-6 up	3.26
5 down-5 up	1.98
10-12	2.85
6 down-7 up	2.50
7 down-14 down	2.79
16 up-17 up	2.58
7 up-7 down	1.79
7 down-15 down	2.81
17 up-17 down	2.00
10-10'	1.83
14 up-14 down	1.75
7 up-8 up	2.31
6 up-8 up	2.77
7 down-8 up	3.35
10'-12'	3.18
3-5 down	2.63
3-5 up	2.69
6 up-6 down	1.72
1-2	2.42
16 up-16 down	1.88
6 up-7 up	2.42

*Internal standard used to calculate distances.

3.6.3 Crystal Structure Data

IT1t X-ray Data (Dr. John Bacsa and Marika Wieliczko, Emory X-ray Crystallography Center, Department of Chemistry)



Single crystals of $C_{23}H_{44}Cl_2N_4O_2S_2$ were recrystallized from ethanol. A suitable crystal was selected and mounted on an apex2_Mo diffractometer. The crystal was kept at 173(2) K during data collection. Using Olex2 (Dolomanov et al., 2009), the structure was solved with the Superflip (L. Palatinus & G. Chapuis, 2007) structure solution program using Charge Flipping and refined with the ShelXL (Sheldrick, 2008) refinement package using Least Squares minimization.

Crystal Data for $C_{23}H_{44}Cl_2N_4O_2S_2$ ($M = 543.64$): monoclinic, space group $P2_1/c$ (no. 14), $a = 8.3244(2)$ Å, $b = 20.1818(5)$ Å, $c = 17.0887(4)$ Å, $\beta = 94.9200(10)^\circ$, $V = 2860.35(12)$ Å³, $Z = 4$, $T = 173(2)$ K, $\mu(\text{MoK}\alpha) = 0.399$ mm⁻¹, $D_{\text{calc}} = 1.262$ g/mm³, 66636 reflections measured ($3.13 \leq 2\theta \leq 73.358$), 14077 unique ($R_{\text{int}} = 0.0499$) which were used in all calculations. The final R_1 was 0.0503 ($I > 2\sigma(I)$) and wR_2 was 0.1498 (all data).

Table 1. Crystal Data and Structure Refinement.

Empirical formula	$C_{23}H_{44}Cl_2N_4O_2S_2$
Formula weight	543.64
Temperature/K	173(2)
Crystal system	monoclinic
Space group	$P2_1/c$
a/Å	8.3244(2)
b/Å	20.1818(5)
c/Å	17.0887(4)
$\alpha/^\circ$	90
$\beta/^\circ$	94.9200(10)
$\gamma/^\circ$	90
Volume/Å ³	2860.35(12)
Z	4
$\rho_{\text{calc}}/\text{mg}/\text{mm}^3$	1.262
m/mm^{-1}	0.399
F(000)	1168.0
Crystal size/ mm^3	$0.658 \times 0.567 \times 0.505$
2 Θ range for data collection	3.13 to 73.358°
Index ranges	$-13 \leq h \leq 13, -33 \leq k \leq 33, -28 \leq l \leq 28$
Reflections collected	66636
Independent reflections	14077[R(int) = 0.0499]
Data/restraints/parameters	14077/1/305
Goodness-of-fit on F ²	1.042
Final R indexes [$I \geq 2\sigma(I)$]	$R_1 = 0.0503, wR_2 = 0.1399$
Final R indexes [all data]	$R_1 = 0.0607, wR_2 = 0.1498$
Largest diff. peak/hole / e Å ⁻³	1.09/-0.57

Table 2. Fractional Atomic Coordinates ($\times 10^4$) and Equivalent Isotropic Displacement Parameters ($\text{Å}^2 \times 10^3$). U_{eq} is defined as 1/3 of the trace of the orthogonalised U_{ij} tensor.

Atom	x	y	z	U(eq)
S2	6965.6(3)	3059.1(2)	5455.8(2)	22.77(6)
Cl2	8786.9(3)	5886.3(2)	3485.8(2)	28.59(7)
Cl1	3512.8(3)	6765.8(2)	6623.2(2)	29.44(7)
N2	7073.3(10)	5046.5(4)	5812.7(5)	18.82(14)
N3	8029.1(11)	3312.1(5)	6959.2(5)	23.05(16)
N4	5913.9(13)	2569.4(5)	6746.7(6)	26.36(18)
N1	6525.7(12)	6078.4(5)	6137.6(7)	27.82(19)
C8	7593.2(12)	3907.4(5)	5352.4(6)	19.34(15)
C7	6512.8(11)	4400.1(5)	5697.2(5)	17.93(15)
C4	8492.4(12)	5416.1(5)	5593.3(6)	21.65(17)

C9	6984.1(12)	2979.6(5)	6483.3(6)	20.36(16)
C6	5011.2(12)	4331.3(5)	5931.2(6)	21.14(17)
C5	6004.0(12)	5462.9(5)	6090.3(6)	20.83(16)
C2	8267.6(13)	6100.7(5)	5995.7(7)	24.01(18)
O1	6719(3)	5846.5(9)	1842.5(13)	84.1(7)
C15	7902.4(14)	3414.4(6)	7806.2(6)	25.55(19)
C16	4531.6(15)	2264.7(6)	6284.2(7)	27.8(2)
C1	8589.3(19)	6687.2(6)	5473.9(10)	36.1(3)
S1	4253.9(3)	5073.6(2)	6291.4(2)	22.20(6)
C14	9383(2)	3164.6(9)	8279.7(8)	39.8(3)
C17	3059.8(16)	2298.8(8)	6760.0(8)	34.9(3)
C3	9265.1(18)	6137.0(9)	6781.4(9)	39.1(3)
C18	1618(2)	1956.6(11)	6316.8(11)	50.4(5)
C13	9259(3)	3286.2(10)	9154.8(9)	50.0(4)
C12	8935(3)	3999.6(10)	9336(1)	50.4(4)
C11	7537(3)	4278.8(12)	8830.1(11)	58.3(5)
C19	2021(3)	1247.9(11)	6112.1(11)	57.4(6)
C20	3482(3)	1217.3(10)	5633.2(11)	55.9(5)
C10	7689(2)	4162.9(8)	7953.6(9)	44.7(4)
C21	4934(2)	1556.9(8)	6070.3(9)	39.4(3)
C22	6621(3)	5198.0(15)	1532.6(17)	71.9(7)
C23	8020(3)	4760.9(16)	1705(2)	79.0(8)
O2	6107(4)	7885.4(11)	6082.1(18)	101.6(9)

Table 3. Anisotropic Displacement Parameters ($\text{\AA}^2 \times 10^3$). The Anisotropic displacement factor exponent takes the form: $-2\pi^2[h^2a^*U_{11} + \dots + 2hka \times b \times U_{12}]$

Atom	U_{11}	U_{22}	U_{33}	U_{23}	U_{13}	U_{12}
S2	30.65(13)	18.76(11)	19.2(1)	-0.74(8)	3.84(8)	-3.71(8)
Cl2	20.90(11)	36.99(15)	28.03(12)	4.23(10)	2.88(9)	-7.05(9)
Cl1	24.77(12)	33.54(14)	30.29(13)	-12.0(1)	3.92(9)	3.56(9)
N2	15.7(3)	18.9(3)	22.7(3)	-0.3(3)	6.5(3)	-0.7(2)
N3	21.7(4)	28.0(4)	19.5(3)	1.3(3)	2.0(3)	-7.0(3)
N4	29.5(4)	26.3(4)	22.4(4)	7.0(3)	-2.5(3)	-10.2(3)
N1	20.5(4)	22.0(4)	42.4(5)	-7.4(4)	11.2(4)	-0.1(3)
C8	20.1(4)	18.4(4)	20.1(4)	2.0(3)	4.7(3)	0.3(3)
C7	16.9(3)	18.8(4)	18.4(3)	2.2(3)	3.1(3)	-0.8(3)
C4	17.7(4)	20.2(4)	28.4(4)	-0.9(3)	9.5(3)	-1.6(3)
C9	22.3(4)	18.4(4)	20.3(4)	2.4(3)	1.6(3)	-1.8(3)
C6	16.4(4)	22.7(4)	24.6(4)	3.0(3)	3.6(3)	-1.7(3)
C5	17.0(4)	22.5(4)	23.8(4)	-1.1(3)	6.1(3)	0.5(3)
C2	20.4(4)	22.1(4)	30.7(5)	-4.7(4)	9.2(3)	-2.9(3)

O1	107.2(15)	54.6(9)	80.2(12)	13.2(8)	-51.7(11)	-10.2(9)
C15	23.6(4)	33.0(5)	19.9(4)	-0.6(4)	1.4(3)	-6.2(4)
C16	30.2(5)	27.2(5)	25.0(4)	5.5(4)	-3.2(4)	-9.8(4)
C1	43.5(7)	19.3(5)	48.4(7)	-1.4(5)	20.4(6)	-2.6(4)
S1	15.1(1)	26.92(12)	25.39(12)	1.76(9)	6.45(8)	0.54(7)
C14	44.2(7)	46.9(8)	26.7(5)	0.2(5)	-6.2(5)	15.6(6)
C17	28.1(5)	41.5(7)	34.6(6)	8.2(5)	0.4(4)	-5.1(5)
C3	30.1(6)	52.4(8)	34.9(6)	-12.2(6)	3.8(5)	-5.9(5)
C18	33.3(7)	73.0(12)	42.6(8)	23.5(8)	-10.8(6)	-20.6(7)
C13	70.3(12)	53.1(10)	24.3(6)	2.8(6)	-9.9(6)	15.1(8)
C12	68.1(11)	50.8(9)	30.0(6)	-10.2(6)	-9.6(7)	0.1(8)
C11	76.2(14)	57.5(11)	39.4(8)	-16.4(8)	-4.4(8)	25(1)
C19	63.8(11)	66.5(12)	39.3(8)	10.4(8)	-10.4(7)	-43.4(10)
C20	81.5(14)	48.3(9)	36.6(7)	-4.9(7)	-1.9(8)	-33.5(9)
C10	62.3(10)	36.8(7)	33.5(6)	-2.4(5)	-5.5(6)	16.3(7)
C21	49.7(8)	32.3(6)	36.5(6)	-4.6(5)	5.1(6)	-9.8(6)
C22	66.4(14)	78.7(17)	66.7(14)	-11.3(12)	-17.3(11)	-6.9(12)
C23	62.9(15)	79.2(18)	95(2)	-16.4(15)	6.1(14)	-16.4(13)
O2	131(2)	56.2(11)	131(2)	-14.7(11)	86.5(18)	-4.5(11)

Table 4. Bond Lengths.

Atom	Atom	Length/Å	Atom	Atom	Length/Å
S2	C8	1.8029(10)	C2	C1	1.5195(18)
S2	C9	1.7620(10)	C2	C3	1.5186(19)
N2	C7	1.3938(13)	O1	C22	1.411(3)
N2	C4	1.4726(13)	C15	C14	1.5025(18)
N2	C5	1.3401(13)	C15	C10	1.544(2)
N3	C9	1.3216(13)	C16	C17	1.5290(19)
N3	C15	1.4748(14)	C16	C21	1.519(2)
N4	C9	1.3230(14)	C14	C13	1.528(2)
N4	C16	1.4734(15)	C17	C18	1.528(2)
N1	C5	1.3160(14)	C18	C19	1.517(3)
N1	C2	1.4911(14)	C13	C12	1.502(3)
C8	C7	1.4952(14)	C12	C11	1.499(3)
C7	C6	1.3518(13)	C11	C10	1.532(2)
C4	C2	1.5618(15)	C19	C20	1.524(3)
C6	S1	1.7569(11)	C20	C21	1.528(2)
C5	S1	1.7158(10)	C22	C23	1.470(4)

Table 5. Bond Angles.

Atom	Atom	Atom	Angle/°
C9	S2	C8	101.90(5)
C7	N2	C4	134.76(8)
C5	N2	C7	114.37(8)
C5	N2	C4	110.13(8)
C9	N3	C15	125.18(9)
C9	N4	C16	126.61(9)
C5	N1	C2	109.81(9)
C7	C8	S2	113.81(7)
N2	C7	C8	118.22(8)
C6	C7	N2	111.16(9)
C6	C7	C8	130.61(9)
N2	C4	C2	101.95(8)
N3	C9	S2	121.06(8)
N3	C9	N4	122.36(10)
N4	C9	S2	116.58(8)
C7	C6	S1	112.63(8)
N2	C5	S1	112.64(8)
N1	C5	N2	112.83(9)
N1	C5	S1	134.53(8)
N1	C2	C4	101.52(8)
N1	C2	C1	109.99(10)
N1	C2	C3	108.86(10)

Atom	Atom	Atom	Angle/°
C1	C2	C4	113.39(10)
C3	C2	C4	110.78(11)
C3	C2	C1	111.77(12)
N3	C15	C14	110.93(11)
N3	C15	C10	108.42(10)
C14	C15	C10	109.94(12)
N4	C16	C17	108.70(11)
N4	C16	C21	110.09(11)
C21	C16	C17	111.93(11)
C5	S1	C6	89.08(5)
C15	C14	C13	110.62(13)
C18	C17	C16	110.31(13)
C19	C18	C17	111.15(15)
C12	C13	C14	112.60(14)
C11	C12	C13	112.71(15)
C12	C11	C10	112.44(17)
C18	C19	C20	111.36(14)
C19	C20	C21	110.70(14)
C11	C10	C15	109.22(14)
C16	C21	C20	110.99(16)
O1	C22	C23	117.5(2)

Table 6. Hydrogen Bonds.

D	H	A	d(D-H)/Å	d(H-A)/Å	d(D-A)/Å	D-H-A/°
O2	H2B	O1 ¹	0.85	2.08	2.896(3)	161.4

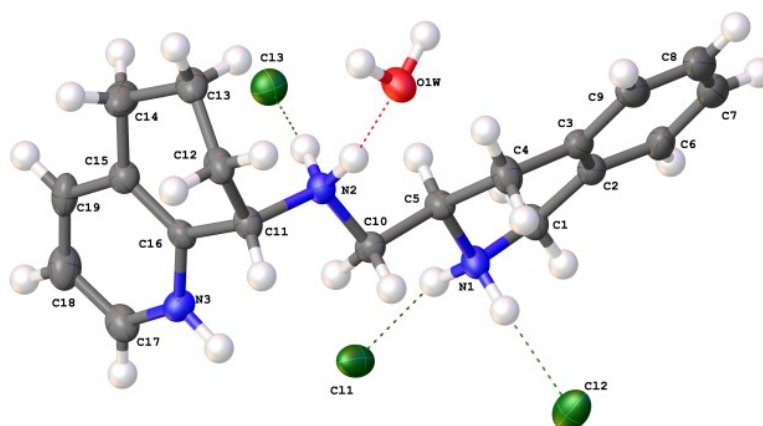
¹+X,3/2-Y,1/2+Z

Table 7. Hydrogen Atom Coordinates (Å×10⁴) and Isotropic Displacement Parameters (Å²×10³).

Atom	x	y	z	U(eq)
H3	8848	3482	6759	28
H4	6038	2471	7238	32
H1	5949	6417	6236	33
H8A	8675	3958	5604	23
H8B	7633	4005	4799	23
H4A	8485	5461	5028	26

H4B	9488	5204	5796	26
H6	4441	3934	5904	25
H1D	7224	5840	2276	126
H15	6957	3176	7964	31
H16	4304	2519	5799	33
H1A	8012	6629	4968	54
H1B	9724	6716	5415	54
H1C	8236	7087	5710	54
H14A	10327	3389	8115	48
H14B	9507	2694	8187	48
H17A	3305	2085	7264	42
H17B	2796	2758	6855	42
H3A	9007	6537	7048	59
H3B	10390	6136	6697	59
H3C	9028	5761	7096	59
H18A	713	1959	6639	60
H18B	1304	2200	5839	60
H13A	8399	3015	9331	60
H13B	10259	3151	9444	60
H12A	8718	4038	9883	61
H12B	9891	4259	9262	61
H11A	7466	4751	8926	70
H11B	6549	4076	8975	70
H19A	1101	1049	5814	69
H19B	2240	995	6592	69
H20A	3228	1434	5131	67
H20B	3743	758	5534	67
H10A	8610	4404	7790	54
H10B	6729	4323	7650	54
H21A	5262	1311	6545	47
H21B	5828	1558	5742	47
H22A	6421	5232	966	86
H22B	5689	4984	1725	86
H23A	7928	4384	1361	119
H23B	8054	4615	2240	119
H23C	8991	4999	1624	119
H2A	5151	7735	6069	122
H2B	6205	8213	6396	122

Compound **21** X-ray Data (Dr. John Bacsca, Emory X-ray Crystallography Center, Department of Chemistry).



Empirical formula	C ₁₉ H ₂₈ Cl ₃ N ₃ O
Formula weight	420.79
Temperature/K	173(2)
Crystal system	monoclinic
Space group	P2 ₁
a/Å	12.536(4)
b/Å	6.965(2)
c/Å	12.871(4)
α/°	90
β/°	110.268(5)
γ/°	90
Volume/Å ³	1054.3(6)
Z	2
ρ _{calc} /mg/mm ³	1.326
m/mm ⁻¹	0.448
F(000)	444.0
Crystal size/mm ³	1.138 × 0.146 × 0.114
Radiation	MoKα (λ = 0.71073)
2θ range for data collection	3.374 to 51.332°
Index ranges	-15 ≤ h ≤ 15, -8 ≤ k ≤ 8, -15 ≤ l ≤ 15
Reflections collected	6798
Independent reflections	3972 [R _{int} = 0.0769, R _{sigma} = 0.1418]
Data/restraints/parameters	3972/125/260
Goodness-of-fit on F ²	1.015
Final R indexes [I ≥ 2σ(I)]	R ₁ = 0.0725, wR ₂ = 0.1328
Final R indexes [all data]	R ₁ = 0.1157, wR ₂ = 0.1554
Largest diff. peak/hole / e Å ⁻³	0.46/-0.30
Flack parameter	-0.07(11)

Single, colourless needle-shaped crystals were recrystallised from ethyl acetate. A suitable crystal ($1.14 \times 0.15 \times 0.11 \text{ mm}^3$) was selected and mounted on loop with paratone oil on a Bruker APEX-II CCD diffractometer. The crystal was kept at $T = 173(2) \text{ K}$ during data collection. Using Olex2 (Dolomanov et al., 2009), the structure was solved with the Superflip (L. Palatinus & G. Chapuis, 2007) structure solution program, using the Charge Flipping solution method. The model was refined with the ShelXL (Sheldrick, 2008) refinement package using Least Squares minimisation.

Crystal Data. $\text{C}_{19}\text{H}_{28}\text{Cl}_3\text{N}_3\text{O}$, $M_r = 420.79$, monoclinic, $\text{P}2_1$ (No. 4) $a = 12.536(4) \text{ \AA}$, $b = 6.965(2) \text{ \AA}$, $c = 12.871(4) \text{ \AA}$, $\beta = 110.268(5)^\circ$, $\alpha = \gamma = 90^\circ$, $V = 1054.3(6) \text{ \AA}^3$, $T = 173(2) \text{ K}$, $Z = 2$, $Z' = 1.000$, $\mu(\text{MoK}_\alpha) = 0.448 \text{ mm}^{-1}$, 6798 reflections measured, 3972 unique ($R_{int} = 0.0769$) which were used in all calculations. The final wR_2 was 0.1554 (all data) and R_1 was 0.0725 ($I > 2(I)$).

Experimental Extended. A colourless needle-shaped crystal with dimensions $1.14 \times 0.15 \times 0.11 \text{ mm}^3$ was mounted on loop with paratone oil. Data were collected using a Bruker APEX-II CCD diffractometer equipped with an Oxford Cryostream low-temperature apparatus operating at $T = 173(2) \text{ K}$.

Data were measured using ϕ and ω scans of 1.00° per frame using MoK_α radiation (fine-focus sealed tube, 45 kV, 30 mA). The total number of runs and images was based on the strategy calculation from the program **APEX2** (Bruker, 2013). The actually achieve resolution was $\theta = 25.666$.

Cell parameters were retrieved using the SAINT v8.34A (Bruker, 2013) software and refined using SAINT v8.34A (Bruker, 2013) on 3565 reflections, 52% of the observed reflections.

Data reduction was performed using the SAINT v8.34A (Bruker, 2013) software which corrects for Lorentz polarisation. The final completeness is 100.00% out to 25.666 in θ . The absorption

coefficient (MU) of this material is 0.448 and the minimum and maximum transmissions are 0.5282 and 0.7456.

The structure was solved by Charge Flipping using the Superflip (L. Palatinus & G. Chapuis, 2007) structure solution program and refined by Least Squares using ShelXL (Sheldrick, 2008).

The structure was solved in the space group $P2_1$ (# 4). All non-hydrogen atoms were refined anisotropically. Hydrogens positions were calculated geometrically and refined using the riding model.

The Flack parameter was refined to -0.07(11), confirming the absolute stereochemistry. Determination of absolute structure using Bayesian statistics on Bijvoet differences using the program within PLATON (Spek, 2003) also report that we have the correct enantiomer based on this comparison. Note: The Flack parameter is used to determine chirality of the crystal studied, the value should be near 0, a value of 1 means that the stereochemistry is wrong and the model should be inverted. A value of 0.5 means that the crystal consists of a racemic mixture of the two enantiomers.

Table 1. Fractional Atomic Coordinates ($\times 10^4$) and Equivalent Isotropic Displacement Parameters ($\text{\AA}^2 \times 10^3$). U_{eq} is defined as 1/3 of the trace of the orthogonalised U_{ij} .

Atom	x	y	z	U_{eq}
C11	3961.9(18)	-1773(3)	4497.3(19)	40.0(6)
C12	3553.5(19)	1828(3)	1561.3(19)	44.5(6)
C13	1347.3(18)	1414(3)	6189.8(18)	37.5(6)
N1	2221(5)	1135(10)	3082(5)	28.8(15)
O1W	1126(5)	7817(9)	4608(5)	38.4(15)
N2	2623(5)	4619(10)	5424(5)	26.0(15)
N3	4833(6)	2559(9)	7146(6)	28.2(16)
C11	3611(7)	5319(12)	6407(7)	28.4(17)
C15	3641(6)	3510(12)	8121(7)	29.8(18)
C9	-641(7)	4470(15)	1271(7)	42(2)
C17	5274(7)	1103(12)	7858(7)	36(2)
C2	316(6)	1414(13)	1626(6)	30.6(16)
C5	1874(6)	2675(11)	3701(7)	27.3(17)

C10	2936(6)	3415(13)	4625(6)	27.9(18)
C19	4096(7)	1969(13)	8862(7)	36(2)
C6	-541(7)	646(15)	690(7)	39(2)
C3	269(6)	3329(14)	1902(6)	30.3(16)
C16	4025(6)	3738(11)	7249(6)	25.2(17)
C13	2325(7)	6366(13)	7415(7)	35.7(19)
C18	4908(8)	801(13)	8722(7)	44(2)
C4	1213(7)	4178(13)	2876(7)	36.4(19)
C8	-1497(8)	3699(16)	367(8)	48(2)
C12	3235(7)	6997(13)	6940(7)	35.0(19)
C7	-1432(7)	1793(18)	82(7)	48(2)
C14	2796(8)	4852(14)	8315(8)	43(2)
C1	1229(7)	76(13)	2311(7)	32.9(18)

Table 2. Anisotropic Displacement Parameters ($\times 10^4$). The anisotropic displacement factor exponent takes the form: $-2\pi^2[a^{*2} \times U_{11} + \dots + 2hka^* \times b^* \times U_{12}]$

Atom	U_{11}	U_{22}	U_{33}	U_{23}	U_{13}	U_{12}
Cl1	38.1(12)	40.1(14)	45.9(13)	18.0(12)	19.9(11)	11.7(11)
Cl2	49.5(13)	45.5(15)	42.1(13)	-12.0(12)	20.5(11)	-20.1(12)
Cl3	41.5(12)	31.0(13)	41.3(12)	3.2(10)	16(1)	-0.6(10)
N1	31(3)	26(4)	25(3)	-1(3)	5(3)	6(3)
O1W	33(3)	39(4)	38(3)	-2(3)	7(3)	7(3)
N2	27(3)	23(4)	26(3)	0(3)	7(3)	-1(3)
N3	35(4)	23(4)	30(4)	0(3)	14(3)	1(3)
C11	30(4)	24(3)	27(3)	-2(3)	4(3)	2(3)
C15	32(4)	27(4)	29(4)	-4(3)	9(3)	0(3)
C9	37(4)	54(5)	39(4)	19(3)	16(3)	15(3)
C17	39(5)	27(5)	36(5)	-5(4)	6(4)	4(4)
C2	29(3)	37(3)	25(3)	4(3)	9(3)	2(3)
C5	27(4)	25(4)	29(3)	-3(3)	8(3)	2(3)
C10	28(4)	27(5)	28(4)	-3(4)	10(4)	-3(4)
C19	50(5)	33(5)	21(4)	0(4)	6(4)	-9(5)
C6	33(4)	58(5)	25(4)	1(3)	11(3)	-5(3)
C3	28(3)	37(3)	27(3)	5(3)	12(3)	3(3)
C16	22(4)	24(4)	26(3)	-2(3)	4(3)	0(3)
C13	40(4)	33(4)	31(4)	-5(3)	9(3)	11(4)
C18	59(6)	32(6)	35(5)	4(4)	11(5)	6(5)
C4	38(4)	32(4)	33(4)	3(3)	4(3)	5(3)
C8	37(4)	74(5)	35(4)	17(4)	14(3)	10(4)
C12	37(4)	32(4)	29(4)	-7(3)	3(3)	7(3)
C7	36(4)	79(5)	32(4)	12(4)	15(3)	4(4)
C14	50(5)	47(5)	37(4)	5(4)	19(4)	19(4)
C1	33(4)	30(4)	30(4)	-1(3)	5(3)	1(3)

Table 3. Bond Lengths.

Atom	Atom	Length/Å
N1	C5	1.488(9)
N1	C1	1.490(10)
N2	C11	1.512(10)
N2	C10	1.481(10)
N3	C17	1.350(10)
N3	C16	1.345(9)
C11	C16	1.507(11)
C11	C12	1.511(11)
C15	C19	1.418(12)
C15	C16	1.375(11)
C15	C14	1.497(11)
C9	C3	1.397(11)
C9	C8	1.388(13)
C17	C18	1.359(12)
C2	C6	1.412(11)
C2	C3	1.387(13)
C2	C1	1.502(11)
C5	C10	1.534(10)
C5	C4	1.516(12)
C19	C18	1.363(12)
C6	C7	1.376(13)
C3	C4	1.515(12)
C13	C12	1.534(11)
C13	C14	1.525(12)
C8	C7	1.387(16)

Table 4. Bond Angles.

Atom	Atom	Atom	Angle/°
C5	N1	C1	112.5(6)
C10	N2	C11	115.3(6)
C16	N3	C17	122.5(7)
C16	C11	N2	110.2(6)
C16	C11	C12	108.8(7)
C12	C11	N2	109.7(6)
C19	C15	C14	120.2(7)
C16	C15	C19	117.6(8)
C16	C15	C14	122.2(8)
C8	C9	C3	120.4(10)
N3	C17	C18	119.8(8)
C6	C2	C1	117.7(8)
C3	C2	C6	119.7(8)
C3	C2	C1	122.5(7)

N1	C5	C10	108.7(6)
N1	C5	C4	108.2(6)
C4	C5	C10	115.3(7)
N2	C10	C5	111.2(6)
C18	C19	C15	120.5(8)
C7	C6	C2	119.5(10)
C9	C3	C4	120.4(8)
C2	C3	C9	119.8(8)
C2	C3	C4	119.8(8)
N3	C16	C11	117.3(7)
N3	C16	C15	119.9(7)
C15	C16	C11	122.7(7)
C14	C13	C12	110.8(7)
C17	C18	C19	119.7(9)
C3	C4	C5	113.0(7)
C7	C8	C9	119.5(9)
C11	C12	C13	110.5(7)
C6	C7	C8	121.0(10)
C15	C14	C13	114.5(7)
N1	C1	C2	112.0(7)

Table 5. Hydrogen Fractional Atomic Coordinates ($\times 10^4$) and Equivalent Isotropic Displacement Parameters ($\text{\AA}^2 \times 10^3$). U_{eq} is defined as 1/3 of the trace of the orthogonalised U_{ij} .

Atom	x	y	z	U_{eq}
H11	4243	5734	6153	34
H9	-675	5780	1461	51
H17	5838	291	7754	43
H5	1354	2099	4053	33
H10A	3399	2305	5021	33
H10B	3407	4182	4294	33
H19	3832	1749	9461	43
H6	-502	-653	482	46
H13A	2061	7503	7733	43
H13B	1657	5828	6809	43
H18	5217	-220	9227	52
H4A	878	5117	3263	44
H4B	1749	4893	2595	44
H8	-2123	4471	-53	58
H12A	2922	8030	6378	42
H12B	3904	7532	7546	42
H7	-2012	1272	-544	58
H14A	3164	5517	9039	52
H14B	2148	4081	8375	52
H1C	907	-786	2748	39
H1D	1490	-744	1809	39

H3	5130(50)	2730(110)	6540(40)	30(20)
H1WA	304(14)	7550(100)	4310(50)	39
H1WB	1200(50)	8760(80)	5200(40)	39
H2A	2140(50)	5710(70)	5050(60)	50(30)
H1A	2680(50)	1490(110)	2620(50)	40(20)
H2B	2140(50)	3740(80)	5680(60)	40(20)
H1B	2630(60)	90(90)	3590(60)	64

3.7 Computational Methods

Conformational Analysis of **IT1t**

Conformational Searches (Performed by Ana Alcaraz, Ph.D.). A 50,000-step Mixed-torsional/Low-mode sampling (MCMM/LMCS) conformational search of **IT1t** was performed on the dication; charge centers assigned consistent with the published pK_a values of the nitrogen atoms in **IT1t** for each of the two resonance forms of the isothiurea moiety. The searches were completed in three force fields (AMBER*, MMFFs, and OPLS-2005) using the MacroModel module in Maestro; each of which delivered the global minimum at least twenty-five times. The GBSA/H₂O solvation model was used along with enhanced torsion sampling and a 30 kJ/mol energy cutoff.

NAMFIS Analysis. The NAMFIS protocol was applied to all dicationic conformations with chair cyclohexyl rings and equatorial amine attachments. Four NOE-derived H-H distances were used to deconvolute the conformer pool, resulting in four conformations with populations of 58, 15, 14 and 13% and a sum of square differences (SSD) of 0.

Conformational Analysis of **AMD11070**

Conformational Searches. A 50,000-step MCMM conformational search of **AMD11070** was performed with three individual force fields (AMBER*, MMFFs, and OPLS-2005) using the MacroModel module in Maestro. The published crystal structure stereochemistry of **AMD11070** was corrected to match the biologically active form (*R* to *S*) and used as the starting structure.

Searches were performed on three forms of the structure: the two stereoisomers of the protonated tertiary nitrogen and the corresponding neutral form. The GBSA/H₂O solvation model was used along with a relaxed 30 kJ/mol energy cut-off, resulting in a total of 10,755 conformations (4,397 in AMBER*, 2,861 in MMFFs, and 3,497 in OPLS-2005). The global minimum was found between twenty-two and two hundred fourteen times for the different searches, assuring complete coverage of conformational space.

NAMFIS Analysis. The NAMFIS protocol was applied to the large pool of conformations. The NOE-derived H-H distances were used to deconvolute the conformer pool, resulting in thirteen conformations and a SSD of 56.

Conformational Analysis of **ECXC00947**

Conformational Searches. A 100,000-step MCMM/LCMS conformational search of **ECXC00947** was performed on the neutral form of the molecule with three individual force fields (AMBER*, MMFFs, and OPLS-2005) using the MacroModel module in Maestro. The GBSA/H₂O solvation model was used along with enhanced torsion sampling and a 30 kJ/mol energy cutoff. The global minimum was found at least twenty-five times for each search.

NAMFIS Analysis. The NAMFIS protocol was applied to the neutral conformations. Twenty two NOE-derived H-H distances were used to deconvolute the conformer pool, resulting in nine conformations and a SSD of 9.

- (1) Kemp, J. A.; McKernan, R. M. *Nat. Neurosci.* **2002**, *5*, 1039.
- (2) Traynelis, S. F.; Wollmuth, L. P.; McBain, C. J.; Menniti, F. S.; Vance, K. M.; Ogden, K. K.; Hansen, K. B.; Yuan, H.; Myers, S. J.; Dingledine, R. *Pharmacol. Rev.* **2010**, *62*, 405.
- (3) Metaferia, B. B.; Hoch, J.; Glass, T. E.; Bane, S. L.; Chatterjee, S. K.; Snyder, J. P.; Lakdawala, A.; Cornett, B.; Kingston, D. G. I. *Org. Lett.* **2001**, *3*, 2461.
- (4) Durand, G. M.; Gregor, P.; Zheng, X.; Bennett, M. V; Uhl, G. R.; Zukin, R. S. *Proc. Natl. Acad. Sci. U.S.A.* **1992**, *89*, 9359.
- (5) Hollmann, M.; Heinemann, S. *Ann. Rev. Neurosci.* **1994**, *17*, 31.
- (6) Monyer, H.; Burnashev, N.; Laurie, D. J.; Sakmann, B.; Seeburg, P. H. *Neuron* **1994**, *12*, 529.
- (7) Santangelo, R. M.; Acker, T. M.; Zimmerman, S. S.; Katzman, B. M.; Strong, K. L.; Traynelis, S. F.; Liotta, D. C. *Expert Opin. Ther. Pat.* **2012**, *22*, 1337.
- (8) Furukawa, H.; Singh, S. K.; Mancusso, R.; Gouaux, E. *Nature* **2005**, *438*, 185.
- (9) Johnson, J. W.; Ascher, P. *Nature* **1987**, *325*, 529.
- (10) Kleckner, N.; Dingledine, R. *Science* **1988**, *241*, 835.
- (11) Nicholls, D. G. *J. Neurochem.* **1989**, *52*, 331.
- (12) Mayer, M. L.; Westbrook, G. L.; Guthrie, P. B. *Nature* **1984**, *309*, 261.
- (13) Nowak, L.; Bregestovski, P.; Ascher, P.; Herbet, A.; Prochiantz, A. *Nature* **1984**, *307*, 462.
- (14) Punnakkal, P.; Jendritza, P.; Kohr, G. *Neuropharmacology* **2012**, *62*, 1985.
- (15) Akazawa, C.; Shigemoto, R.; Bessho, Y.; Nakanishi, S.; Mizuno, N. *J. Comp. Neurol.* **1994**, *347*, 150.
- (16) Furukawa, H.; Gouaux, E. *EMBO* **2003**, *22*, 2873.
- (17) Chen, P. E.; Geballe, M. T.; Katz, E.; Erreger, K.; Livesey, M. R.; O'Toole, K. K.; Le, P.; Lee, C. J.; Snyder, J. P.; Traynelis, S. F.; Wyllie, D. J. A. *J. Physiol.* **2008**, *586*, 227.
- (18) Wafford, K.; Kathoria, M.; Bain, C.; Marshall, G.; Le Bourdelles, B.; Kemp, J.; Whiting, P. *Mol. Pharmacol.* **1995**, *47*, 374.
- (19) Clausen, R. P.; Christensen, C.; Hansen, K. B.; Greenwood, J. R.; Jørgensen, L.; Micalé, N.; Madsen, J. C.; Nielsen, B.; Egebjerg, J.; Bräuner-Osborne, H.; Traynelis, S. F.; Kristensen, J. L. *J. Med. Chem.* **2008**, *51*, 4179.

- (20) Fleck, M.; Henze, D.; Barrionuevo, G.; Palmer, A. *J. Neurosci.* **1993**, *13*, 3944.
- (21) Patneau, D.; Mayer, M. *J. Neurosci.* **1990**, *10*, 2385.
- (22) Priestley, T.; Laughton, P.; Myers, J.; Le Bourdelles, B.; Kerby, J.; Whiting, P. *Mol. Pharmacol.* **1995**, *48*, 841.
- (23) Shinozaki, H.; Ishida, M.; Shimamoto, K.; Ohfune, Y. *Brain Res.* **1989**, *480*, 355.
- (24) Sivaprakasam, M.; Hansen, K. B.; David, O.; Nielsen, B.; Traynelis, S. F.; Clausen, R. P.; Couty, F.; Bunch, L. *ChemMedChem* **2009**, *4*, 110.
- (25) Vance, K. M.; Simorowski, N.; Traynelis, S. F.; Furukawa, H. *Nat. Commun.* **2011**, *2*, 294.
- (26) Do, K. Q.; Herrling, P. L.; Streit, P.; Cuenod, M. *J. Neural Transm.* **1988**, *72*, 185.
- (27) Do, K.; Herrling, P.; Streit, P.; Turski, W.; Cuenod, M. *J. Neurosci.* **1986**, *6*, 2226.
- (28) Olney, J. W.; Price, M. T.; Salles, K. S.; Labruyere, J.; Ryerson, R.; Mahan, K.; Frierdich, G.; Samson, L. *Brain Res. Bull.* **1987**, *19*, 597.
- (29) Karakas, E.; Simorowski, N.; Furukawa, H. *Nature* **2011**, *475*, 249.
- (30) Chenard, B. L.; Bordner, J.; Butler, T. W.; Chambers, L. K.; Collins, M. A.; De Costa, D. L.; Ducat, M. F.; Dumont, M. L.; Fox, C. B. *J. Med. Chem.* **1995**, *38*, 3138.
- (31) Fischer, G.; Mutel, V.; Trube, G.; Malherbe, P.; Kew, J. N. C.; Mohacsi, E.; Heitz, M. P.; Kemp, J. A. *J. Pharmacol. Exp. Ther.* **1997**, *283*, 1285.
- (32) Mony, L.; Kew, J. N. C.; Gunthorpe, M. J.; Paoletti, P. *Br. J. Pharmacol.* **2009**, *157*, 1301.
- (33) Williams, K. *Mol. Pharmacol.* **1993**, *44*, 851.
- (34) Burnashev, N.; Schoepfer, R.; Monyer, H.; Ruppersberg, J.; Gunther, W.; Seeburg, P.; Sakmann, B. *Science* **1992**, *257*, 1415.
- (35) Jin, L.; Sugiyama, H.; Takigawa, M.; Katagiri, D.; Tomitori, H.; Nishimura, K.; Kaur, N.; Phanstiel, O.; Kitajima, M.; Takayama, H.; Okawara, T.; Williams, K.; Kashiwagi, K.; Igarashi, K. *J. Pharmacol. Exp. Ther.* **2007**, *320*, 47.
- (36) Kashiwagi, K. *Mol. Pharmacol.* **2002**, *61*, 533.
- (37) Blanpied, T. A.; Boeckman, F. A.; Aizenman, E.; Johnson, J. W. *J Neurophysiol.* **1997**, *77*, 309.
- (38) Chen, H.-S. V.; Lipton, S. A. *J. Neurochem.* **2006**, *97*, 1611.

- (39) Parsons, C. G.; Quack, G.; Bresink, I.; Baran, L.; Przegalinski, E.; Kostowski, W.; Krzascik, P.; Hartmann, S.; Danysz, W. *Neuropharmacology* **1995**, *34*, 1239.
- (40) Jentsch, J. D.; Roth, R. H. *Neuropsychopharmacology* **1999**, *20*, 201.
- (41) Luby, E. D. *Arch. Neurol. Psychiatry* **1959**, *81*, 363.
- (42) Acker, T. M.; Yuan, H.; Hansen, K. B.; Vance, K. M.; Ogden, K. K.; Jensen, H. S.; Burger, P. B.; Mullasseril, P.; Snyder, J. P.; Liotta, D. C.; Traynelis, S. F. *Mol. Pharmacol.* **2011**, *80*, 782.
- (43) Costa, B. M.; Irvine, M. W.; Fang, G.; Eaves, R. J.; Mayo-Martin, M. B.; Skifter, D. A.; Jane, D. E.; Monaghan, D. T. *J. Pharmacol. Exp. Ther.* **2010**, *335*, 614.
- (44) Hansen, K. B.; Traynelis, S. F. *J. Neurosci.* **2011**, *31*, 3650.
- (45) Mosley, C. A.; Acker, T. M.; Hansen, K. B.; Mullasseril, P.; Andersen, K. T.; Le, P.; Vellano, K. M.; Bräuner-Osborne, H.; Liotta, D. C.; Traynelis, S. F. *J. Med. Chem.* **2010**, *53*, 5476.
- (46) Mullasseril, P.; Hansen, K. B.; Vance, K. M.; Ogden, K. K.; Yuan, H.; Kurtkaya, N. L.; Santangelo, R.; Orr, A. G.; Le, P.; Vellano, K. M.; Liotta, D. C.; Traynelis, S. F. *Nat. Commun.* **2010**, *1*, 90.
- (47) Kim, J. S.; Kornhuber, H. H.; Schmid-Burgk, W.; Holzmüller, B. *Neurosci. Lett.* **1980**, *20*, 379.
- (48) Gattaz, W. F.; Gattaz, D.; Beckmann, H. *Arch. Psychiatr. Nervenkr.* **1982**, *231*, 221.
- (49) Korpi, E. R.; Kaufmann, C. A.; Marnela, K. M.; Weinberger, D. R. *Psychiatry Res.* **1987**, *20*, 337.
- (50) Perry, T. L. *Neurosci. Lett.* **1982**, *28*, 81.
- (51) Albers, G. W.; Goldstein, L. B.; Hall, D.; Lesko, L. M. *JAMA* **2001**, *286*, 2673.
- (52) Davis, S. M.; Albers, G. W.; Diener, H.-C.; Lees, E. R.; Norris, J. *Lancet* **1997**, *349*, 32.
- (53) Lees, G. J. *Drugs* **2000**, *59*, 33.
- (54) Yurkewicz, L.; Weaver, J.; Bullock, M. R.; Marshall, L. F. *J. Neurotrauma* **2005**, *22*, 1428.
- (55) Kalia, L. V.; Kalia, S. K.; Salter, M. W. *Lancet Neurol.* **2008**, *7*, 742.
- (56) Dirnagl, U.; Iadecola, C.; Moskowitz, M. A. *Trends Neurosci.* **1999**, *22*, 391.

- (57) Danysz, W.; Parsons, C. G.; Möbius, H.-Jö.; Stöffler, A.; Quack, Gü. *Neurotox. Res.* **2000**, *2*, 85.
- (58) Andersen, H. S.; Olsen, O. H.; Iversen, L. F.; Sørensen, A. L. P.; Mortensen, S. B.; Christensen, M. S.; Branner, S.; Hansen, T. K.; Lau, J. F.; Jeppesen, L.; Moran, E. J.; Su, J.; Bakir, F.; Judge, L.; Shahbaz, M.; Collins, T.; Vo, T.; Newman, M. J.; Ripka, W. C.; Møller, N. P. H. *J. Med. Chem.* **2002**, *45*, 4443.
- (59) Gopalsamy, A.; Shi, M. Iminothiazolidinone Derivatives as SFRP-1 Antagonists. WO/2006/124887, November 24, 2006.
- (60) Arakelian, A.; Dunn, Jr., H.; Grieshammer, L.; Coleman, L. *J. Org. Chem.* **1960**, *25*, 465.
- (61) Tedenborg, L.; Barf, T.; Nordin, S.; Vallagarda, J.; Williams, M.; Kurz, G. Thiazol-Compounds as 11-Beta-Hydroxysteroid Dehydrogenase Type 1 Inhibitors. WO/2005/075471, August 19, 2005.
- (62) Vorbrüggen, H.; Krolikiewicz, K. *Chem. Ber.* **1984**, *117*, 1523.
- (63) Montalbetti, C. A. G. N.; Falque, V. *Tetrahedron* **2005**, *61*, 10827.
- (64) Balasubramaniyan, V.; Balasubramaniyan, P.; Wani, M. J. *Proc. Indian Acad. Sci. (Chem. Sci.)* **1991**, *103*, 621.
- (65) Ulbricht, T. L. V.; Price, C. C. *J. Org. Chem.* **1956**, *21*, 567.
- (66) Hirota, K.; Sajiki, H.; Kitade, Y.; Maki, Y. *J. Chem. Soc. Perkin Trans. 1* **1990**, 123.
- (67) Wang, X.; Sharp, J. S.; Handel, T. M.; Prestegard, J. H. *Prog. Mol. Biol. Transl. Sci.* **2013**, *117*, 531.
- (68) Sodhi, A.; Montaner, S.; Gutkind, J. S. *Nat. Rev. Nat. Cell Biol.* **2004**, *5*, 998.
- (69) Proudfoot, A. E. I.; Power, C. a; Schwarz, M. K. *Expert Opin. Investig. Drugs* **2010**, *19*, 345.
- (70) Raman, D.; Sobolik-delmaire, T.; Richmond, A. *Exp. Cell Res.* **2011**, *317*, 575.
- (71) Gozansky, E. K.; Louis, J. M.; Caffrey, M.; Clore, G. M. *J. Mol. Biol.* **2005**, *345*, 651.
- (72) Zhang, W.-B.; Navenot, J.-M.; Haribabu, B.; Tamamura, H.; Hiramatu, K.; Omagari, A.; Pei, G.; Manfredi, J. P.; Fujii, N.; Broach, J. R.; Peiper, S. C. *J. Biol. Chem.* **2002**, *277*, 24515.
- (73) Nguyen, L. T.; Vogel, H. J. *Front. Immunol.* **2012**, *3*, 384.
- (74) Proudfoot, A. E. I. *Nat. Rev. Immunol.* **2002**, *2*, 106.

- (75) Feng, Y.; Broder, C. C.; Kennedy, P. E.; Berger, E. A. *Science* **1996**, *272*, 872.
- (76) Ratajczak, J.; Wysoczynski, M.; Hayek, F.; Janowska-Wieczorek, A.; Ratajczak, M. Z. *Leukemia* **2006**, *20*, 1487.
- (77) Kofuku, Y.; Yoshiura, C.; Ueda, T.; Terasawa, H.; Hirai, T.; Tominaga, S.; Hirose, M.; Maeda, Y.; Takahashi, H.; Terashima, Y.; Matsushima, K.; Shimada, I. *J. Biol. Chem.* **2009**, *284* (50), 35240.
- (78) Sun, X.; Cheng, G.; Hao, M.; Zheng, J.; Zhou, X.; Zhang, J.; Taichman, R. S.; Pienta, K. J.; Wang, J. *Cancer Metastasis Rev.* **2010**, *29*, 709.
- (79) Dealwis, C.; Fernandez, E. J.; Thompson, D. A.; Simon, R. J.; Siani, M. A.; Lolis, E. *Proc. Natl. Acad. Sci. U.S.A.* **1998**, *95*, 6941.
- (80) Ratajczak, M. Z.; Kim, C. H.; Abdel-Latif, A.; Schneider, G.; Kucia, M.; Morris, A. J.; Laughlin, M. J.; Ratajczak, J. *Leukemia* **2012**, *26*, 63.
- (81) Lapidot, T.; Kollet, O. *Leukemia* **2002**, *16*, 1992.
- (82) Abraham, M.; Biyder, K.; Begin, M.; Wald, H.; Weiss, I. D.; Galun, E.; Nagler, A.; Peled, A. *Stem Cells* **2007**, *25*, 2158.
- (83) Wu, B.; Chien, E. Y. T.; Mol, C. D.; Fenalti, G.; Liu, W.; Katritch, V.; Abagyan, R.; Brooun, A.; Wells, P.; Bi, F. C.; Hamel, D. J.; Kuhn, P.; Handel, T. M.; Cherezov, V.; Stevens, R. C. *Science* **2010**, *330*, 1066.
- (84) Müller, A.; Homey, B.; Soto, H.; Ge, N.; Catron, D.; Buchanan, M. E.; McClanahan, T.; Murphy, E.; Yuan, W.; Wagner, S. N.; Barrera, J. L.; Mohar, A.; Verástegui, E.; Zlotnik, A. *Nature* **2001**, *410*, 50.
- (85) Taichman, R. S.; Cooper, C.; Keller, E. T.; Pienta, K. J.; Taichman, N. S.; McCauley, L. K. *Cancer Res.* **2002**, *62*, 1832.
- (86) Choi, W.-T.; Duggineni, S.; Xu, Y.; Huang, Z.; An, J. *J. Med. Chem.* **2011**, *55*, 977.
- (87) Truax, V. M.; Zhao, H.; Katzman, B. M.; Prosser, A. R.; Alcaraz, A. A.; Saindane, M. T.; Howard, R. B.; Culver, D.; Arrendale, R. F.; Gruddanti, P. R.; Evers, T. J.; Natchus, M. G.; Snyder, J. P.; Liotta, D. C.; Wilson, L. J. *ACS Med. Chem. Lett.* **2013**, *4*, 1025.
- (88) Riveiro-Falkenbach, E.; Soengas, M. S. *Clin. Cancer Res.* **2010**, *16*, 2932.
- (89) Teicher, B. A.; Fricker, S. P. *Clin. Cancer Res.* **2010**, *16*, 2927.
- (90) Hesselgesser, J.; Liang, M.; Hoxie, J.; Greenberg, M.; Brass, L. F.; Orsini, M. J.; Taub, D.; Horuk, R. *J. Immunol.* **1998**, *160*, 877.
- (91) De Clercq, E. *Nat. Rev. Drug Discov.* **2003**, *2*, 581.

- (92) Daar, E.; Kesler, K.; Petropoulos, C.; Huang, W.; Bates, M.; Lail, A.; Coakley, E.; Gomperts, E.; Donfield, S. *Clin. Infect. Dis.* **2007**, *45*, 1656.
- (93) Broxmeyer, H. E.; Orschell, C. M.; Clapp, D. W.; Hangoc, G.; Cooper, S.; Plett, P. A.; Liles, W. C.; Li, X.; Graham-Evans, B.; Campbell, T. B.; Calandra, G.; Bridger, G.; Dale, D. C.; Srouf, E. F. *J. Exp. Med.* **2005**, *201*, 1307.
- (94) Zlotnik, A.; Burkhardt, A. M.; Homey, B. *Nat. Rev. Immunol.* **2011**, *11*, 597.
- (95) DiPersio, J. F.; Micallef, I. N.; Stiff, P. J.; Bolwell, B. J.; Maziarz, R. T.; Jacobsen, E.; Nademanee, A.; McCarty, J.; Bridger, G.; Calandra, G. *J. Clin. Oncol.* **2009**, *27*, 4767.
- (96) Larochelle, A.; Krouse, A.; Metzger, M.; Orlic, D.; Donahue, R. E.; Fricker, S.; Bridger, G.; Dunbar, C. E.; Hematti, P. *Blood* **2006**, *107*, 3772.
- (97) Devine, S. M.; Flomenberg, N.; Vesole, D. H.; Liesveld, J.; Weisdorf, D.; Badel, K.; Calandra, G.; DiPersio, J. F. *J. Clin. Oncol.* **2004**, *22*, 1095.
- (98) Flomenberg, N.; Devine, S. M.; Dipersio, J. F.; Liesveld, J. L.; McCarty, J. M.; Rowley, S. D.; Vesole, D. H.; Badel, K.; Calandra, G. *Blood* **2005**, *106*, 1867.
- (99) Taylor, D. D.; Gercel-Taylor, C. *Gynecol. Oncol.* **2008**, *110*, 13.
- (100) Kobayashi, K.; Oishi, S.; Hayashi, R.; Tomita, K.; Kubo, T.; Tanahara, N.; Ohno, H.; Yoshikawa, Y.; Furuya, T.; Hoshino, M.; Fujii, N. *J. Med. Chem.* **2012**, *55*, 2746.
- (101) Ueda, S.; Oishi, S.; Wang, Z.; Araki, T.; Tamamura, H.; Cluzeau, J.; Ohno, H.; Kusano, S.; Nakashima, H.; Trent, J. O.; Peiper, S. C.; Fujii, N. *J. Med. Chem.* **2007**, *50*, 192.
- (102) Singh, I. P.; Chauthe, S. K. *Expert Opin. Ther. Pat.* **2011**, *21*, 227.
- (103) Skerlj, R. T.; Bridger, G. J.; Kaller, A.; McEachern, E. J.; Crawford, J. B.; Zhou, Y.; Atsma, B.; Langille, J.; Nan, S.; Veale, D.; Wilson, T.; Harwig, C.; Hatse, S.; Princen, K.; De Clercq, E.; Schols, D. *J. Med. Chem.* **2010**, *53*, 3376.
- (104) Grande, F.; Garofalo, A.; Neamati, N. *Curr. Pharm. Des.* **2008**, *14*, 385.
- (105) De Clercq, E. *Pharmacol. Ther.* **2010**, *128*, 509.
- (106) Burger, J. A.; Stewart, D. J. *Expert Opin. Invest. Drugs* **2009**, *18*, 481.
- (107) Ichiyama, K.; Yokoyama-Kumakura, S.; Tanaka, Y.; Tanaka, R.; Hirose, K.; Bannai, K.; Edamatsu, T.; Yanaka, M.; Niitani, Y.; Miyano-Kurosaki, N.; Takaku, H.; Koyanagi, Y.; Yamamoto, N. *Proc. Natl. Acad. Sci. U. S. A.* **2003**, *100*, 4185.
- (108) Murakami, T.; Kumakura, S.; Yamazaki, T.; Tanaka, R.; Hamatake, M.; Okuma, K.; Huang, W.; Toma, J.; Komano, J.; Yanaka, M.; Tanaka, Y.; Yamamoto, N. *Antimicrob. Agents Chemother.* **2009**, *53*, 2940.

- (109) Iwasaki, Y.; Akari, H.; Murakami, T.; Kumakura, S.; Dewan, M. Z.; Yanaka, M.; Yamamoto, N. *Cancer Sci.* **2009**, *100*, 778.
- (110) De Clercq, E. *Biochem. Pharmacol.* **2009**, *77*, 1655.
- (111) Crawford, J. B.; Chen, G.; Gauthier, D.; Wilson, T.; Carpenter, B.; Baird, I. R.; McEachern, E.; Kaller, A.; Harwig, C.; Atsma, B.; Skerlj, R. T.; Bridger, G. J. *Org. Proc. Res. Dev.* **2008**, *12*, 823.
- (112) Lipinski, C.; Hopkins, A. *Nature* **2004**, *432*, 855.
- (113) Hamilton, R.; Walker, B. J.; Walker, B. *Tet. Lett.* **1993**, *34*, 2847.
- (114) Riggs-Sauthier, J. Protease Inhibitors. WO/2010/144869 A2, 2010.
- (115) Thompson, L. A.; Boy, K. M.; Shi, J.; Macor, J. E.; Good, A. C.; Marcin, L. R. Substituted Tetrahydroisoquinolines as beta-secretase Inhibitors. US/2008/0153868 A1, 2008.
- (116) Morris, D. J.; Partridge, A. S.; Manville, C. V.; Racys, D. T.; Woodward, G.; Docherty, G.; Wills, M. *Tet. Lett.* **2010**, *51*, 209.
- (117) Abdel-Magid, A. F.; Carson, K. G.; Harris, B. D.; Maryanoff, C. A.; Shah, R. D. *J. Org. Chem.* **1996**, *61*, 3849.
- (118) Xu, F.; Simmons, B.; Armstrong, J.; Murry, J. *J. Org. Chem.* **2005**, *70*, 6105.
- (119) Surmont, R.; Verniest, G.; Thuring, J. W.; Ten Holte, P.; Deroose, F.; De Kimpe, N. *Org. Biomol. Chem.* **2010**, *8*, 4514.
- (120) Kendrick, D. A.; Danzin, C.; Kolb, M. *J. Med. Chem.* **1989**, *32*, 170.
- (121) Cyprotex. Caco-2 Permeability www.cyprotex.com.
- (122) Sneader, W. *Drug Discovery: A History*; 2006; pp. 1–468.
- (123) Silverstein, A. M. *Bull. Hist. Med.* **2002**, *76*, 335.
- (124) Rosenthal, S. A. *Yale J. Biol. Med.* **1984**, *57*, 718.
- (125) Kingston, W. *J. Hist. Med. Allied Sci.*, **2004**, *59*, 441.
- (126) Jorgensen, W. L. *Science* **2004**, *303*, 1813.
- (127) Silverman, R. B.; Holladay, M. W. *The Organic Chemistry of Drug Design and Drug Action*, Elsevier Science, 2014; 3rd edition, p. 1–17.
- (128) Perola, E.; Charifson, P. S. *J. Med. Chem.* **2004**, *47*, 2499.

- (129) Nicolaou, K. C.; Frederick, M. O. *Angew. Chem. Int. Ed.* **2007**, *46*, 5278.
- (130) Wüthrich, K. *Nat. Struct. Biol.* **2001**, *8*, 923.
- (131) Freeman, R. *Magnetic Resonance in Chemistry and Medicine*; Oxford University Press: New York, **2003**.
- (132) Karplus, M. *J. Am. Chem. Soc.* **1963**, *85*, 2870.
- (133) Haasnoot, C. A. G.; de Leeuw, F. A. A. M.; Altona, C. *Tetrahedron* **1980**, *36*, 2783.
- (134) Phillips, L.; Cooper, M. K.; Haaland, A.; Samdal, S.; Giricheva, N. I.; Girichev, G. V. *Dalton Trans.* **2010**, *39*, 4631.
- (135) Kegley, S. E. *Problems and Solutions in Organometallic Chemistry*; University Science Books, **1986**; Vol. 2, p. 323.
- (136) Cicero, D. O.; Barbato, G.; Bazzo, R. *J. Am. Chem. Soc.* **1995**, *117*, 1027.
- (137) Thepchatrri, P.; Cicero, D. O.; Monteagudo, E.; Ghosh, A. K.; Cornett, B.; Weeks, E. R.; Snyder, J. P. *J. Am. Chem. Soc.* **2005**, *127*, 12838.
- (138) Snyder, J. P.; Nevins, N.; Cicero, D. O.; Jansen, J. *J. Am. Chem. Soc.* **2000**, *122*, 724.
- (139) Monteagudo, E.; Cicero, D. O.; Cornett, B.; Myles, D. C.; Snyder, J. P. *J. Am. Chem. Soc.* **2001**, *123*, 6929.
- (140) Lynn, D. G.; Snyder, J. P.; Lakdawala, A. S.; Dong, J.; Lu, K. *Structure*, **2003**, *11*, 242.
- (141) Thoma, G.; Streiff, M. B.; Kovarik, J.; Glickman, F.; Wagner, T.; Beerli, C.; Zerwes, H.-G. *J. Med. Chem.* **2008**, *51*, 7915.
- (142) Beuming, T.; Sherman, W. *J. Chem. Inf. Model* **2012**, *52*, 3263.
- (143) Cox, B. D.; Prosser, A. R.; Katzman, B. M.; Alcaraz, A. A.; Liotta, D. C.; Wilson, L. J.; Snyder, J. P. *ChemBioChem* **2014**, online.